國 立 交 通 大 學

機 械 工 程 學 系

碩 士 論 文

加裝可移動的尼龍線在一小水平加熱銅板上對 FC-72 池沸騰熱傳增強及氣泡特性研究

Pool Boiling Heat Transfer Enhancement of FC-72 and Associated Bubble Characteristics over a Small Horizontal Plate by Placing Flexible Nylon Strings above the Plate

研 究 生：陳 俊 州

指 導 老 師：林 清 發 教授

中 華 民 國 99 年 6 月

加裝可移動的尼龍線在一小水平加熱銅板上對 FC-72 池沸騰熱傳增強及氣泡特性研究

Pool Boiling Heat Transfer Enhancement of FC-72 and Associated Bubble Characteristics over a Small Horizontal Plate by Placing Flexible Nylon Strings above the Plate

研 究 生 ： 陳 俊 州　　Student：Chun-Chou Chen

指導教授 ： 林 清 發　　Advisor：Prof. Tsing-Fa Lin

國立交通大學

機械工程學系

碩士論文

A Thesis

Submitted to Department of Mechanical Engineering

College of Engineering

National Chiao Tung University

In partial Fulfillment of the Requirements

For the Degree of

Master of Science

In

Mechanical Engineering

April 2010

Hsinchu, Taiwan, Republic of China

中華民國 99 年 6 月

加裝可移動的尼龍線在一小水平加熱銅板上

對 FC-72 池沸騰熱傳增強及氣泡特性研究

研 究 生：陳 俊 州　　指 導 老 師：林 清 發 教授

國立交通大學機械工程學系

摘要

本論文針對加裝可饒性且具有活動力的尼龍線於加熱銅塊邊緣之FC-72 池沸騰飽和態和次冷態的熱傳增強實驗研究。尼龍線的端點固定在銅塊邊緣且線和線之間彼此互相平行。在實驗中探討尼龍線線徑、尼龍線固定端點和加熱面的距離、尼龍線的長度藉以控制鬆弛程度以及部分線和線之間間距的效應。在實驗參數範圍上，熱通量q從 0.1 到 7 W/cm^2，尼龍線直徑從 74 到 259 μm，尼龍線和加熱面的距離從 0 到 2 mm，線的長度由 10 到 12 mm以及線和線之間間距 1 mm和 2 mm，工作流體次冷度從 0°C到 10°C。

實驗數據以壁過熱度對應輸入的熱通量及熱傳係數表示，比較對於光滑加熱銅塊下熱傳增強的表現，由數據呈現的圖形可得，熱傳增強的表現會因其不同的參數搭配而有不同的增強效果，理想且良好的熱傳增強表現在於適當的線徑、長度和固定端點的高度搭配，並且在次冷態的熱傳增強方面和飽和態有近似的趨勢。

Pool Boiling Heat Transfer Enhancement of FC-72 and Associated Bubble Characteristics over a Small Horizontal Plate by Placing Flexible Nylon Strings above the Plate

Student: Chun-Chou Chen Advisor: Prof. Tsing-Fa Lin

Department of Mechanical Engineering

National Chiao Tung University

ABSTRACT

An experiment is carried out here to investigate how the saturated and subcooled pool boiling of liquid FC-72 over a small horizontal heated copper surface is affected by placing flexible and movable nylon strings above the surface, intending to explore the possible pool boiling heat transfer enhancement by the strings. The strings of uniform size are fixed only at their ends and are parallel with each other. In the experiment, the imposed heat flux is varied from 0.1 to 7 W/cm^2, the diameter of strings from 74 to 259μm, the string-heated surface separation from 0 to 2 mm, and the length of the strings from 10 to 12 mm for the pitch of the strings mainly fixed at 2 mm. Besides, the subcooling in the bulk FC-72 liquid is chosen to be at 5°C and 10°C. The measured data are presented in terms of boiling curves and the boiling heat transfer coefficient at the heating surface with the installation of the strings and for a bare surface. Effects of the experimental parameters on the possible boiling heat transfer enhancement are examined in detail.

The data obtained from the present study for the saturated and subcooled pool boiling indicate that placing the flexible and movable nylon strings can increase the pool boiling heat transfer coefficient of FC-72 more than 100% over that for a bare surface for a certain combination of the experimental parameters. However, the

boiling heat transfer enhancement varies nonmonotonically with the string size, length and height, reflecting the complicate influence of the strings on the bubble motion near the heated surface. An optimal boiling heat transfer enhancement can be procured by a suitable choice of the experimental parameters. Besides, the effects of the experimental parameters on the boiling heat transfer enhancement are similar at different subcoolings of FC-72.

TABLE OF CONTENTS

LIST OF TABLES

LIST OF FIGURES

Experimental Apparatus

Data Reduction

Saturated Pool Boiling Heat Transfer

NOMENCLATURE

A	area, mm^2
d_w	wire diameters, μm
h_w	wire height
ℓ_w	wire length
h	heat transfer coefficient, $W/m^2 \cdot K$
I	measured current from DC power supply, A
k	thermal conductivity, W/m·K
L	characteristic length, m
Nu_L	Nusselt number, $Nu_L = \frac{hL}{k_\ell}$
P	system pressure, kPa
Q	heat transfer rate, W
q_n	net wall heat flux, W/cm^2
Ra	Rayleigh number, dimensionless
T	temperature, ^oC
V	measured voltage from DC power supply, V

CHAPTER 1

INTRODUCTION

1.1 Motive of the Present Study

With the recent quick development of the microelectronic fabrication technology, the power dissipation density in various micro processors increases significantly. How to effectively remove the large amount of dissipating heat from the processors poses a great challenge to heat transfer research community. In order to transfer the large quantity of the dissipating heat from the chips with an ultra high component density, highly efficient heat transfer methods are required to control their temperatures at allowable level. Although air cooling is used commonly today, this method has reached its upper limit and is unable to solve the cooling problems encountered in the current electronics industry [1]. Therefore, alternate means of cooling based on liquid convection and liquid-vapor phase-change heat transfer have been considered. Among these, boiling heat transfer is regarded to be one of the most effective methods in electronics cooling comparing with the methods based on single-phase heat transfer because of the exchange of latent heat involved in the boiling processes. Methods to further improve the boiling heat transfer are therefore of great interest.

Over the past decades considerable effort has been devoted to investigating how the change in the heating surface structure can enhance the pool boiling heat transfer. The prominent examples include adding the micro-structures, pin fins and grooves to the surfaces. Besides, coating the surfaces with particles and covering the surfaces with screens have been known to be effective. These enhancement methods are based on various forms of extended surface fixed firmly onto the surfaces or directly fabricated on the surfaces. The possible pool boiling heat transfer enhancement by placing flexible and movable strings above the heating plate will be investigated in the present study. The strings are only fixed at their ends and

should be fine enough so that they can move to a certain extent near the surface by the forces induced in the boiling flow.

The working fluid FC-72, a dielectric fluorocarbon liquid manufactured by the 3M Company, is gaining popularity in electronics cooling application. It not only has suitable phase-change temperature for thermal control of I.C. components but also owns the quality that does not foul the boiling surface. More importantly, FC-72 has less impact on our environment than alternative liquids like chlorofluorocarbons or organic liquids. Copper has properties of better thermal conductivity than most metal and is often considered to be suitable for heat dissipating elements. Thus the heat transfer enhancement characteristics of pool boiling of the dielectric liquid on a copper plate by placing flexible strings above the heating surface immersed in FC-72 liquid are explored in the present study.

1.2 Literature Review

In what follows the literature relevant to the present study is briefly reviewed. Pool boiling heat transfer is a process of vigorous heat transfer resulting from latent heat exchange associated with liquid-to-vapor phase change in a quiescent liquid. Nukiyama [2] conducted a pioneering pool boiling experiment in 1934 and arranged the experimental heat transfer data as a form of the wall superheat versus the heat flux, which is known as the “boiling curve” today. After that, the pool boiling heat transfer research has received considerable attention.

The state of the art cooling technologies for handling heat dissipation in microelectronic equipments have been developed extensively over the past 30 years. Several products were released including Air-Cooled Modules, High Thermal Conduction Modules, and Liquid-Cooled Modules, as discussed by Bar-Cohen [3].

In an early attempt to improve pool boiling heat transfer by using a micro-configured surface, Miller et al. [4] found that vapor retention could be a function of the scale and geometry of the micro-configurations. They pointed out that the relation between the stability

of the potential nucleation sites and the micro-configuration size and geometry required further investigation, so that the size and the site density of the cavities could be optimized for boiling heat transfer enhancement.

A few studies have been carried out to examine the influences of the surface fabricated microstructures on the pool boiling heat transfer. These include boiling of FC-72 on micro-porous surfaces with particle coating tested by Chang and You [5], adding microporous pin-fins and coating particles to the surface in the mean time investigated by Rainey and You [6] and by Rainey et al. [7], and fabricating micro-pin-fins and submicron-scale roughness on the surfaces by Honda et al. [8] and Wei et al. [9]. The study of Rainey and You [6] and Rainey et al. [7] concluded that the microporous coating can significantly enhance the boiling heat transfer performance over the pin-finned surfaces. In examining the pool boiling on the micro-pin-fin surfaces, Honda et al. [8] and Wei et al. [9] noted that the boiling curves were characterized by that a very small increase in the wall superheat can cause a large increase in the heat flux. And increasing the fin height was found to provide better heat transfer in the nucleate boiling regime and result in a higher critical heat flux. Anderson and Mudawar [10] reported that microstructures in the forms of fins, studs, grooves and vapor-trapping cavities on the boiling surface significantly shifted the boiling curve toward lower superheats while increasing the incipience excursion. Their results also suggest that the maximum boiling heat flux is a function of surface geometry and orientation but independent of the initial conditions, surface roughness, or the presence of large artificial cavities. Intending to augment boiling heat transfer, O'Connor and You [11] painted silver flakes on the boiling surface. Their experimental data show that the incipience boiling superheats are 70-85% lower and the nucleate boiling superheats are 70-80% lower than the bare surface. Besides the critical heat flux is increased by 109%. O'Connor et al. [12] then compared two methods of generating surface microstructures, "spraying" and "painting", for pool boiling heat transfer enhancement. They noted that the incipient boiling superheat has 33-55% reduction for the sprayed alumina

and 63-85% reduction for the painted diamond. The enhancement in the critical heat flux can be up to 47% for the sprayed alumina and 103% for the painted diamond microstructures. Chang and You [13] further studied the effects of coating different sizes of the diamond particles on the pool boiling performances. They classified the coating thickness into two groups. For coatings thinner than 100μm, increasing the coating thickness would generate a higher active nucleation density. But for coatings thicker than 100μm, a further increase in the coating thickness does not always enhance the pool boiling heat transfer. They attributed this result to higher impedance for liquid-vapor exchange channels and higher thermal resistance for the thicker coating. Jung and Kwak [14] investigated the effects of submicron-scale roughness on the subcooled boiling heat transfer for a boiling surface anodized in DMF (dimethylforamide) and HF (hydrofluoric acid). Both surface treatments were found to increase the effective boiling area and serve for increasing the nucleation sites and hence show considerable enhancement in the boiling heat transfer. The critical heat flux also increases linearly. Honda and Wei [15] reviewed recent advances in enhancing boiling heat transfer from electronic components immersed in dielectric liquids through the use of surface microstructures and concluded that most of the surface microstructures were effective in decreasing the wall superheat at the boiling incipience. The nucleate boiling heat transfer also can be improved and the critical heat flux is raised. Rainey and You [16] and Rainey et al. [17] respectively studied the effects of the orientation and pressure on the pool boiling heat transfer from microporous surface. Their data show that nucleate boiling performance increases slightly for the surface inclined from 0^{o}(horizontal) to 45^{o} and then decreases for the inclination angle from 90^{o} to 180^{o}. Moreover, for the plain and microporous surfaces increases in boiling performance and critical heat flux and decrease in the incipience wall superheat were noted as the pressure increased.

Chou et al. [18] arranged several grooved patterns on surfaces intending to enhance boiling heat transfer of distilled water. Their experimental data reveal that the radial grooved

pattern has the best enhanced boiling heat transfer performance and the spiral or concentric grooved pattern has poorer boiling heat transfer coefficient. The worst performance is noted for the grid or the spotted grooved pattern. All grooved patterns they investigated have better heat transfer performance than the plain surface and the denser groove is better than the sparser one for the same patterns.

Hasegawa et al. [19] covered a heat pipe with a woven screen to investigate the associated boiling characteristics and burnout phenomena. Their results disclose that the additional screen produces two opposite effects of inhibiting and enhancing the boiling heat transfer. Tsay et al. [20] explored pool boiling heat transfer enhancement by covering the boiling surface with a screen in distilled water. They found that the screen coverage could raise bubble generation frequency and enhance the boiling heat transfer. But the screen can also cover some nucleation sites and hence may retard the boiling heat transfer. They also noted that the boiling heat transfer decreased at lowering the liquid level. They concluded that covering the heated surface with a screen can augment the pool boiling heat transfer if the mesh size is comparable with the bubble departure diameter. In boiling of methanol and HFE-7100, Liu et al. [21] pointed out that placing a fine mesh layer on the boiling surface enhances nucleate boiling heat transfer at low wall superheat (ΔT<10K) but an opposite trend results at a high superheat (ΔT>10K). They also reported that the heat transfer in nucleate boiling always becomes worse with a coarse mesh on the boiling surface when compared with that on a smooth surface. Moreover, Franco et al. [22] used dielectric refrigerant R141b to investigate enhancement in the boiling heat transfer performance by covering the heated surface with wire meshes. The boiling heat transfer coefficient was noted to increase significantly, especially at relatively low heat fluxes. They also found that the wire mesh coverage on the heating surface results in slower transition to steady film boiling. In studying the effects of the wall superheat and the mesh layer covering on boiling heat transfer, Kurihara and Myers [23] tested several working fluids including water, acetone, n-hexane, carbon

tetrachloride, and carbon disulfide. They found that active nucleation sites on the heating plate increased due to the mesh covering and the boiling heat transfer coefficient was proportional to the one-third power of the bubble column numbers at high numbers.

1.3 Objective of Present Study

The above literature review clearly reveals that considerable works have been carried out in the past to investigate the enhancement in the pool boiling heat transfer over a surface by using the surface microstructures such as roughness, micro-pin-fins, mesh screens, and particle coating. All these microstructures are fixed firmly onto the boiling surface. In this study, an experimental study is conducted to explore the possible enhancement in the FC-72 pool boiling heat transfer by placing flexible and movable fine wires above the boiling surface. The wires are loosely fixed at their two ends on the surface and hence are allowed to move adjacent to the heating surface during the boiling processes to some degree. This movement of the wires adjacent to the boiling surface is expected to greatly affect the bubble dynamics near the surface and hence the boiling heat transfer from the surface. Besides, in the present study we will also examine the associated bubble behavior in the boiling flow by visualizing the flow. Both the possible saturated and subcooled pool boiling heat transfer enhancement will be examined.

CHAPTER 2

EXPERIMENTAL APPARATUS AND PROCEDURES

A schematic arrangement of the experimental apparatus for the present investigation of the pool boiling heat transfer enhancement by flexible strings is shown in Fig. 2.1. The experimental system includes a main test chamber, a test heater assembly, and other auxiliary parts such as a D.C. power supply, a data acquisition unit and a high-speed photographic unit. The working fluid, FC-72, is a highly wetting dielectric fluorocarbon liquid produced by 3M Industrial Chemical Products Division, which has been considered as a good candidate fluid for liquid immersion cooling applications. It is chemically stable, dielectric, and has a relatively low boiling point (T_{sat}=56°C at atmospheric pressure). Some thermophysical properties of FC-72 are given in Table 2.1.

2.1 Main Test Chamber

The main test chamber is a hermetic stainless steel pressure vessel of 205mm in height and 216mm in diameter. An internal water condenser is installed inside the chamber and connects with a thermostat (LAUDA RK20) to maintain the bulk temperature of the working fluid in the chamber at the preset level. The maximum cooling power of the thermostat is 200W (at 20°C). We further use an external temperature controller (FENWAL MYSPEC Digital Temperature Controller) to control the bulk temperature of FC-72 in the test chamber with an accuracy of ±0.1°C. Besides, a cartridge heater is located near the bottom of the test chamber to provide additional heating during the degassing process. In order to prevent the heat loss from the vessel to the ambient, a superlon layer of 10-mm thick is wrapped

around the chamber. Moreover, a pressure transducer with an operating range of 0-980kPa is located at the gate valve to measure the pressure of the work fluid. Meanwhile, the working fluid temperature is measured by two resistance temperature detectors (RTDs) located at the gate valve and at a selected location 5cm above the bottom surface of the chamber with a calibrated accuracy of $\pm 0.1°C$. An auxiliary tank of 10-liter liquid FC-72 is placed right above the test vessel and it is only used for subcooled pool boiling experiment to prevent regassing of the working fluid after degassing. A pressure transducer and a RTD are placed in the auxiliary tank to measure the internal gas pressure and liquid temperature. In addition, a test heater assembly is mounted to a stainless steel shelf to fix the Teflon substrate. The working fluid is maintained at approximately 80mm above the heated surface in the experiment.

2.2 Test Heater Assembly

A schematic of the test heater assembly is shown in Fig. 2.2. The assembly consists mainly of a film heater and is adhered to a square copper block with epoxy Omegabond 200 . The heater supplies the required power input to the copper block. The copper block is flush mounted onto a much larger Teflon block. Liquid FC-72 boils on the upper surface of the copper block and its side is 10-mm long. More specifically, the copper block is heated by the D.C. current delivered from the film heater adhering to the lower surface of the copper block. Besides, three calibrated copper-constantan thermocouples (T-type) with a calibrated accuracy of $\pm 0.2°C$ are installed at selected locations in the copper block right below the boiling surface. They are used for the control and determination of the boiling surface temperature. The detailed locations of the thermocouples are shown in Fig. 2.3. Note that the whole

copper block is inserted into a Teflon block which serves as a heat insulator ($k_T \approx 0.35\text{W/m}\cdot\text{K}$) intending to reduce the heat loss from the lateral and bottom surfaces of the block to the ambient.

2.3 Installation of Strings on Boiling Surface

The strings are fixed on the upper surface of the copper block by paste at their ends, as schematically shown in Fig. 2.4. The nylon threads are chosen in the present experiment because of its good flexibility. Specifically, each the nylon thread has the same mean diameter. The nylon strings are installed uniformly at the same pitch and height above the heating surface. Besides, the vertical distance between the strings and boiling surface will be varied in the test to investigate its effects on the pool boiling heat transfer. Moreover, the looseness of the strings measured by their length relative to the length of the boiling surface on the boiling heat transfer will be investigated. The measured data apparently will be compared with that of a bare heating surface (without the presence of the strings).

2.4 DC Power Supply

The power generated in the film heater in the test heater assembly is provided by a programmable D.C. power supply (Chroma 6203-15). It offers a maximum D.C. power of 300W for an output voltage of 15V and an output current of 20A. The power input to the copper block is transmitted through a GPIB interface to a personal computer. In order to measure the D.C. current, a precision ammeter (KYORITSU A.C./D.C. DIGITAL CLAMP METER) is arranged in series connection with the electric circuit. Besides, a YOKOGAWA data recorder is used to measure the voltage drop across the test heater assembly. All the voltage, current and power measurement

devices are calibrated by a YOKOGAWA WT200 power meter according to the Center of Measurement Standards in Industrial Technology Research Institute of Taiwan.

2.5 Data Acquisition

A 30-channel YOKOGAWA data recorder (MX-100) combined with a personal computer is used to acquire and process the data from various transducers. All signals detected from the T-type thermocouples, RTDs, pressure transducer, ammeter, data recorders and power meter are all collected and converted by the internal calibration equations in the computer during the data acquisition.

2.6 Experimental Procedures

Prior to putting all the devices and components for the experimental system together, the boiling surface is polished by fine sand paper (Number 3000) and cleaned by alcohol. In each test, we need to remove the non-condensable gases in the empty test chamber by running a vacuum pump for about 15 minutes and then fill the FC-72 liquid into the test chamber. Next, the FC-72 liquid in the test chamber is heated to the saturation state by employing a digital temperature controller and cartridge heater. Moreover, the FC-72 liquid is boiled vigorously for 2 hours to remove the dissolved noncondensible gases in it. After the working fluid pressure and temperature stabilize to one atmosphere and at the saturation state, we turn on the test heater. The imposed heat flux on the boiling surface is adjusted by controlling the electric current delivered to the heater from the D.C. power supply. Upon reaching the statistical state, we begin collecting the required heat transfer data and visualizing the boiling activity.

Table 2.1 Thermophysical properties of FC-72.

Properties at 25°C	**FC-72**
Appearance	Clear, colorless
Average Molecular Weight	338
Boiling Point (1atm)	56°C
Pour Point (1atm)	-90°C
Estimated Critical Temperature	449K
Estimated Critical Pressure	1.83×10^{6} Pa
Vapor Pressure	3.09×10^{4} Pa
Latent Heat of Vaporization h_{fg} (at normal boiling point)	88 J/g
Liquid Density ρ_l	1680 kg/m^3
Absolute Viscosity μ	6.4×10^{-3} poises ; 6.4×10^{-4} kg/m·s
Kinematic Viscosity ν	3.8×10^{-3} stokes ; 3.8×10^{-7} m^2/ s
Liquid Specific Heat c_p	1100 J/kg·°C
Liquid Thermal Conductivity k	0.057 W/m·°C
Coefficient of Expansion β	0.00156 /°C
Surface Tension σ	10 dynes/cm ; 10^{-2} N/m

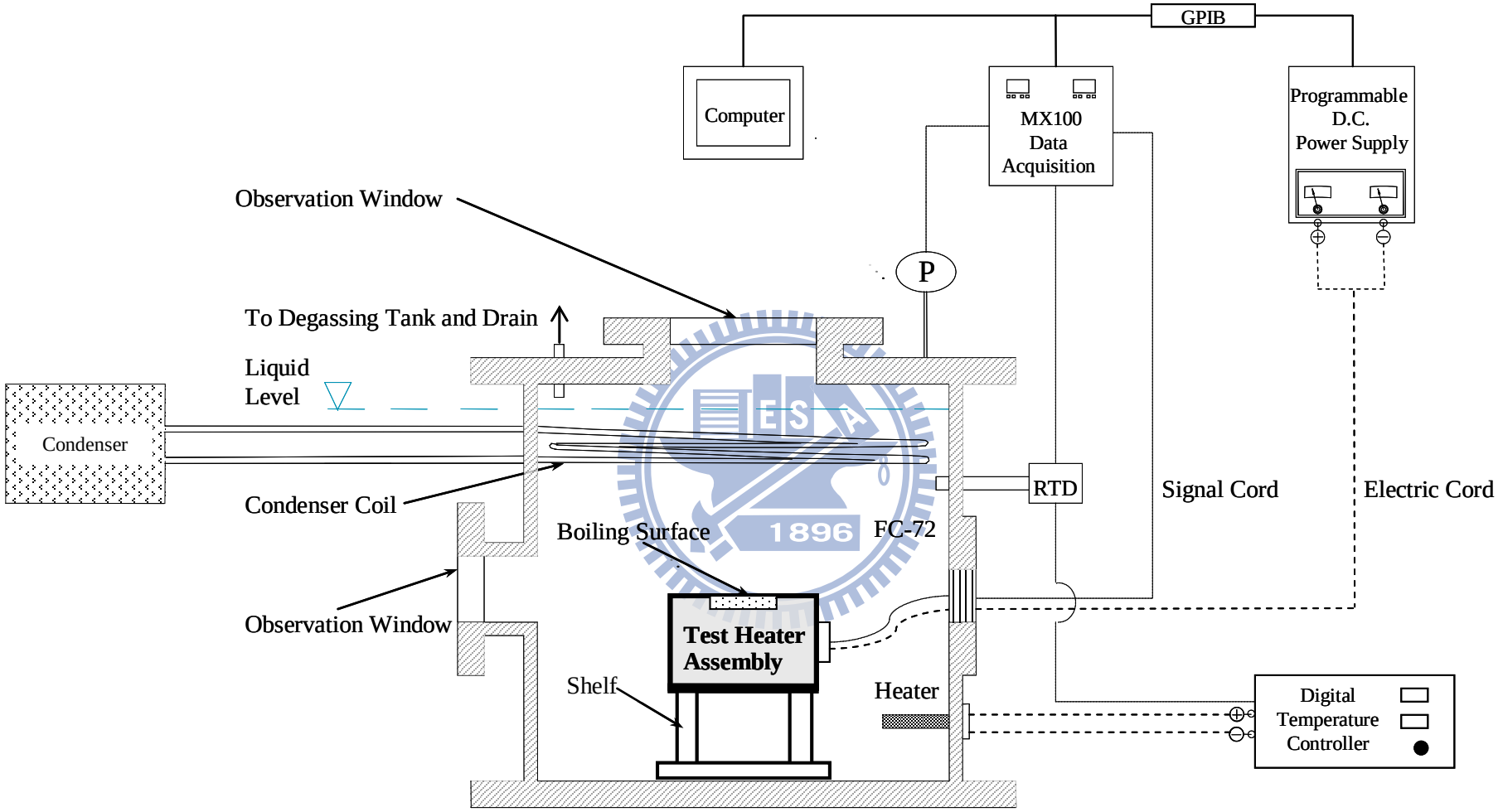

Fig. 2.1 Schematic diagram of the test apparatus.

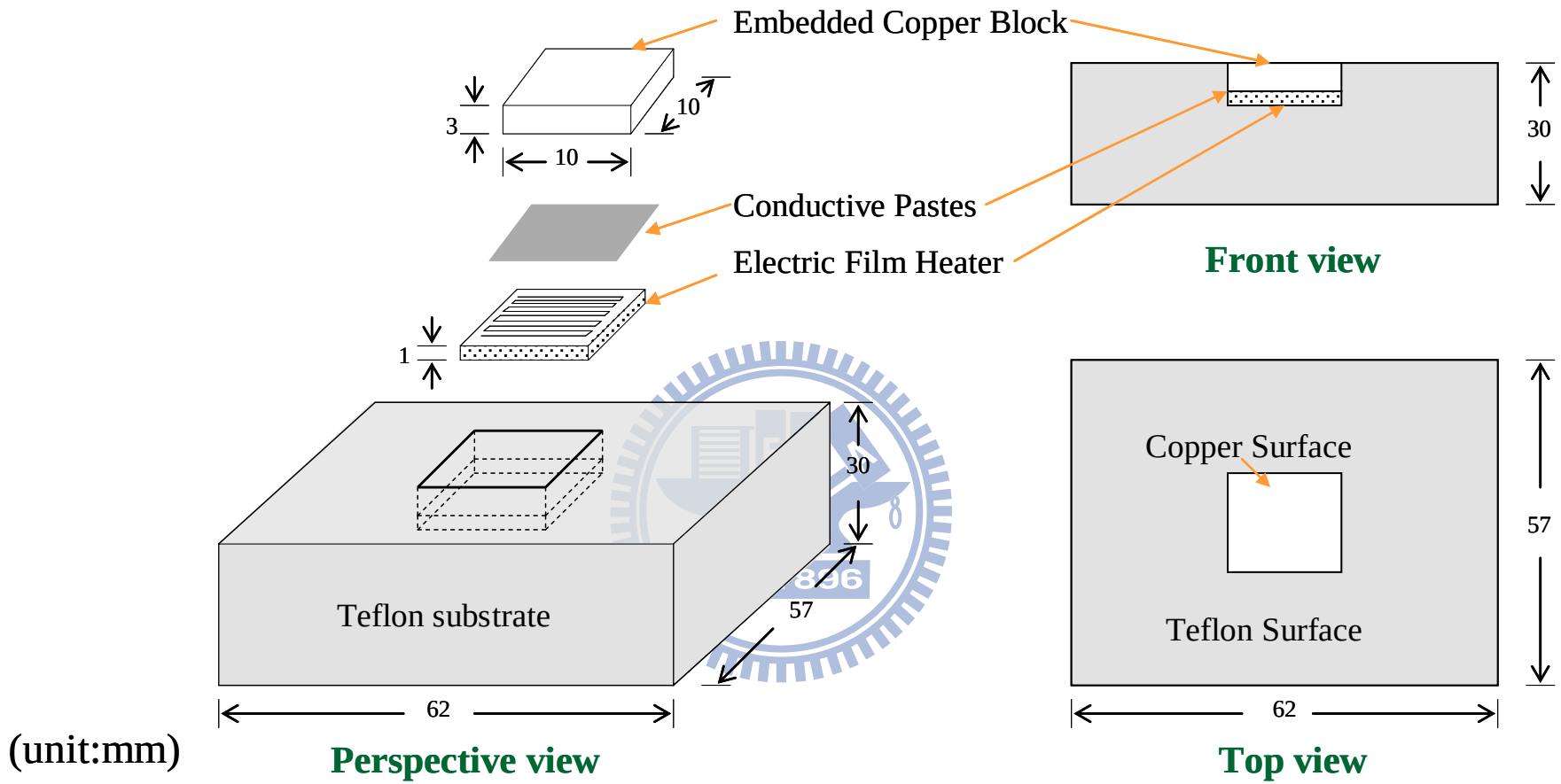

Fig. 2.2 Schematic diagram of the test heater assembly (not to scale).

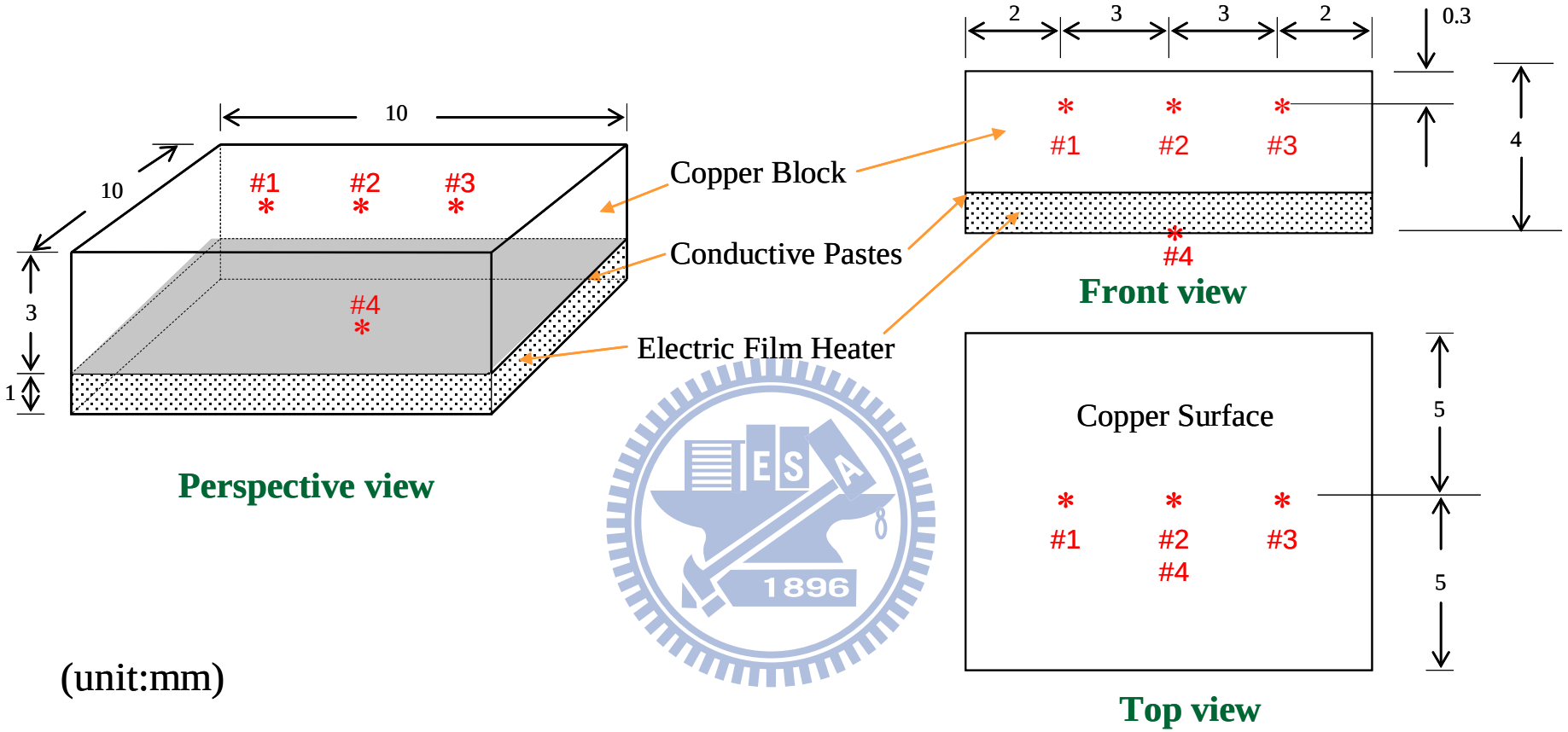

Fig. 2.3 Locations of three thermocouples in the copper block and one thermocouple below the heater (not to scale).

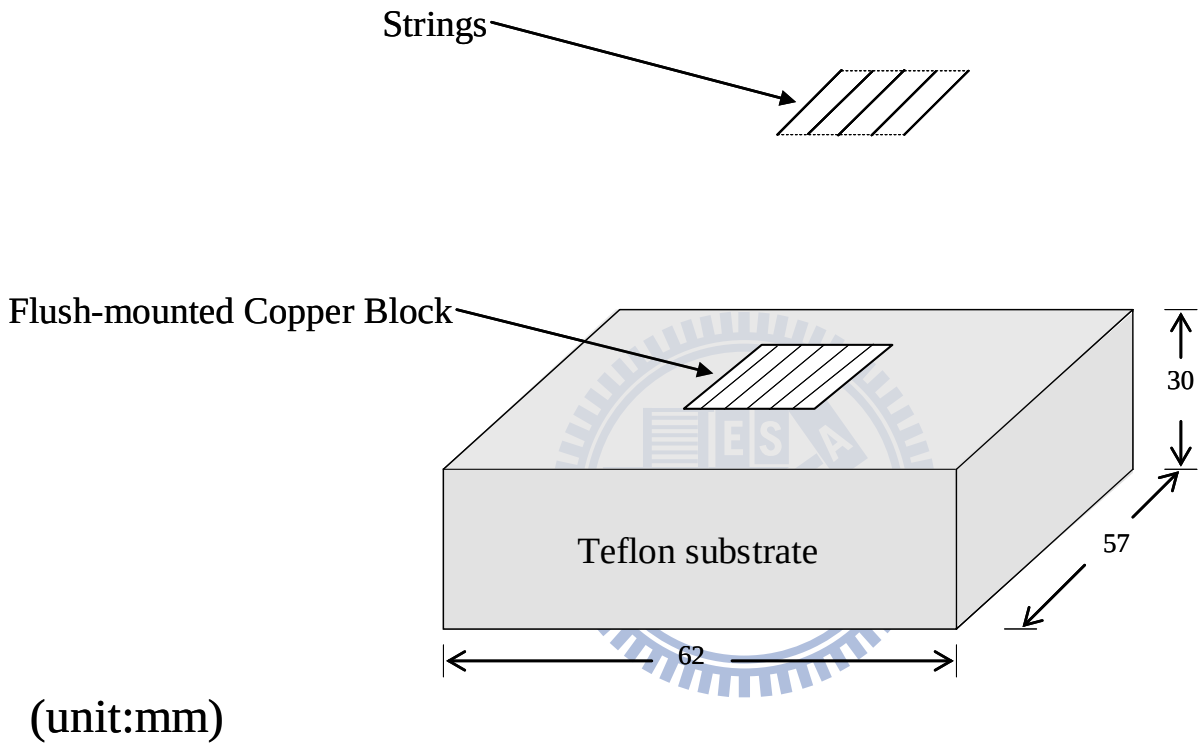

Fig. 2.4 Schematic diagram of placing strings on heating surface (not to scale).

CHAPTER 3

DATA REDUCTION

3.1 Boiling Heat Transfer Coefficient

The space-average boiling heat transfer coefficient over the upper surface of the heated square copper block at long time when the flow is at a statistical state is defined as

$$h = q_n / \Delta T_{sat} \tag{3.1}$$

where q_n is the net heat flux imposed on the upper surface and ΔT_{sat} is the wall superheat defined as the difference between the average surface temperature and the saturated temperature of FC-72. The average heated surface temperature is estimated from the measured average temperature from the thermocouples installed at locations near the upper surface of the copper block according to the steady-state one-dimensional conduction heat transfer. Specifically,

$$T_w = T_{Cu} - \left(q_n \times \frac{\delta}{k_{Cu}} \right) \tag{3.2}$$

where

T_{Cu} = the average measured temperature from the thermocouples (°C)

k_{Cu} = the thermal conductivity of copper (W/m·K)

δ = the vertical distance between the thermocouple tips and the upper surface of the copper block (m)

The total power input Q_t to the copper block can be obtained from the voltage drop across the film heater in the test heater assembly and the current passing through it,

$$Q_t = I \cdot V \tag{3.3}$$

where

Q_t = total power input to the upper surface of the copper block (W)

I = electric current passing through the film heater (Amp.)

V = voltage drop across the film heater (Volts)

In fact, the Teflon insulator cannot completely prevent the heat loss from the surfaces of the copper block. Heat loss across the insulator does exist, mainly from the lateral sides of the copper block and heater and from the bottom of the heater. The heat loss is estimated by one-dimensional heat conduction in the Teflon insulator and convection from the insulator surface to the ambient based on a model schematically shown in Fig. 3.1. Thus, we have

$$Q_{loss} = \frac{(T_5 - T_{sur})A_{T,5}}{\frac{L_5}{k_T} + \frac{1}{h_5}} + 2 \cdot \frac{(T_6 - T_{sur})A_{T,6}}{\frac{L_6}{k_T} + \frac{1}{h_6}} + 2 \cdot \frac{(T_7 - T_{sur})A_{T,7}}{\frac{L_7}{k_T} + \frac{1}{h_7}} \tag{3.4}$$

where

T_{sur} : the ambient temperature (°C)

T_5 , T_6 , T_7 : the average measured temperatures at the measured locations inside the Teflon insulator, as schematically shown in Fig. 3.1

k_T : thermal conductivity of the Teflon insulator (W/m·K)

L_5 , L_6 , L_7 : shortest distances between locations #5, #6, #7 and the insulator surfaces (m)

$A_{T,5}$, $A_{T,6}$, $A_{T,7}$: bottom and lateral surface areas of the Teflon block

$$A_{T,5} = \frac{62 \times 57}{2}\,\text{mm}^2,\ A_{T,6} = \frac{30 \times 57}{2}\,\text{mm}^2,\ A_{T,7} = \frac{30 \times 62}{2}\,\text{mm}^2$$

h_i : estimated natural convection heat transfer coefficient from the Teflon block surfaces to the surroundings by correlations from Incropera et al. [24]. (W/m^2·K)

h_5: estimated from $\mathrm{Nu_L} = 0.27\mathrm{Ra_L}^{1/4}$ for the bottom surface of the Teflon block.

h_6 , h_7: estimated from $\mathrm{Nu_L} = 0.68 + \dfrac{0.670\mathrm{Ra_L}^{1/4}}{\left[1+(0.492/\mathrm{Pr})^{9/16}\right]^{4/9}}$ for the lateral surfaces of the Teflon Block.

Finally, the net imposed input heat flux to the upper surface of copper square can be evaluated from the relation

$$q_n = \frac{Q_t - Q_{loss}}{A_{Cu}} \tag{3.5}$$

where A_{Cu} is the area of the upper surface of the copper block.

3.2 Uncertainty Analysis

An uncertainty analysis is carried out here to estimate the uncertainty levels in the experiment. Kline and McClintock [25] proposed a formula for evaluating the uncertainty in the result F as a function of independent variables, X_1, X_2, X_3……X_n,

$$F=F\,(X_1\,,X_2,\,X_3\cdots\cdots\cdots X_n) \tag{3.6}$$

The absolute uncertainty of F is expressed as

$$\delta F = \left\{\left[\left(\frac{\partial F}{\partial X_1}\right)\delta X_1\right]^2 + \left[\left(\frac{\partial F}{\partial X_2}\right)\delta X_2\right]^2 + \left[\left(\frac{\partial F}{\partial X_3}\right)\delta X_3\right]^2 + \cdots + \left[\left(\frac{\partial F}{\partial X_n}\right)\delta X_n\right]^2\right\}^{\frac{1}{2}} \tag{3.7}$$

and the relative uncertainty of F is

$$\frac{\delta F}{F} = \left\{\left[\left(\frac{\partial \ell nF}{\partial \ell nX_1}\right)\left(\frac{\delta X_1}{X_1}\right)\right]^2 + \left[\left(\frac{\partial \ell nF}{\partial \ell nX_2}\right)\left(\frac{\delta X_2}{X_2}\right)\right]^2 + \left[\left(\frac{\partial \ell nF}{\partial \ell nX_3}\right)\left(\frac{\delta X_3}{X_3}\right)\right]^2 + \cdots + \left[\left(\frac{\partial \ell nF}{\partial \ell nX_n}\right)\left(\frac{\delta X_n}{X_n}\right)\right]^2\right\}^{\frac{1}{2}} \tag{3.8}$$

If $F = X_1^a X_2^b X_3^c \ldots\ldots$, then the relative uncertainty is

$$\frac{\delta F}{F} = \left\{ \left[a\left(\frac{\delta X_1}{X_1}\right) \right]^2 + \left[b\left(\frac{\delta X_2}{X_2}\right) \right]^2 + \left[c\left(\frac{\delta X_3}{X_3}\right) \right]^2 + \cdots\cdots \right\}^{\frac{1}{2}} \tag{3.9}$$

where $\frac{\partial F}{\partial X_i}$ and ∂X_i are, respectively, the sensitivity coefficient and uncertainty level associated with the variable X_i. The values of the uncertainty intervals ∂X_i are obtained by a root-mean-square combination of the precision uncertainty of the instruments and the unsteadiness uncertainty, as recommended by Moffat [26]. The choice of the variable X_i to be included in the calculation of the total uncertainty level of the result F depends on the purpose of the analysis.

The uncertainties of the parameters in the present study are calculated as follows:

(1) Uncertainty of temperature difference, $\Delta T_{sat}=T_w-T_{sat}$

$$\frac{\delta(T_w - T_{sat})}{(T_w - T_{sat})} = \left\{ \left[\left(\frac{\partial \ell n(T_w - T_{sat})}{\partial \ell n T_w} \right)\left(\frac{\delta T_w}{T_w} \right) \right]^2 + \left[\left(\frac{\partial \ell n(T_w - T_{sat})}{\partial \ell n T_{sat}} \right)\left(\frac{\delta T_{sat}}{T_{sat}} \right) \right]^2 \right\}^{\frac{1}{2}}$$

$$= \left\{ \left[\left(\frac{T_w}{T_w - T_{sat}} \right)\left(\frac{\delta T_w}{T_w} \right) \right]^2 + \left[\left(\frac{T_{sat}}{T_w - T_{sat}} \right)\left(\frac{\delta T_{sat}}{T_{sat}} \right) \right]^2 \right\}^{\frac{1}{2}}$$

$$= \left\{ \left[\frac{\delta T_w}{T_w - T_{sat}} \right]^2 + \left[\frac{\delta T_{sat}}{T_w - T_{sat}} \right]^2 \right\}^{\frac{1}{2}}$$

(3.10)

(2) Uncertainty of total power input, Q_t

$$Q_t = I \cdot V \tag{3.3}$$

and $$\frac{\delta Q_t}{Q_t} = \left[\left(\frac{\delta I}{I} \right)^2 + \left(\frac{\delta V}{V} \right)^2 \right]^{\frac{1}{2}} \tag{3.11}$$

(3) Uncertainty of net wall heat flux, q_e

$$q_n = \frac{Q_t - Q_{loss}}{A_{Cu}} \tag{3.5}$$

and

$$\frac{\delta q_n}{q_n} = \left\{ \left[\left(\frac{\partial \ell n q_n}{\partial \ell n A_{Cu}} \right) \left(\frac{\delta A_{Cu}}{A_{Cu}} \right) \right]^2 + \left[\left(\frac{\partial \ell n q_n}{\partial \ell n Q_t} \right) \left(\frac{\delta Q_t}{Q_t} \right) \right]^2 + \left[\left(\frac{\partial \ell n q_n}{\partial \ell n Q_{loss}} \right) \left(\frac{\delta Q_{loss}}{Q_{loss}} \right) \right]^2 \right\}^{\frac{1}{2}}$$

$$= \left\{ \left[1 \cdot \left(\frac{\delta A_{Cu}}{A_{Cu}} \right) \right]^2 + \left[\left(\frac{Q_t}{Q_t - Q_{loss}} \right) \left(\frac{\delta Q_t}{Q_t} \right) \right]^2 + \left[\left(\frac{Q_{loss}}{Q_t - Q_{loss}} \right) \left(\frac{\delta Q_{loss}}{Q_{loss}} \right) \right]^2 \right\}^{\frac{1}{2}}$$

$$= \left\{ \left[\frac{\delta A_{Cu}}{A_{Cu}} \right]^2 + \left[\frac{\delta Q_t}{Q_t - Q_{loss}} \right]^2 + \left[\frac{\delta Q_{loss}}{Q_t - Q_{loss}} \right]^2 \right\}^{\frac{1}{2}} \tag{3.12}$$

where $$Q_{loss} = \frac{(T_5 - T_{sur})A_{T,5}}{\frac{L_5}{k_T} + \frac{1}{h_5}} + 2 \cdot \frac{(T_6 - T_{sur})A_{T,6}}{\frac{L_6}{k_T} + \frac{1}{h_6}} + 2 \cdot \frac{(T_7 - T_{sur})A_{T,7}}{\frac{L_7}{k_T} + \frac{1}{h_7}} \tag{3.4}$$

(4) Uncertainty of space-average heat transfer coefficient, h

$$h = q_n / \Delta T_{sat} \tag{3.1}$$

and

$$\frac{\delta h}{h} = \left\{ \left[\left(\frac{\partial \ell n h}{\partial \ell n q_n} \right) \left(\frac{\delta q_n}{q_n} \right) \right]^2 + \left[\left(\frac{\partial \ell n h}{\partial \ell n (T_w - T_{sat})} \right) \left(\frac{\delta (T_w - T_{sat})}{T_w - T_{sat}} \right) \right]^2 \right\}^{\frac{1}{2}}$$

$$= \left\{ \left[1 \cdot \left(\frac{\delta q_n}{q_n} \right) \right]^2 + \left[1 \cdot \left(\frac{\delta T_w - T_{sat}}{T_w - T_{sat}} \right) \right]^2 \right\}^{\frac{1}{2}}$$

$$= \left\{ \left[\frac{\delta q_n}{q_n} \right]^2 + \left[\frac{\delta T_w - T_{sat}}{T_w - T_{sat}} \right]^2 \right\}^{\frac{1}{2}}$$

(3.13)

A summary of the results from the present uncertaintly analysis is given in Table 3.1.

Table 3.1 Summary of the results from the uncertainty analysis.

Parameter	**Uncertainty**
Geometry	
Length & thickness (%)	± 0.5%
Area (%)	± 1.0%
Parameter measurement	
Temperature, T (°C)	± 0.2
Temperature difference (°C)	± 0.4
System pressure, P (kPa)	± 0.5
Boiling heat transfer on the copper flat plate	
Power input, Q_t (%)	± 8.2%
Imposed effective heat flux, q_n (%)	± 14.8%
Heat transfer coefficient, h (%)	± 13.4%

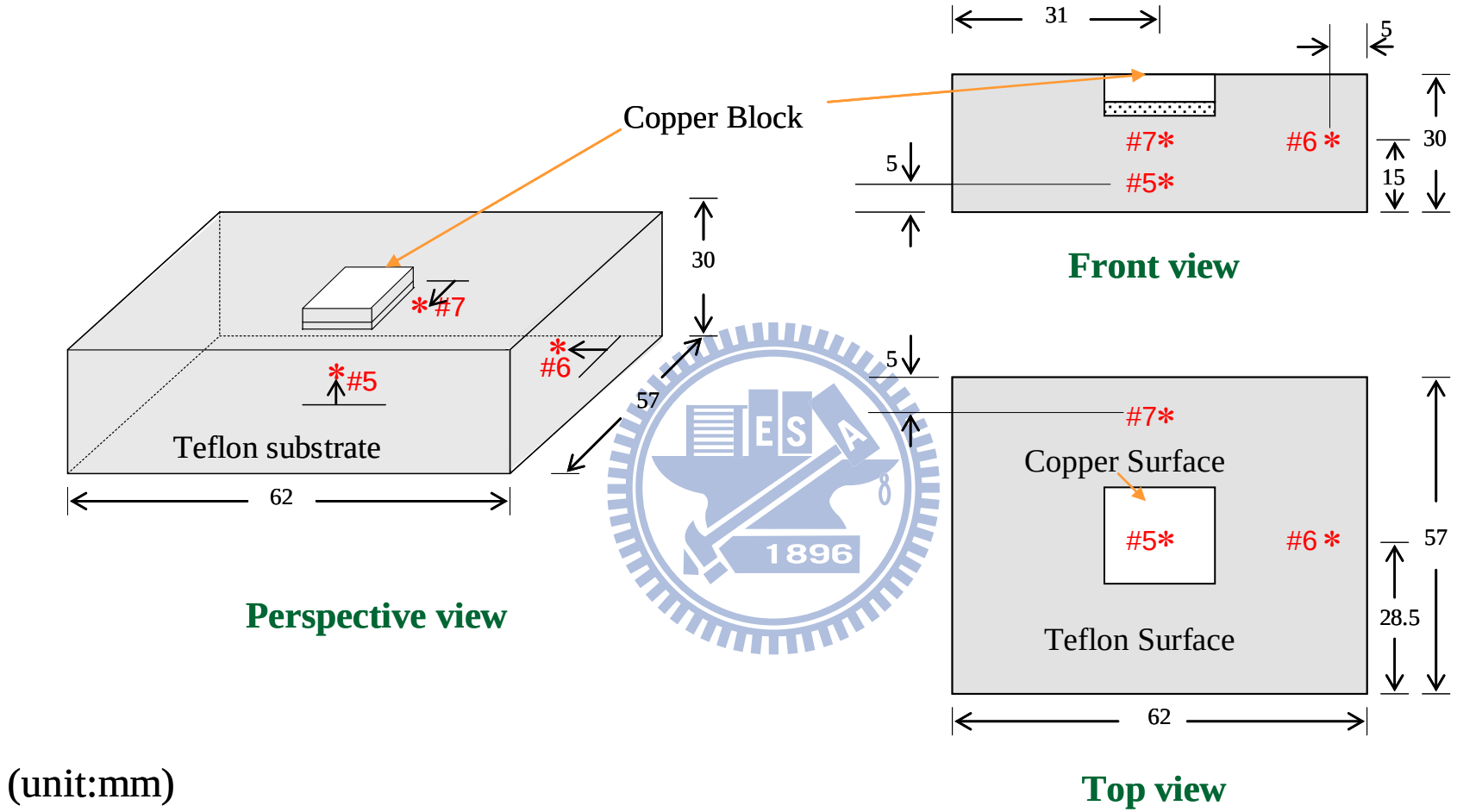

Fig. 3.1 Locations of three thermocouples in the Teflon substrate in order to estimate heat loss (not to scale).

CHAPTER 4

SATURATED POOL BOILING HEAT TRANSFER ENHANCEMENT OF FC-72 OVER A SMALL HEATED HORIZONTAL COPPER SURFACE

The experimental results for the possible enhancement of saturated pool boiling heat transfer of FC-72 by placing flexible strings above the heating surface measured in the present study are examined in this chapter. The present experiments are carried out for the diameter of the nylon strings varied from 74 to 259 μm, the height of the strings from 0 to 2 mm, and the length of the strings from 10 to 12 mm for the pitch of the strings mainly fixed at 2.0 mm with the FC-72 liquid in the test chamber maintained at saturated liquid state corresponding to the atmospheric pressure. The measured data are presented in terms of the boiling curves and boiling heat transfer coefficients for various diameters, heights, length of the flexible strings and for a bare heating surface. Effects of the experimental parameters on the possible boiling heat transfer enhancement will be examined in detail. Selected results are presented in the following to illustrate the possible pool boiling heat transfer enhancement by the flexible strings.

4.1 Single-phase Natural Convection Heat Transfer

Before conducting the pool boiling experiment, we first measure steady natural convection heat transfer over the heated small copper surface without the installation of the strings which prevails at low imposed heat flux, intending to verify the present experimental setup. The measured data for the natural convection heat transfer coefficient are compared with the empirical correlation of Radziemska and Lewandowski [27] in Fig. 4.1. Their correlation is

$$Nu_L=(2.1e^{-48W}+1.2)Ra_L^{0.2} \quad (4.1)$$

where w is the width of the heating plate (m). The correlation given in Eq.(4.1) is based on the data for a small horizontal plate heated from below for $10^5<Ra_L<10^8$. Note that the characteristic length L used in defining the dimensionless groups in the above equation is chosen to be the ratio of the heated surface area and its perimeter, and the Nusselt and Rayleigh numbers are respectively defined as

$$Nu_L = \frac{hL}{k_\ell} \tag{4.2}$$

and

$$Ra_L = \frac{g\beta(\Delta T_{sat})L^3}{\alpha\nu} \tag{4.3}$$

The results in Fig. 4.1 indicate that our natural convection data are in good agreement with that calculated from Eq. (4.1). Thus the experimental system established here is considered to be suitable for the present study.

4.2 Saturated Pool Boiling on Bare Copper Surface

To further verify the suitability of the present experimental facility, the boiling curve for saturated pool boiling of FC-72 on a bare heated copper surface is also obtained. These data are compared with those from Chang and You [28] for pool boiling of FC-72 on a small square copper plate of $1cm^2$ in surface area in Fig. 4.2. The results indicate that the present data are in qualitative agreement with those of Chang and You [28] before and after the onset nucleate boiling.

4.3 Effects of String Diameter on Boiling Heat Transfer Enhancement

Attention is then turned to examining how the diameter of the flexible strings affects the boiling heat transfer of FC-72 on the heated plate. This is illustrated in Figs. 4.3-4.11 by showing the boiling curves and the variations of the boiling heat transfer coefficients with the wall superheat for various string diameters at different string heights and lengths. The results for the boiling curves clearly indicate that the presence of the flexible strings significantly reduces the temperature overshoot at the

onset of boiling and hence the boiling hysteresis. Besides, the inception of the boiling takes place at a much lower wall superheat with the strings installed. It is also noted that at the same wall superheat ΔT_{sat} the boiling heat transfer coefficients are substantially higher for the surface covered by the strings for certain d_w, ℓ_w and h_w when compared with that for the bare heated surface, as clearly seen by checking with the data for the variations of the heat transfer coefficient with ΔT_{sat}. These data show that an increase in the boiling heat transfer coefficient of more than 100% over that for a bare heated surface by placing the flexible strings on the heating surface can be obtained. Note that at a small ΔT_{sat} the boiling heat transfer coefficient is already relatively high for the plate covered with the strings but the flow over the bare surface is still in single-phase state. Moreover, the extent of the boiling heat transfer enhancement varies nonmonotonically with size, looseness and height of the strings. This is attributed to the complex effects of these parameters on the bubble dynamics in the boiling flow. A close inspection of these data reveals that when the strings directly contact the heating surface (h_w=0 mm) and the strings are tightly fixed at their ends (ℓ_w=10 mm), placing the strings with the largest diameter of 259 μm results in the highest heat transfer enhancement (Fig. 4.3). While for the strings with d_w=74 μm & 158 μm the enhancements are somewhat smaller and nearly the same. Note that for the strings being slightly loose at ℓ_w=11 mm the heat transfer enhancement for the three different string size do not differ significantly with each other, as evident from the data given in Fig. 4.4. The boiling heat transfer coefficient is enhanced by about 60 to 80%. But for the strings loosened substantially at ℓ_w = 12 mm the data in Fig.4.5 show that the boiling heat transfer is noticeably better for the smaller strings. At d_w=74 μm a boiling heat transfer coefficient enhancement of more than 100% can be procured.

Now when the strings are installed at a slightly higher position with h_w=1 mm the effects of the string diameter on the boiling heat transfer enhancement shown in

Figs. 4.6-4.8 are relatively different. For the tight strings with ℓ_w=10 mm the boiling heat transfer enhancement does not change significantly with the string size (Fig. 4.6). The heat transfer enhancement is larger for smaller-diameter strings when ℓ_w is slightly increased to 11 mm (Fig. 4.7). While for ℓ_w is increased further to 12 mm it is of interest to note that the enhancement is largest for the mid-size strings with d_w=158 μm and smallest for the large strings (Fig. 4.8).

For the string height increased further to 2 mm the situation again is somewhat different. At ℓ_w=10 mm the string diameter exhibits a much smaller influence on the boiling heat enhancement and the enhancement is all less than 50% (Fig. 4.9). But for the strings being loosened slightly at ℓ_w=11 & 12 mm the smallest string with d_w=74 μm clearly gives the largest enhancement (Figs. 4.10 & 4.11). And, the enhancement is more significant for ℓ_w=11 mm .

4.4 Effects of String Height on Boiling Heat Transfer Enhancement

Next, how the boiling heat transfer is affected by the string height is illustrated in Figs. 4.12-4.20. These results indicate that for the small-diameter strings with d_w=74 μm and tightly fixed at ℓ_w=10 mm the heat transfer enhancement is largest for the strings directly contacting the heating surface, as seen in Fig. 4.12. Then, for the strings fixed slightly loosely at ℓ_w=11 mm the strings placed slightly away from the heating surface with h_w=1 mm give the best boiling heat transfer performance (Fig. 4.13). But for the strings fixed loosely at ℓ_w=12 mm, the case with the strings directly contacting the heating surface (h_w=0 mm) gives the substantially higher boiling heat transfer enhancement (Fig. 4.14). For the mid-size strings at d_w=158 μm the enhancement is most prominent at h_w=0 mm for the strings tightly fixed at ℓ_w=10 mm, as noted from the data given in Fig. 4.15. But for ℓ_w=11 mm the enhancement is largest at h_w=1 mm and lowest at h_w=2 mm (Fig. 4.16). While for the strings loosely fixed at ℓ_w=12 mm the enhancement is rather large and

comparable for h_w=0 & 1 mm (Fig. 4.17). Note that the heat transfer enhancement nearly vanishes when the strings are far away from the heating surface at h_w=2 mm. The data in Figs. 4.18-4.20 for the large-diameter strings at d_w=259 μm indicate that the enhancement is significant for the strings directly contacting the heating surface (h_w=0 mm) and tightly fixed (ℓ_w=10 mm). For the strings loosely fixed at ℓ_w=12 mm only small heat transfer enhancement can be obtained by placing strings of large size (Fig. 4.20).

4.5 Effects of String Length on Boiling Heat Transfer Enhancement

Then, the effects of the string length on the boiling heat transfer are shown in Figs. 4.21-4.29. The results in Figs 4.21-4.23 for the small-diameter strings at d_w=74 μm indicate that for the strings directly contacting the heating surface h_w=0mm the longest strings with ℓ_w=12 mm have a substantially larger boiling heat transfer enhancement (Fig. 4.21). However, for the strings fixed away from the heating surface at h_w=1 & 2 mm the slightly shorter strings of ℓ_w=11 mm give the best heat transfer performance (Figs. 4.22 & 4.23). For the mid-size strings (d_w=158 μm) the boiling heat transfer enhancement is largest for the longest strings (ℓ_w=12 mm) at h_w=0 mm (Fig. 4.24). But at h_w=1 mm the boiling heat transfer enhancement are rather close for ℓ_w=11 mm and ℓ_w=12 mm (Fig. 4.25). While for the strings fixed at a higher position with h_w=2 mm the slightly loosened strings with ℓ_w=11 mm show the best performance (Fig. 4.26). Now for the large-diameter strings with d_w=259 μm the enhancement is better for the shorter strings when they contact the boiling surface at h_w=0 mm, as evident from data given in Fig. 4.27. But at h_w=1 & 2mm the slightly loosely fixed strings at ℓ_w=11 mm show the best heat transfer performance (Figs. 4.28 & 4.29).

4.6 Effects of String Pitch on Boiling Heat Transfer Enhancement

Finally, we examine the effects of the string pitch on the boiling heat transfer in Figs. 4.30-4.35. The results in Figs 4.30-4.32 for the small-diameter strings at d_w=74 μm and h_w=1 mm indicate that an reduction of the string pitch from 2 mm to 1 mm can enhance the boiling heat transfer to a larger degree by increase the string looseness. But for the mid-size strings (d_w=158 μm) the reduction in the string pitch only slightly affects the boiling heat transfer, as evident from the data shown in Figs 4.33-4.35.

4.7 Concluding Remarks

In this chapter how the installation of the flexible nylon strings on the saturated pool boiling heat transfer of FC-72 over a small heated horizontal square plate have been investigated. The effects of the string diameter, length and height on the boiling heat transfer enhancement have been examined in detail. The major results from this investigation can be summarized at follows.

(1) The extent of the boiling heat transfer enhancement by the flexible strings depends strongly on all experimental parameters, namely, the string diameter, length and height.

(2) A boiling heat transfer coefficient enhancement of more than 100% over that for a bare heated plate can be obtained by a suitable choice of the experimental parameters.

(3) The bubble dynamics near the heated surface is conjectured to be affected substantially by the string size, looseness and position. But the details on how these parameters affect the near-wall bubbles requires further investigation.

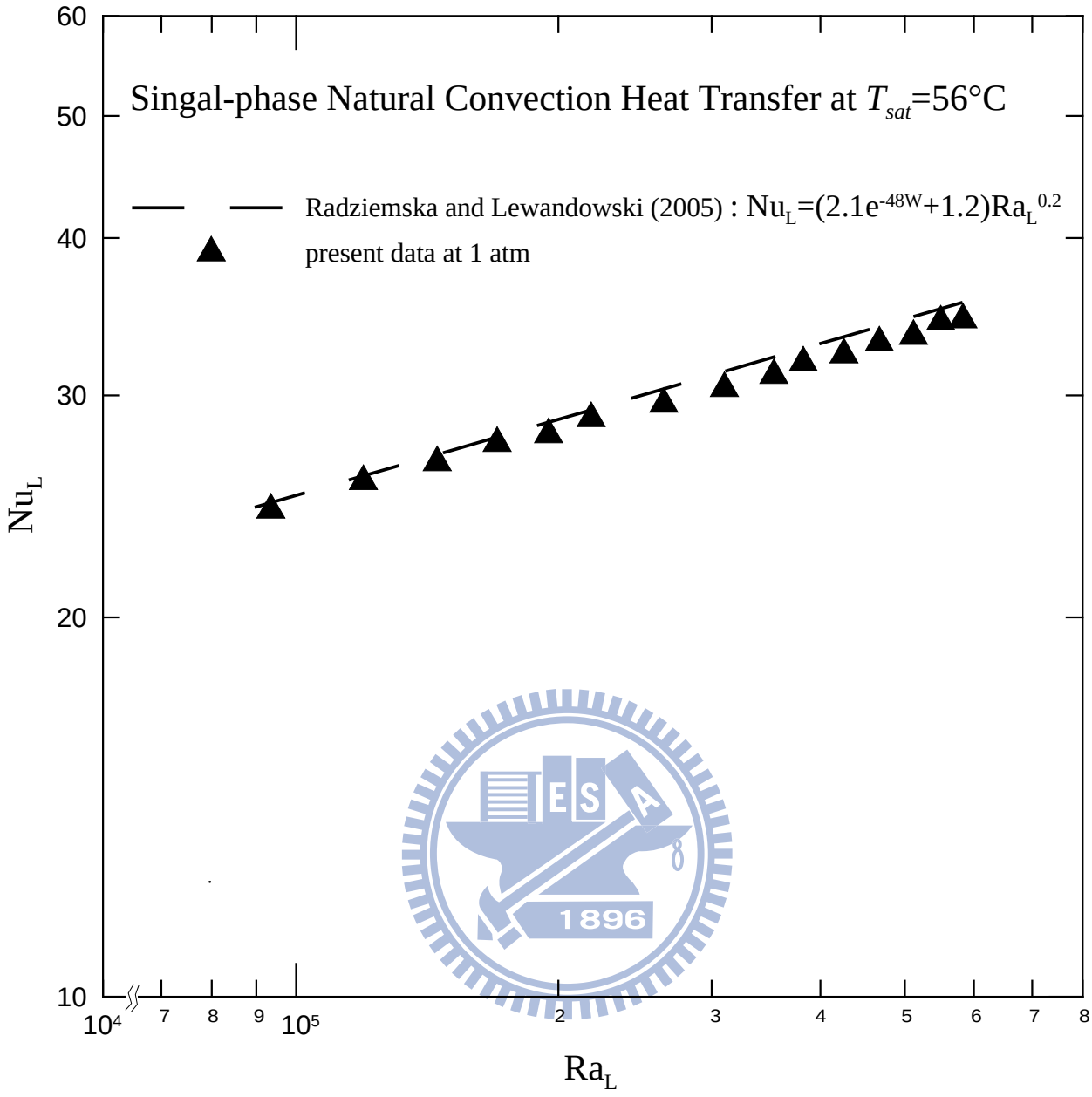

Fig. 4.1 Comparison of the present single-phase natural convection data with the empirical correlation of Radziemska and Lewandowski (2005).

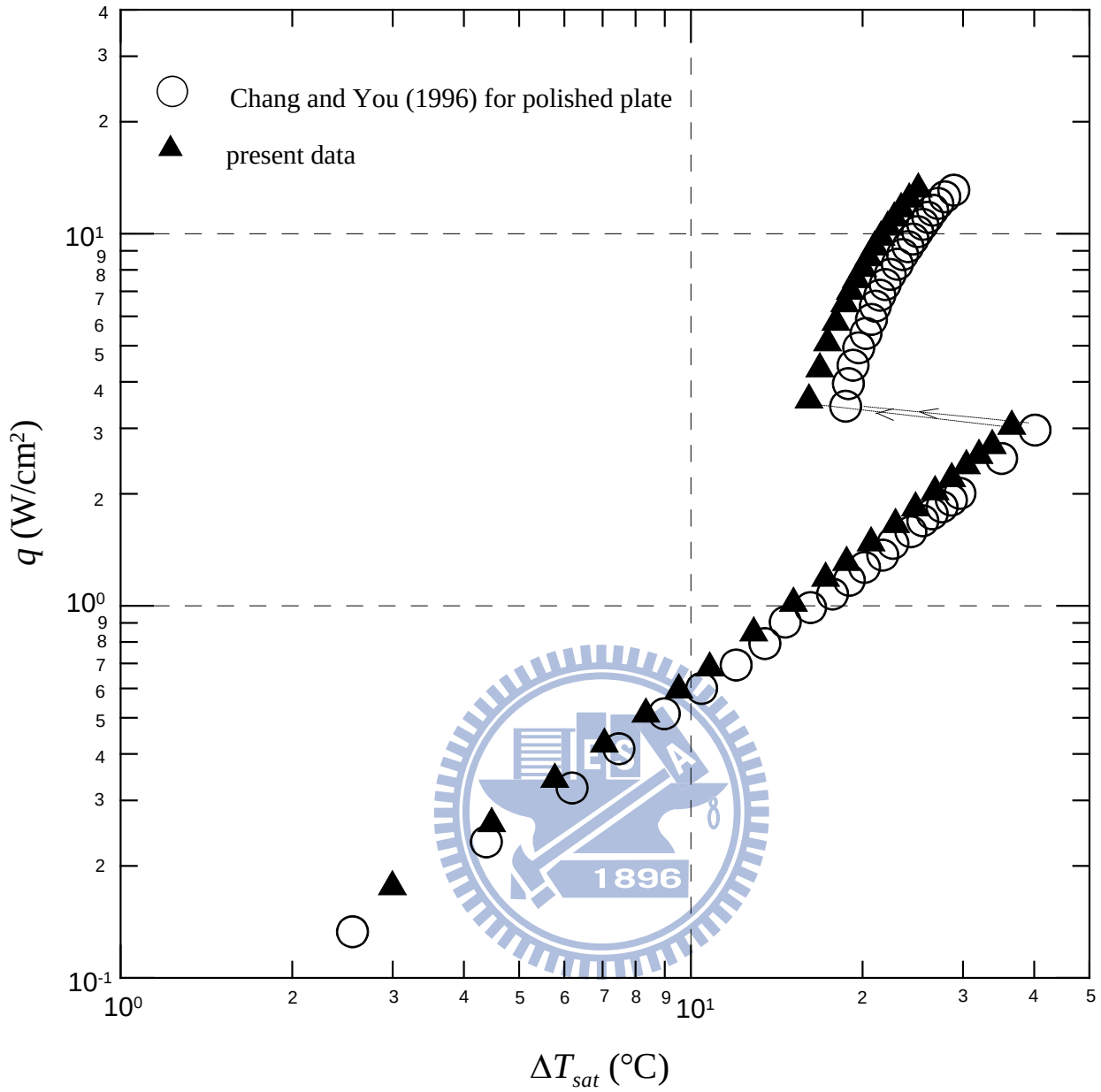

Fig. 4.2 Comparison of the present nucleate boiling heat transfer data on smooth plate with Chang and You (1996).

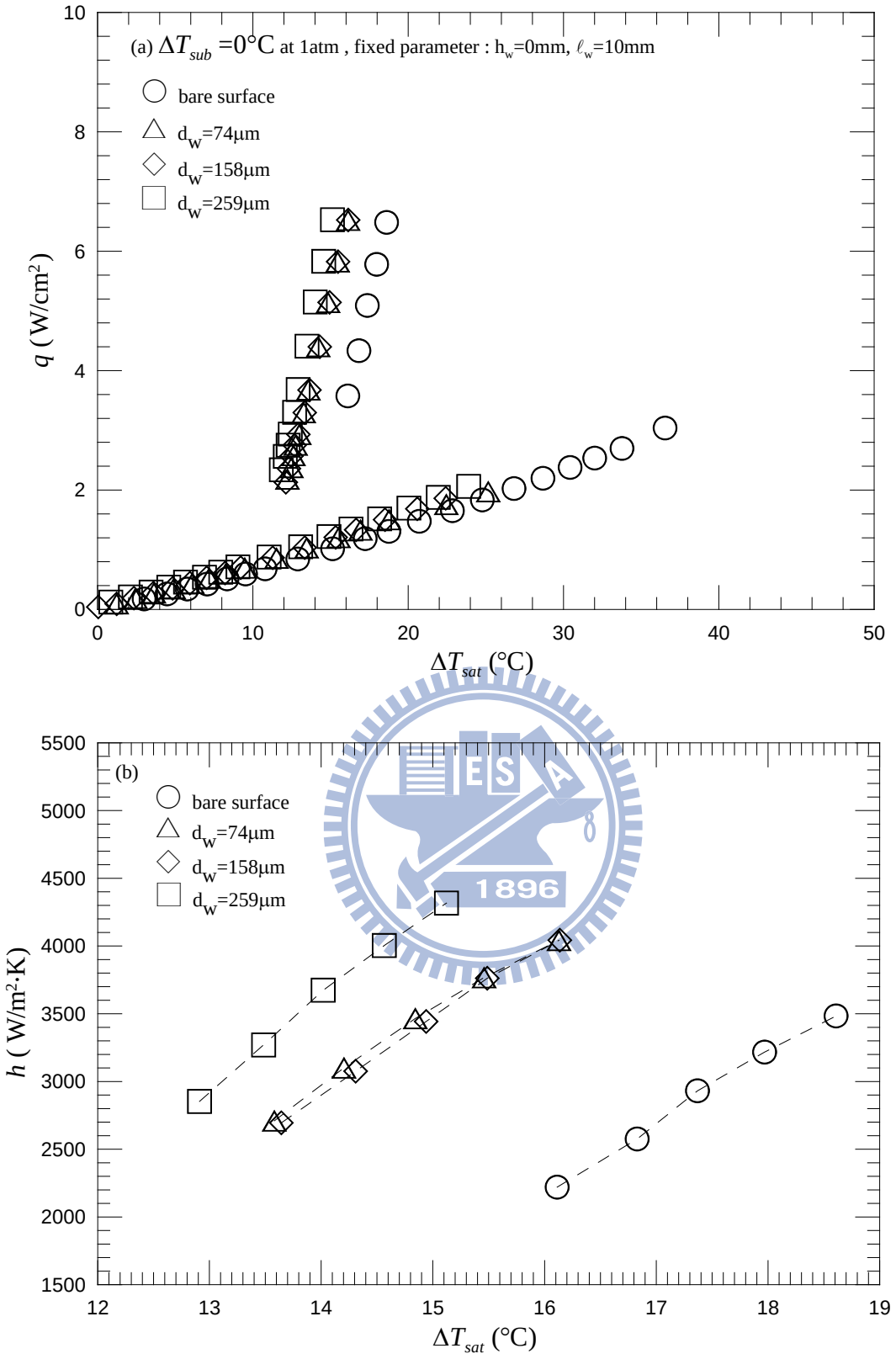

Fig. 4.3 Effects of string diameter on saturated pool boiling curves (a) and boiling heat transfer coefficients (b) at h_w=0mm and ℓ_w=10mm.

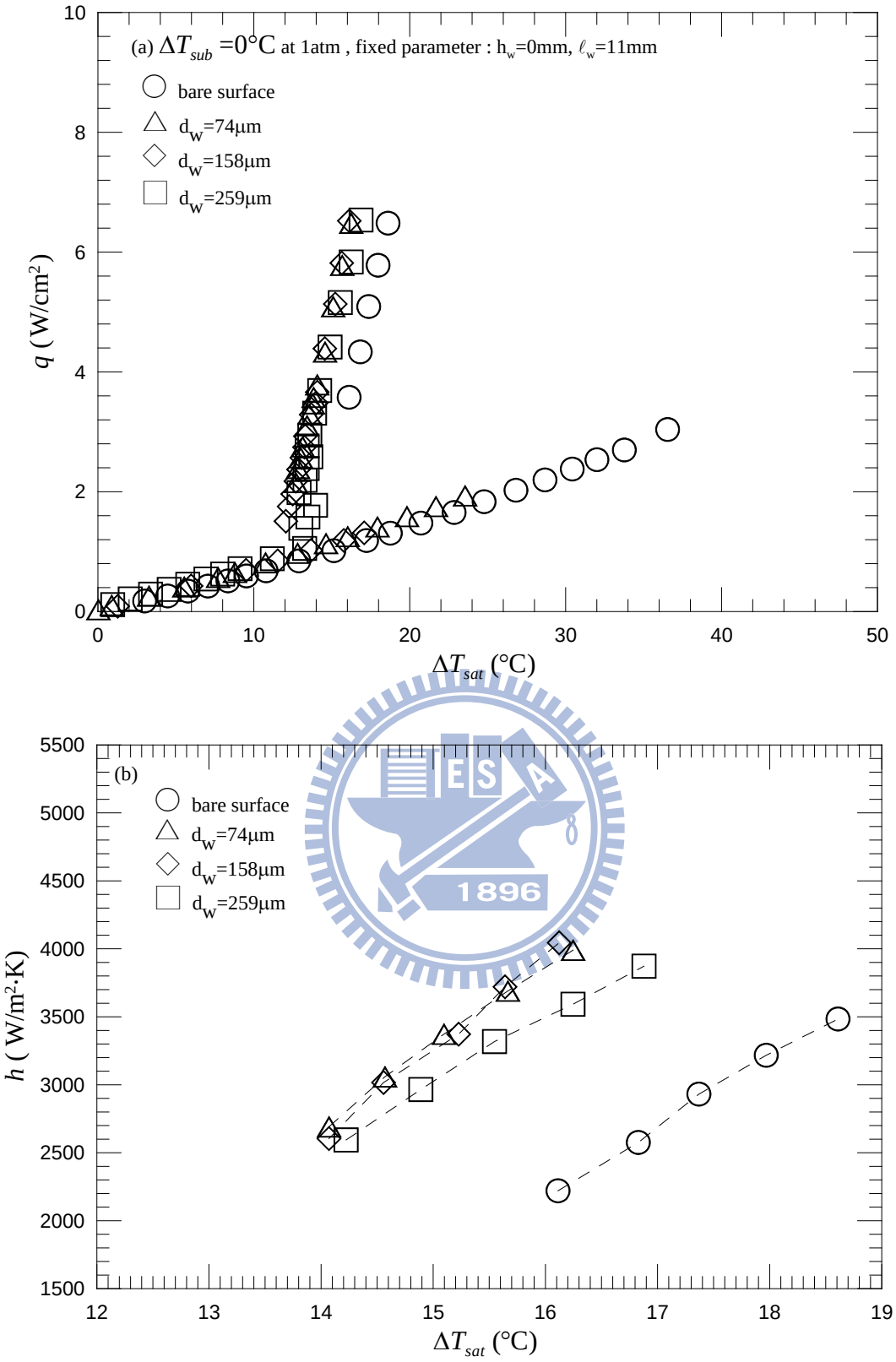

Fig. 4.4 Effects of string diameter on saturated pool boiling curves (a) and boiling heat transfer coefficients (b) at h_w=0mm and ℓ_w =11mm.

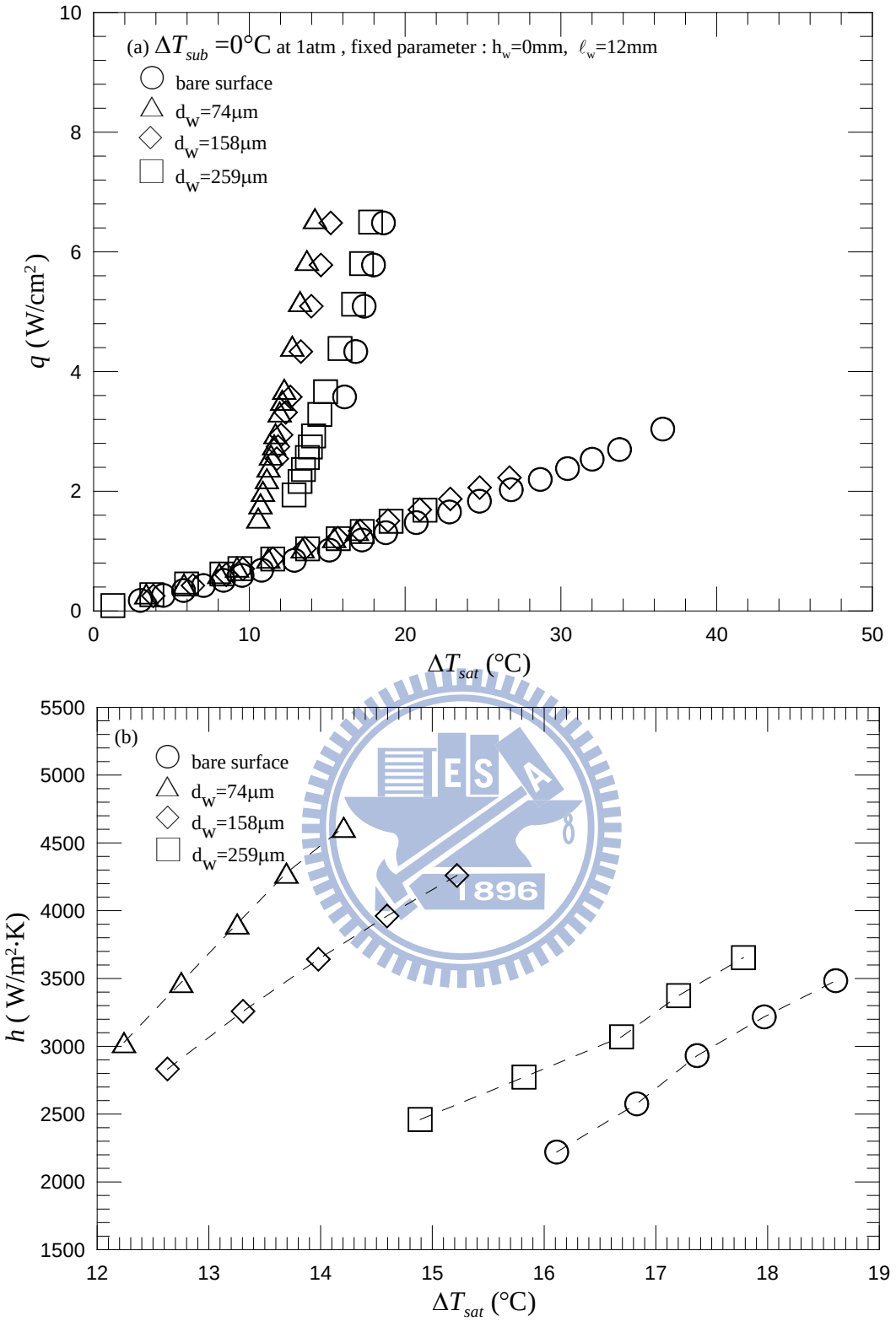

Fig. 4.5 Effects of string diameter on saturated pool boiling curves (a) and boiling heat transfer coefficients (b) at h_w=0mm and ℓ_w=12mm.

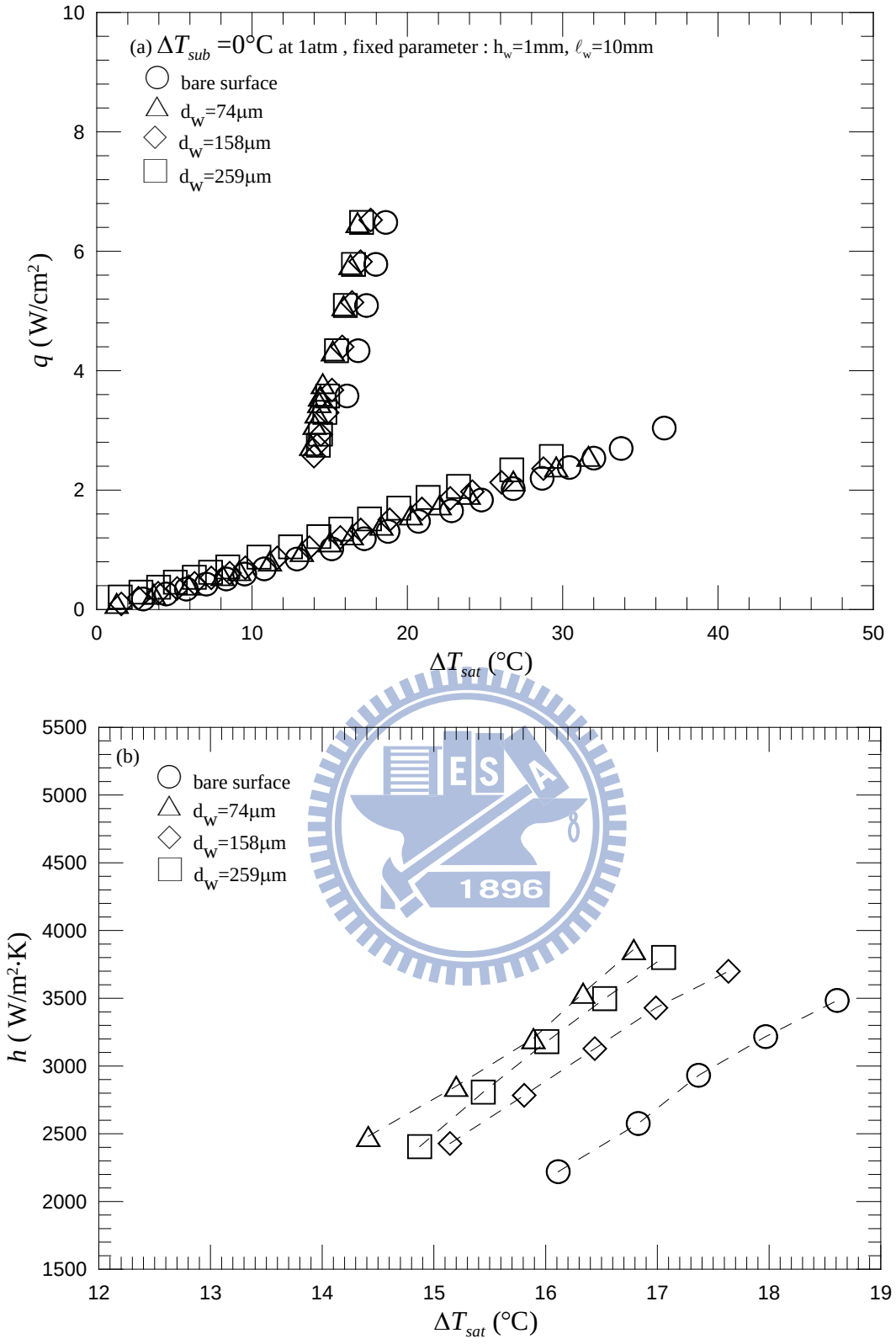

Fig. 4.6 Effects of string diameter on saturated pool boiling curves (a) and boiling heat transfer coefficients (b) at h_w=1mm and ℓ_w=10mm.

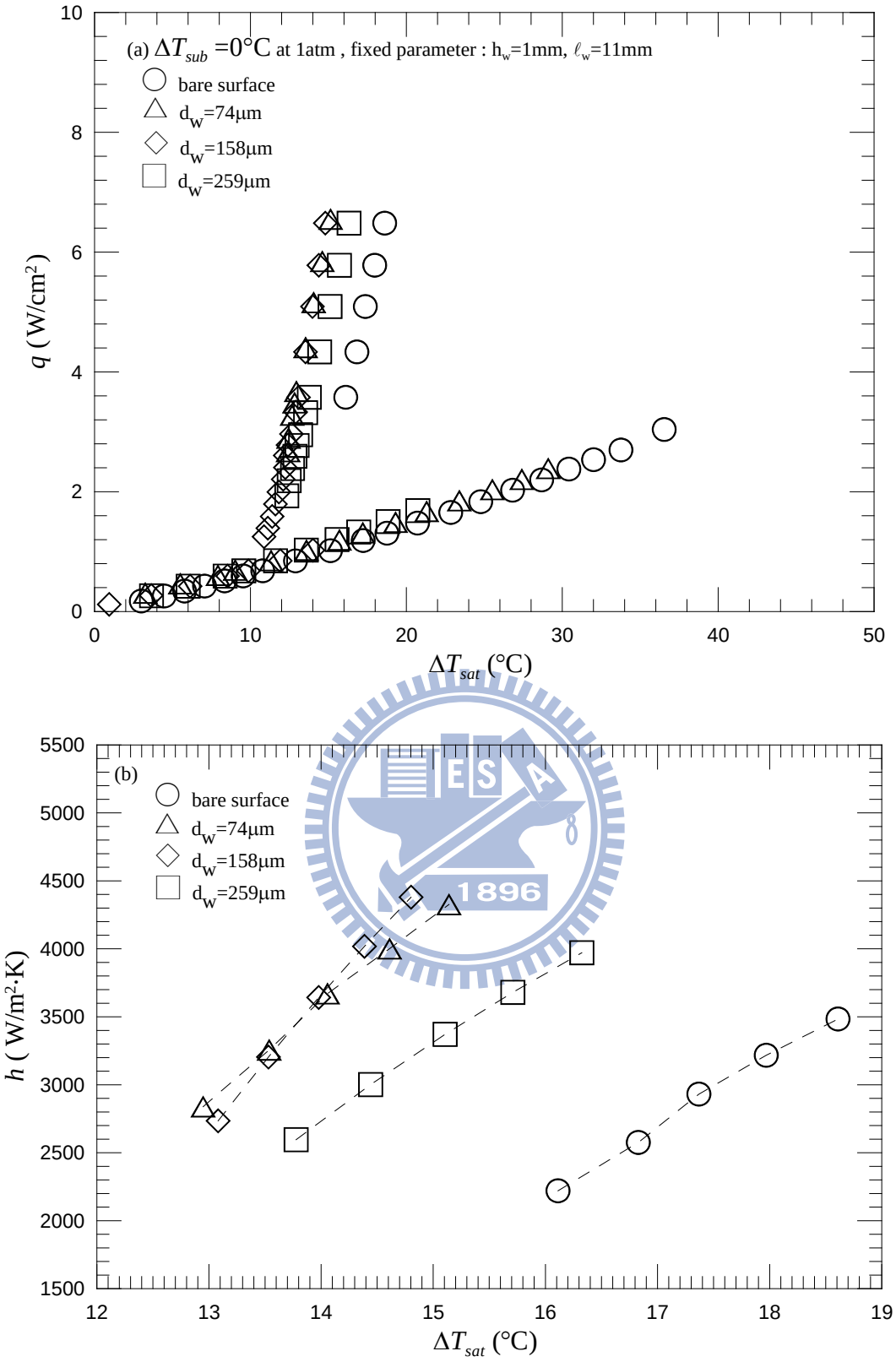

Fig. 4.7 Effects of string diameter on saturated pool boiling curves (a) and boiling heat transfer coefficients (b) at h_w=1mm and ℓ_w =11mm.

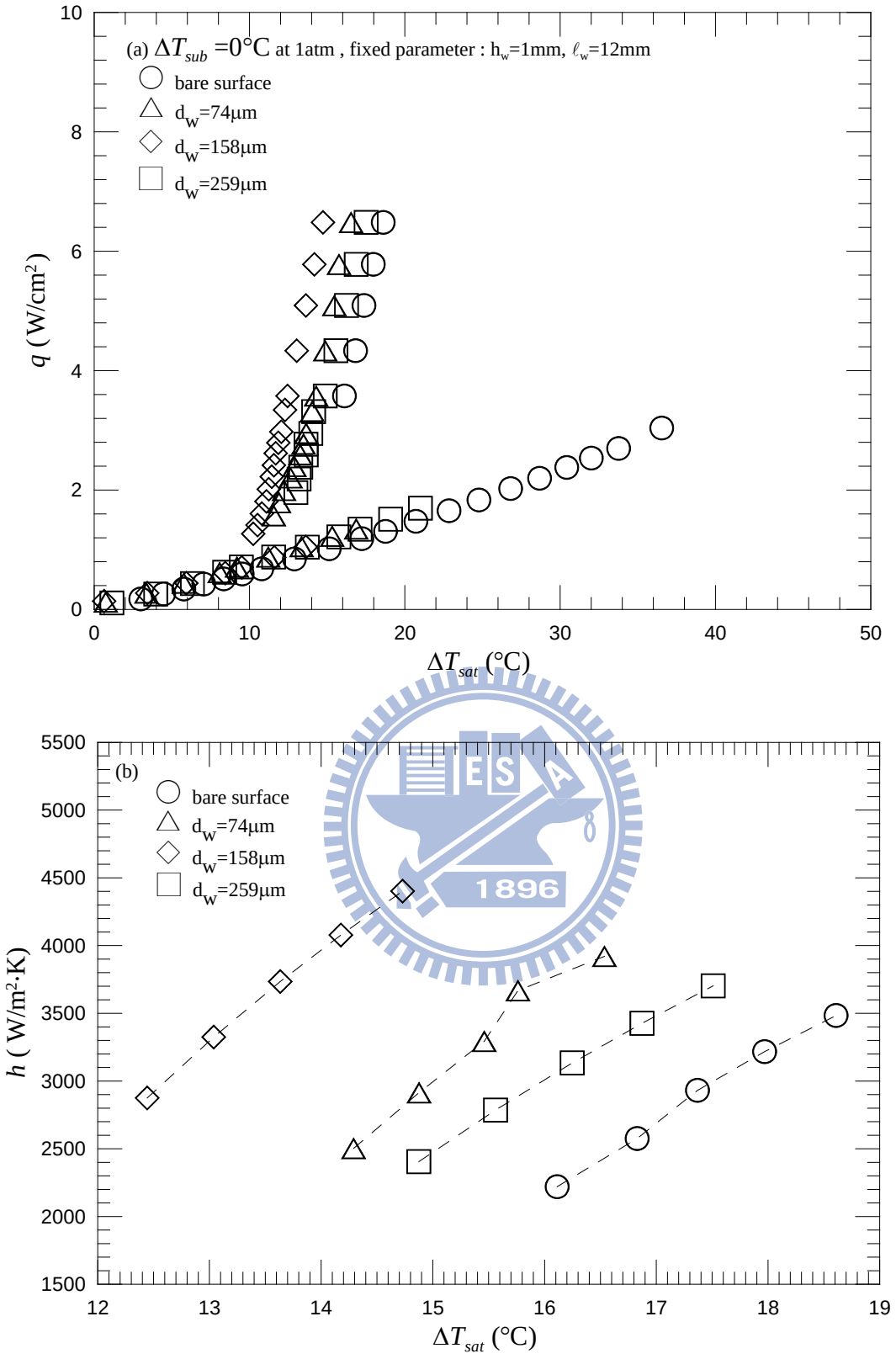

Fig. 4.8 Effects of string diameter on saturated pool boiling curves (a) and boiling heat transfer coefficients (b) at h_w=1mm and ℓ_w =12mm.

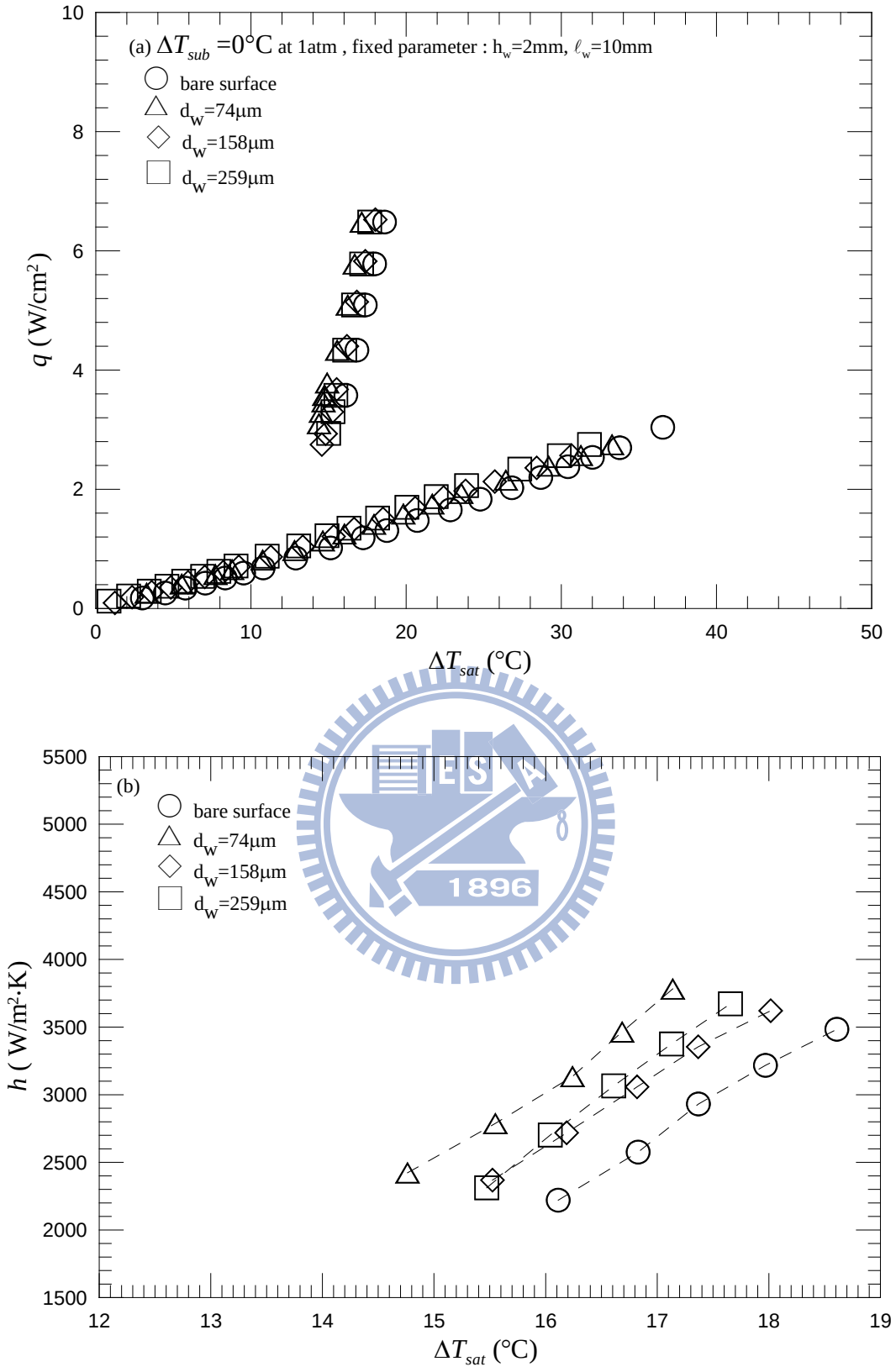

Fig. 4.9 Effects of string diameter on saturated pool boiling curves (a) and boiling heat transfer coefficients (b) at h_w=2mm and ℓ_w=10mm.

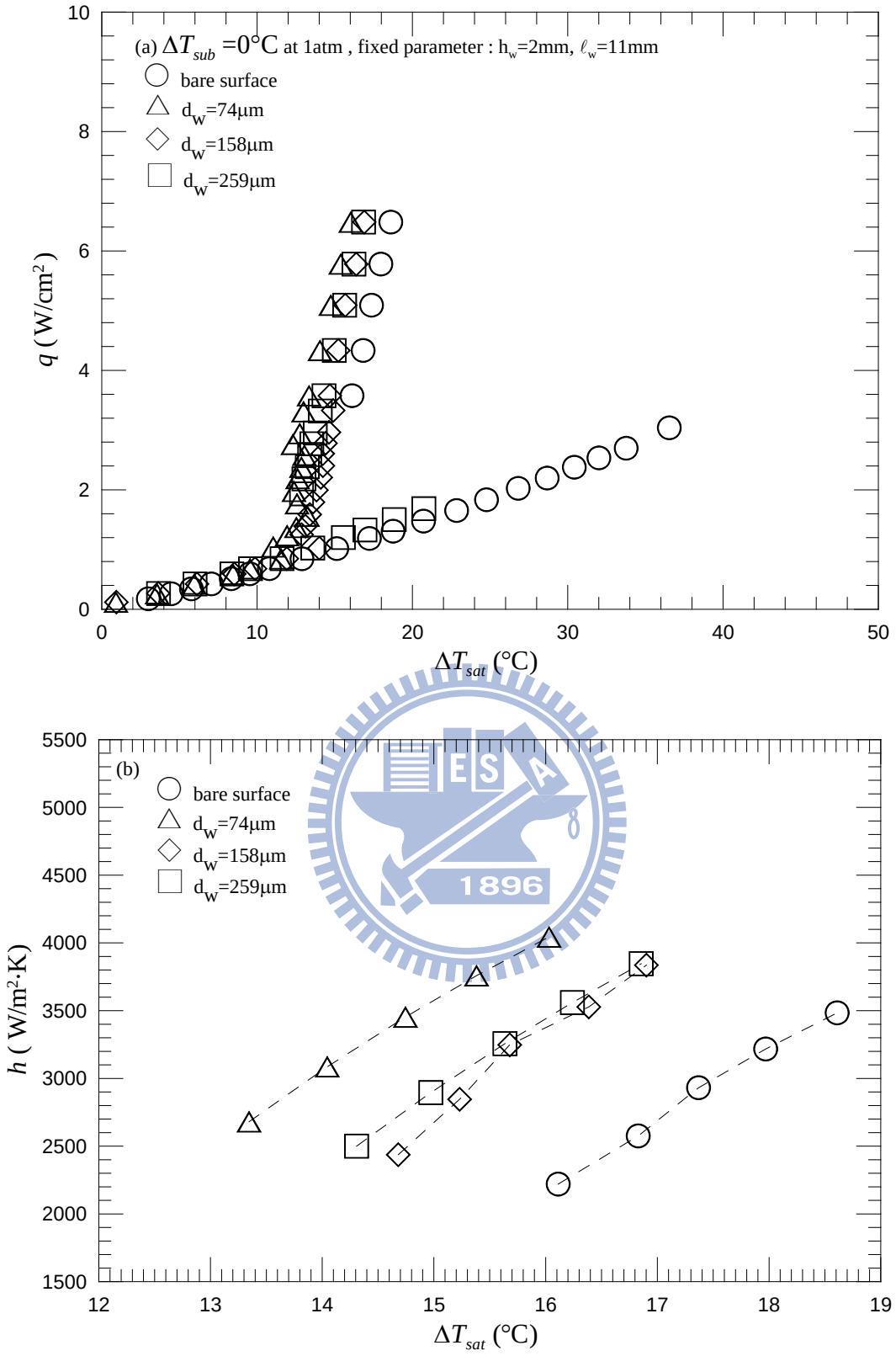

Fig. 4.10 Effects of string diameter on saturated pool boiling curves (a) and boiling heat transfer coefficients (b) at h_w=2mm and ℓ_w =11mm.

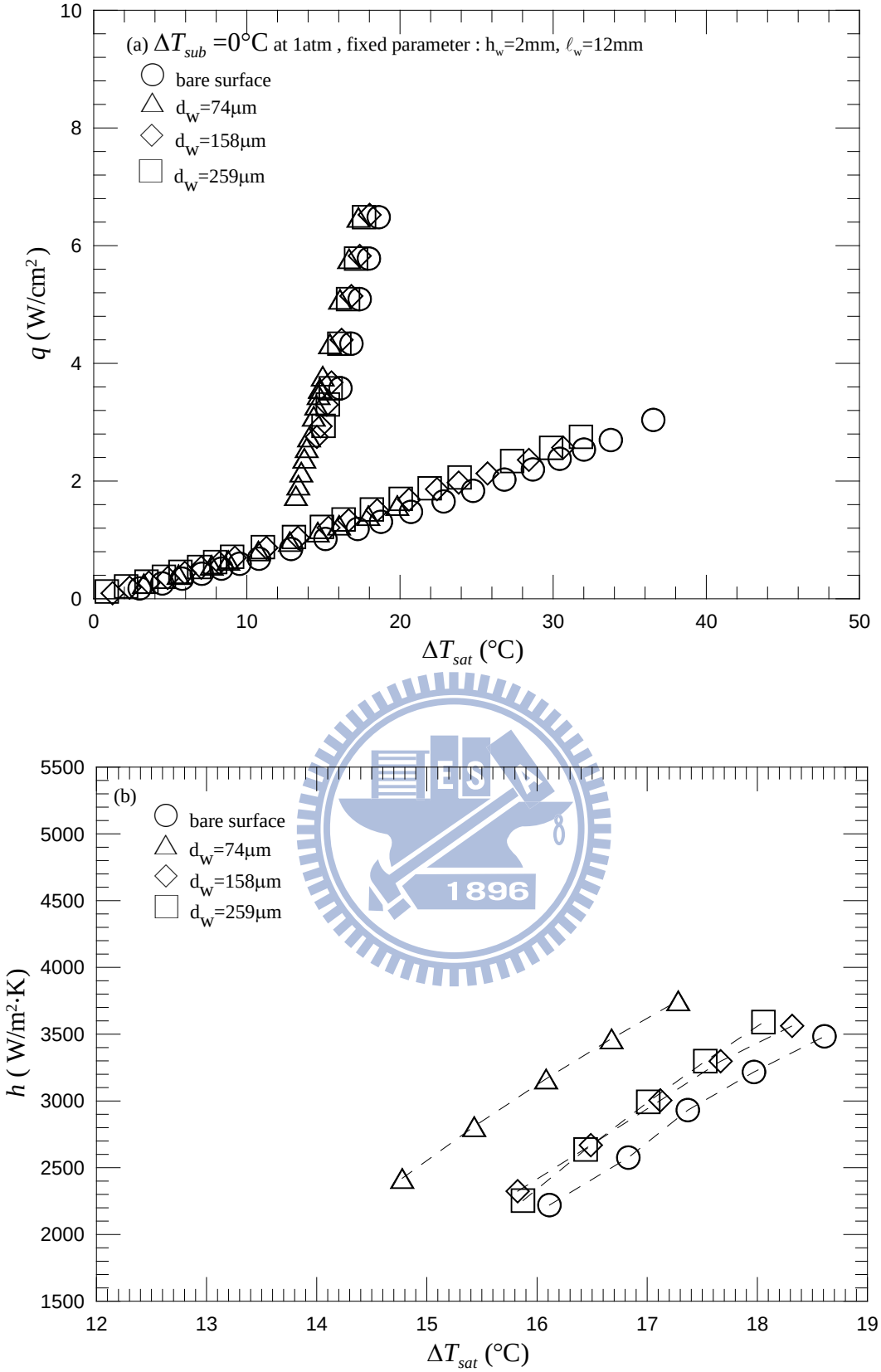

Fig. 4.11 Effects of string diameter on saturated pool boiling curves (a) and boiling heat transfer coefficients (b) at h_w=2mm and ℓ_w=12mm.

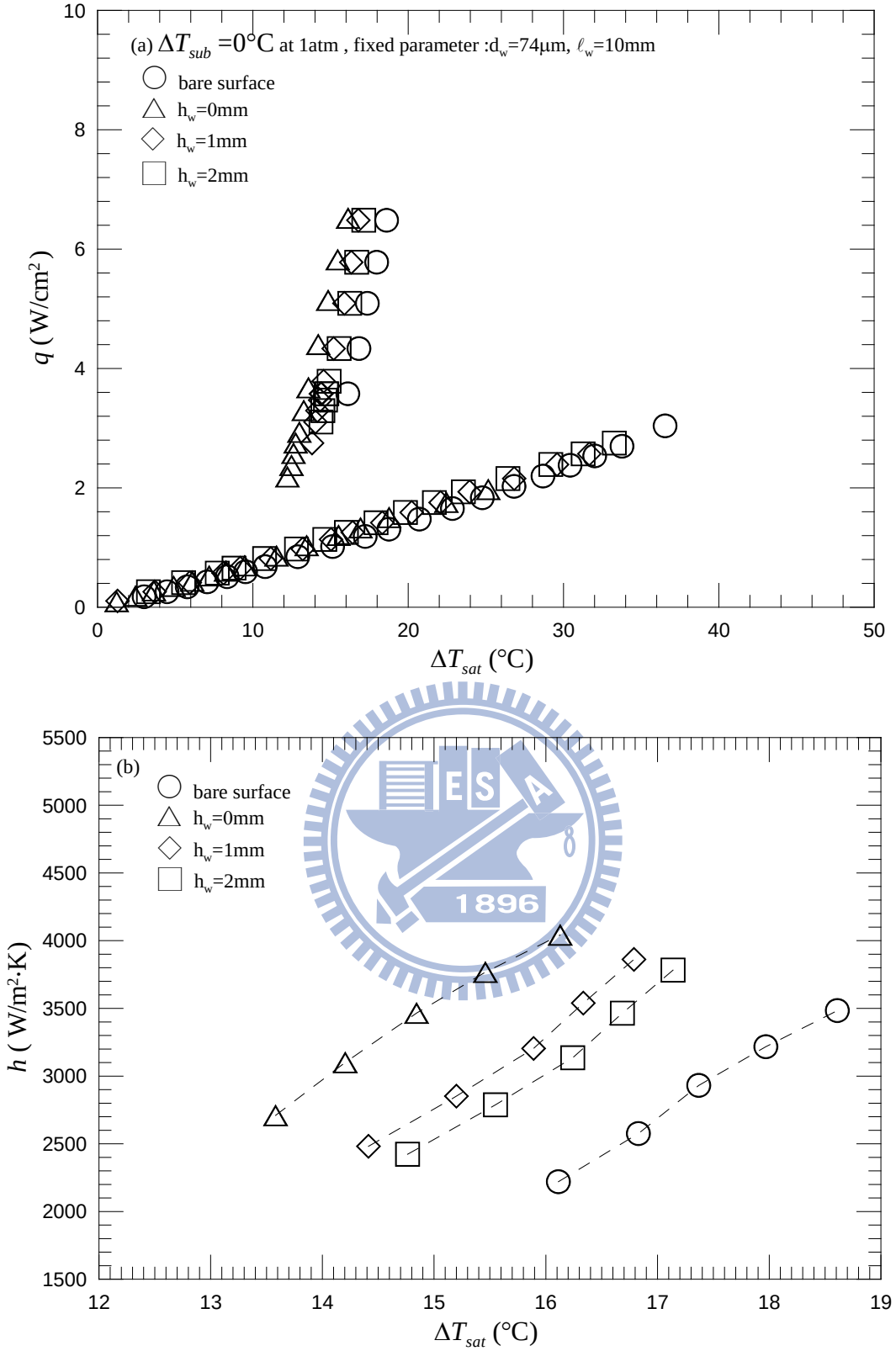

Fig. 4.12 Effects of string height on saturated pool boiling curves (a) and boiling heat transfer coefficients (b) at d_w=74μm and ℓ_w=10mm.

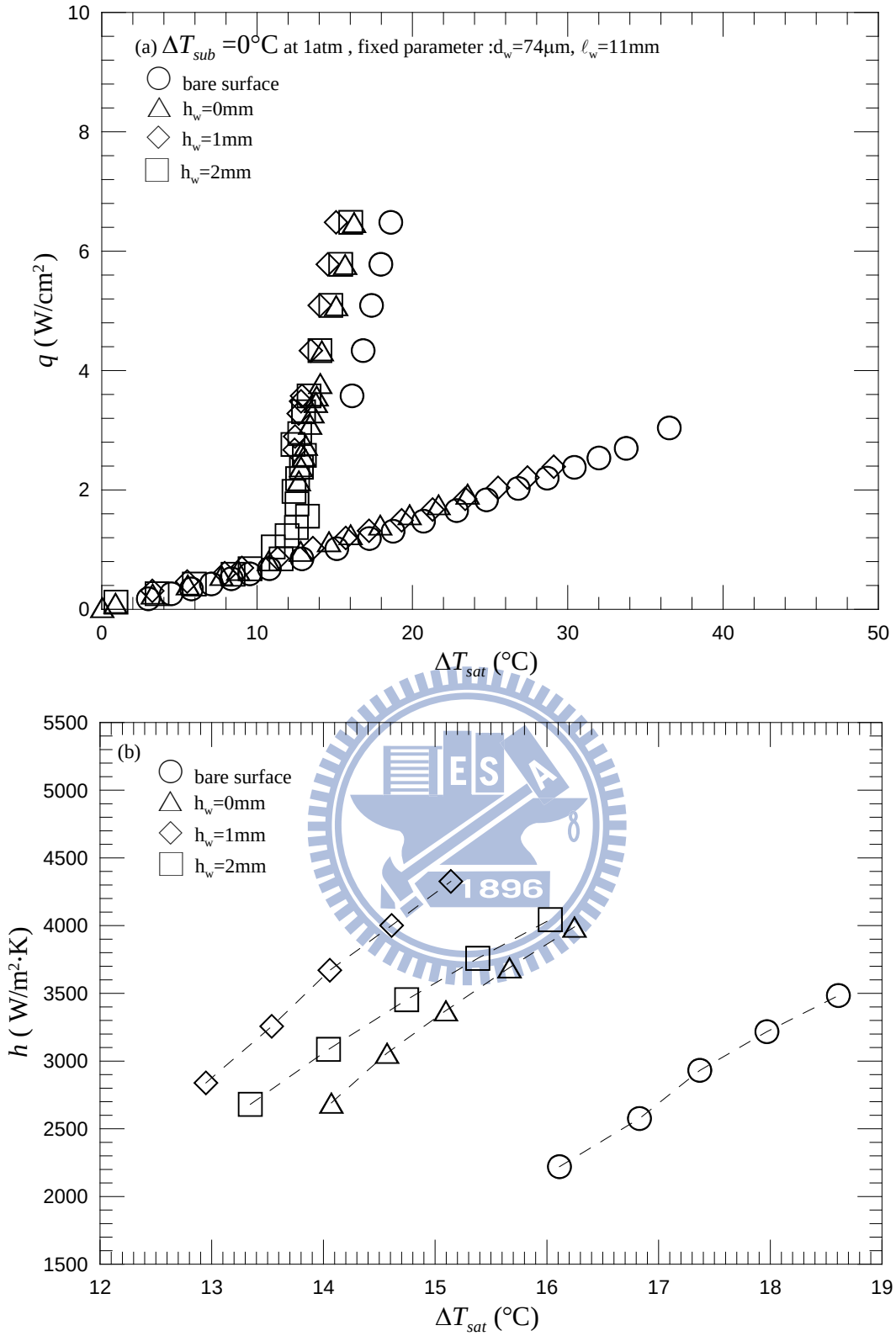

Fig. 4.13 Effects of string height on saturated pool boiling curves (a) and boiling heat transfer coefficients (b) at d_w=74μm and ℓ_w =11mm.

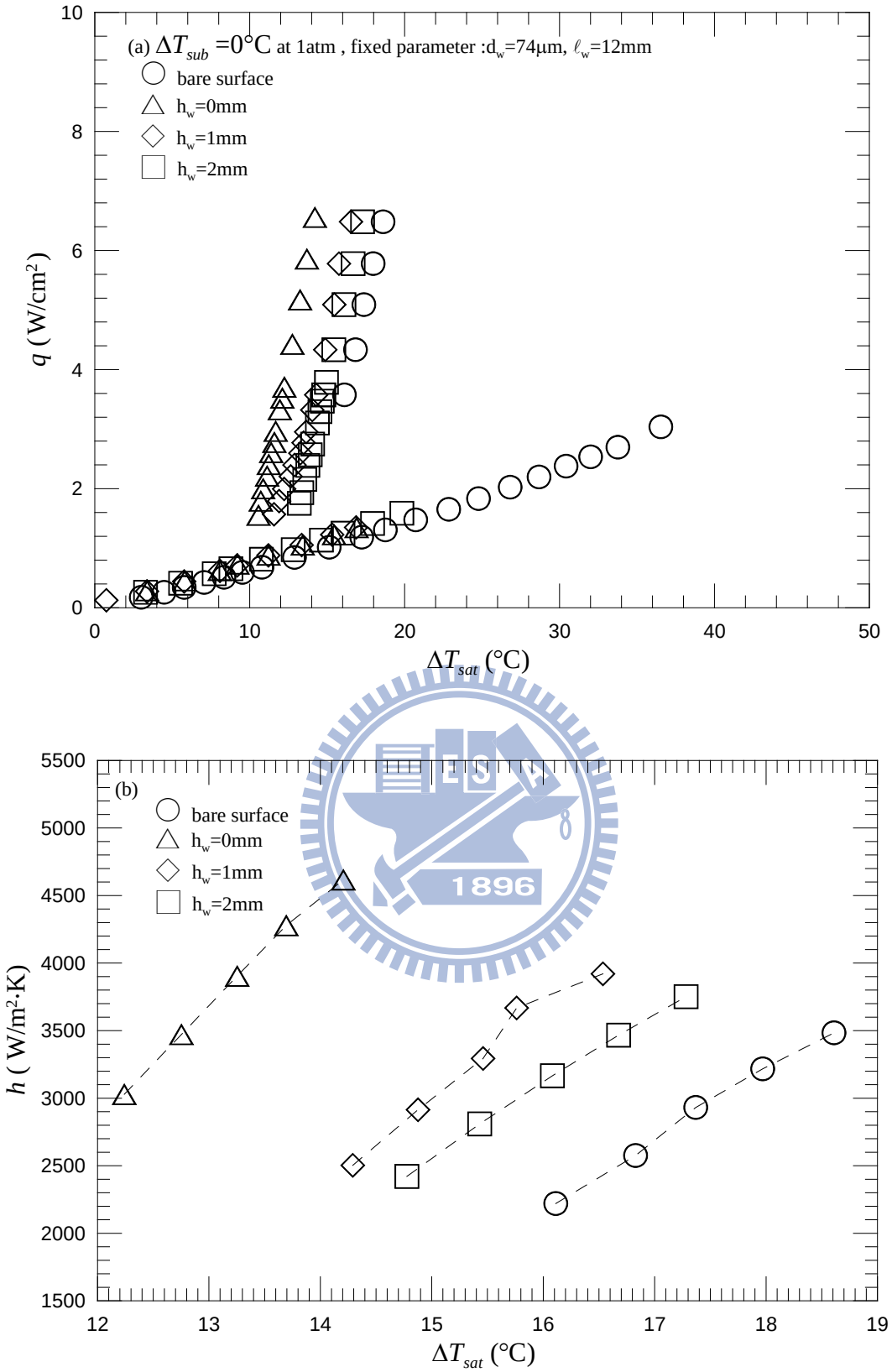

Fig. 4.14 Effects of string height on saturated pool boiling curves (a) and boiling heat transfer coefficients (b) at d_w=74μm and ℓ_w=12mm.

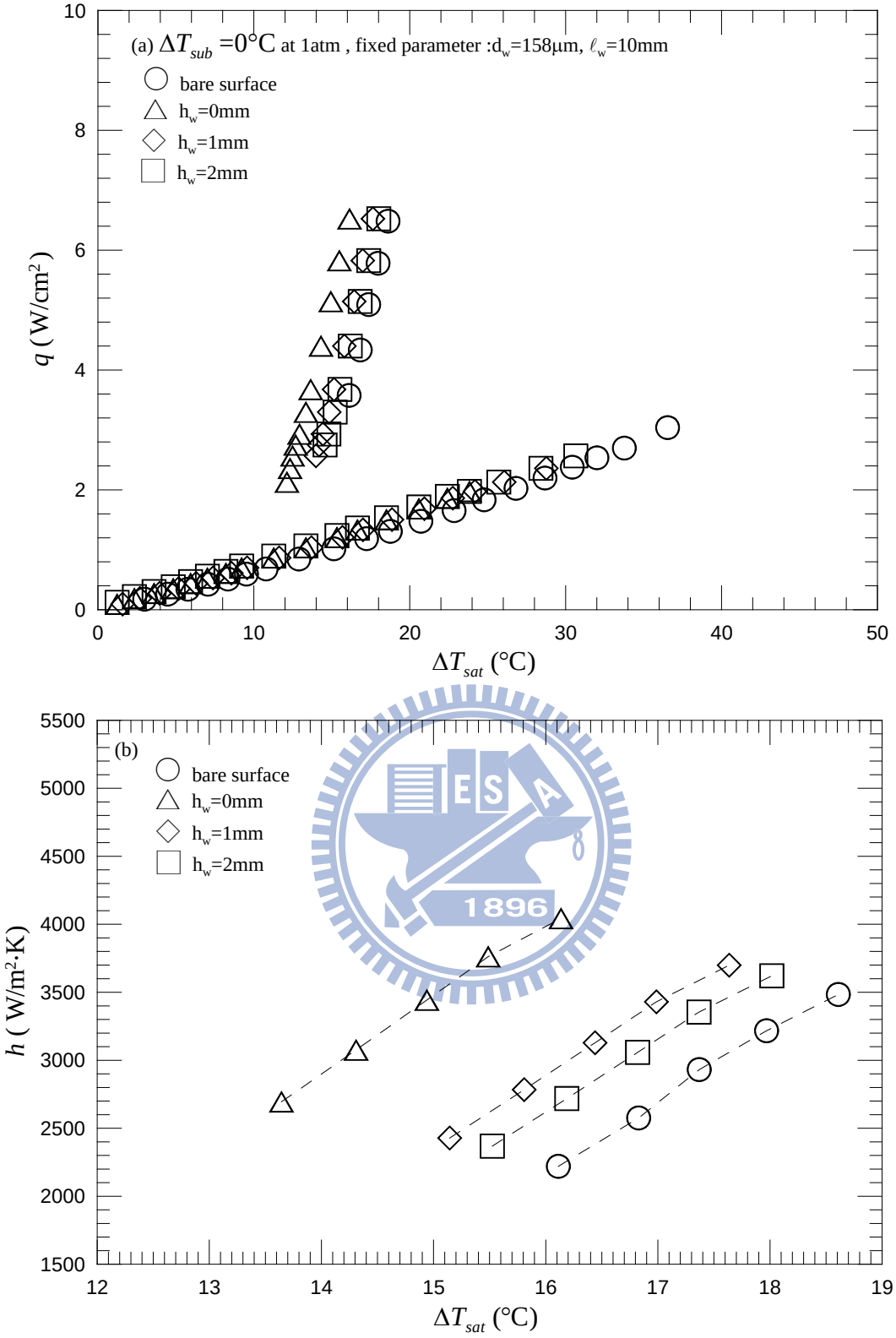

Fig. 4.15 Effects of string height on saturated pool boiling curves (a) and boiling heat transfer coefficients (b) at d_w=158μm and ℓ_w=10mm.

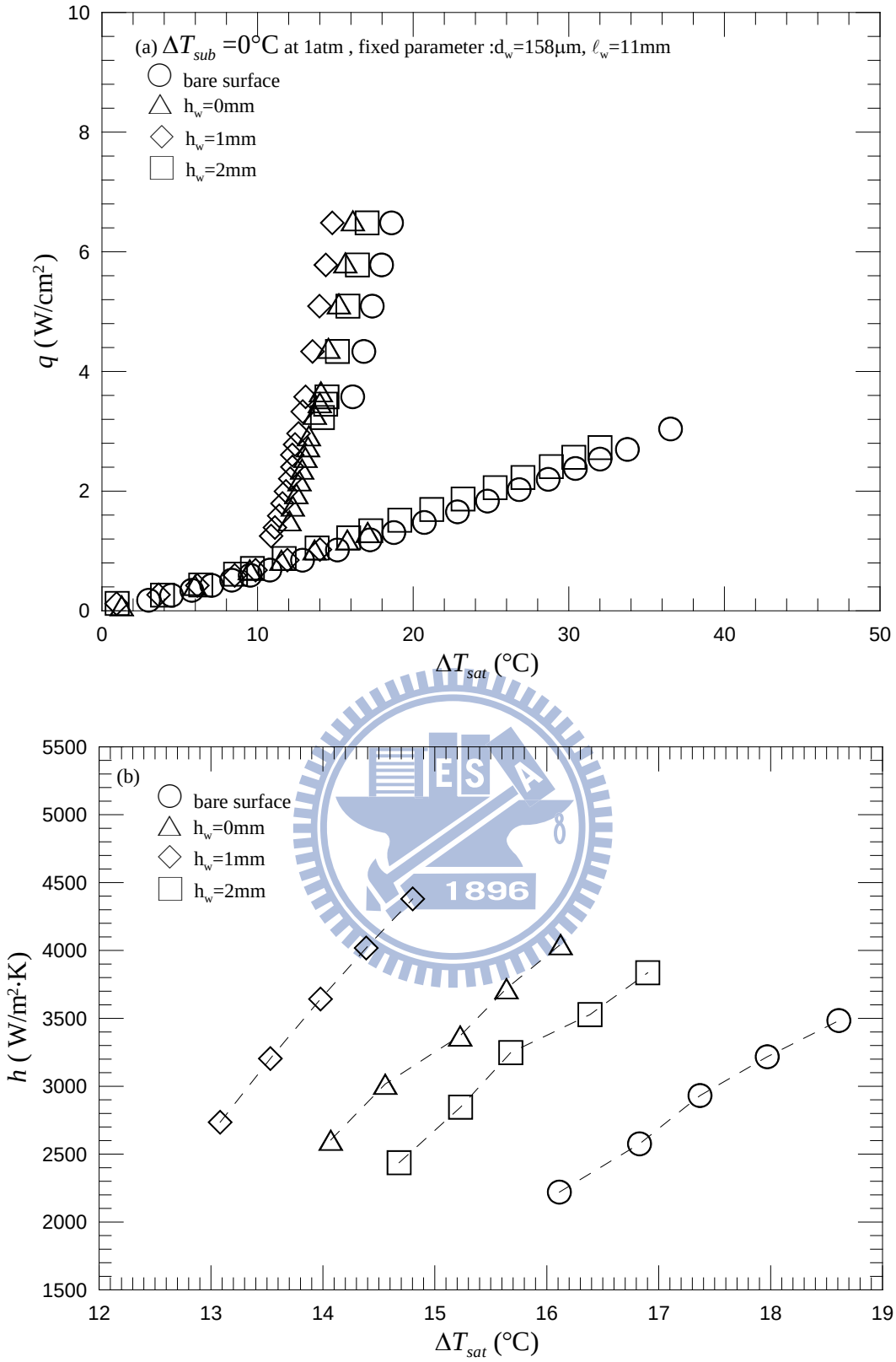

Fig. 4.16 Effects of string height on saturated pool boiling curves (a) and boiling heat transfer coefficients (b) at d_w=158μm and ℓ_w=11mm.

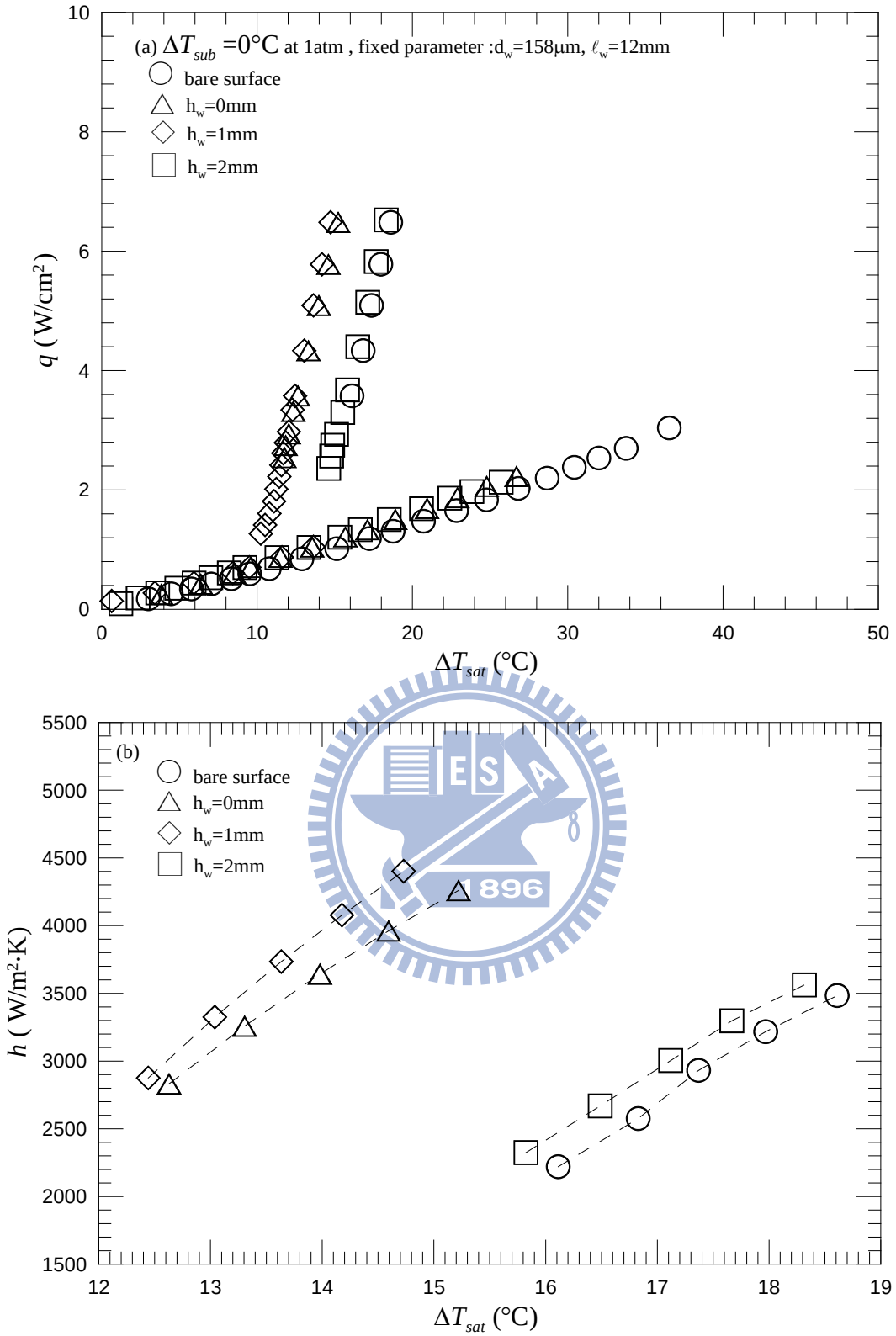

Fig. 4.17 Effects of string height on saturated pool boiling curves (a) and boiling heat transfer coefficients (b) at d_w=158μm and ℓ_w=12mm.

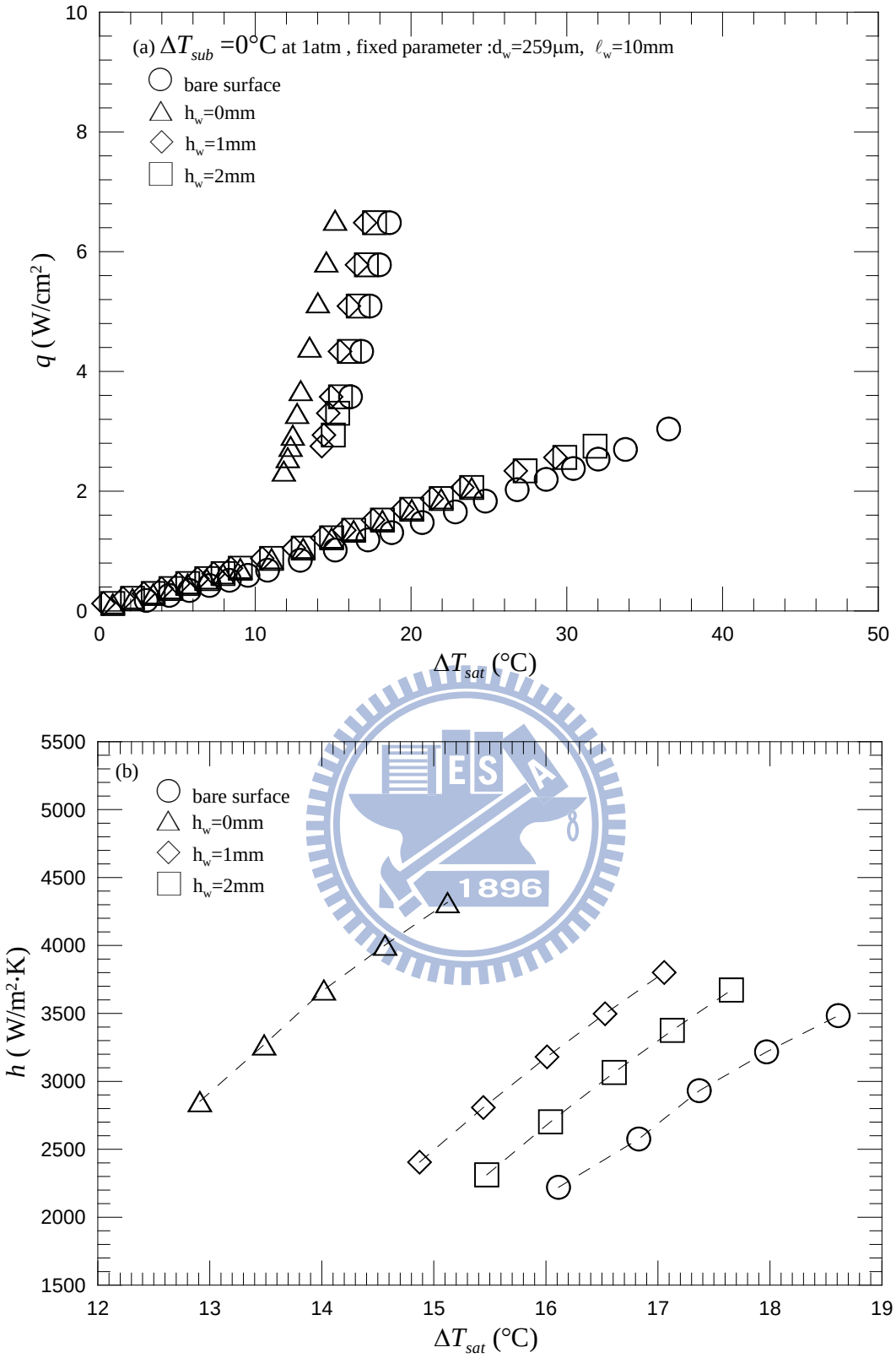

Fig. 4.18 Effects of string height on saturated pool boiling curves (a) and boiling heat transfer coefficients (b) at d_w=259μm and ℓ_w=10mm.

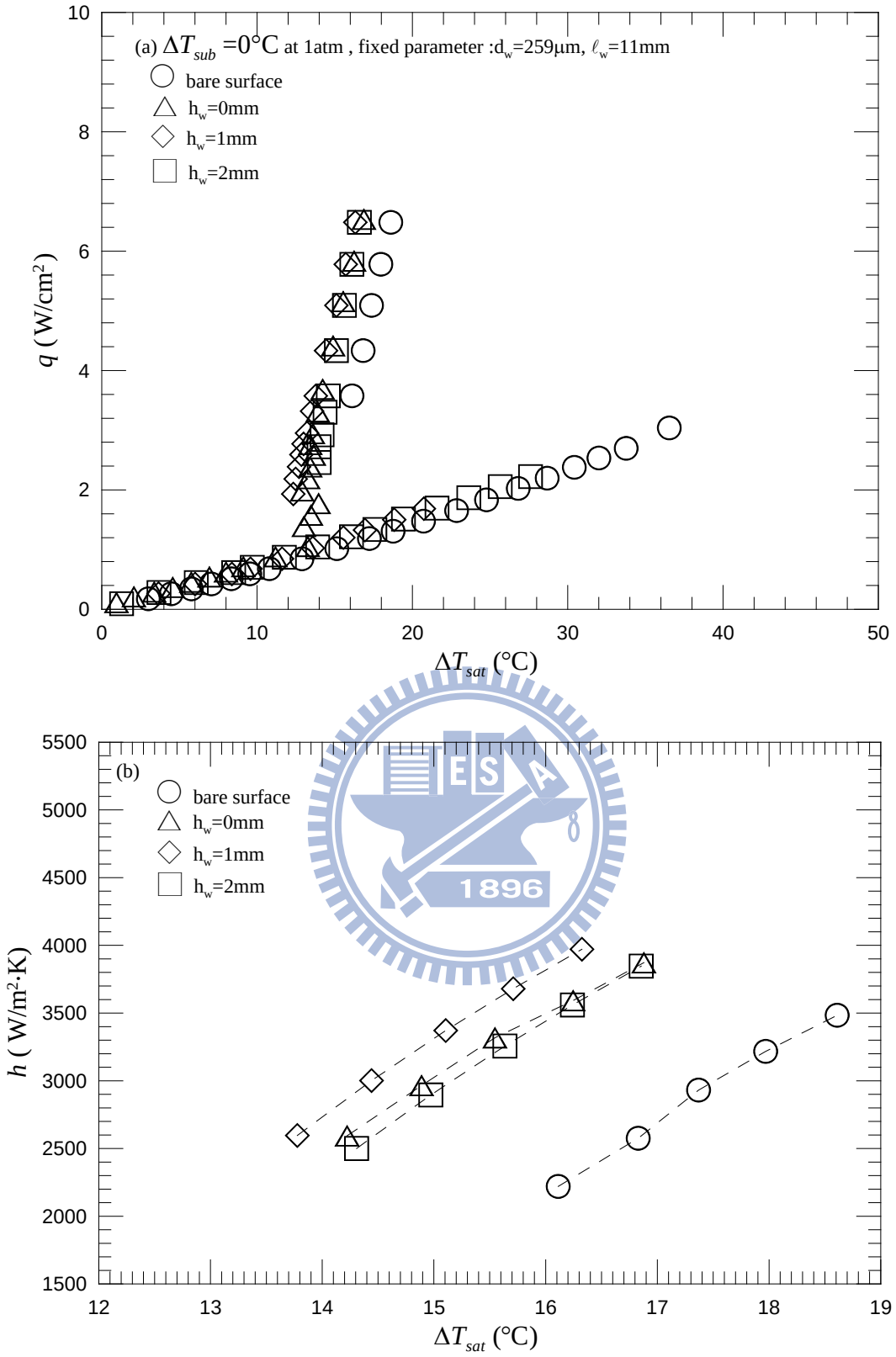

Fig. 4.19 Effects of string height on saturated pool boiling curves (a) and boiling heat transfer coefficients (b) at d_w=259μm and ℓ_w=11mm.

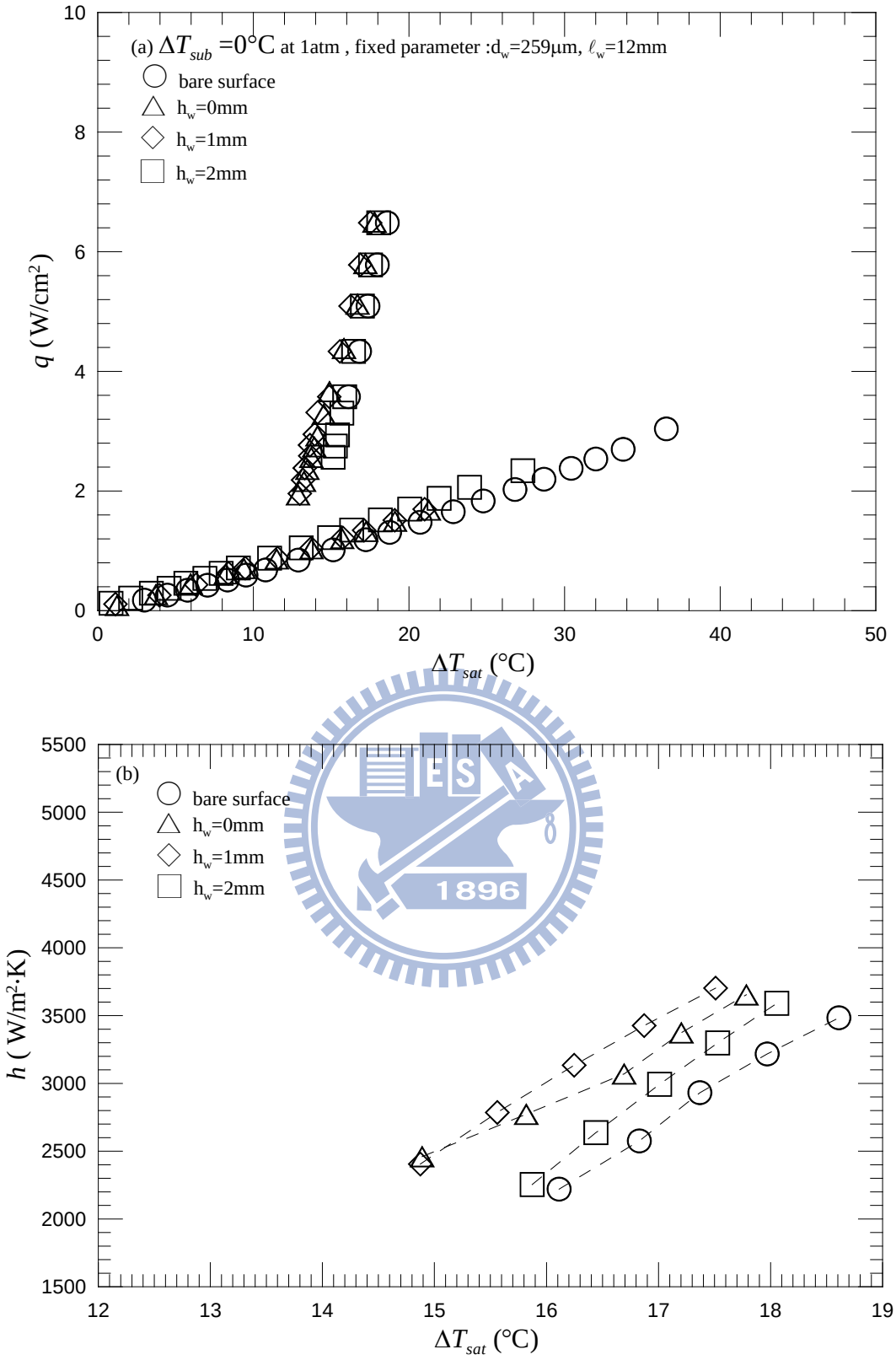

Fig. 4.20 Effects of string height on saturated pool boiling curves (a) and boiling heat transfer coefficients (b) at d_w=259μm and ℓ_w=12mm.

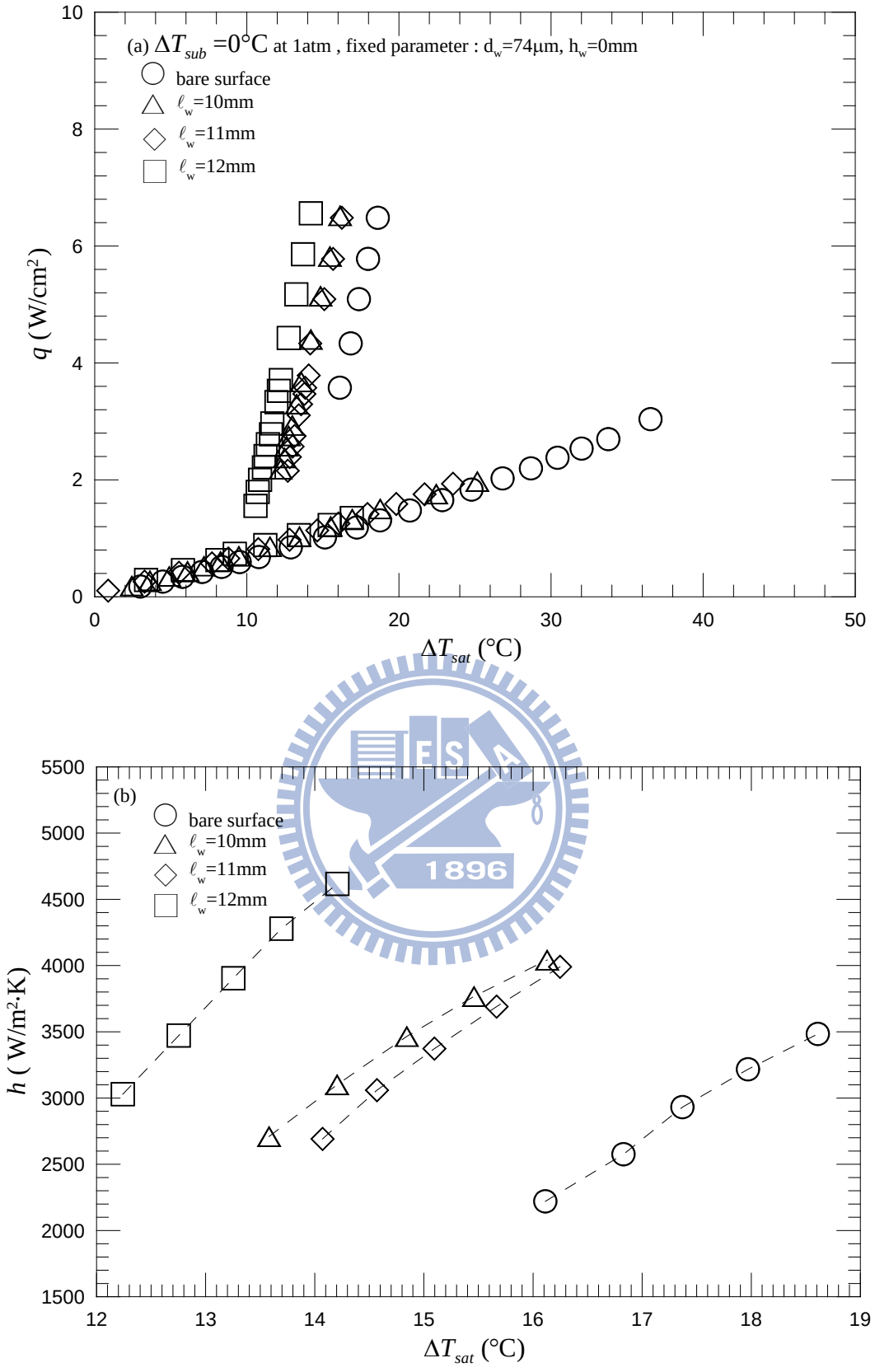

Fig. 4.21 Effects of string length on saturated pool boiling curves (a) and boiling heat transfer coefficients (b) at d_w=74μm and h_w=0mm.

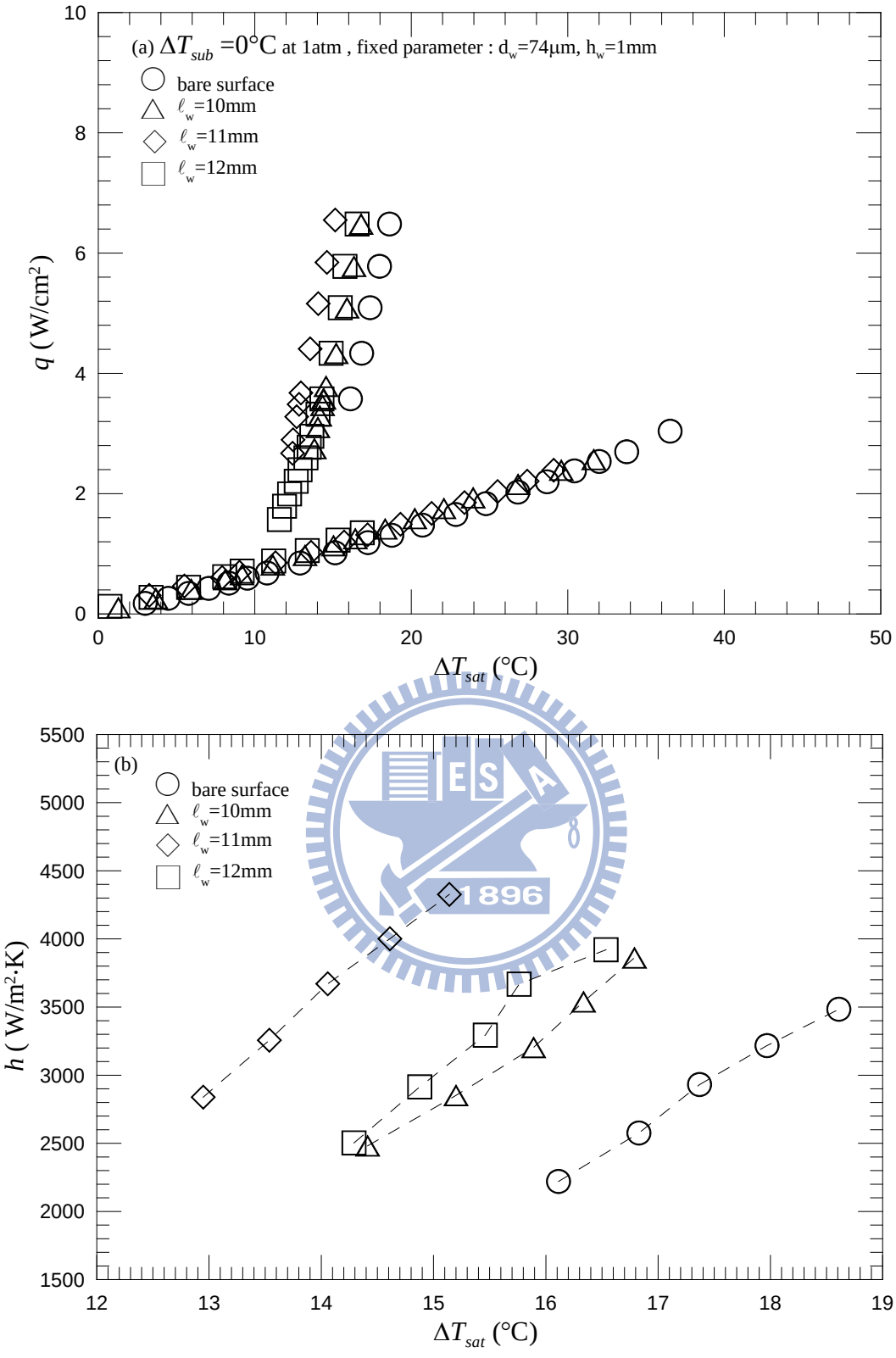

Fig. 4.22 Effects of string length on saturated pool boiling curves (a) and boiling heat transfer coefficients (b) at d_w=74μm and h_w=1mm.

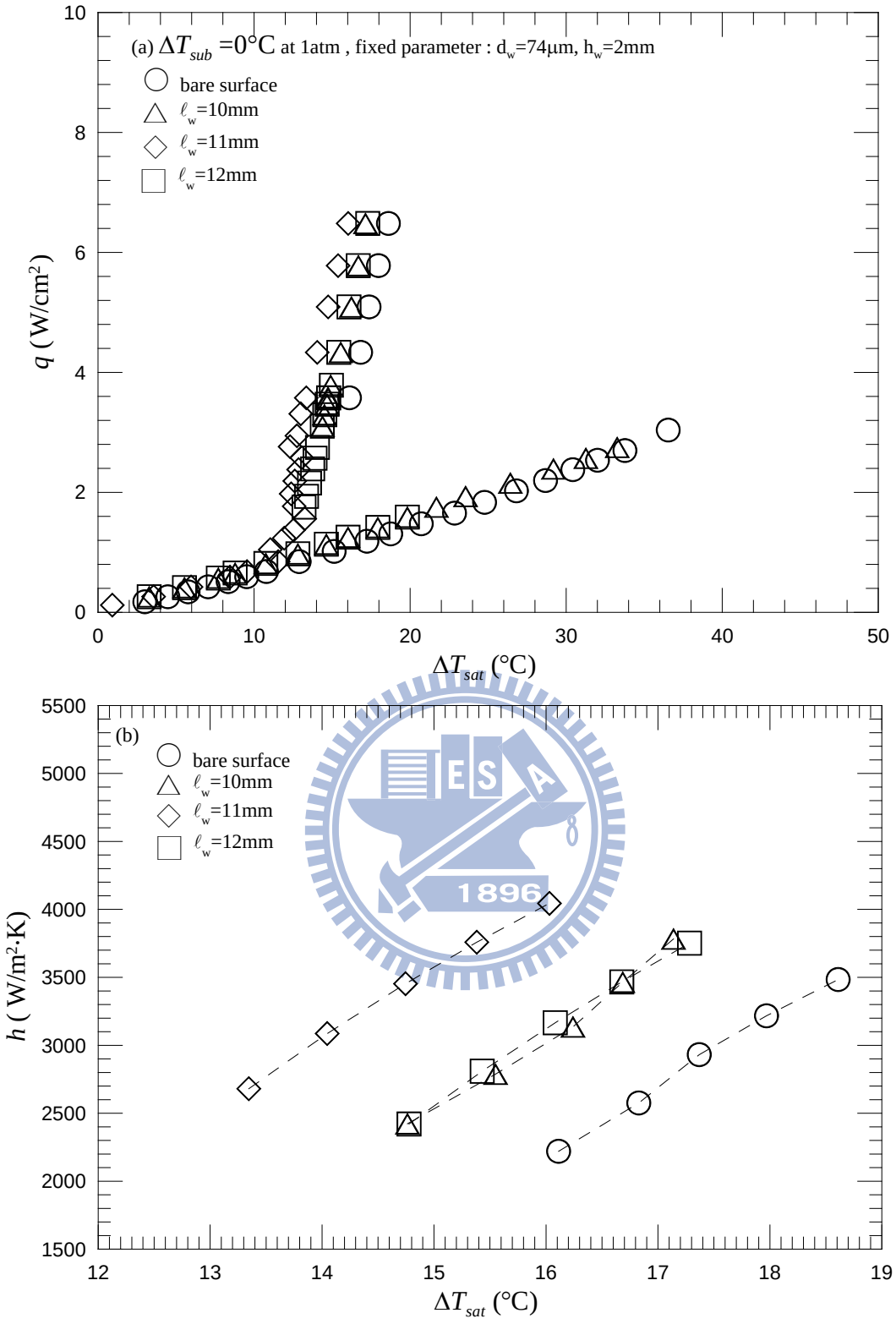

Fig. 4.23 Effects of string length on saturated pool boiling curves (a) and boiling heat transfer coefficients (b) at d_w=74μm and h_w=2mm.

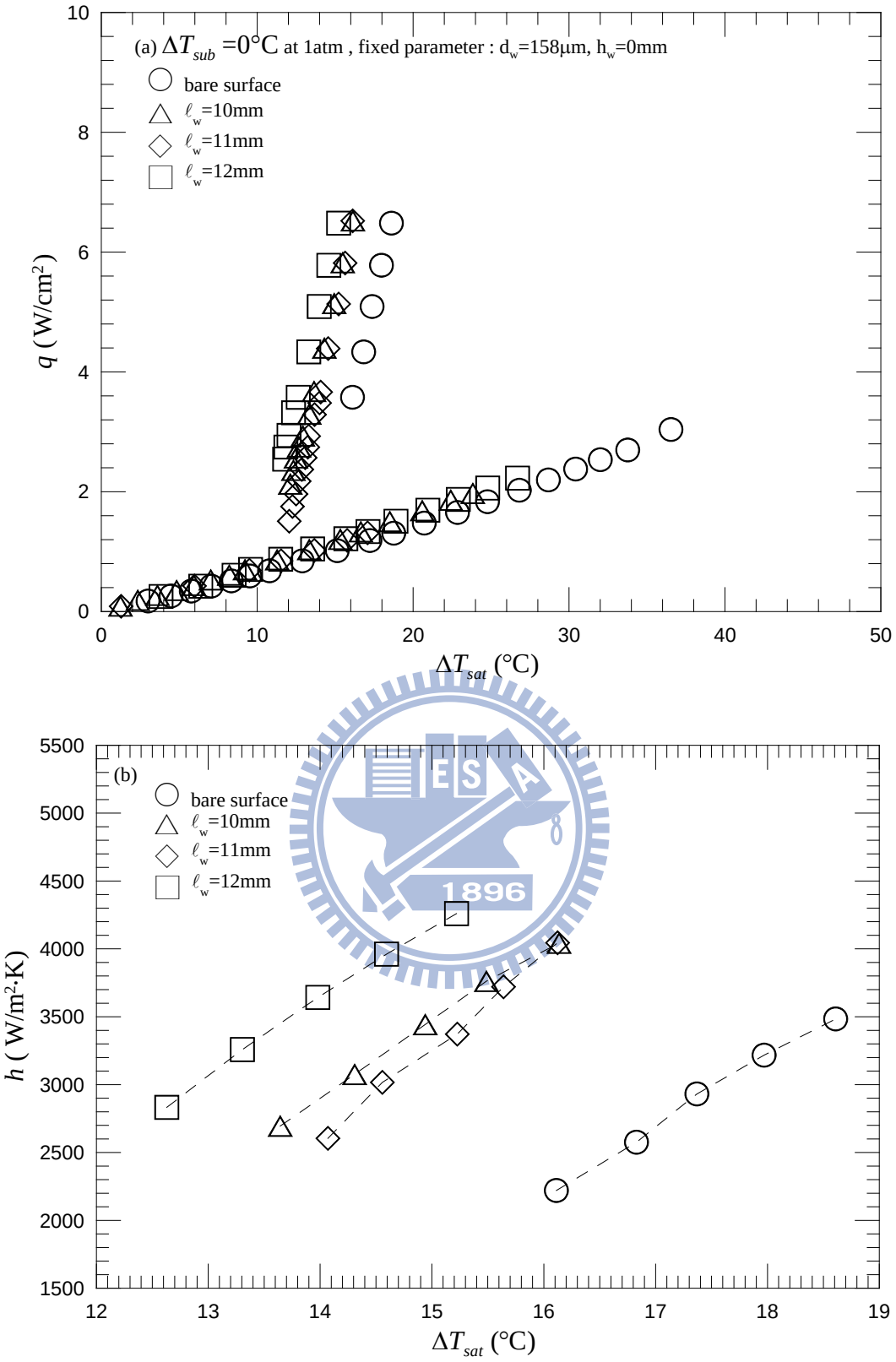

Fig. 4.24 Effects of string length on saturated pool boiling curves (a) and boiling heat transfer coefficients (b) at d_w=158μm and h_w=0mm.

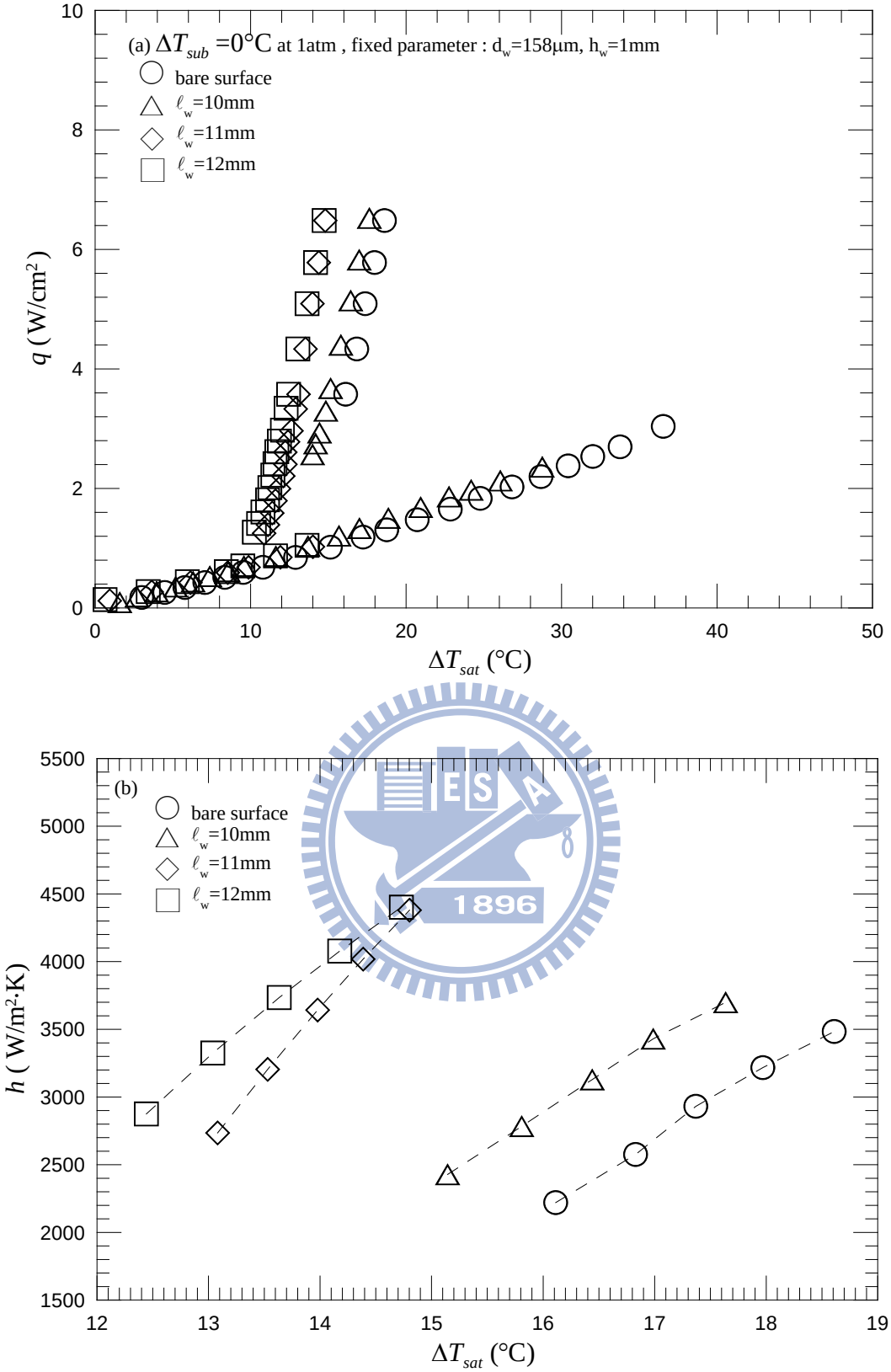

Fig. 4.25 Effects of string length on saturated pool boiling curves (a) and boiling heat transfer coefficients (b) at d_w=158μm and h_w=1mm.

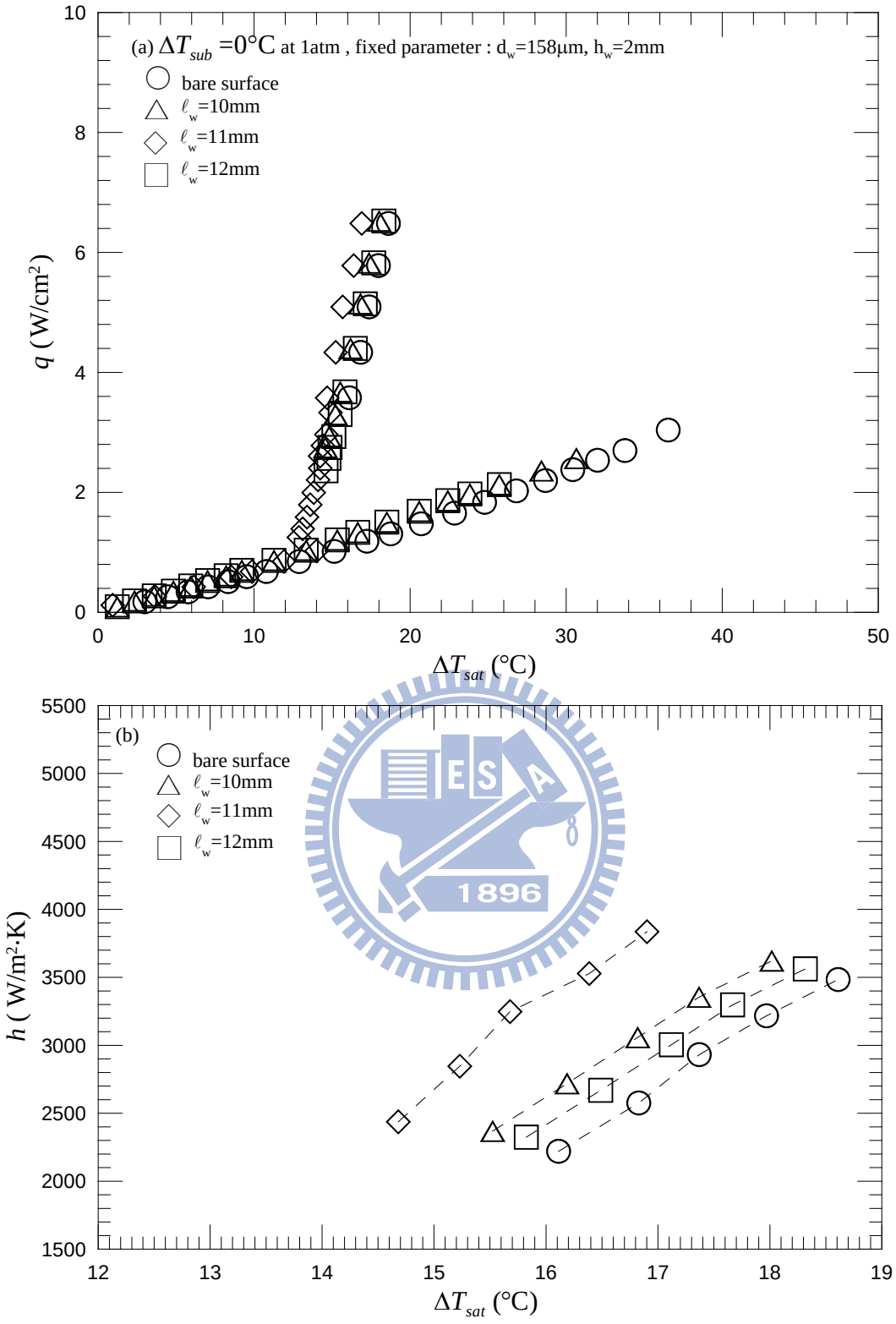

Fig. 4.26 Effects of string length on saturated pool boiling curves (a) and boiling heat transfer coefficients (b) at d_w=158μm and h_w=2mm.

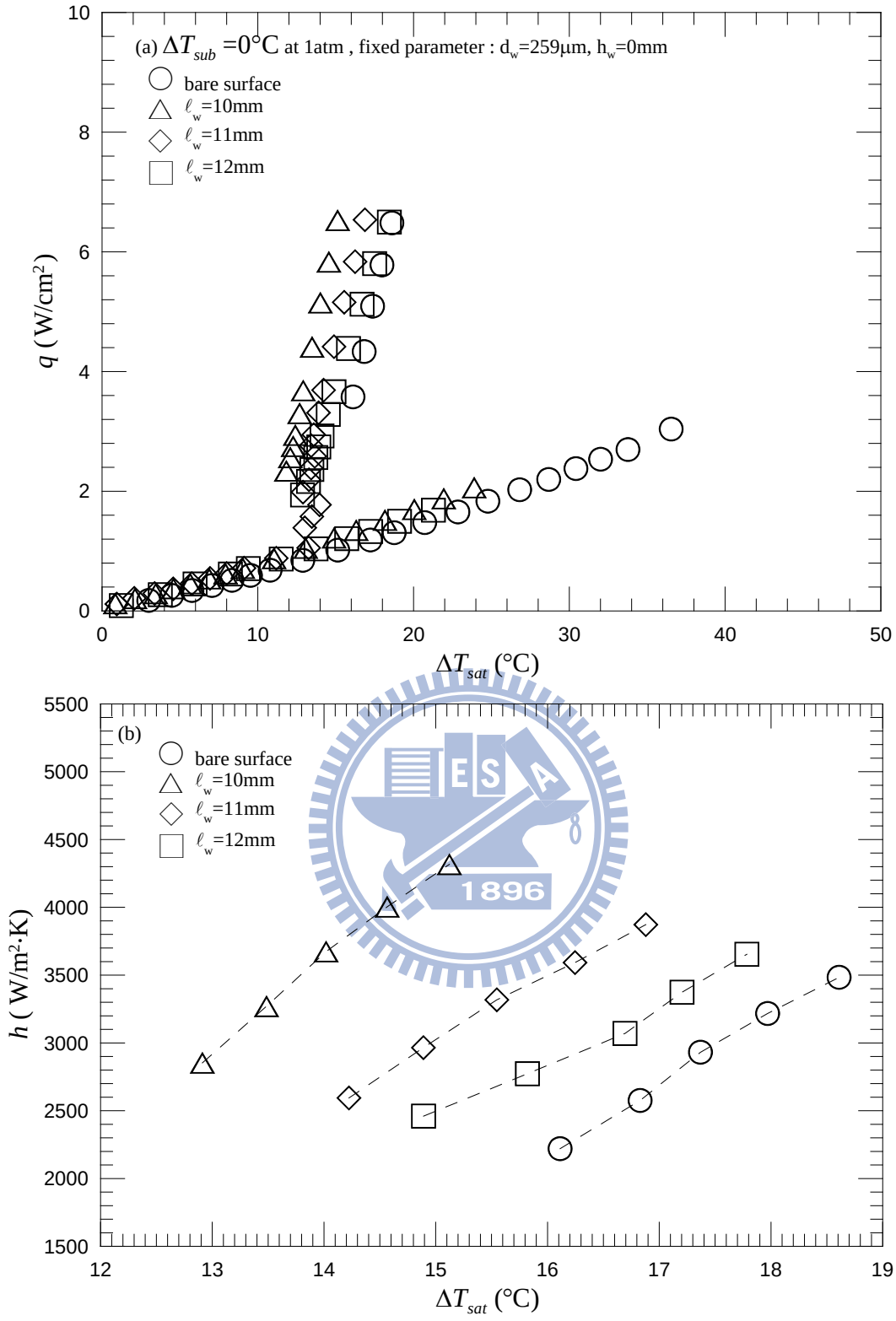

Fig. 4.27 Effects of string length on saturated pool boiling curves (a) and boiling heat transfer coefficients (b) at d_w=259μm and h_w=0mm.

.

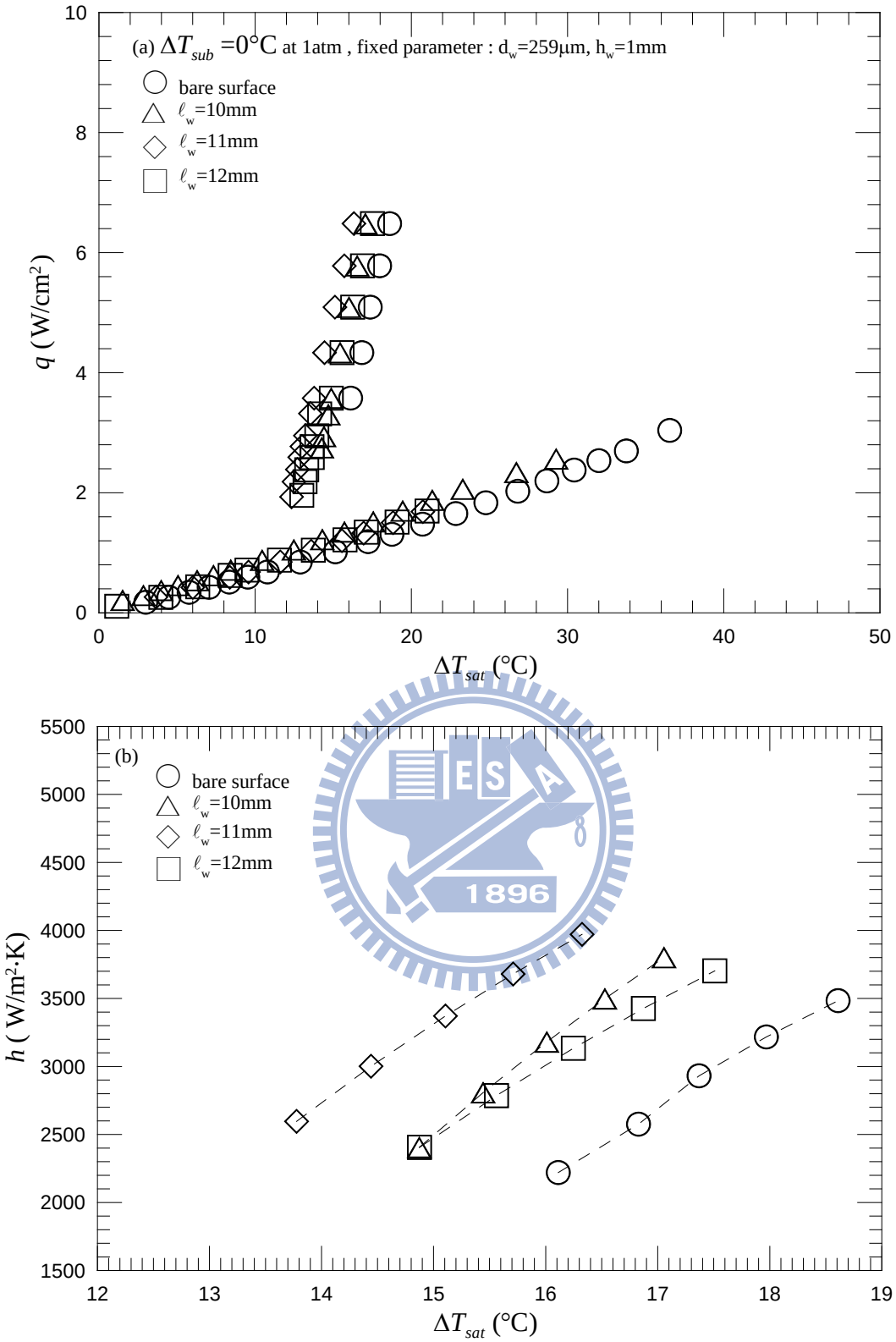

Fig. 4.28 Effects of string length on saturated pool boiling curves (a) and boiling heat transfer coefficients (b) at d_w=259μm and h_w=1mm.

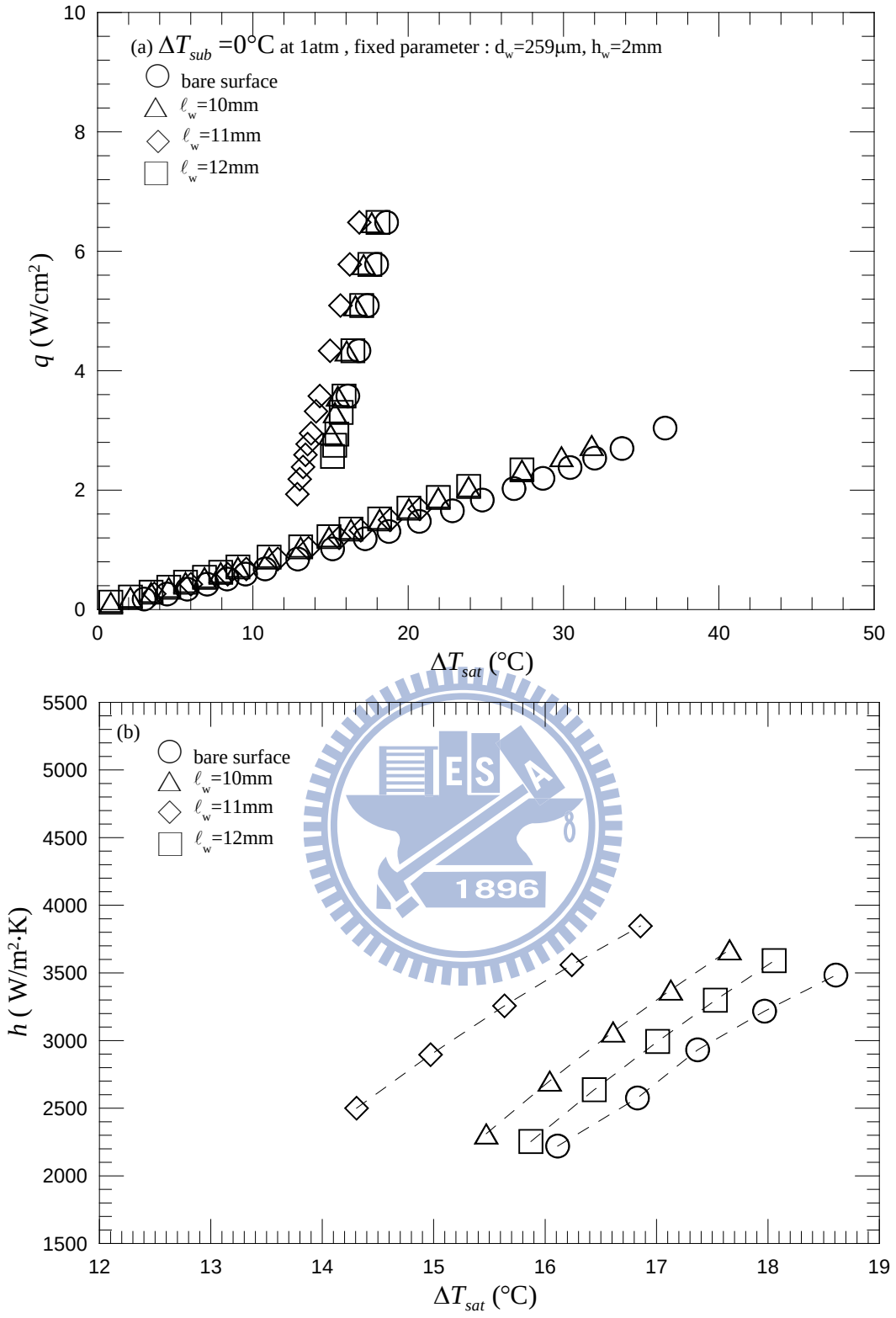

Fig. 4.29 Effects of string length on saturated pool boiling curves (a) and boiling heat transfer coefficients (b) at d_w=259μm and h_w=2mm.

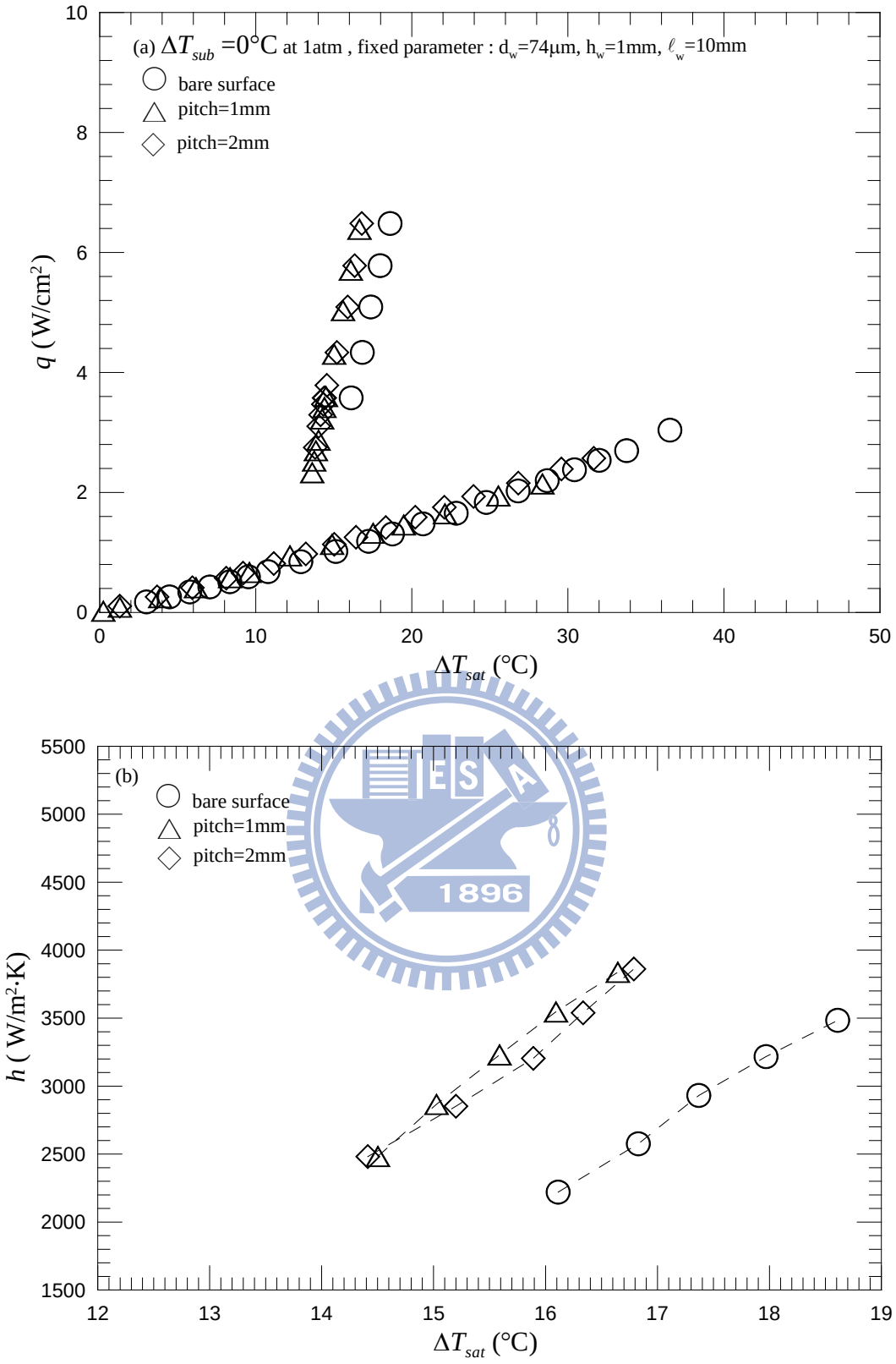

Fig. 4.30 Effects of string-string pitch on saturated pool boiling curves (a) and boiling heat transfer coefficients (b) at d_w=74μm, h_w=1mm and ℓ_w =10mm.

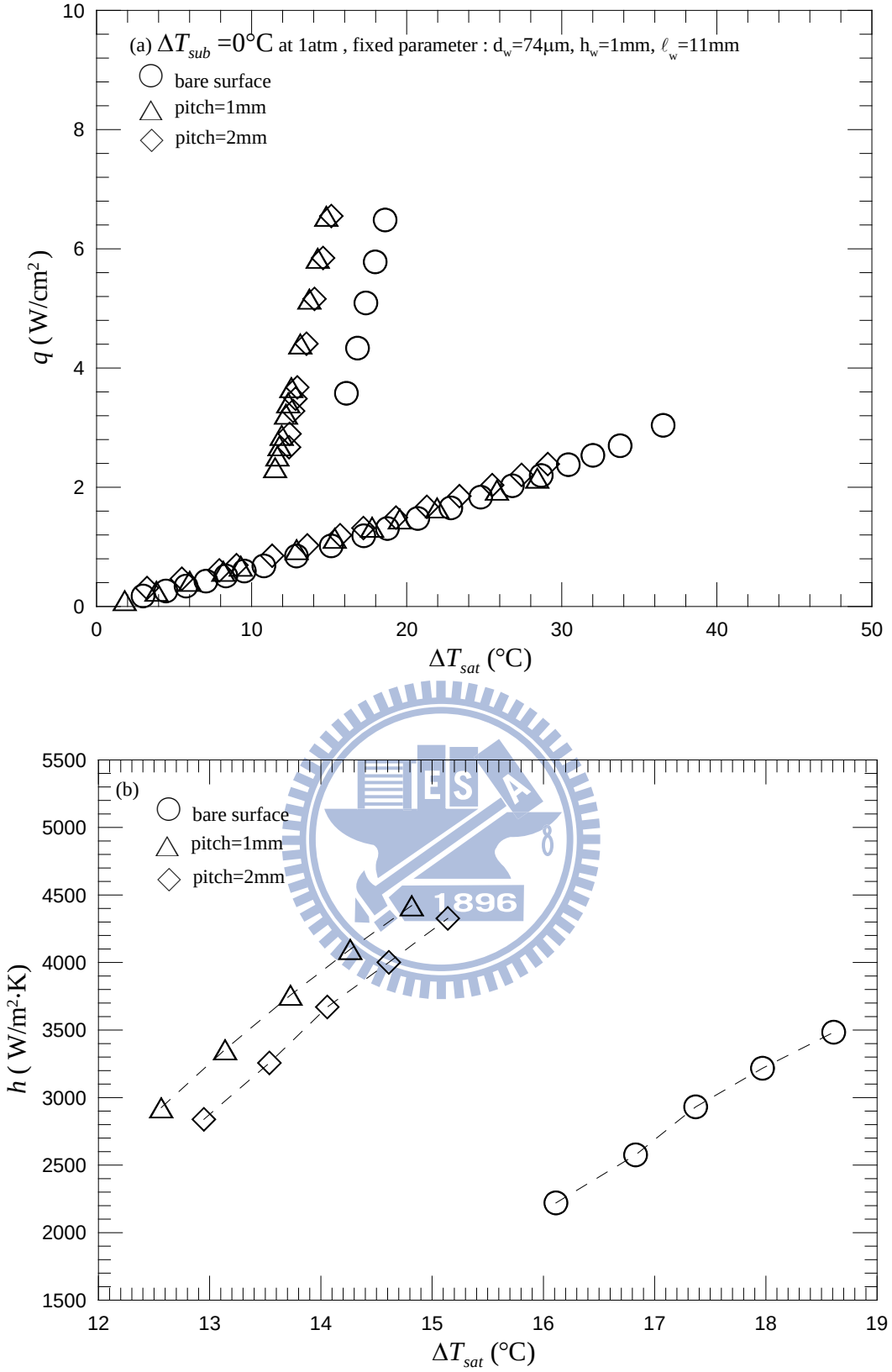

Fig. 4.31 Effects of string-string pitch on saturated pool boiling curves (a) and boiling heat transfer coefficients (b) at d_w=74μm, h_w=1mm and ℓ_w =11mm.

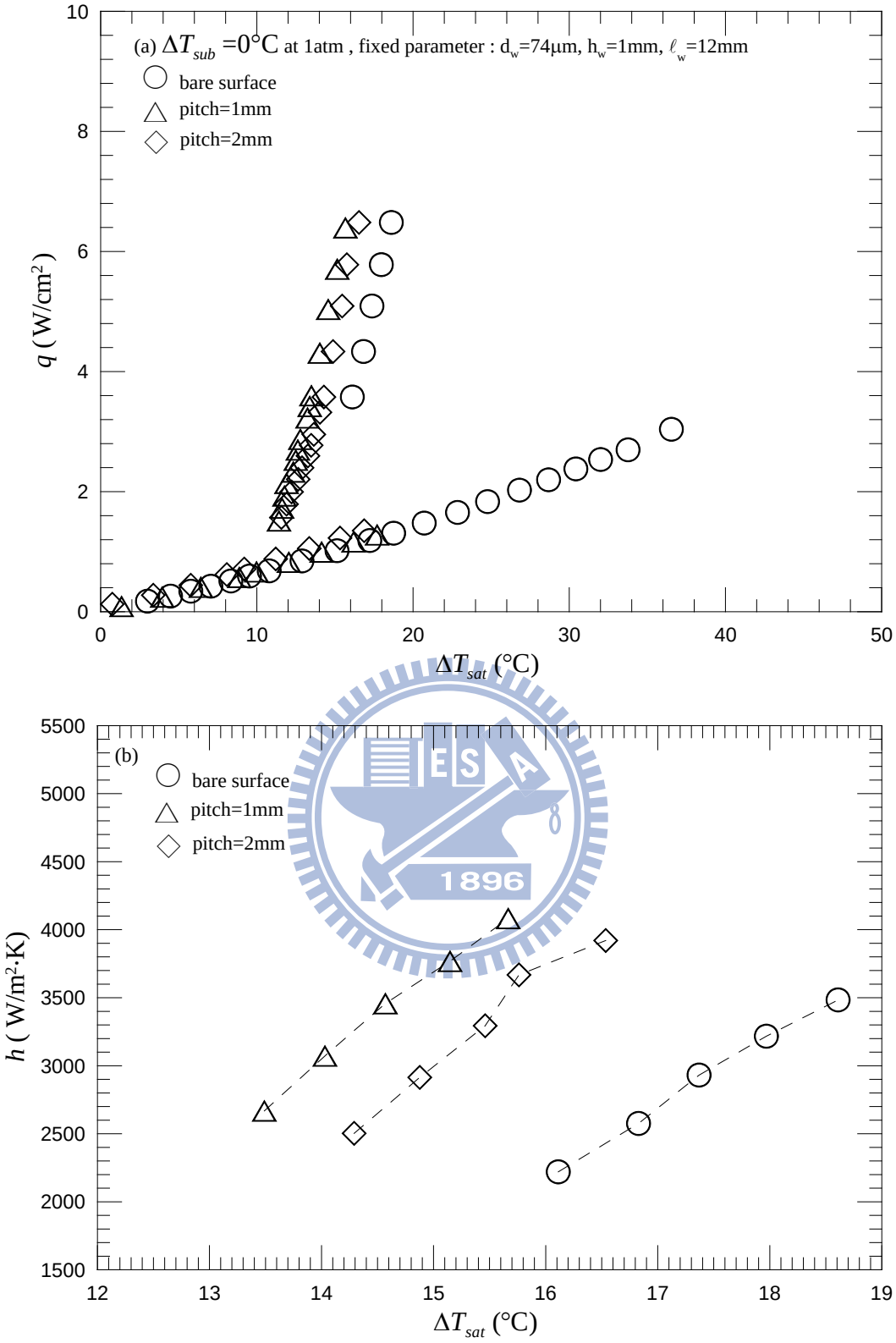

Fig. 4.32 Effects of string-string pitch on saturated pool boiling curves (a) and boiling heat transfer coefficients (b) at d_w=74μm, h_w=1mm and ℓ_w =12mm.

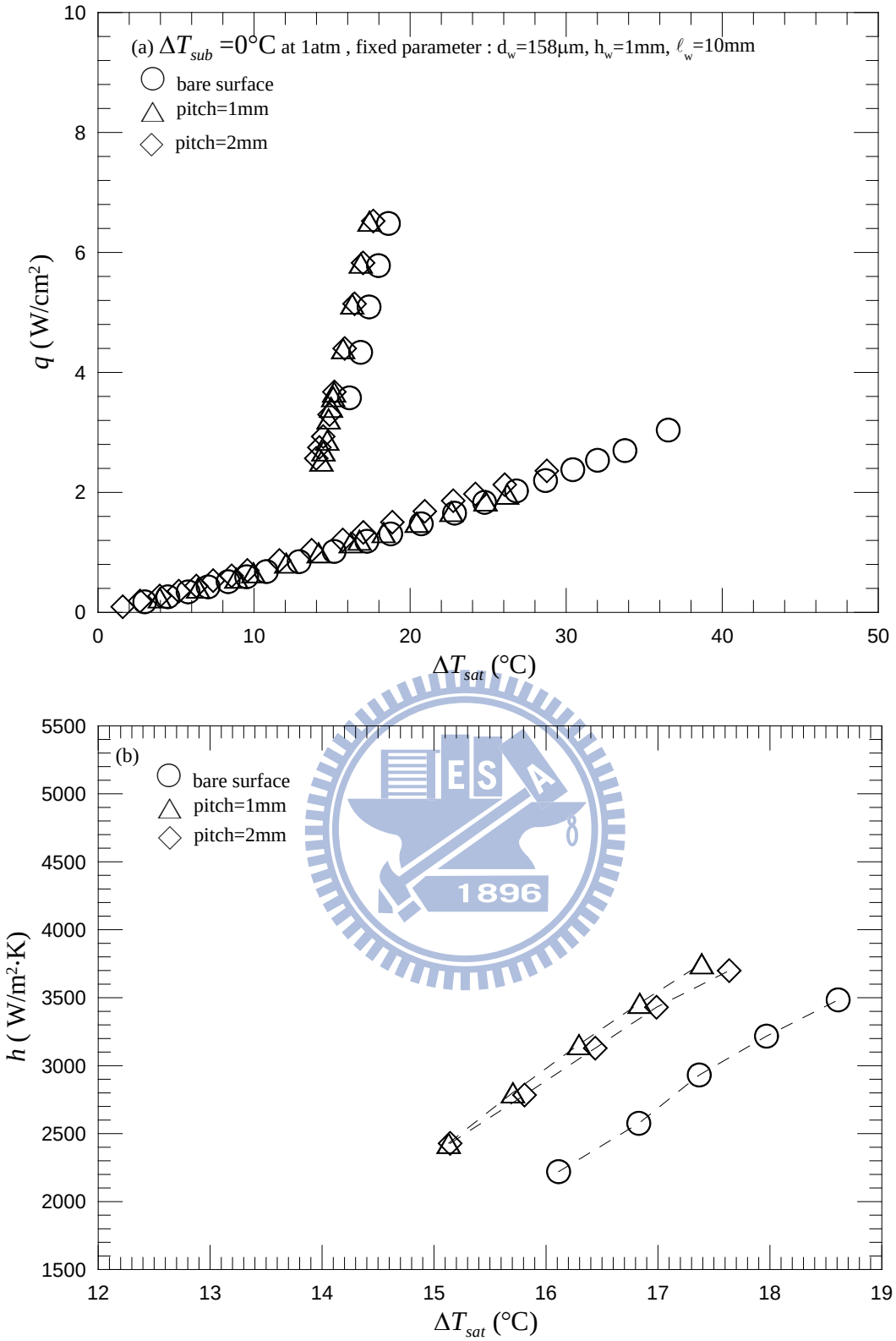

Fig. 4.33 Effects of string-string pitch on saturated pool boiling curves (a) and boiling heat transfer coefficients (b) at d_w=158μm, h_w=1mm and ℓ_w=10mm.

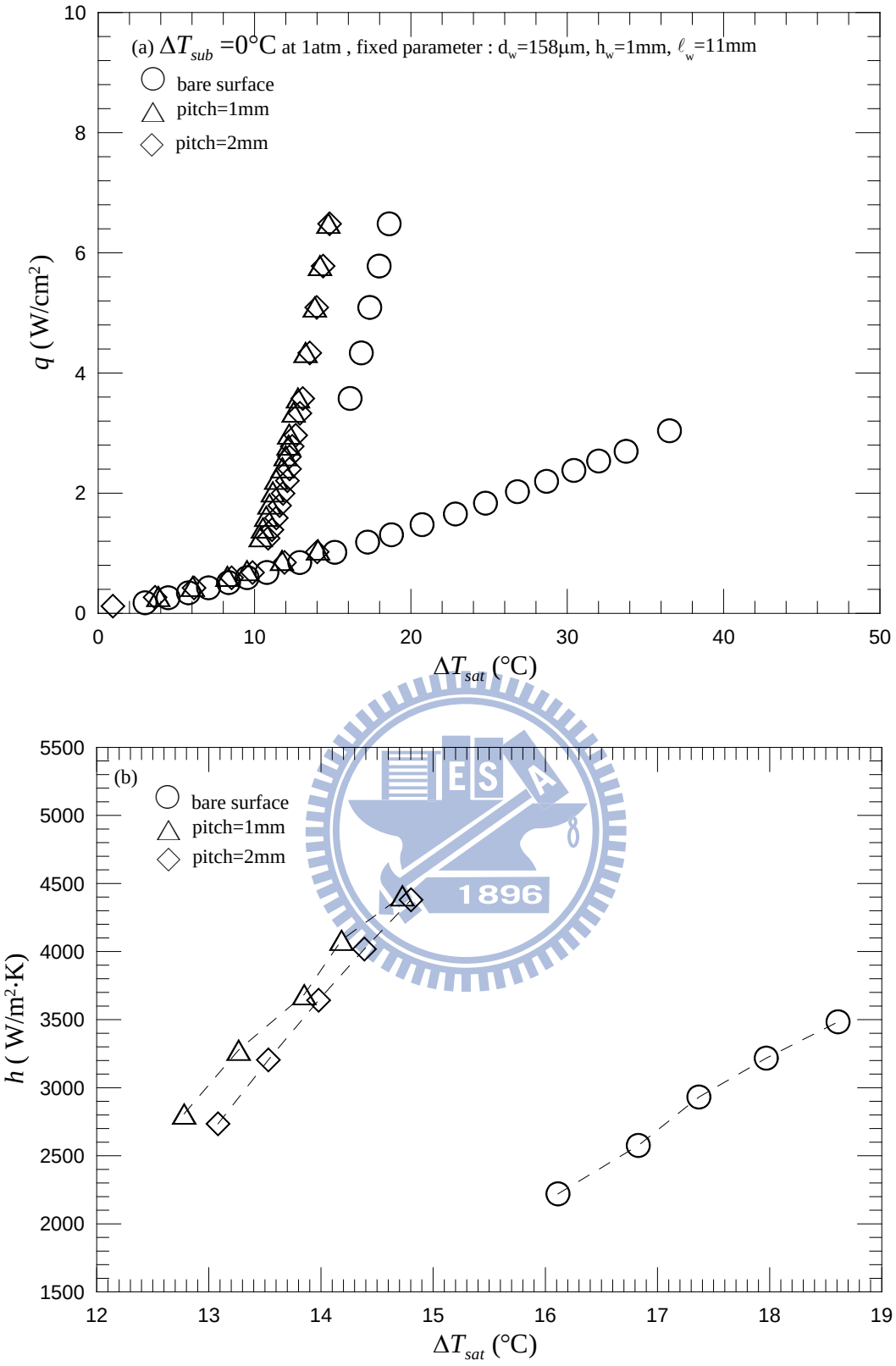

Fig. 4.34 Effects of string-string pitch on saturated pool boiling curves (a) and boiling heat transfer coefficients (b) at d_w=158μm, h_w=1mm and ℓ_w =11mm.

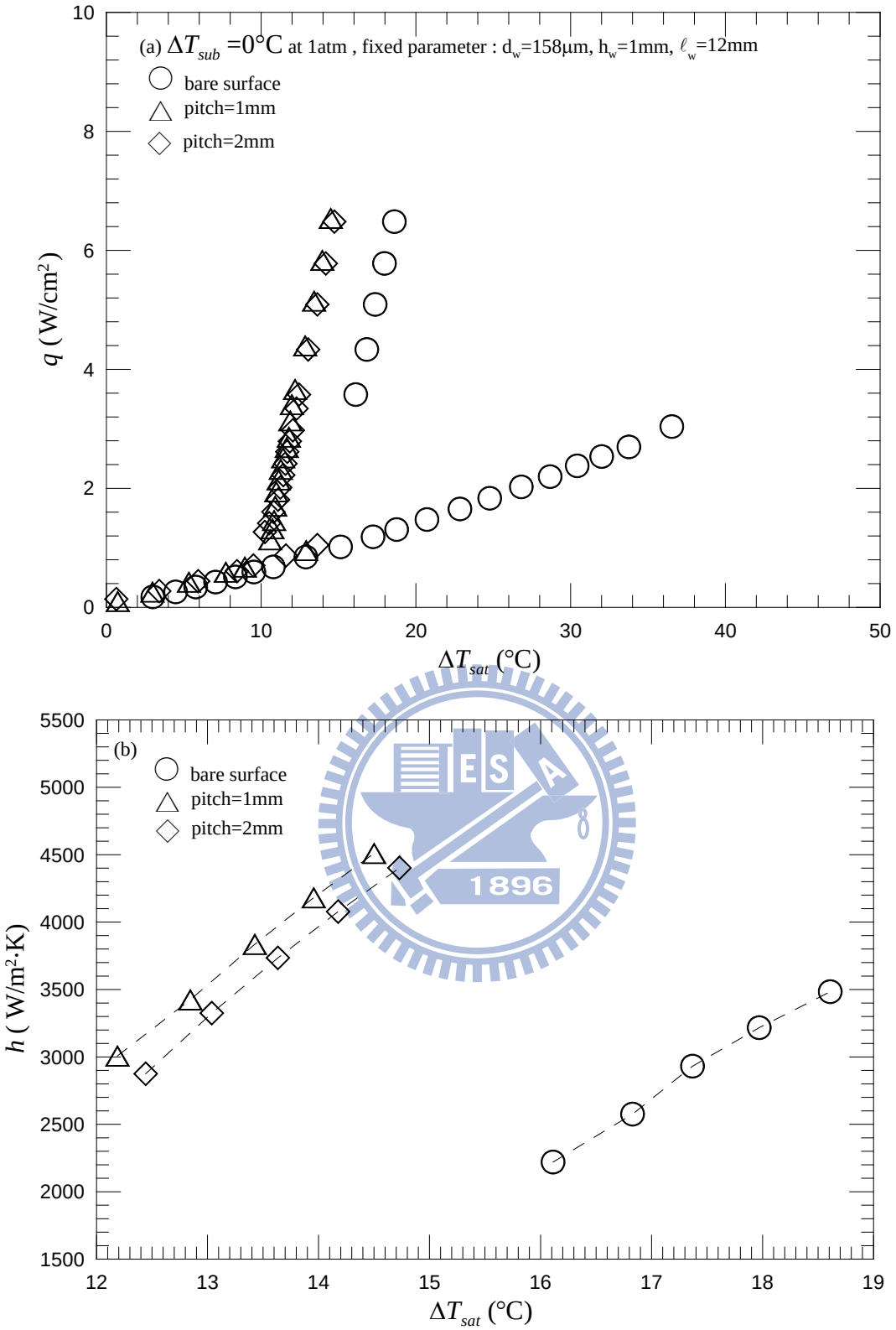

Fig. 4.35 Effects of string-string pitch on saturated pool boiling curves (a) and boiling heat transfer coefficients (b) at d_w=158μm, h_w=1mm and ℓ_w=12mm.

CHAPTER 5

SUBCOOLED POOL BOILING HEAT TRANSFER ENHANCEMENT OF FC-72 OVER A SMALL HEATED HORIZONTAL COPPER SURFACE

The data obtained in the second part of this study are presented in this chapter to illustrate the possible enhancement of subcooled pool boiling heat transfer of FC-72 by placing flexible strings above the heating surface. The liquid subcooling in the FC-72 inside the container is chosen to be at 5°C and 10°C. The coolant FC-72 in the test chamber is at the atmospheric pressure of 101.3 kPa with T_{sat}=56°C for FC-72. Selected data again are presented here to demonstrate the effects of the flexible strings on the FC-72 subcooled pool boiling heat transfer enhancement.

5.1 Subcooled Pool Boiling on Bare Copper Surface

In their study of boiling heat transfer of FC-72 from microporous surface, Rainey et al. [17] noted that the nucleate boiling curves collapse onto a single line regardless of the subcooling temperature and a higher subcooling level causes higher natural convection heat transfer before the onset of nucleate boiling. The boiling curves from the present study of the subcooled pool boiling heat transfer of FC-72 over a bare heated shown in Fig. 5.1 also exhibit these characteristics.

5.2 Effects of String Diameter on Subcooled Pool Boiling Heat Transfer Enhancement

At first, the effects of the string diameter on the subcooled nucleate boiling heat transfer of FC-72 over the small heated copper surface are illustrated by the boiling curves and boiling heat transfer coefficients in Figs. 5.2-5.10 for the liquid subcooling

of 5°C and in Figs. 5.11-5.19 for the liquid subcooling of 10°C. For comparison purpose the measured data for FC-72 over the bare surface without the presence of the strings are also given in these plots. The results in Fig. 5.2 for ΔT_{sub}=5°C show that when the strings are tight at ℓ_w=10mm and directly contact the heated surface at h_w=0 mm the boiling heat transfer coefficients are substantially higher with the installation of the flexible strings than that for the bare surface. More specifically, the boiling heat transfer enhancement is most prominent for the large-diameter strings with d_w=259 μm. An enhancement of more than 100% can be reached when compared to the bare surface. The enhancements for the medium- and small-diameter strings with d_w=158 μm & 74 μm are very close. We also note that the onset of nucleate boiling is significantly earlier with the string installation. Similar trend can be seen in Fig. 5.11 at higher liquid subcooling of 10°C except that the boiling heat transfer for the small-diameter strings becomes better than the medium-diameter strings as the wall superheat increases. As the strings are loosened slightly at ℓ_w=11 mm but still contact the boiling surface the results in Figs. 5.3 and 5.12 for ΔT_{sub}=5°C & 10°C indicate that the extents of the boiling heat transfer enhancements for the three different string sizes do not differ greatly from each other. For a further increase in the looseness of the strings to ℓ_w=12mm the large strings, however, only result in a small boiling heat transfer enhancement. The boiling heat transfer is substantially enhanced by the small- and medium-diameter strings for ΔT_{sub}=5°C & 10°C (Figs.5.4 and 5.13). Besides, the enhancements for these two strings are rather close and they increase with the wall superheat.

The effects of the string diameter on the boiling heat transfer enhancement are somewhat different when the strings are installed at a slightly higher position with the separation distance between the strings and heated surface h_w=1 mm. Note that when strings are tightly fixed at ℓ_w=10mm the data in Fig. 5.5(b) and 5.14(b) show that

the enhancement is largest for the small-diameter strings. Besides, the medium- and large-diameter strings causes a similar degree of the enhancement for ΔT_{sub}=5°C. But at ΔT_{sub}=10°C the enhancement is larger for a smaller string size. This trend is also noted when the strings are loosened slightly at ℓ_w=11 mm, as evident from the data given in Figs. 5.6 and 5.15. But for a further loosening of the strings to ℓ_w=12 mm the installation of the medium-diameter strings results in the best boiling heat transfer enhancement (Figs. 5.7 and 5.16). And the large-diameter strings provide the worst enhancement.

It is of interest to note from the data given in Figs. 5.8-5.10 for ΔT_{sub}=5°C and in 5.17-19 for ΔT_{sub}=10°C that for the strings-surface separation distance is increased to 2 mm the effects of the string diameter on the boiling heat transfer enhancement is less pronounced. Besides, the enhancement is smaller. By and large at their higher string position the enhancement is largest for the small-diameter strings for all string length. Even for h_w=2 mm a boiling heat transfer enhancement of more than 80% can be procured at d_w=74 μm and ℓ_w=11 mm (Figs. 5.9 and 5.18).

The results presented above clearly indicate that in the subcooled pool boiling of FC-72 over the small heated surface the influences of the string diameter on the nucleate boiling heat transfer are also nonmonotonic, similar to that in saturated pool boiling examined in Chapter 4.

5.3 Effects of String Height on Subcooled Pool Boiling Heat Transfer Enhancement

Next, how the subcooled boiling heat transfer is affected by the height of the flexible strings are shown in Figs. 5.20-5.28 for ΔT_{sub}=5°C and in Figs. 5.29-5.37 for ΔT_{sub}=10°C. These data also indicate that the boiling heat transfer coefficient varies nonmobotonically with the string height. Note that for the small-diameter

strings tightly and loosely fixed at their ends at ℓ_w=10mm and 12mm the boiling heat transfer enhancement is larger for the strings closer to the heating surface, as evident from Figs. 5.20 & 5.22 and 5.29 & 5.31. But for a slightly loose strings at ℓ_w=11mm the enhancement is largest for the strings placed at a slightly higher position with h_w=1 mm (Figs. 5.21 and 5.30).

The data shown in Figs. 5.23 and 5.32 for the medium-diameter strings manifest that the boiling heat transfer enhancement is largest when the strings directly contact the heating surface as they are tightly fixed. But with a slightly looseness of the strings at ℓ_w=11mm both the strings placed at h_w=0 mm and 1 mm result in best boiling heat transfer performance (Fig. 5.24) at ΔT_{sub}=5°C. For the strings loosely fixed at ℓ_w=12mm again the strings placed at h_w=0 mm and 1 mm give a much better boiling heat transfer performance (Figs. 5.25 and 5.34).

A somewhat different situation arises when the large-diameter strings are installed. The data in Figs. 5.26 and 5.35 show that a best boiling heat transfer performance is obtained when the strings are tight and directly contace the heating surface. However, for the strings loosely fixed at ℓ_w=11mm and 12mm the effects of the string height on the boiling heat transfer enhancement are relatively mild (Figs. 5.27, 5.28, 5.36 & 5.37).

5.4 Effects of String Length on Subcooled Pool Boiling Heat Transfer Enhancement

Then, the effects of the string length on the boiling heat transfer enhancement are presented in Figs. 5.38-5.46 for ΔT_{sub}=5°C and in 5.47-5.55 for ΔT_{sub}=10°C. The data in Figs. 5.38 and 5.47 for the small-diameter strings indicate that for the strings directly contacting the heating surface the loosely fixed strings at ℓ_w=12mm result in the largest boiling heat transfer enhancement. But for the strings installed at a

higher position at h_w=1 mm and 2 mm the enhancement is largest for the slightly loosely fixed strings (Figs. 5.39, 5.40. 5.48 and 5.49).

For the medium-diameter strings we have the best boiling heat transfer enhancement for the loosely fixed strings at ℓ_w=12 mm when they are installed at h_w=0 mm and 1 mm, as clearly seen in Figs. 5.41, 5.42, 5.50 and 5.51. While for the strings fixed position at h_w=2 mm the slightly loose strings cause the largest enhancement (Figs.5.43 and 5.52). The situation is different for the large-diameter strings. As the strings directly contact the heating surface, the enhancement is most effective for the tightly fixed strings (ℓ_w=10 mm), as seen in Figs. 5.44 and 5.53. But for the strings placed at higher positions at h_w=1 mm and 2 mm the strings fixed slightly loosely at ℓ_w=11 mm provide the largest boiling heat transfer enhancement (Figs.5.45, 5.46, 5.54 and 5.55).

5.5 Effects of String Pitch on Subcooled Pool Boiling Heat Transfer Enhancement

Finally, we examine the effects of the string pitch on the boiling heat transfer in Figs. 5.56-5.67. The results in Figs 5.56-5.58 and Figs 5.62-5.64 for the small-diameter strings at d_w=74 μm and h_w=1 mm indicate that an reduction of the string pitch from 2 mm to 1 mm can enhance the boiling heat transfer to a larger degree by increase the string looseness. But for the mid-size strings (d_w=158 μm) the reduction in the string pitch only slightly affects the boiling heat transfer, as evident from the data shown in Figs 5.59-5.61 and Figs 5.65-5.67.

5.6 Bubble Characteristics

The qualitative characteristics of the bubble motion in the flow affected by the flexible strings are illustrated by the top view photos of the bubbly flow in Figs.

5.56-5.64 for various experimental parameters. The photos for the limiting case of the bare surface are also given here for comparison. Note that with the installation of the strings the pictures of the bubbles somewhat blur (Figs. 5.59, 5.61-5.64). This qualitatively reflects the increases of the bubble departure frequency and active nucleation site density resulting from the motion of the strings.

5.7 Concluding Remarks

In this chapter the enhancement of the subcooled boiling heat transfer of FC-72 over a small horizontal heated surface by installing nylon strings above the surface is explored. The effects of the string diameter, height and length on the boiling heat transfer enhancement are examined. The major results from their study can be summarized as follows.

(1) The degree of the subcooled boiling heat transfer enhanced by the flexible strings again depends strongly on all experimental parameters, namely, the string diameter, height and length and the liquid subcooling. The dependence is nonmonotonic.

(2) In the subcooled boiling a heat transfer enhancement of more than 100% can be procured by a proper choice of the experimental parameters.

(3) The bubble behavior near the heated surface is considered to be affected greatly by the string size, position and looseness. But the detail on how these parameters influence near-wall bubbles needs further investigation.

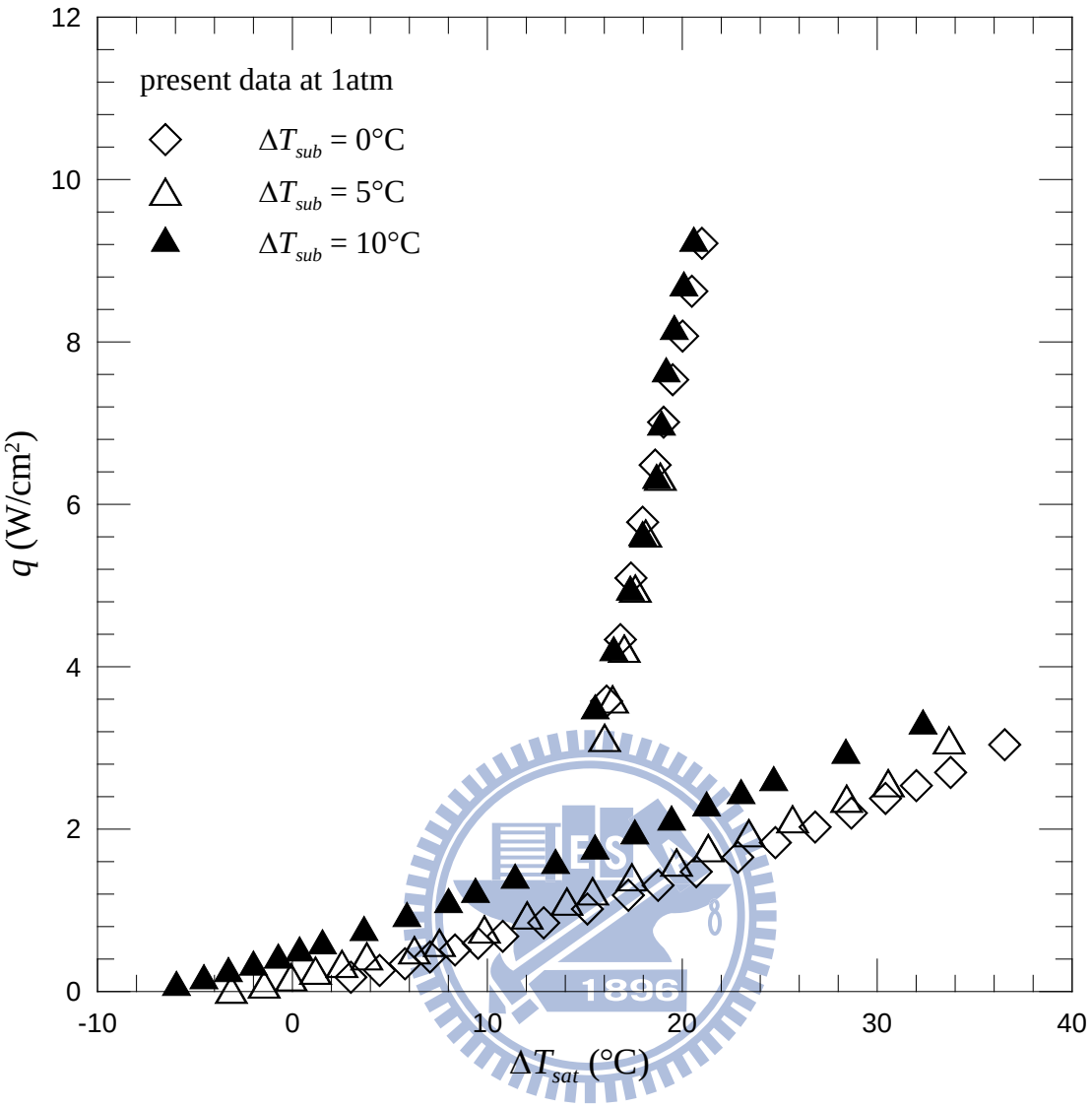

Fig. 5.1 Present data of saturated and subcooled boiling curve.

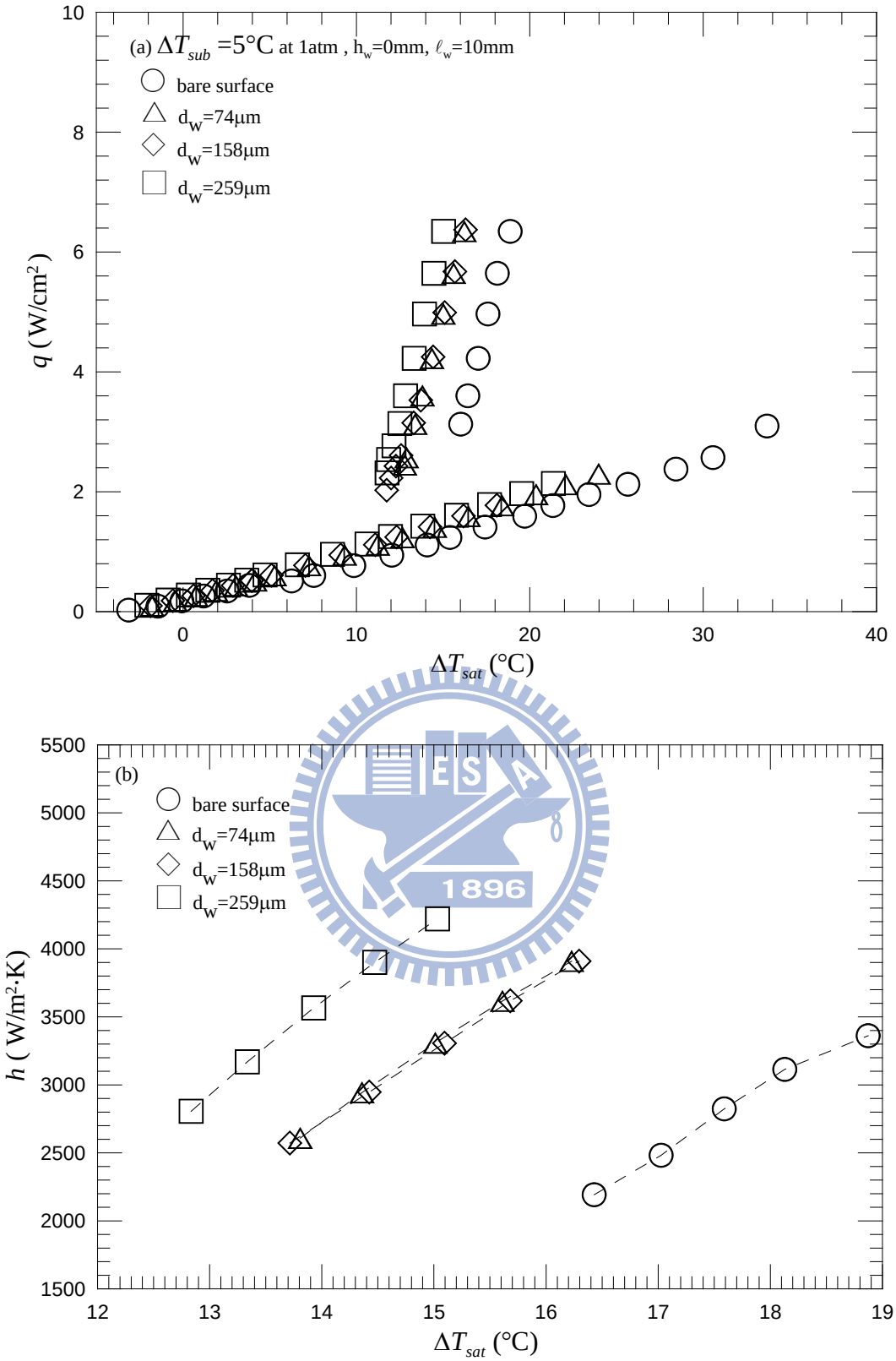

Fig. 5.2 Effects of string diameter on subcooled pool boiling curves (a) and boiling heat transfer coefficients (b) for ΔT_{sub}= 5°C at h_w=0mm and ℓ_w =10mm.

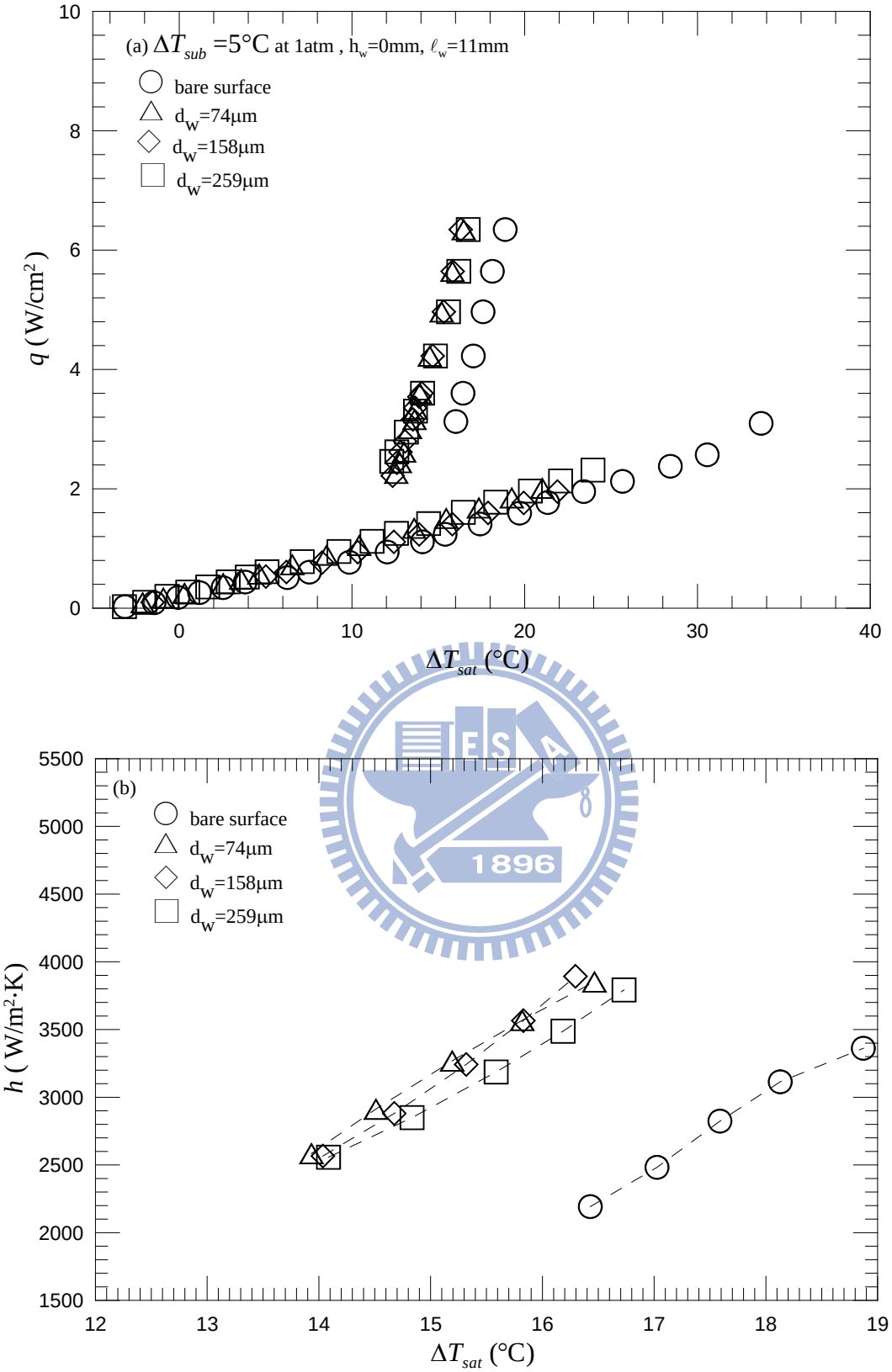

Fig. 5.3 Effects of string diameter on subcooled pool boiling curves (a) and boiling heat transfer coefficients (b) for ΔT_{sub}= 5°C at h_w=0mm and ℓ_w =11mm.

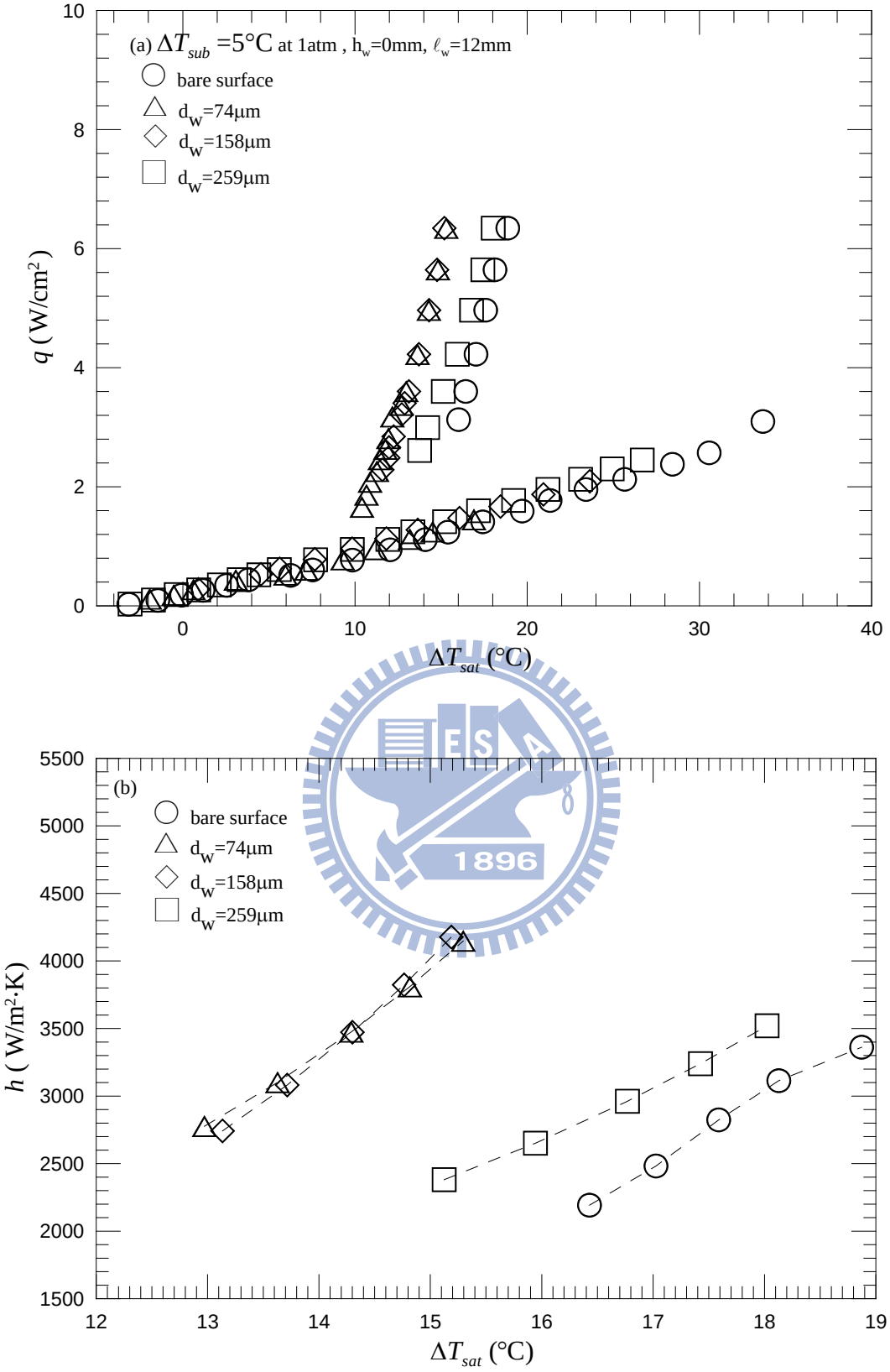

Fig. 5.4 Effects of string diameter on subcooled pool boiling curves (a) and boiling heat transfer coefficients (b) for ΔT_{sub}= 5°C at h_w=0mm and ℓ_w =12mm.

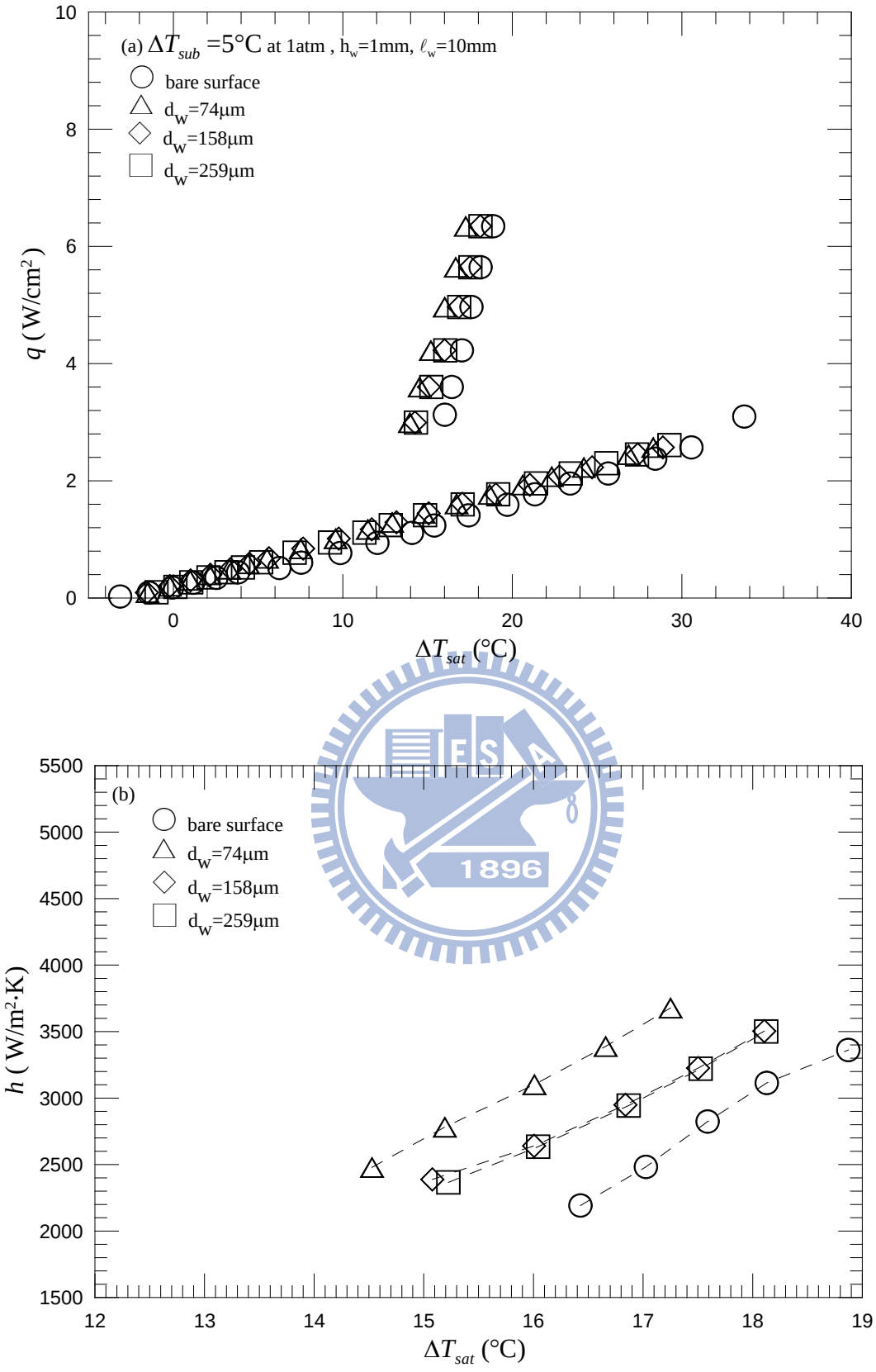

Fig. 5.5 Effects of string diameter on subcooled pool boiling curves (a) and boiling heat transfer coefficients (b) for ΔT_{sub}= 5°C at h_w=1mm and ℓ_w =10mm.

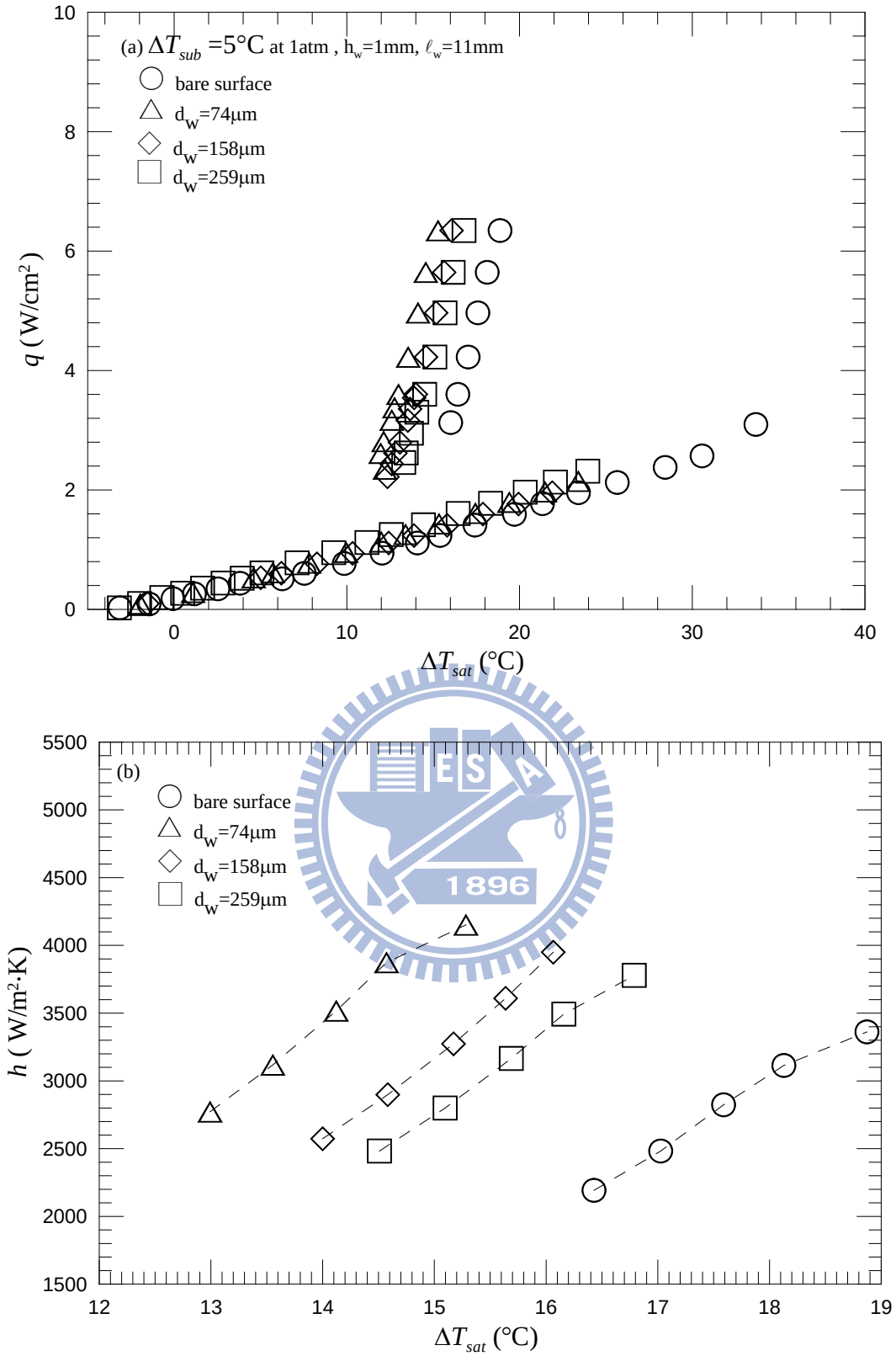

Fig. 5.6 Effects of string diameter on subcooled pool boiling curves (a) and boiling heat transfer coefficients (b) for ΔT_{sub}= 5°C at h_w=1mm and ℓ_w =11mm.

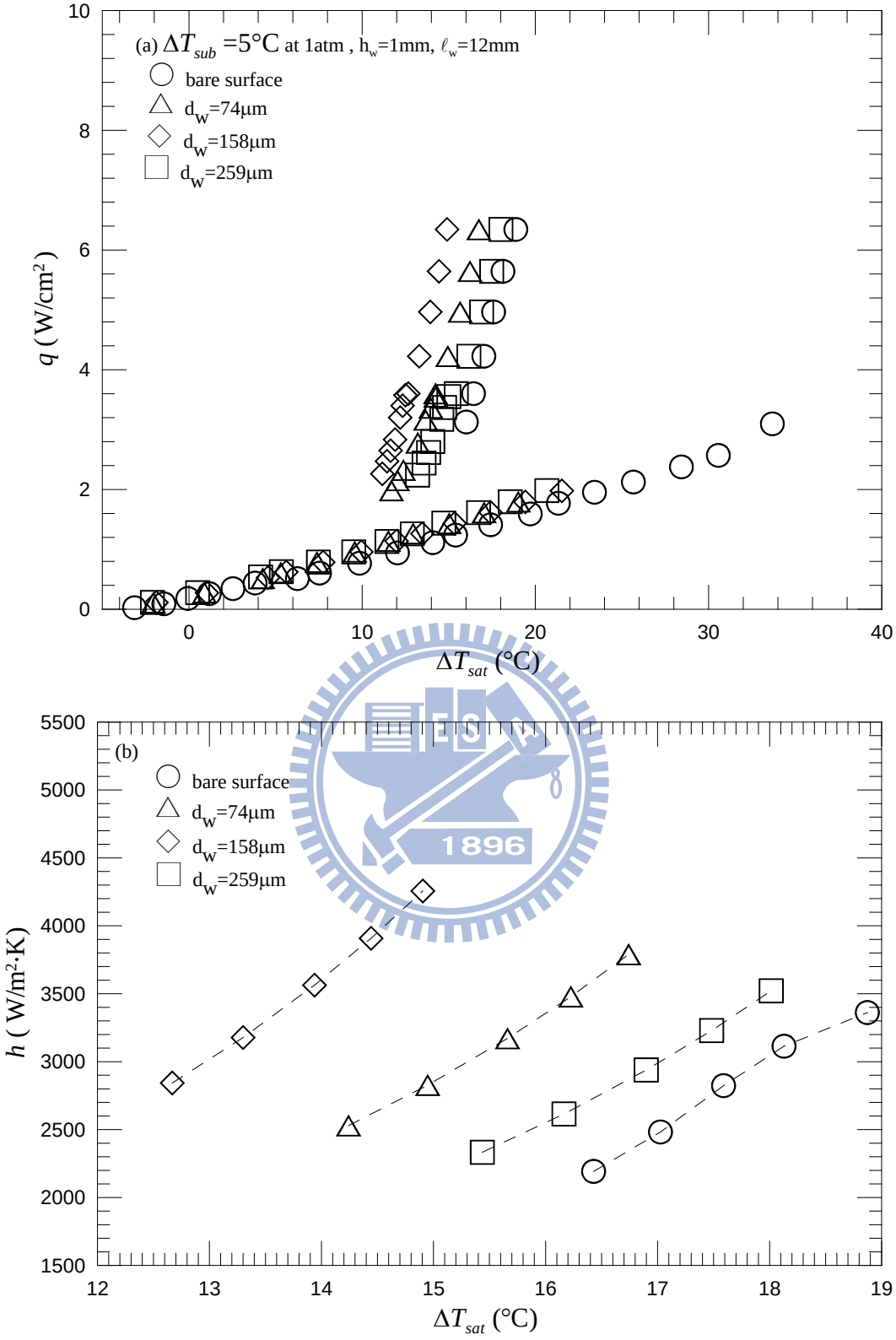

Fig. 5.7 Effects of string diameter on subcooled pool boiling curves (a) and boiling heat transfer coefficients (b) for ΔT_{sub}= 5°C at h_w=1mm and ℓ_w =12mm.

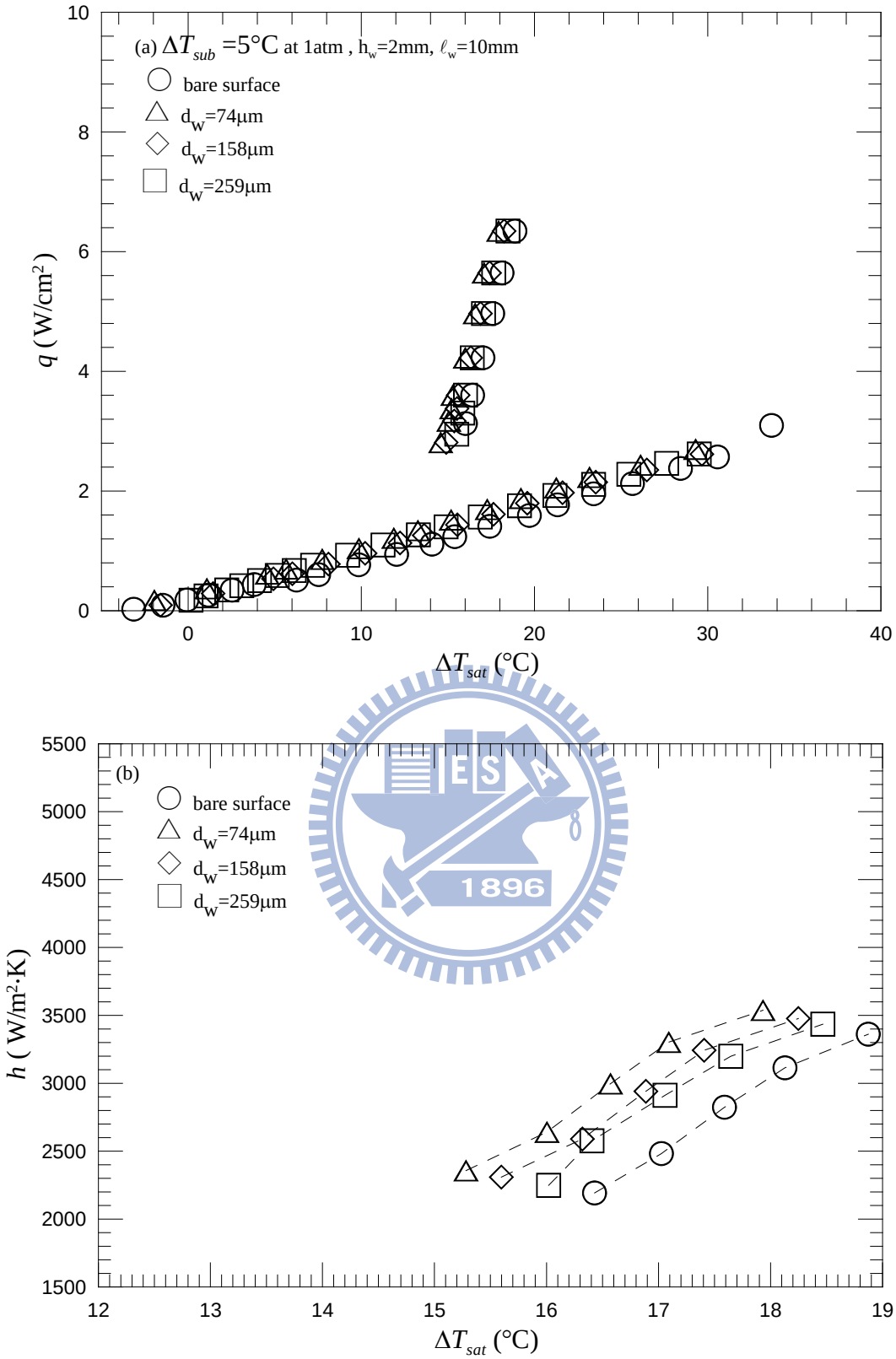

Fig. 5.8 Effects of string diameter on subcooled pool boiling curves (a) and boiling heat transfer coefficients (b) for ΔT_{sub}= 5°C at h_w=2mm and ℓ_w =10mm.

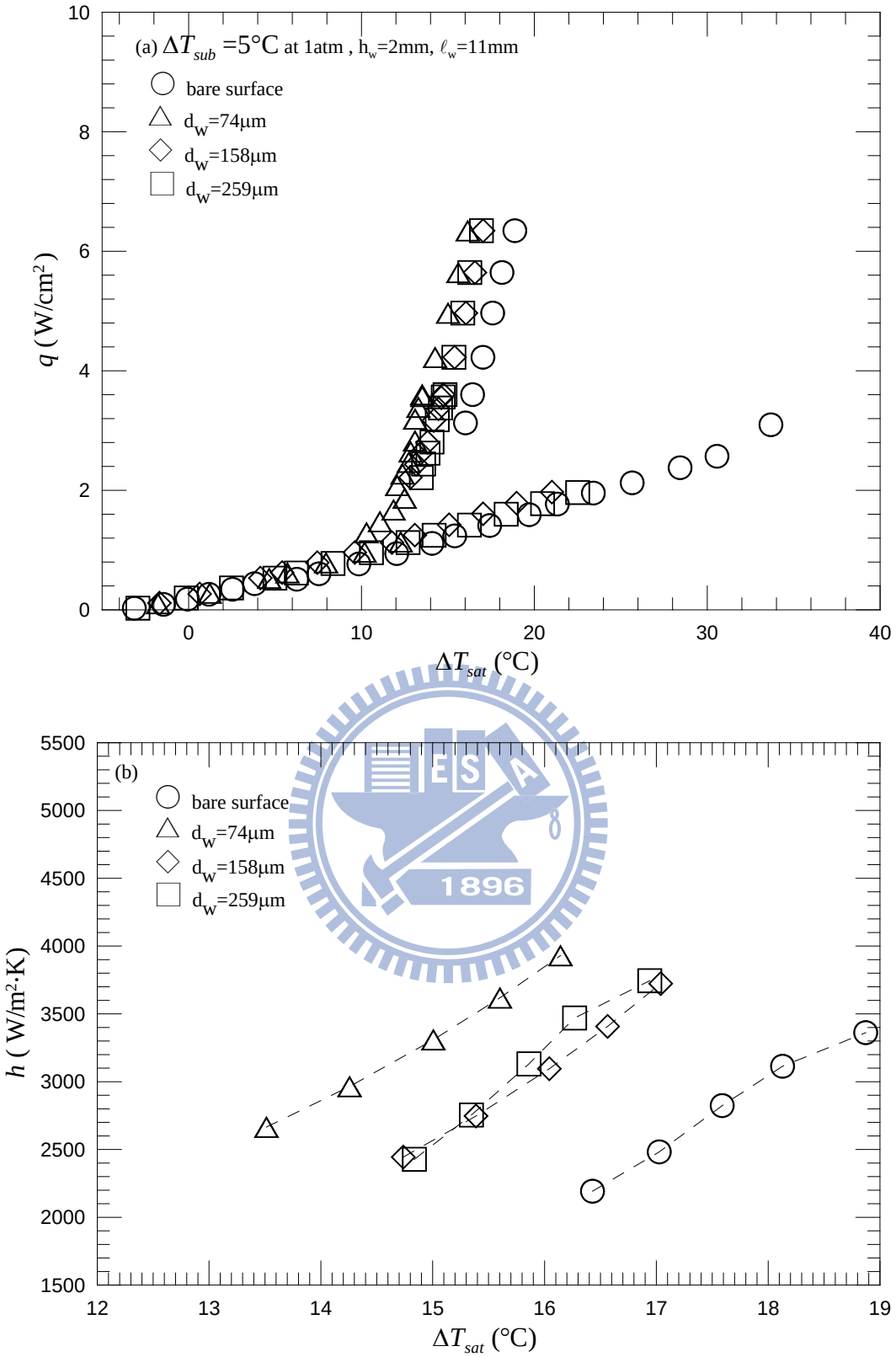

Fig. 5.9 Effects of string diameter on subcooled pool boiling curves (a) and boiling heat transfer coefficients (b) for ΔT_{sub}= 5°C at h_w=2mm and ℓ_w =11mm.

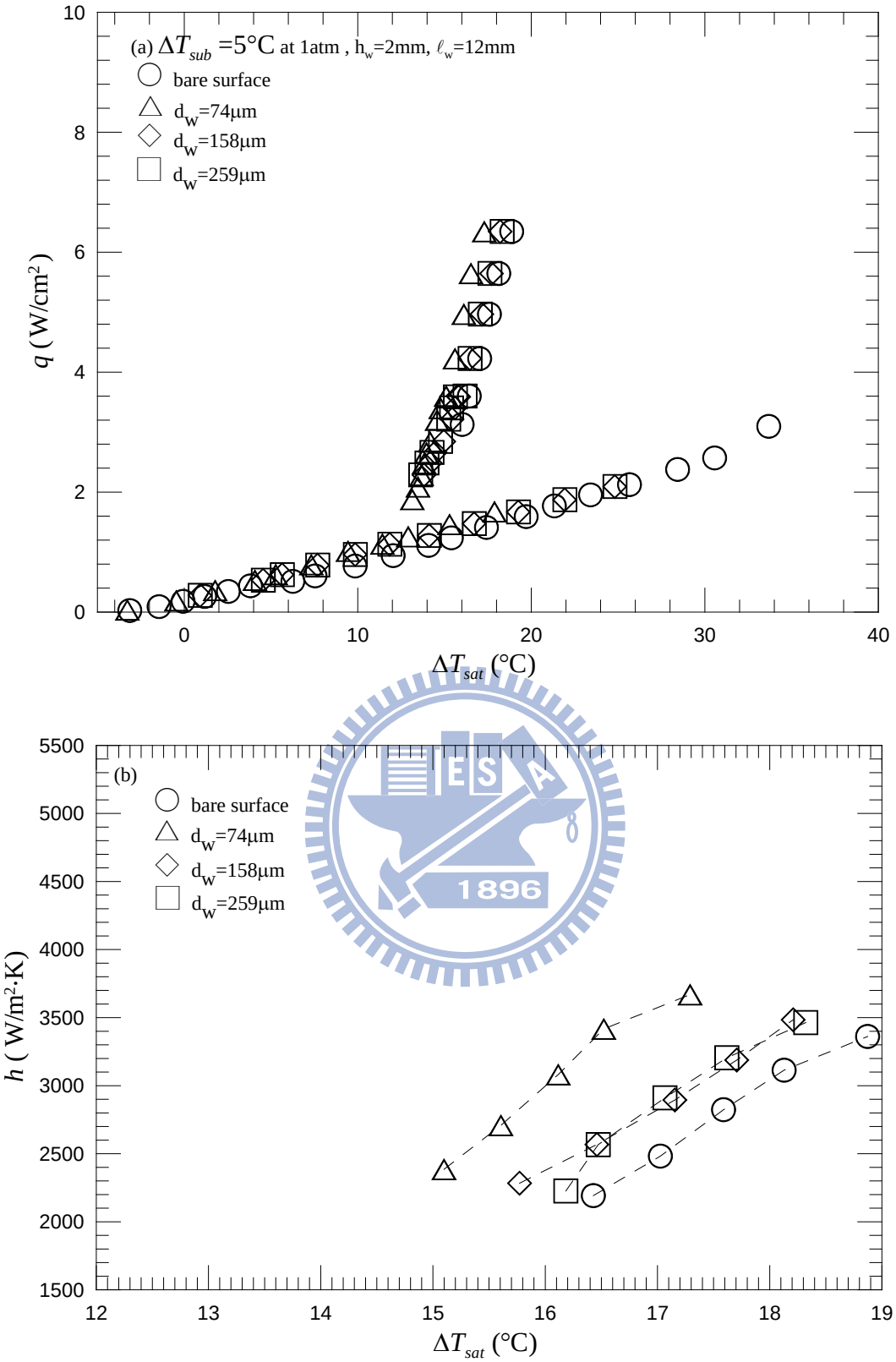

Fig. 5.10 Effects of string diameter on subcooled pool boiling curves (a) and boiling heat transfer coefficients (b) for ΔT_{sub}= 5°C at h_w=2mm and ℓ_w =12mm.

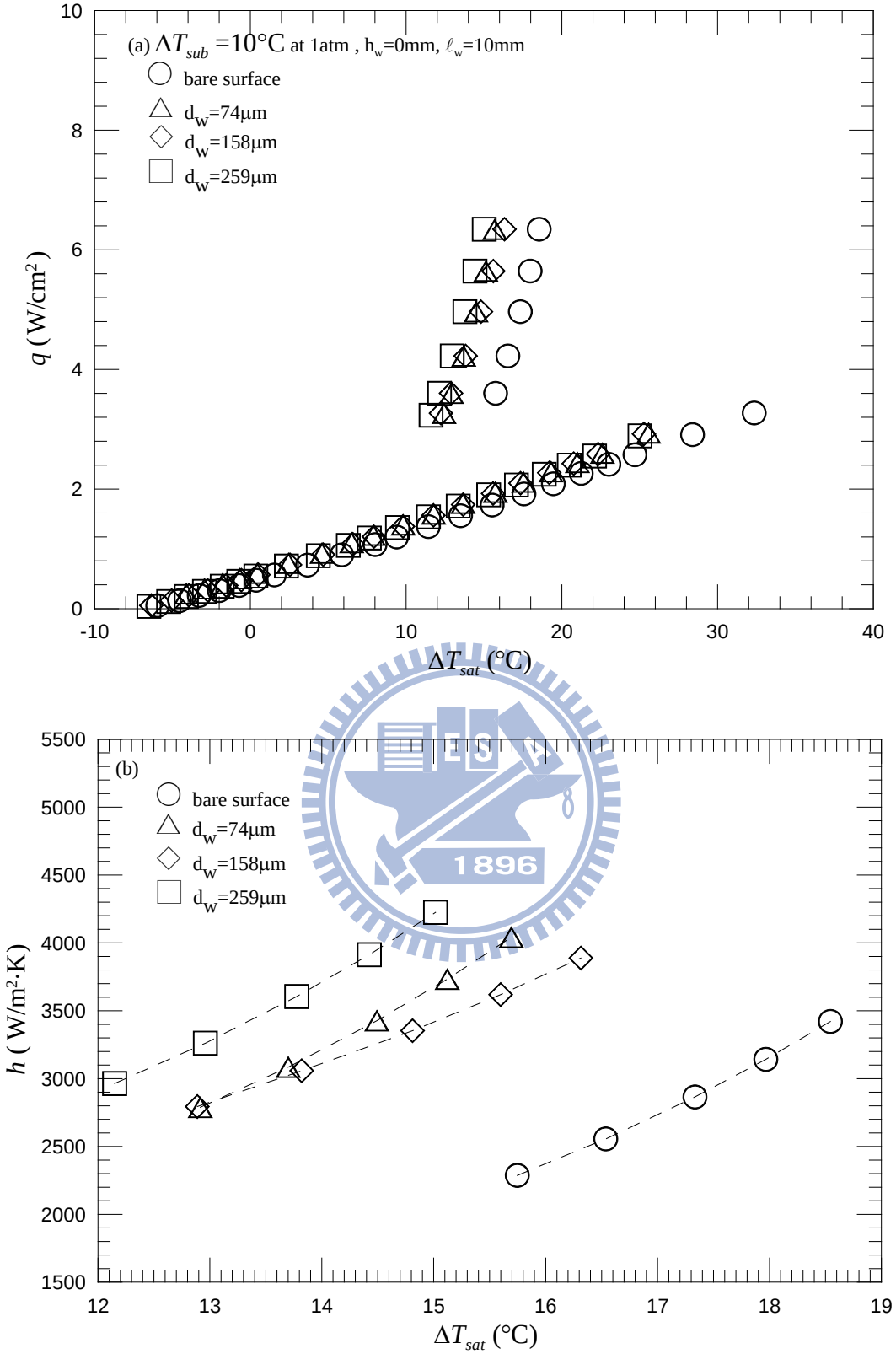

Fig. 5.11 Effects of string diameter on subcooled pool boiling curves (a) and boiling heat transfer coefficients (b) for ΔT_{sub}= 10°C at h_w=0mm and ℓ_w =10mm.

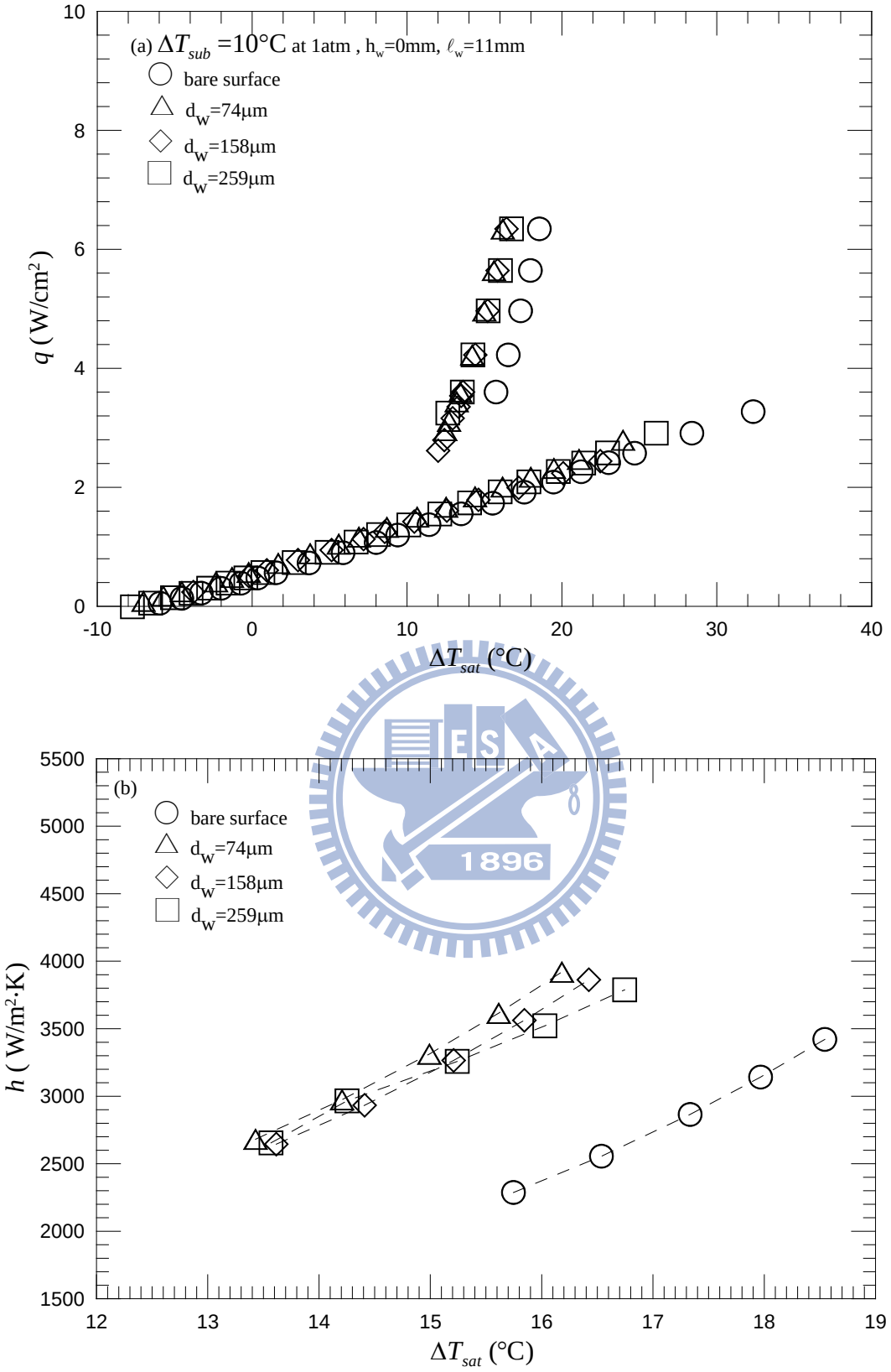

Fig. 5.12 Effects of string diameter on subcooled pool boiling curves (a) and boiling heat transfer coefficients (b) for ΔT_{sub}= 10°C at h_w=0mm and ℓ_w =11mm.

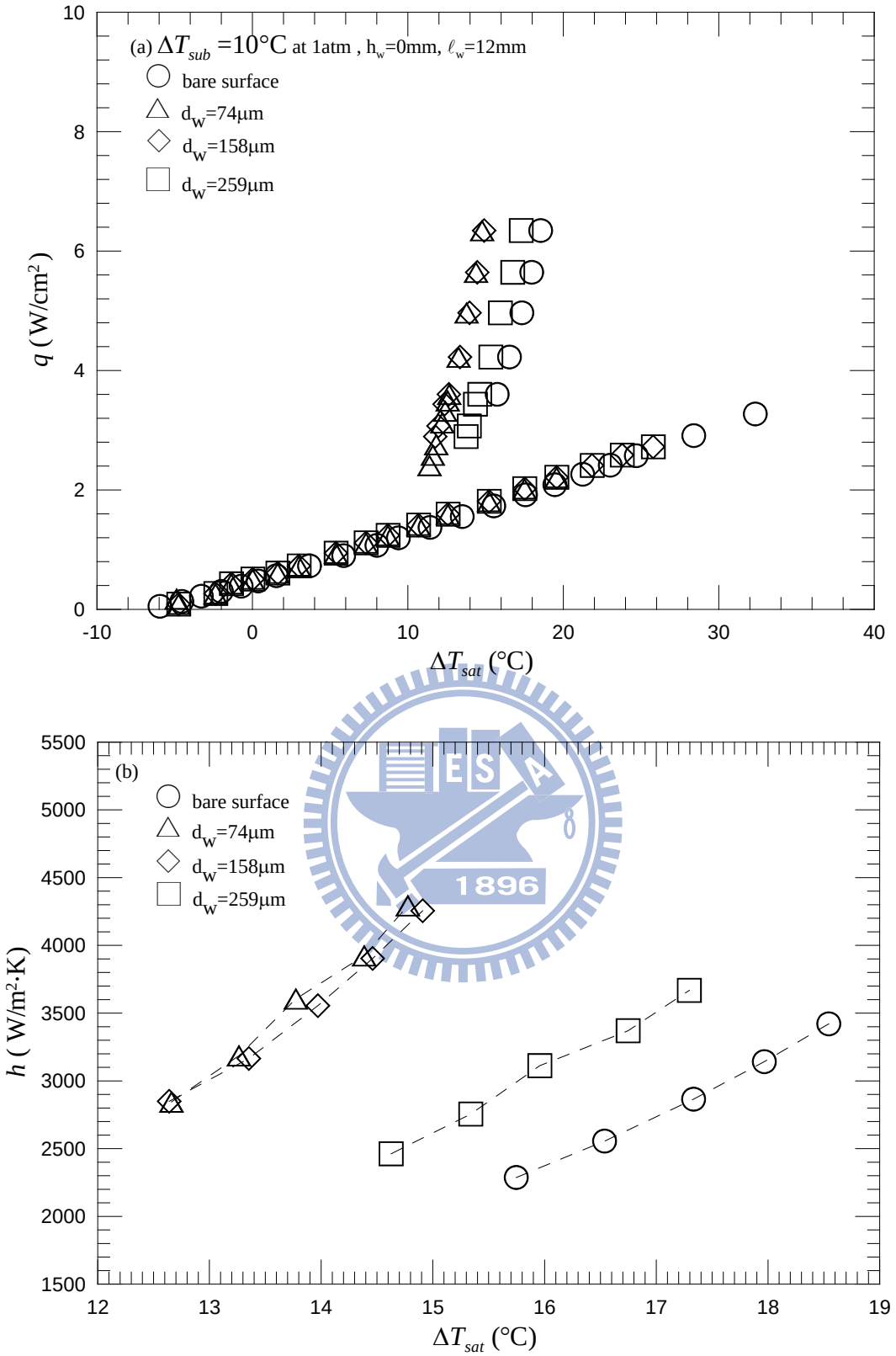

Fig. 5.13 Effects of string diameter on subcooled pool boiling curves (a) and boiling heat transfer coefficients (b) for ΔT_{sub}= 10°C at h_w=0mm and ℓ_w =12mm.

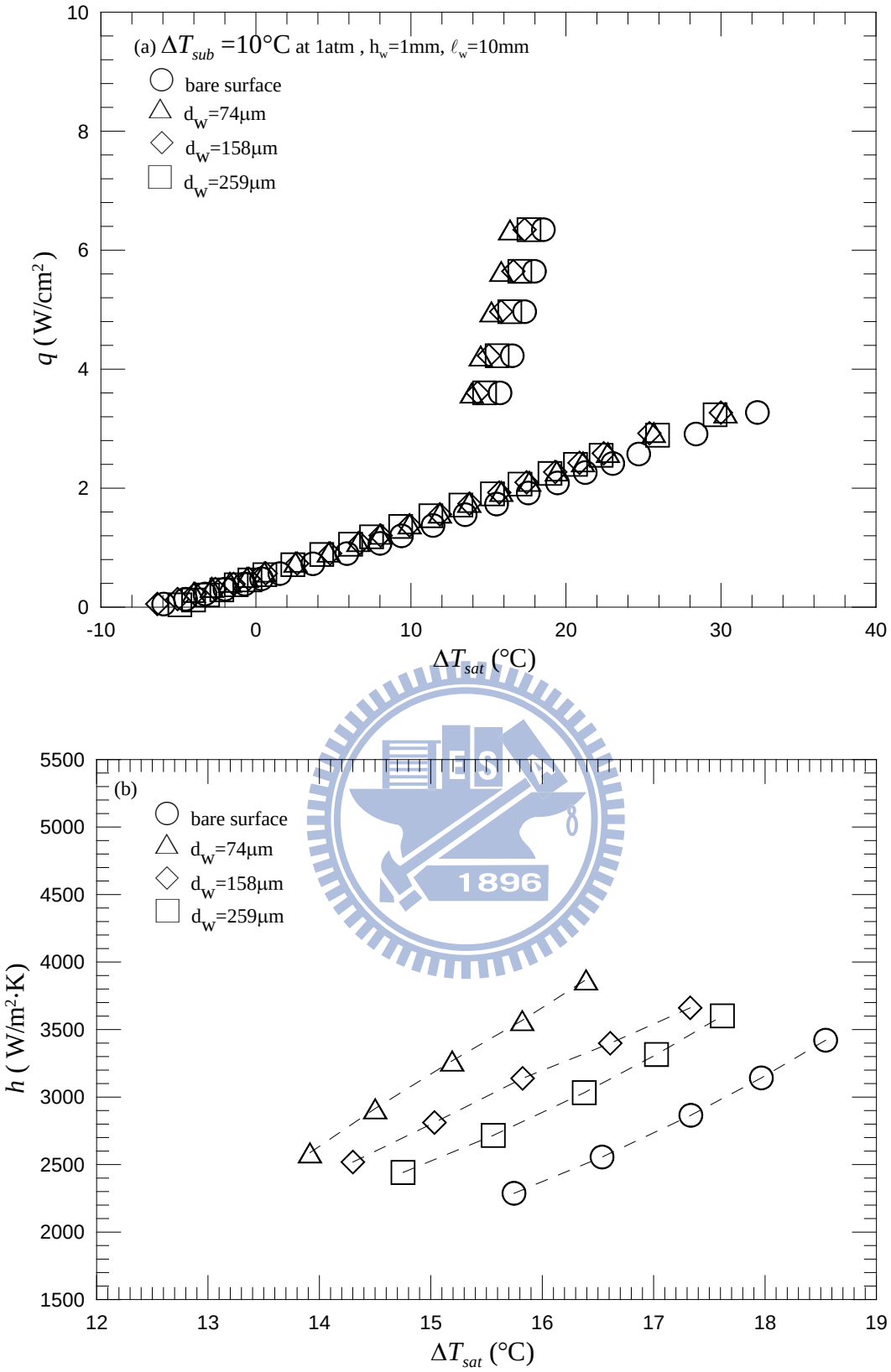

Fig. 5.14 Effects of string diameter on subcooled pool boiling curves (a) and boiling heat transfer coefficients (b) for ΔT_{sub}= 10°C at h_w=1mm and ℓ_w =10mm.

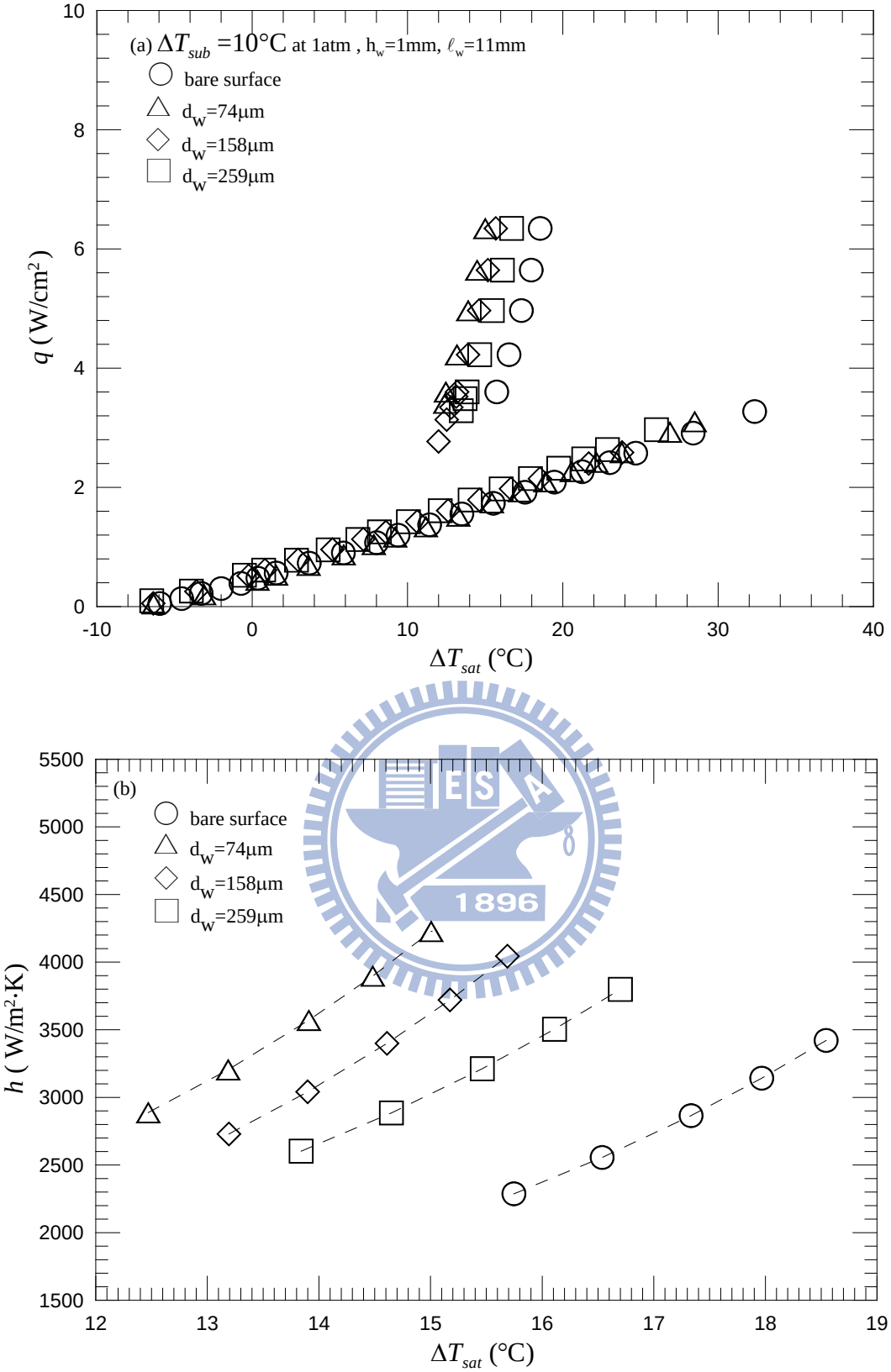

Fig. 5.15 Effects of string diameter on subcooled pool boiling curves (a) and boiling heat transfer coefficients (b) for ΔT_{sub}= 10°C at h_w=1mm and ℓ_w =11mm.

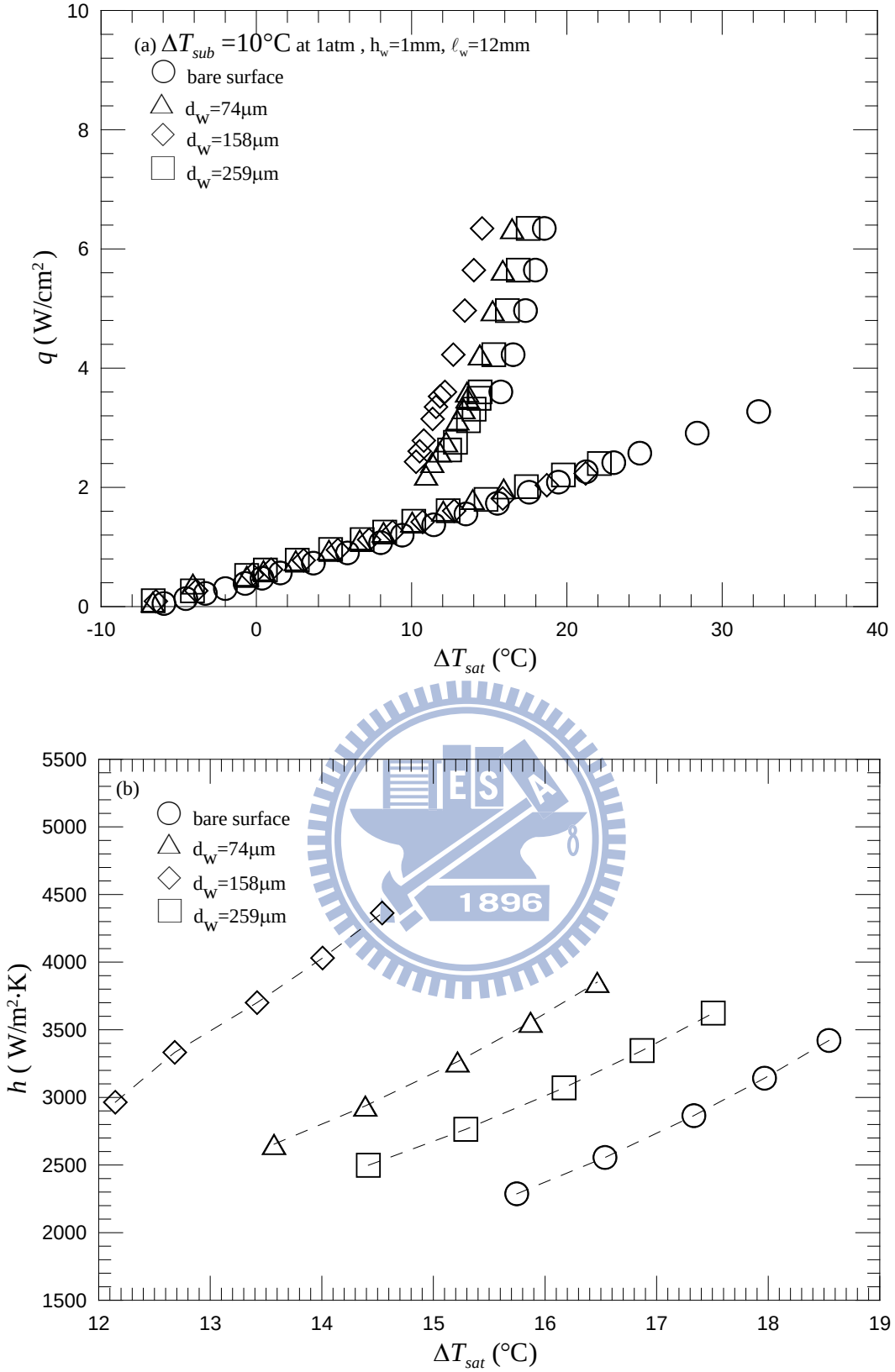

Fig. 5.16 Effects of string diameter on subcooled pool boiling curves (a) and boiling heat transfer coefficients (b) for ΔT_{sub}= 10°C at h_w=1mm and ℓ_w =12mm.

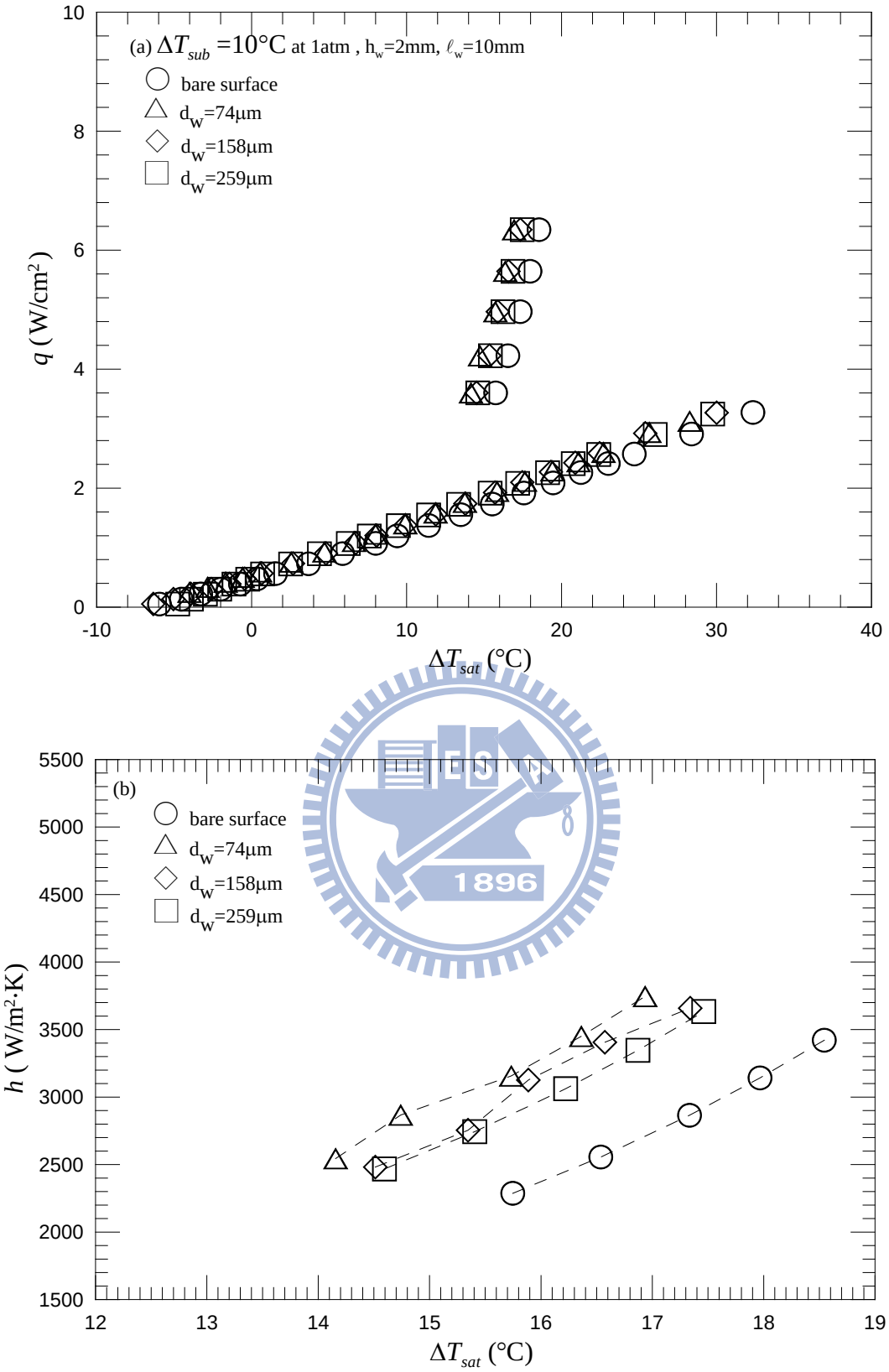

Fig. 5.17 Effects of string diameter on subcooled pool boiling curves (a) and boiling heat transfer coefficients (b) for ΔT_{sub}= 10°C at h_w=2mm and ℓ_w =10mm.

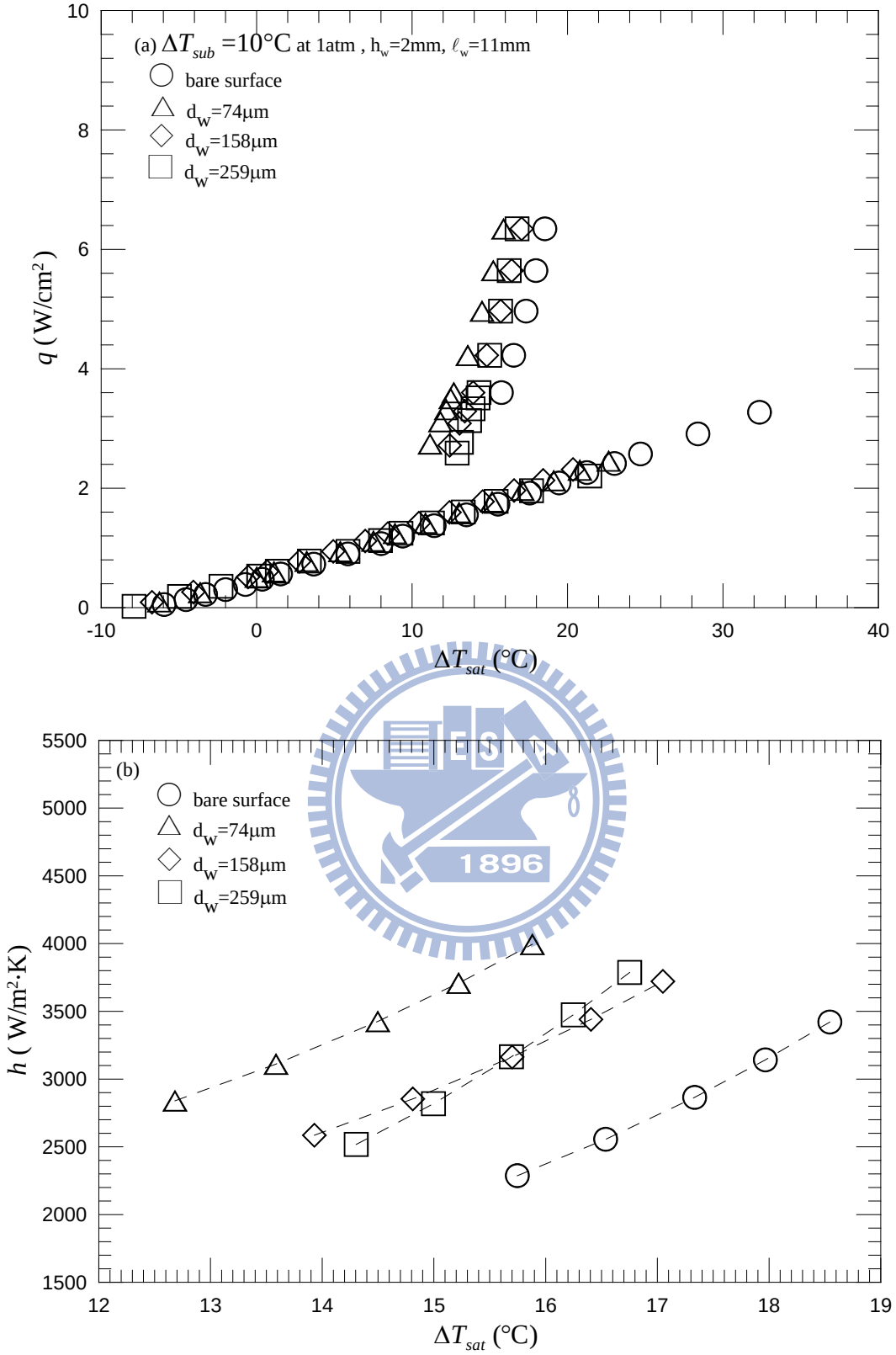

Fig. 5.18 Effects of string diameter on subcooled pool boiling curves (a) and boiling heat transfer coefficients (b) for ΔT_{sub}= 10°C at h_w=2mm and ℓ_w =11mm.

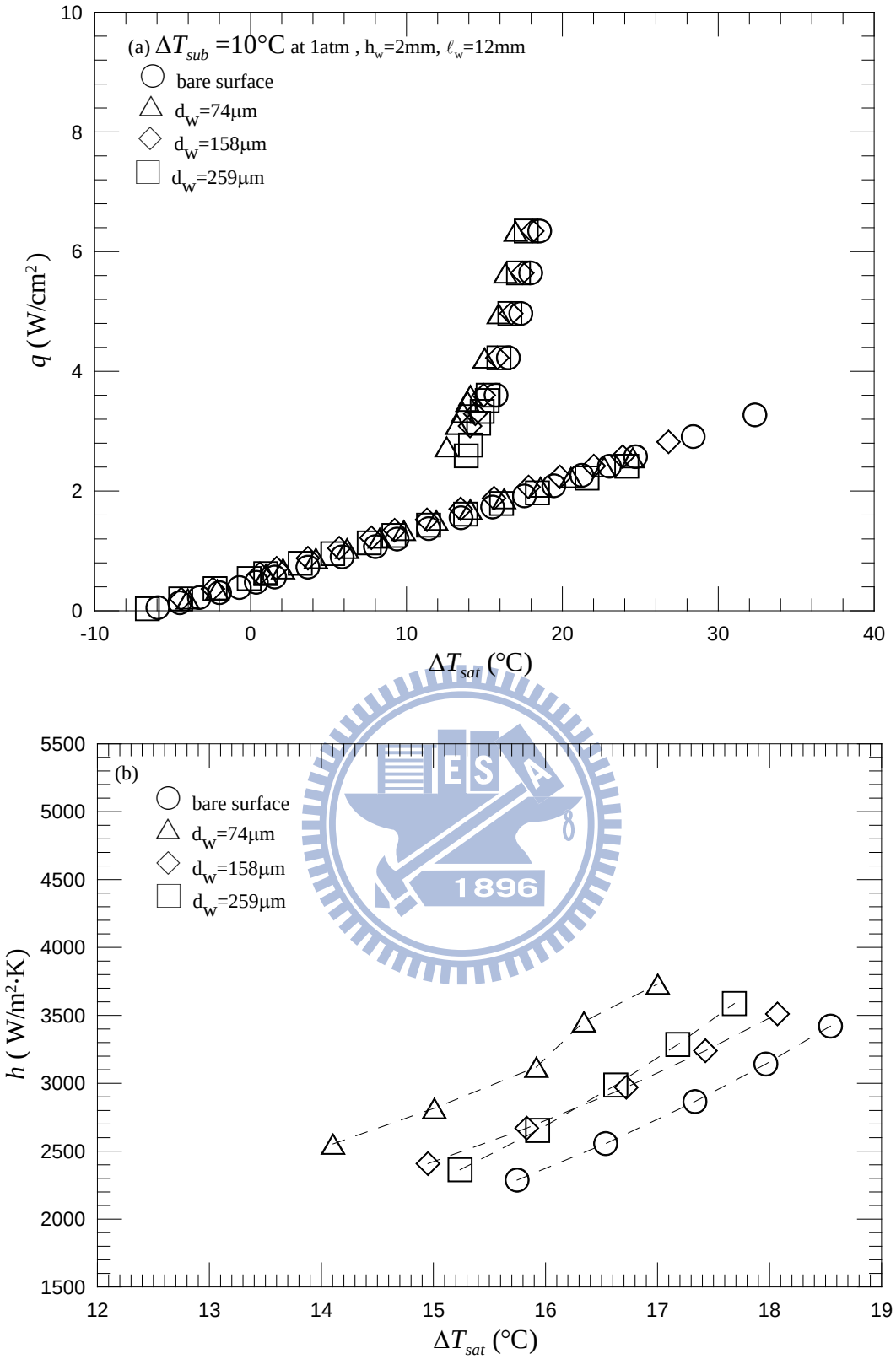

Fig. 5.19 Effects of string diameter on subcooled pool boiling curves (a) and boiling heat transfer coefficients (b) for ΔT_{sub}= 10°C at h_w=2mm and ℓ_w =12mm.

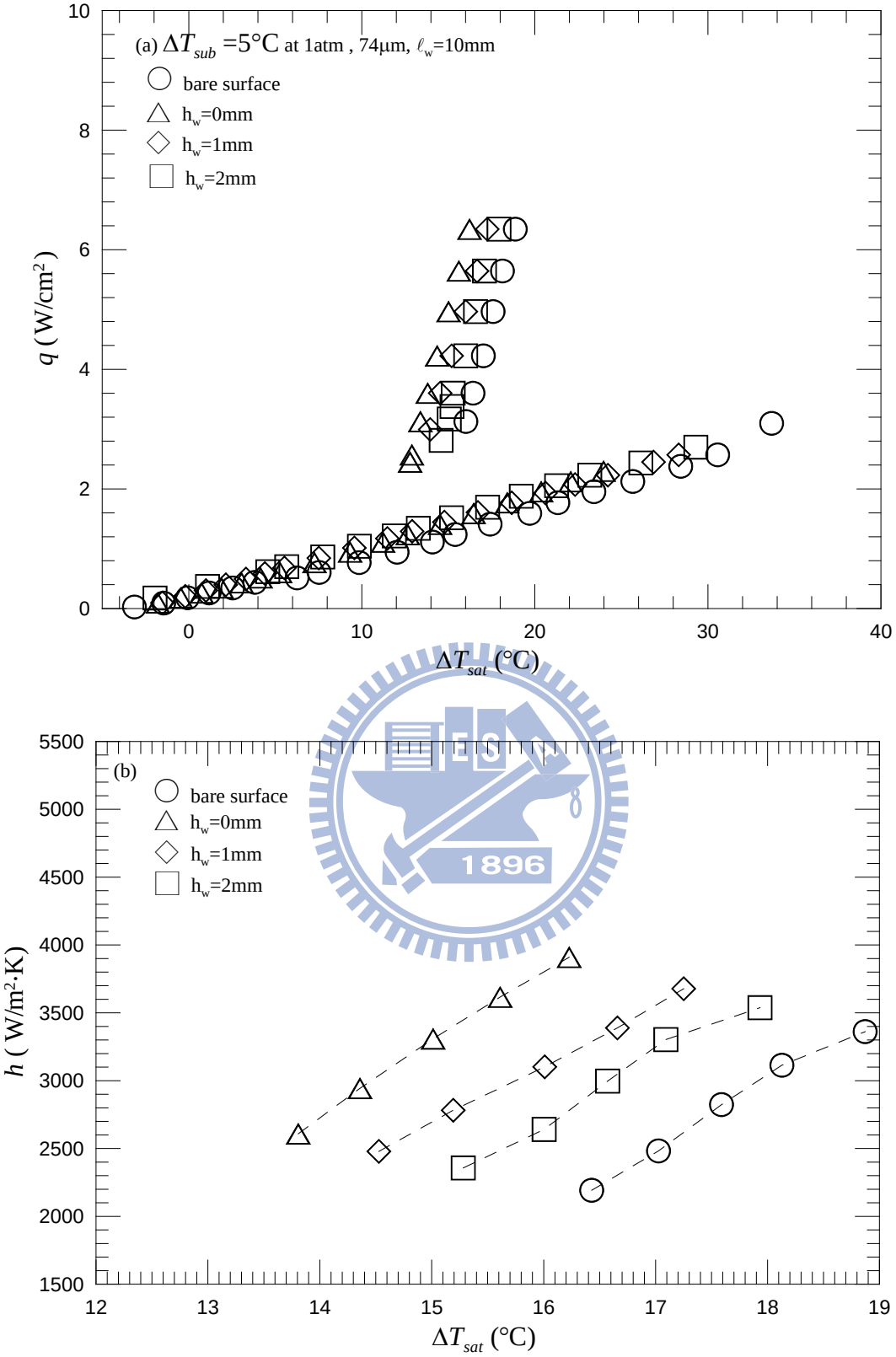

Fig. 5.20 Effects of string height on subcooled pool boiling curves (a) and boiling heat transfer coefficients (b) for ΔT_{sub}= 5°C at d_w=74μm and ℓ_w =10mm.

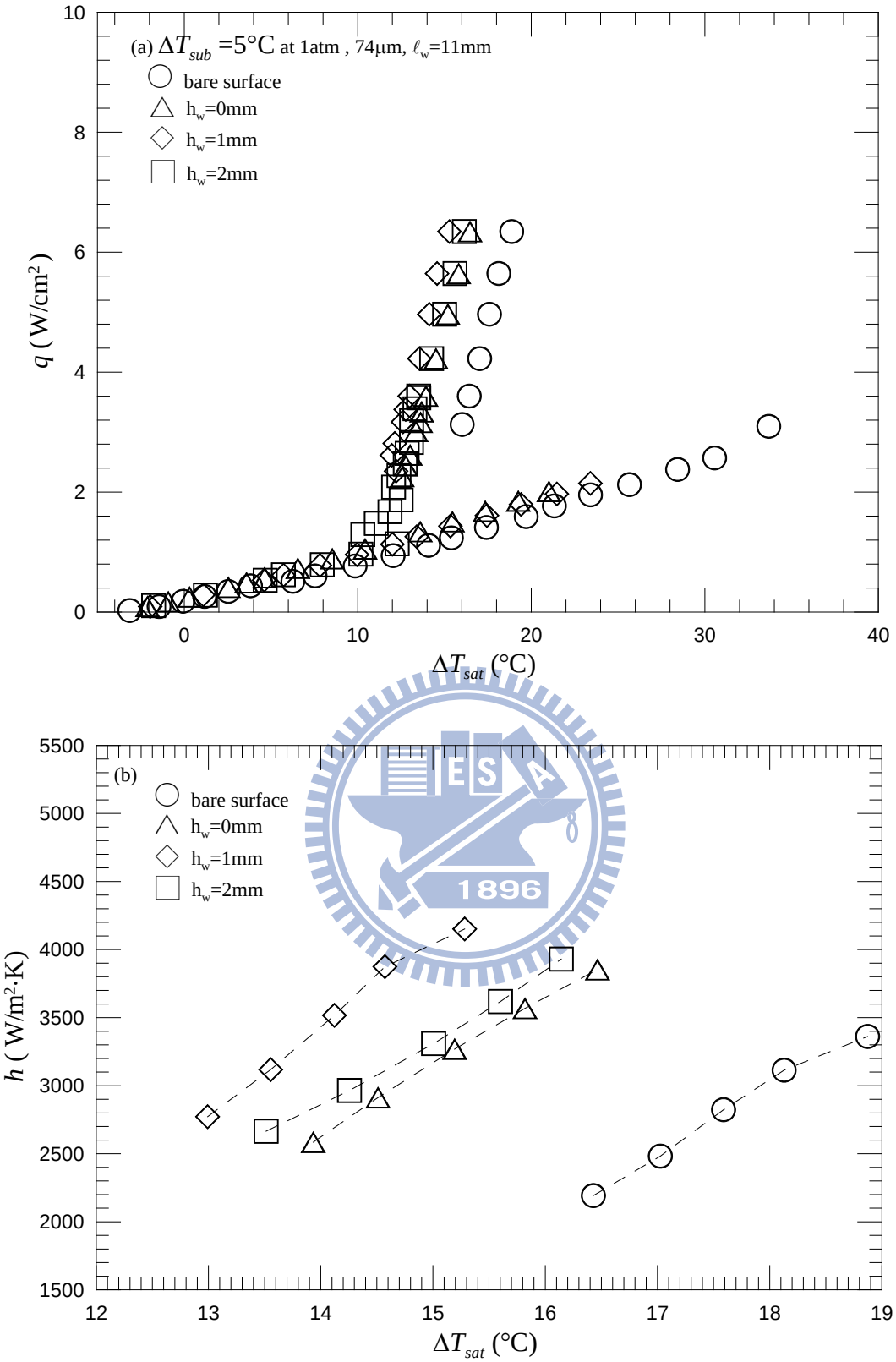

Fig. 5.21 Effects of string height on subcooled pool boiling curves (a) and boiling heat transfer coefficients (b) for ΔT_{sub}= 5°C at d_w=74μm and ℓ_w =11mm.

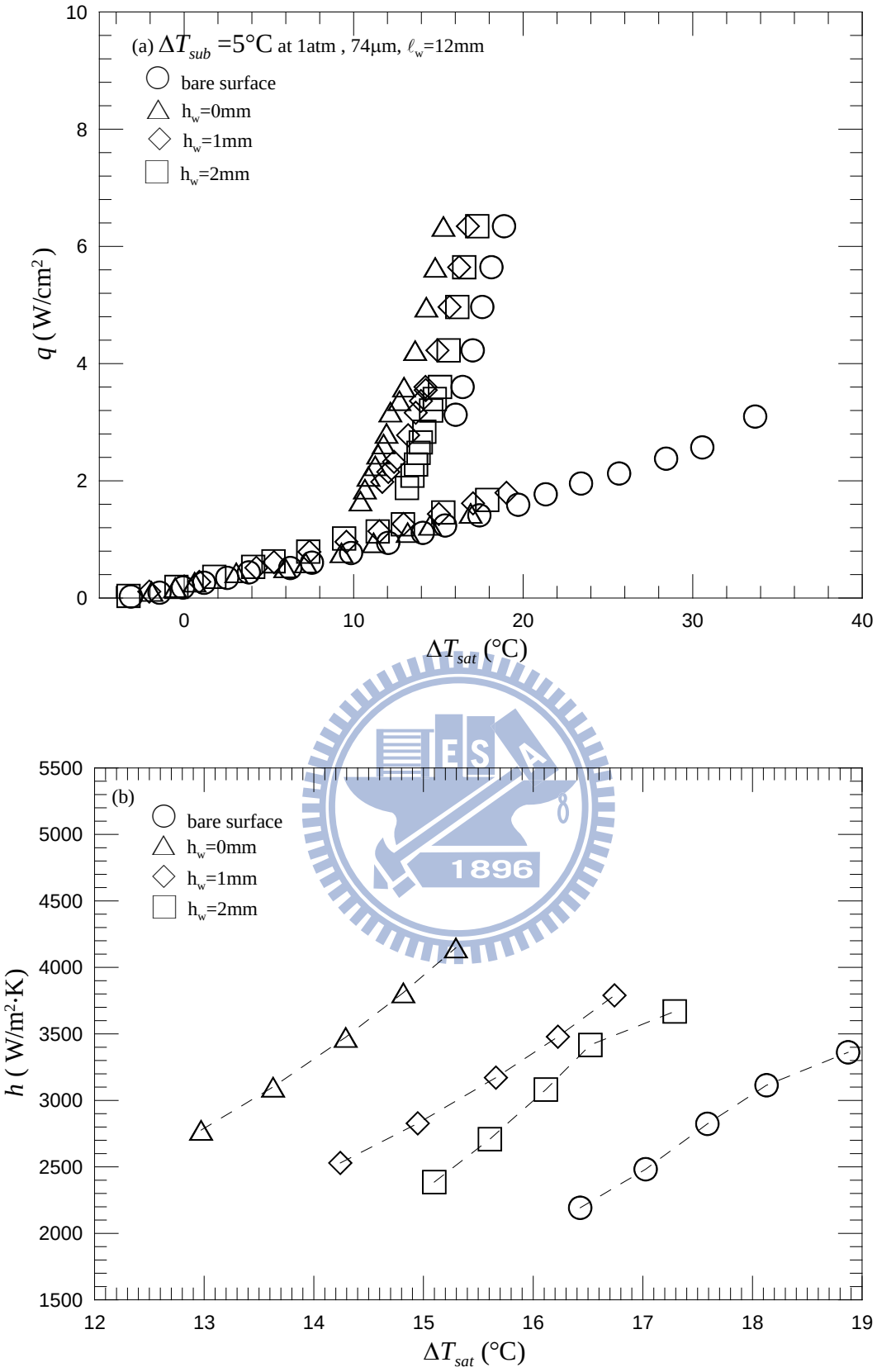

Fig. 5.22 Effects of string height on subcooled pool boiling curves (a) and boiling heat transfer coefficients (b) for ΔT_{sub}= 5°C at d_w=74μm and ℓ_w =12mm.

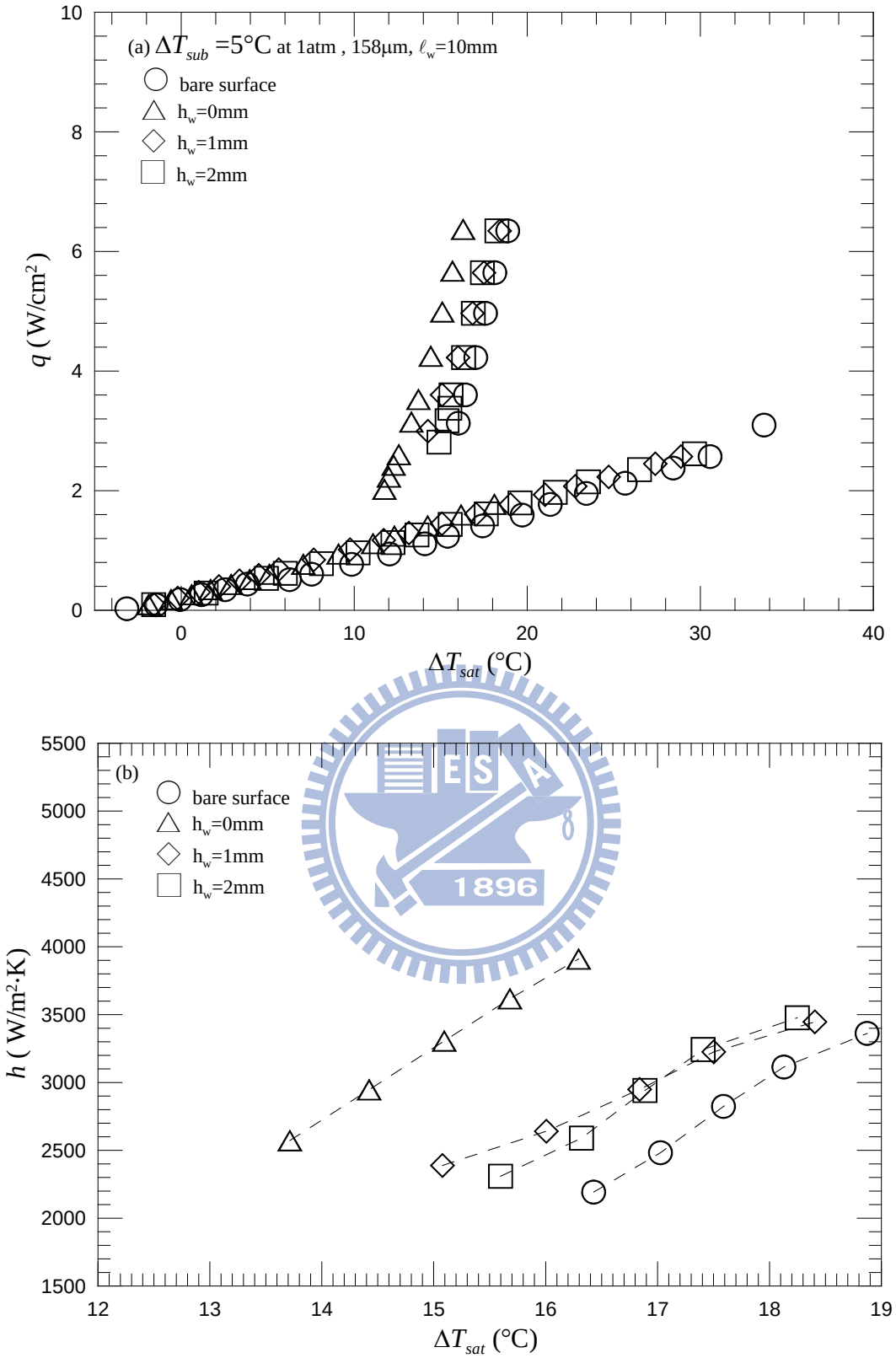

Fig. 5.23 Effects of string height on subcooled pool boiling curves (a) and boiling heat transfer coefficients (b) for ΔT_{sub}= 5°C at d_w=158μm and ℓ_w =10mm.

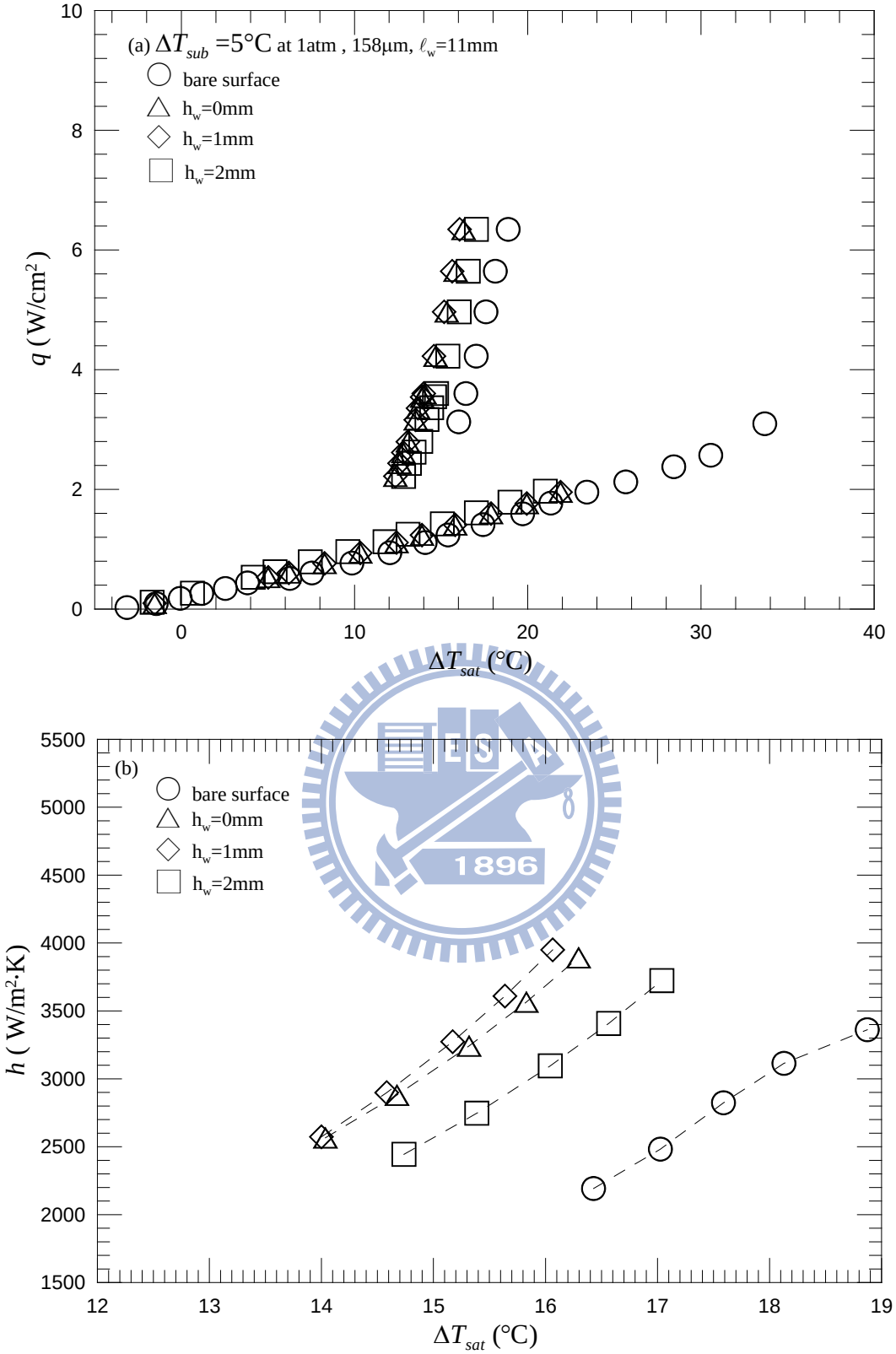

Fig. 5.24 Effects of string height on subcooled pool boiling curves (a) and boiling heat transfer coefficients (b) for ΔT_{sub}= 5°C at d_w=158μm and ℓ_w =11mm.

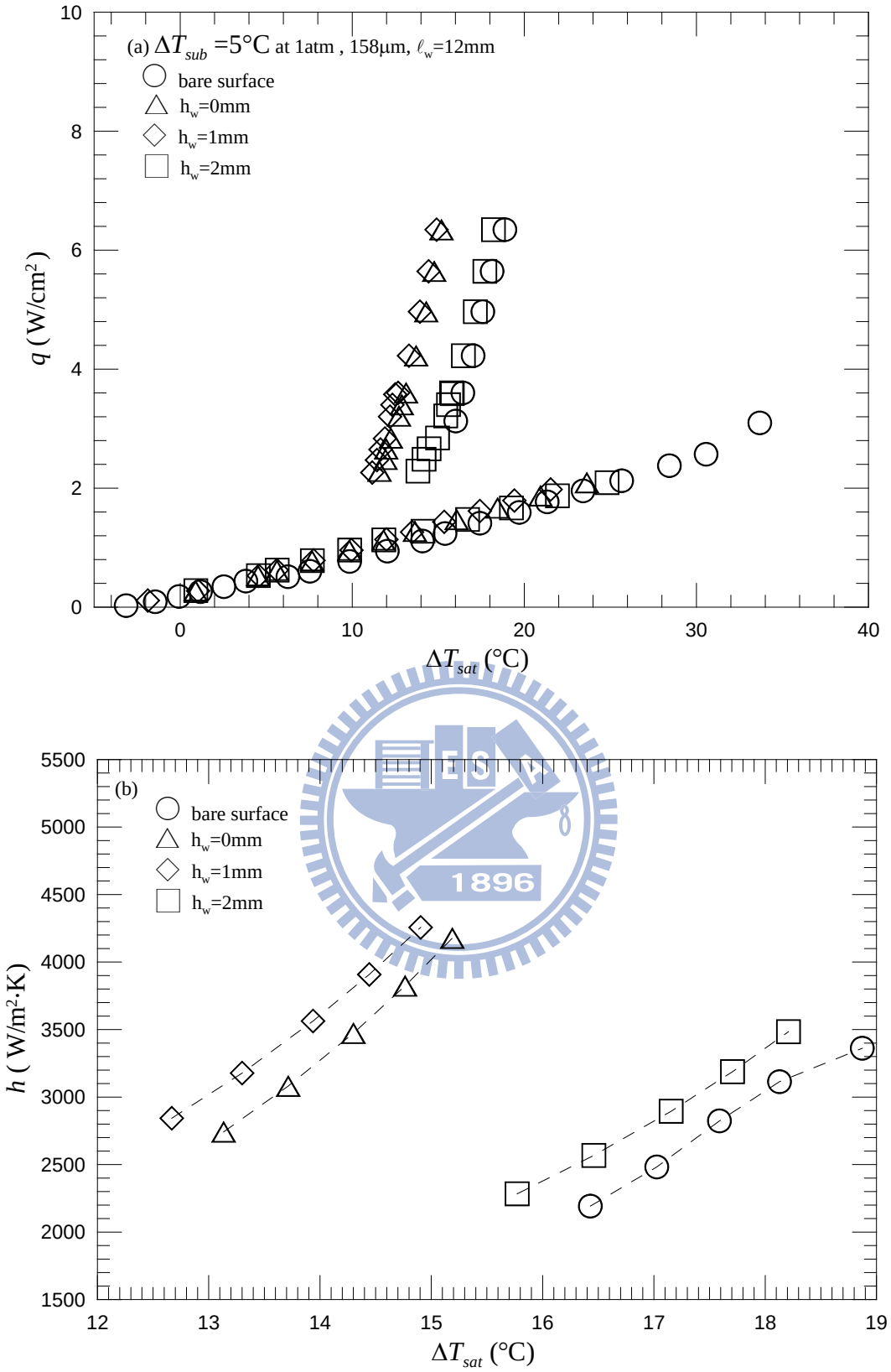

Fig. 5.25 Effects of string height on subcooled pool boiling curves (a) and boiling heat transfer coefficients (b) for ΔT_{sub}= 5°C at d_w=158μm and ℓ_w =12mm.

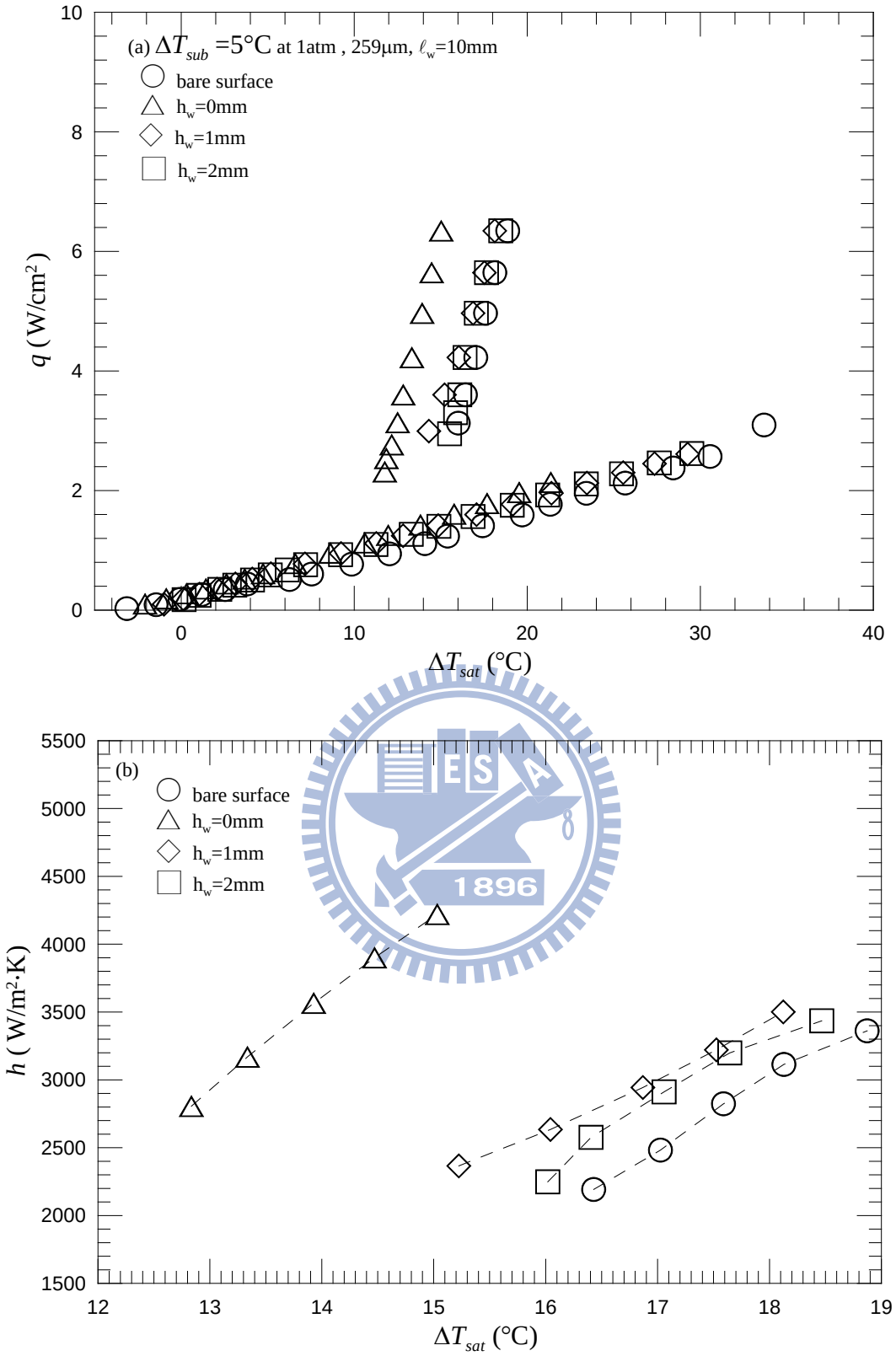

Fig. 5.26 Effects of string height on subcooled pool boiling curves (a) and boiling heat transfer coefficients (b) for ΔT_{sub}= 5°C at d_w=259μm and ℓ_w =10mm.

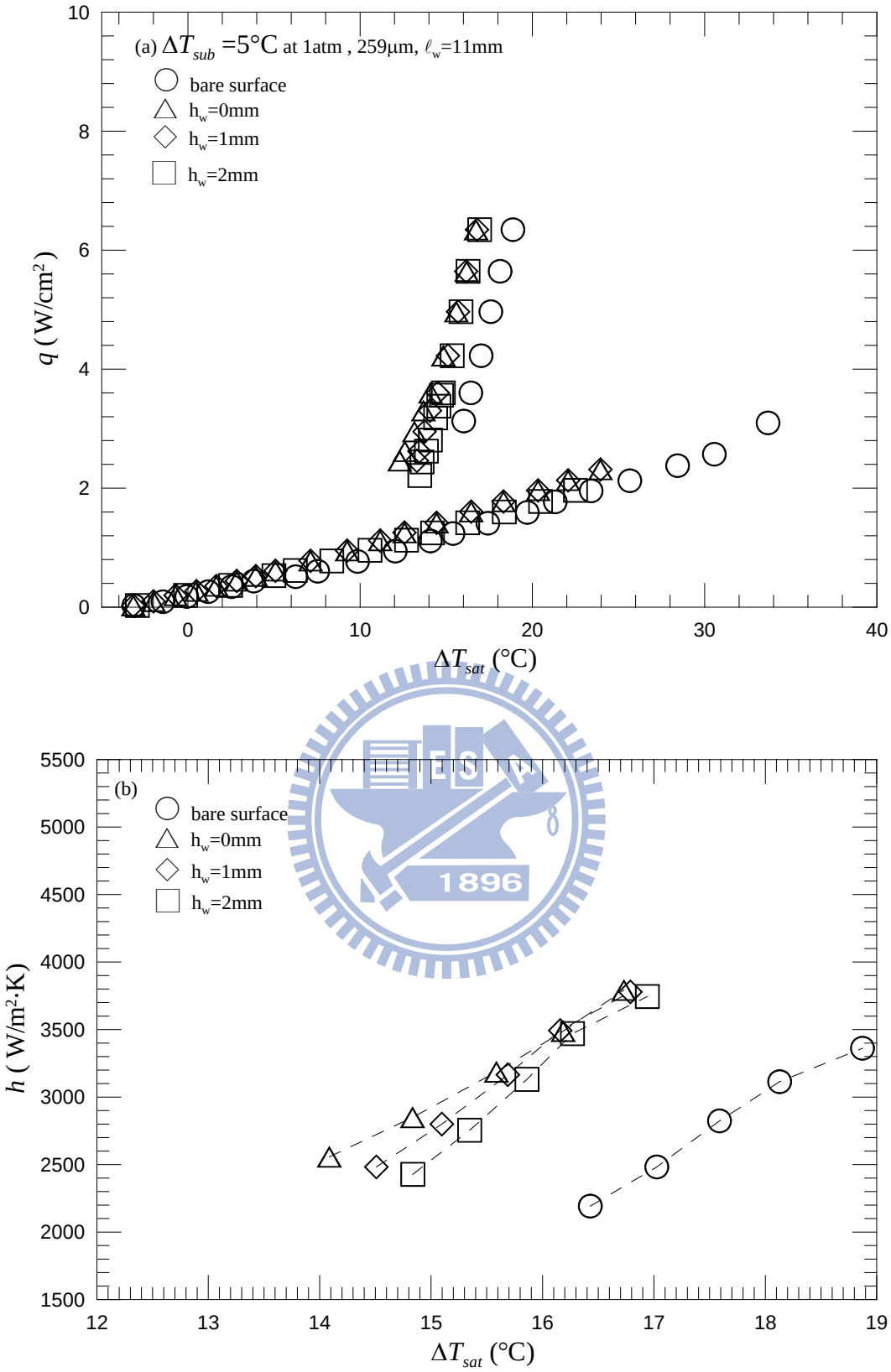

Fig. 5.27 Effects of string height on subcooled pool boiling curves (a) and boiling heat transfer coefficients (b) for ΔT_{sub}= 5°C at d_w=259μm and ℓ_w =11mm.

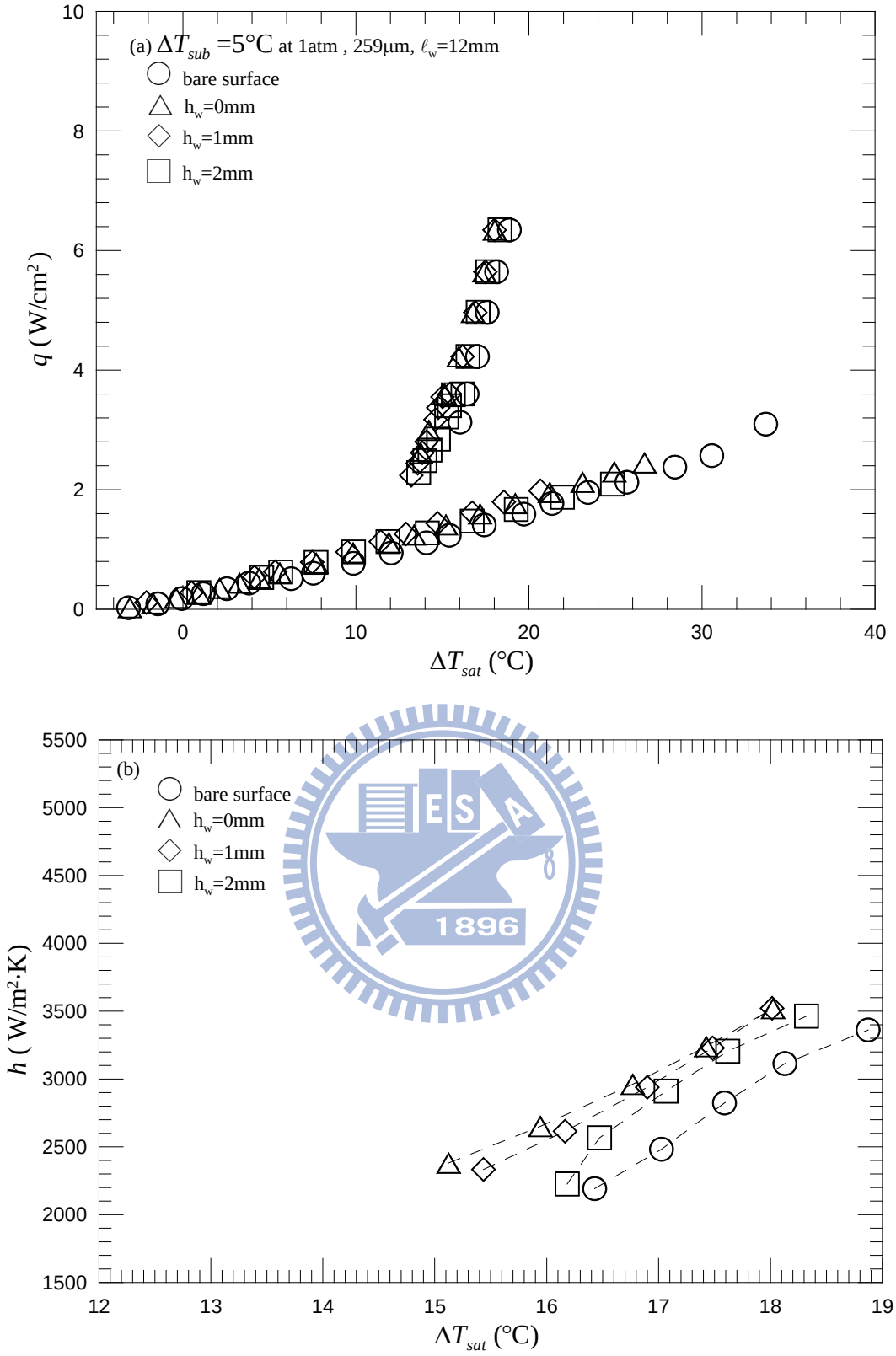

Fig. 5.28 Effects of string height on subcooled pool boiling curves (a) and boiling heat transfer coefficients (b) for ΔT_{sub}= 5°C at d_w=259μm and ℓ_w =12mm.

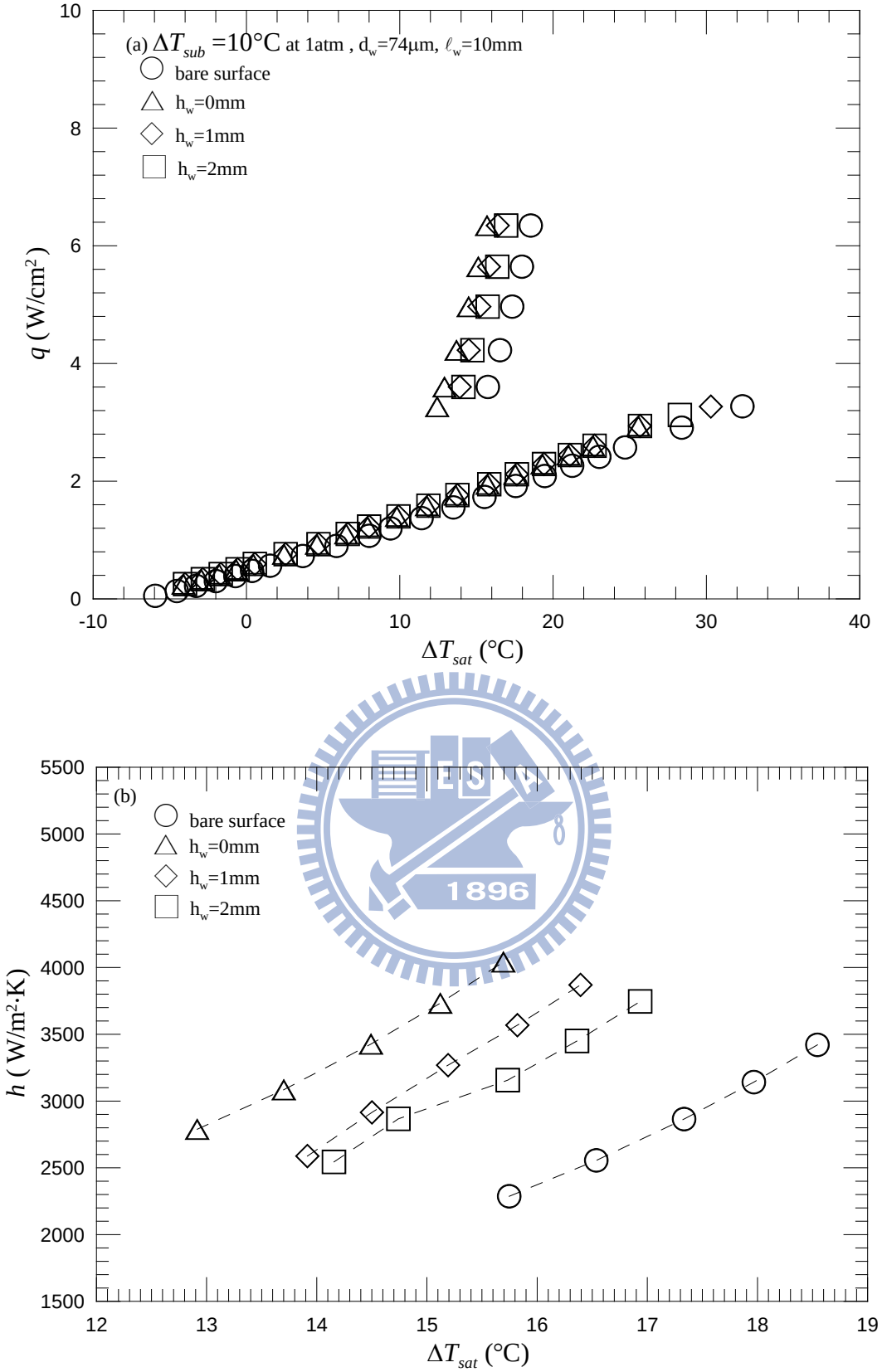

Fig. 5.29 Effects of string height on subcooled pool boiling curves (a) and boiling heat transfer coefficients (b) for ΔT_{sub}= 10°C at d_w=74μm and ℓ_w =10mm.

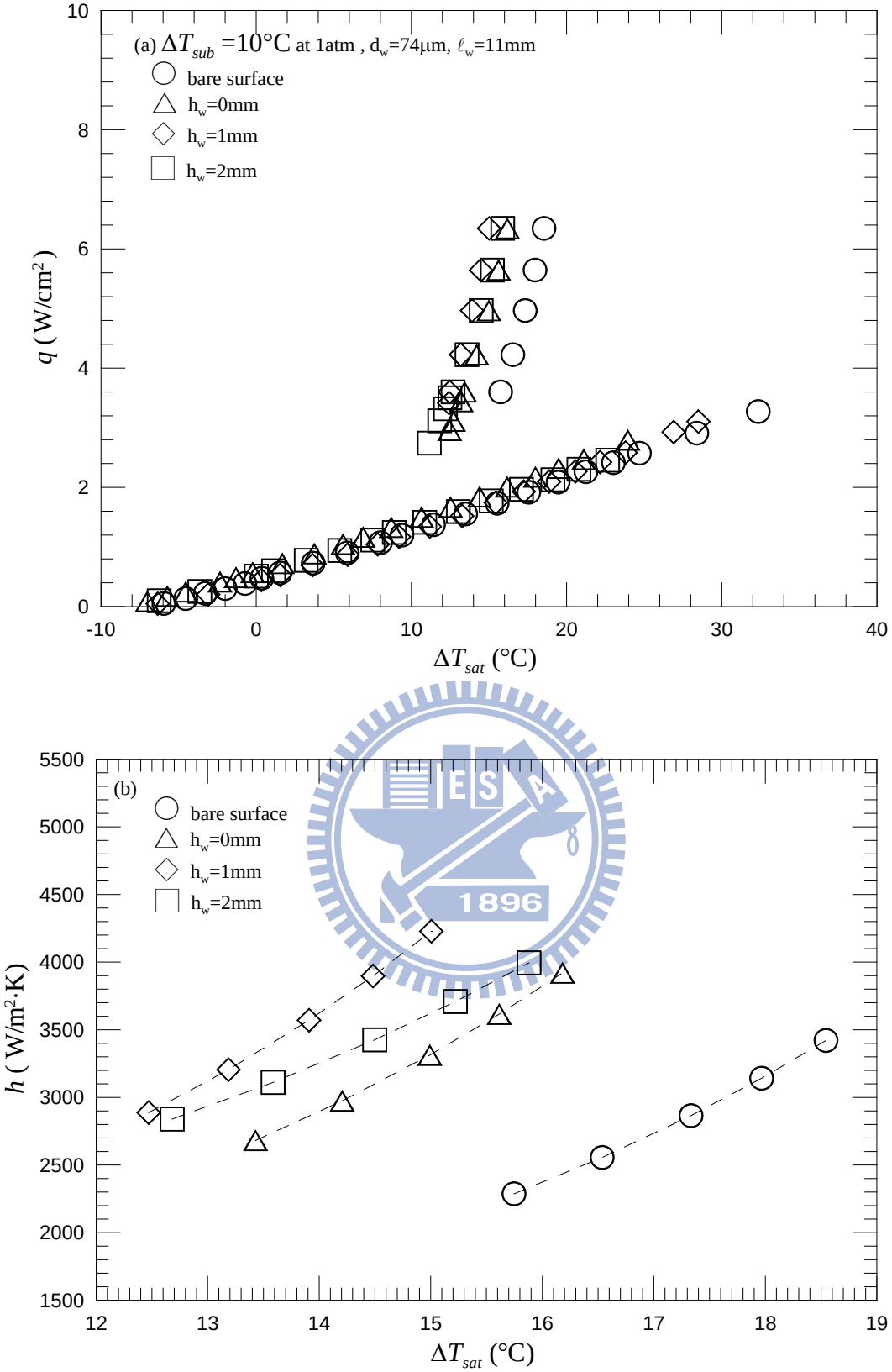

Fig. 5.30 Effects of string height on subcooled pool boiling curves (a) and boiling heat transfer coefficients (b) for ΔT_{sub}= 10°C at d_w=74μm and ℓ_w =11mm.

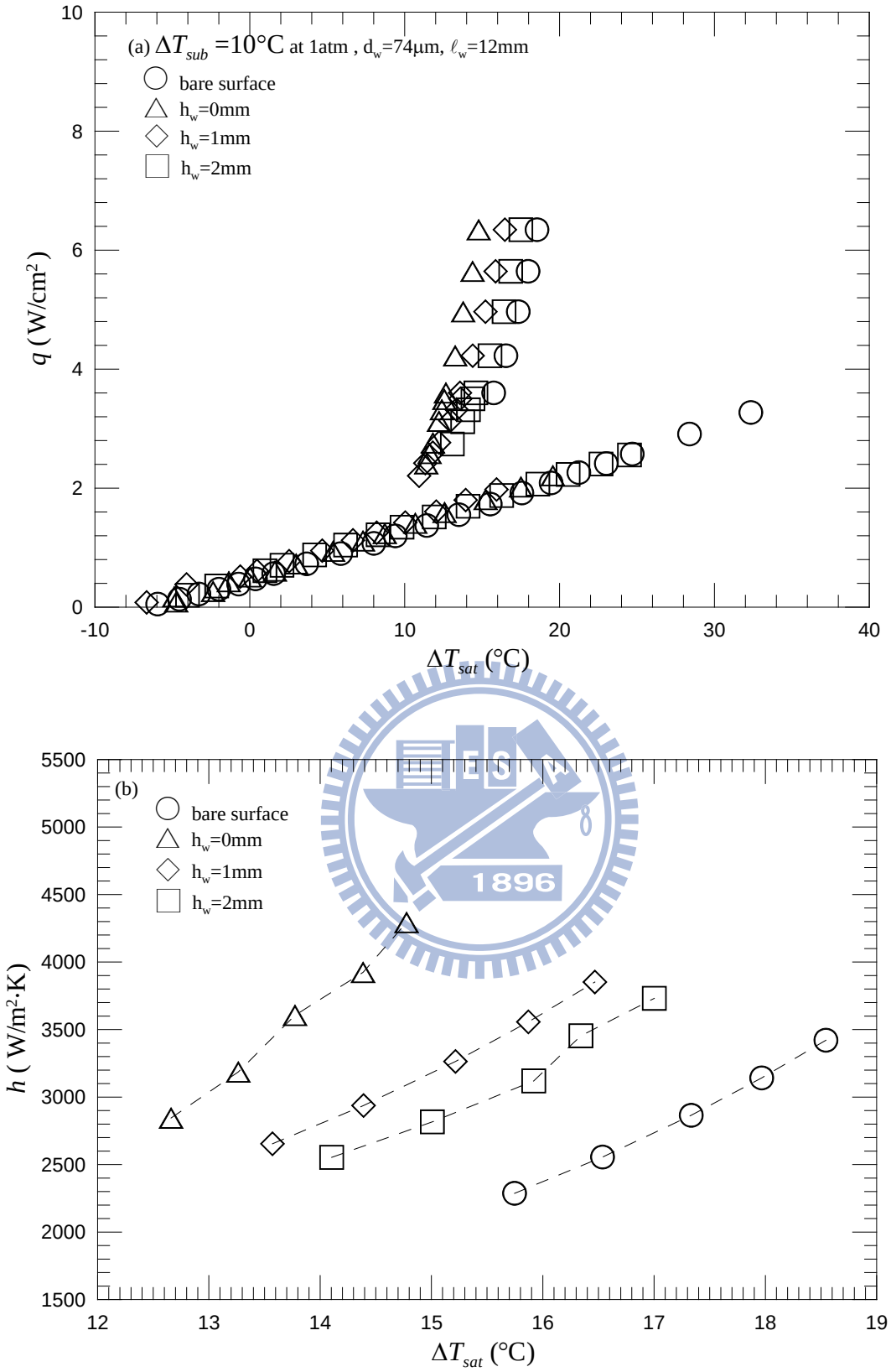

Fig. 5.31 Effects of string height on subcooled pool boiling curves (a) and boiling heat transfer coefficients (b) for ΔT_{sub}= 10°C at d_w=74μm and ℓ_w =12mm.

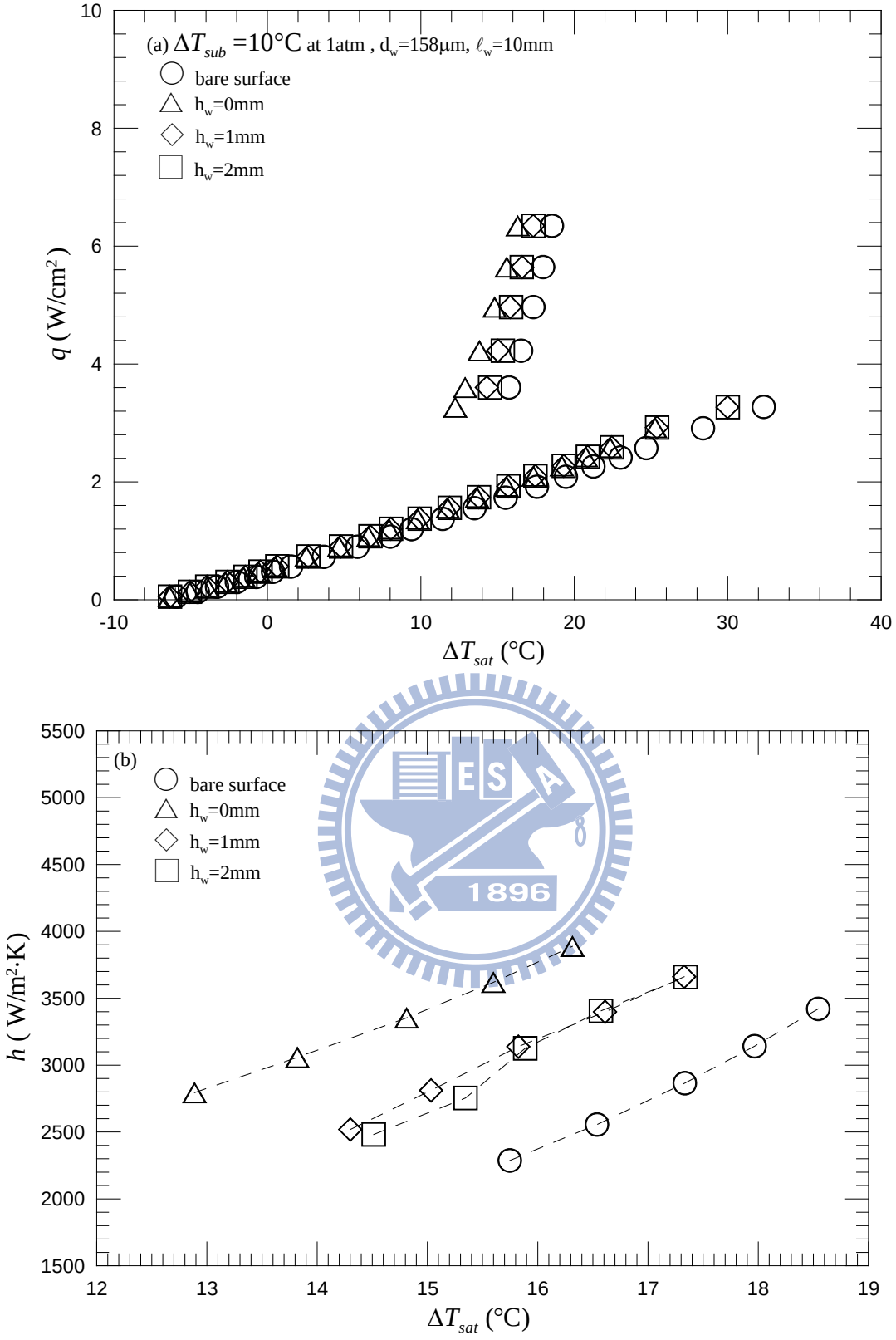

Fig. 5.32 Effects of string height on subcooled pool boiling curves (a) and boiling heat transfer coefficients (b) for ΔT_{sub}= 10°C at d_w=158μm and ℓ_w =10mm.

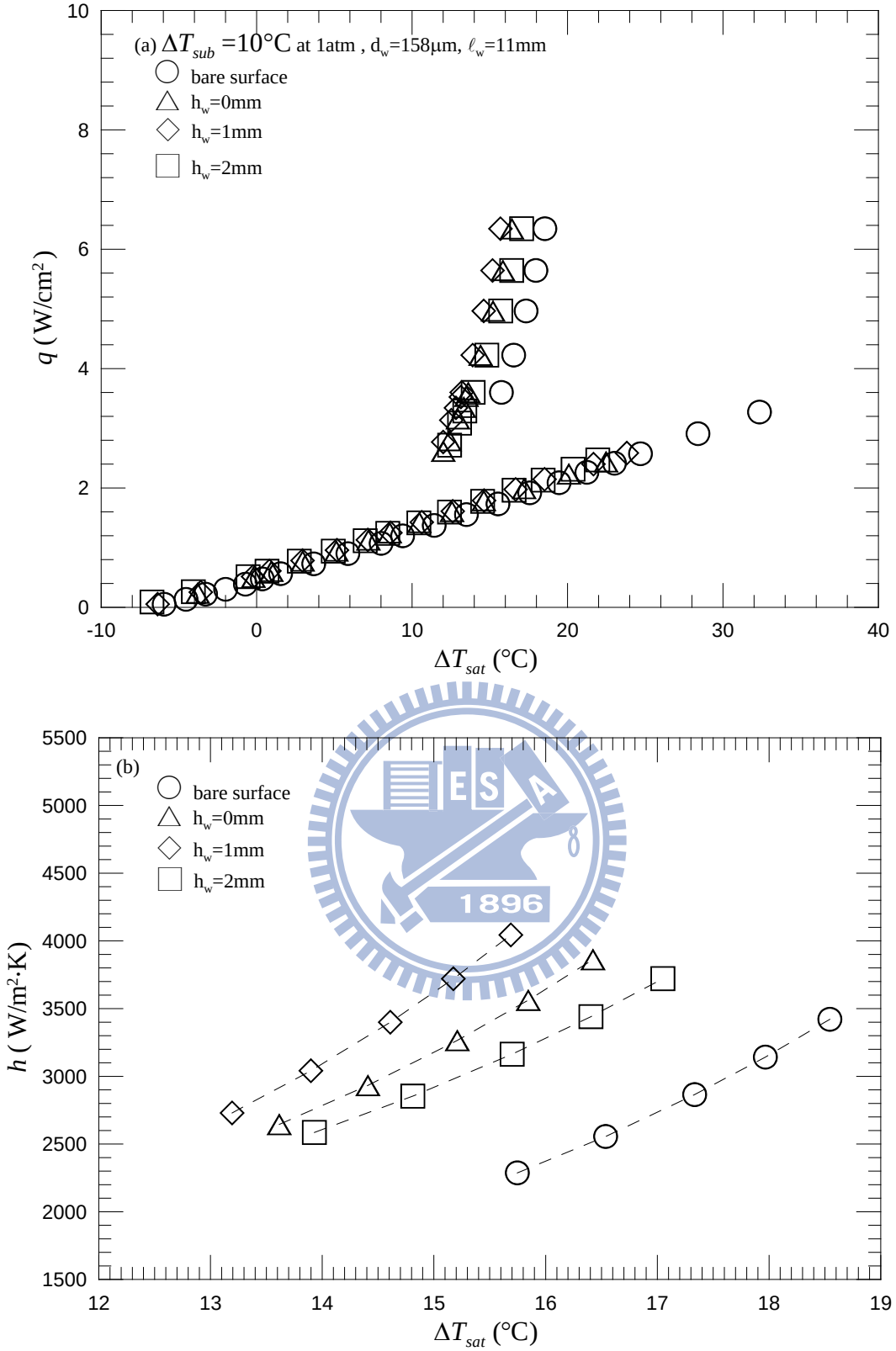

Fig. 5.33 Effects of string height on subcooled pool boiling curves (a) and boiling heat transfer coefficients (b) for ΔT_{sub}= 10°C at d_w=158μm and ℓ_w =11mm.

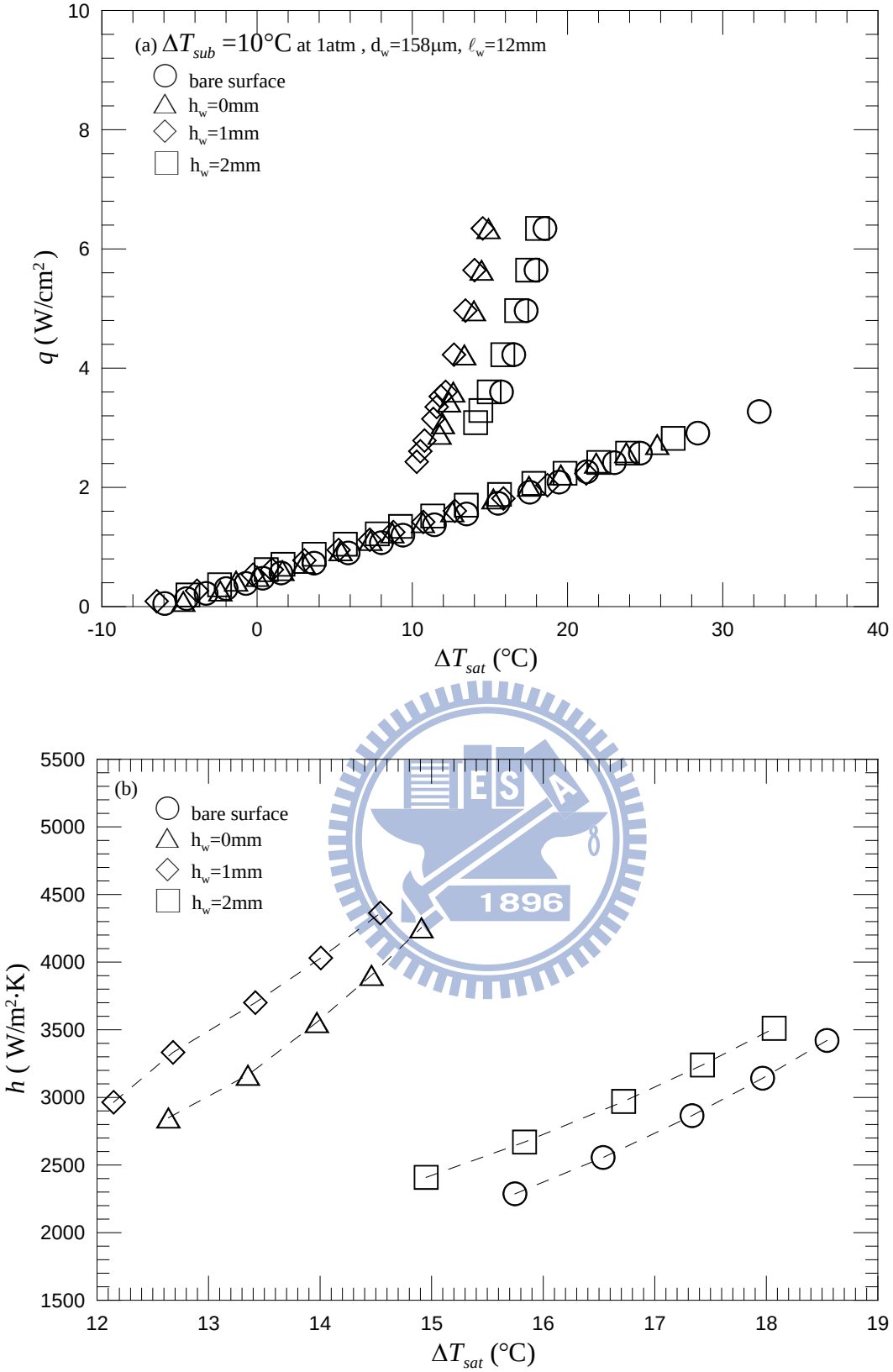

Fig. 5.34 Effects of string height on subcooled pool boiling curves (a) and boiling heat transfer coefficients (b) for ΔT_{sub}= 10°C at d_w=158μm and ℓ_w =12mm.

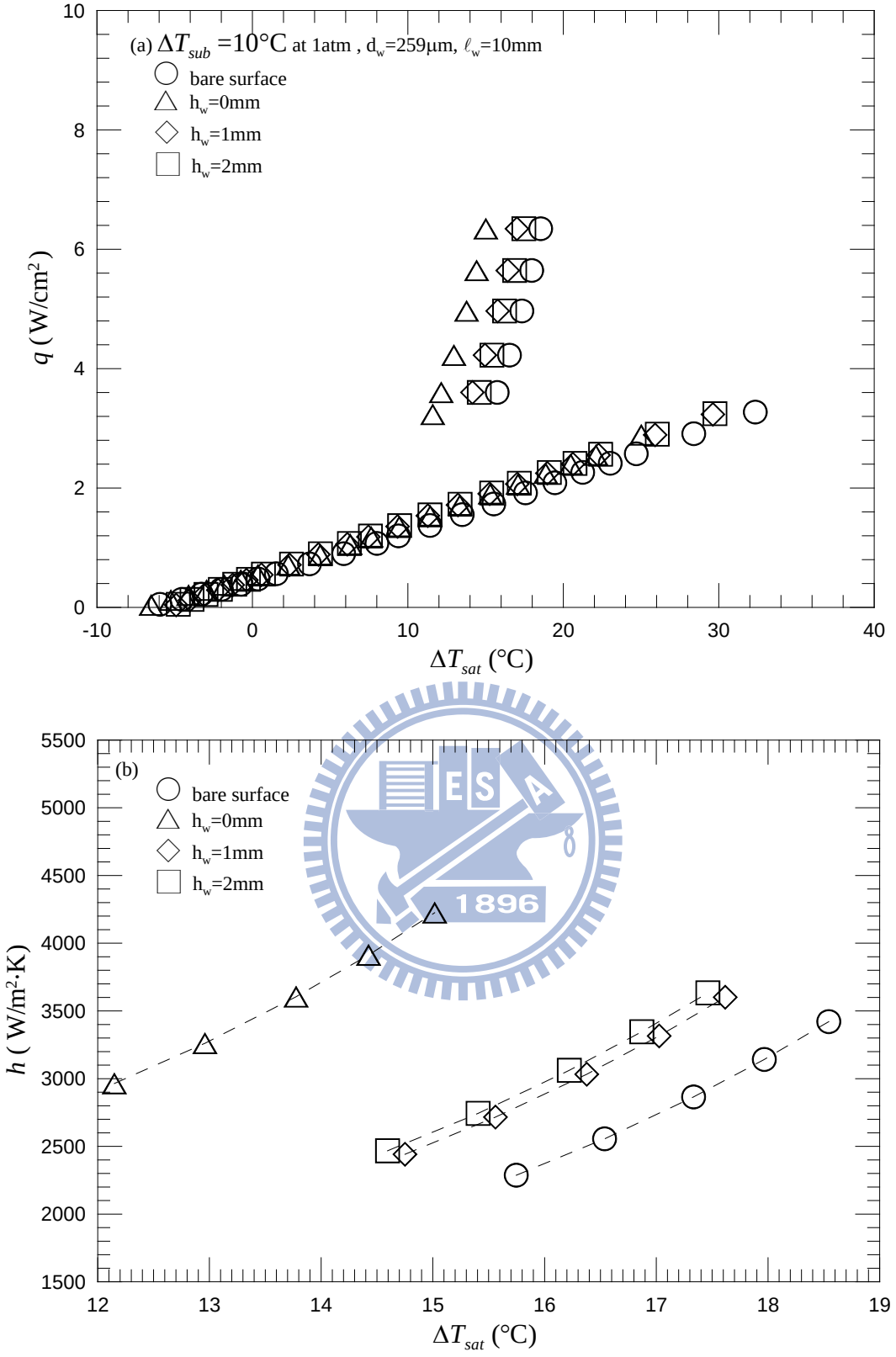

Fig. 5.35 Effects of string height on subcooled pool boiling curves (a) and boiling heat transfer coefficients (b) for ΔT_{sub}= 10°C at d_w=259μm and ℓ_w =10mm.

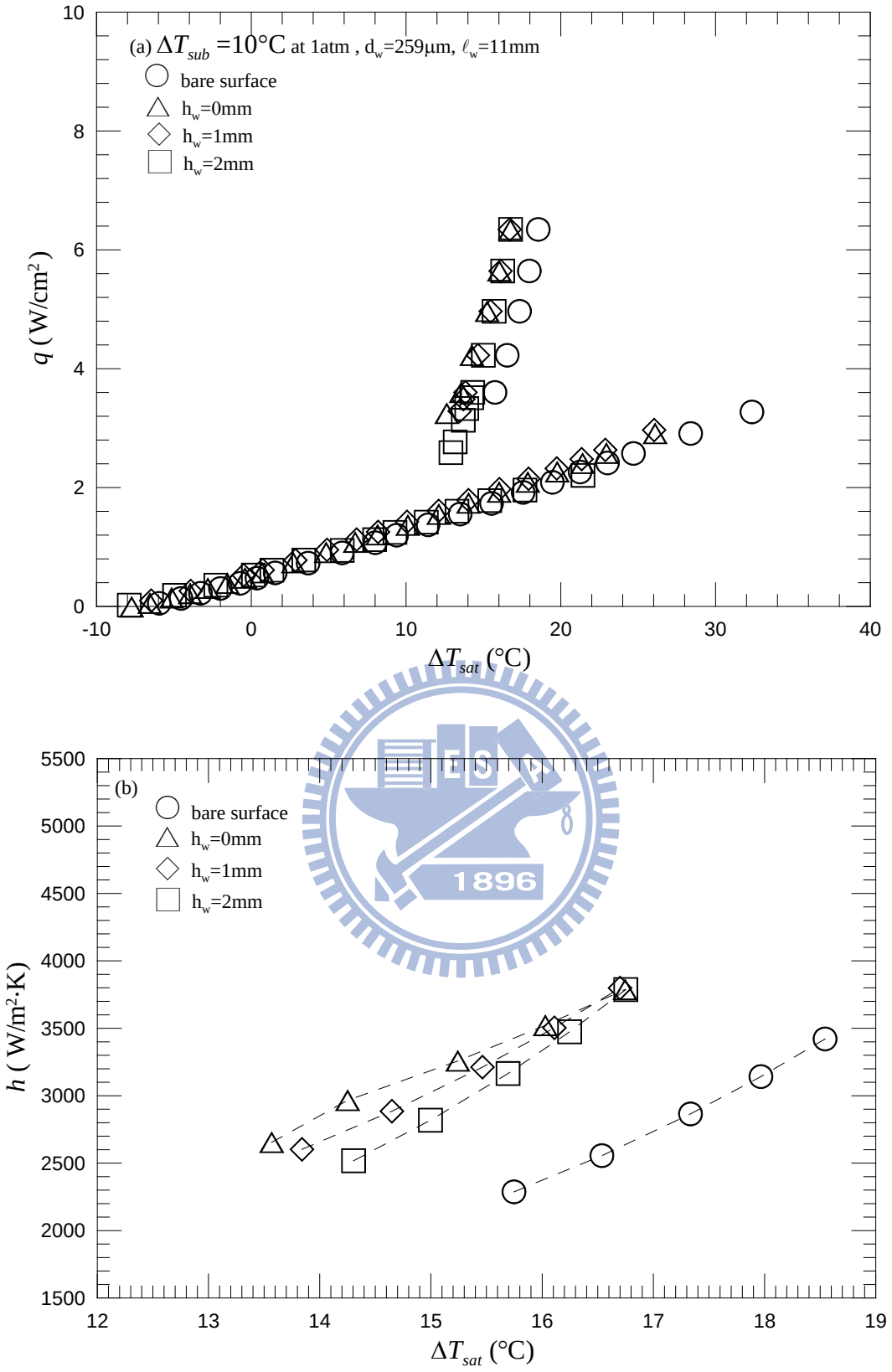

Fig. 5.36 Effects of string height on subcooled pool boiling curves (a) and boiling heat transfer coefficients (b) for ΔT_{sub}= 10°C at d_w=259μm and ℓ_w =11mm.

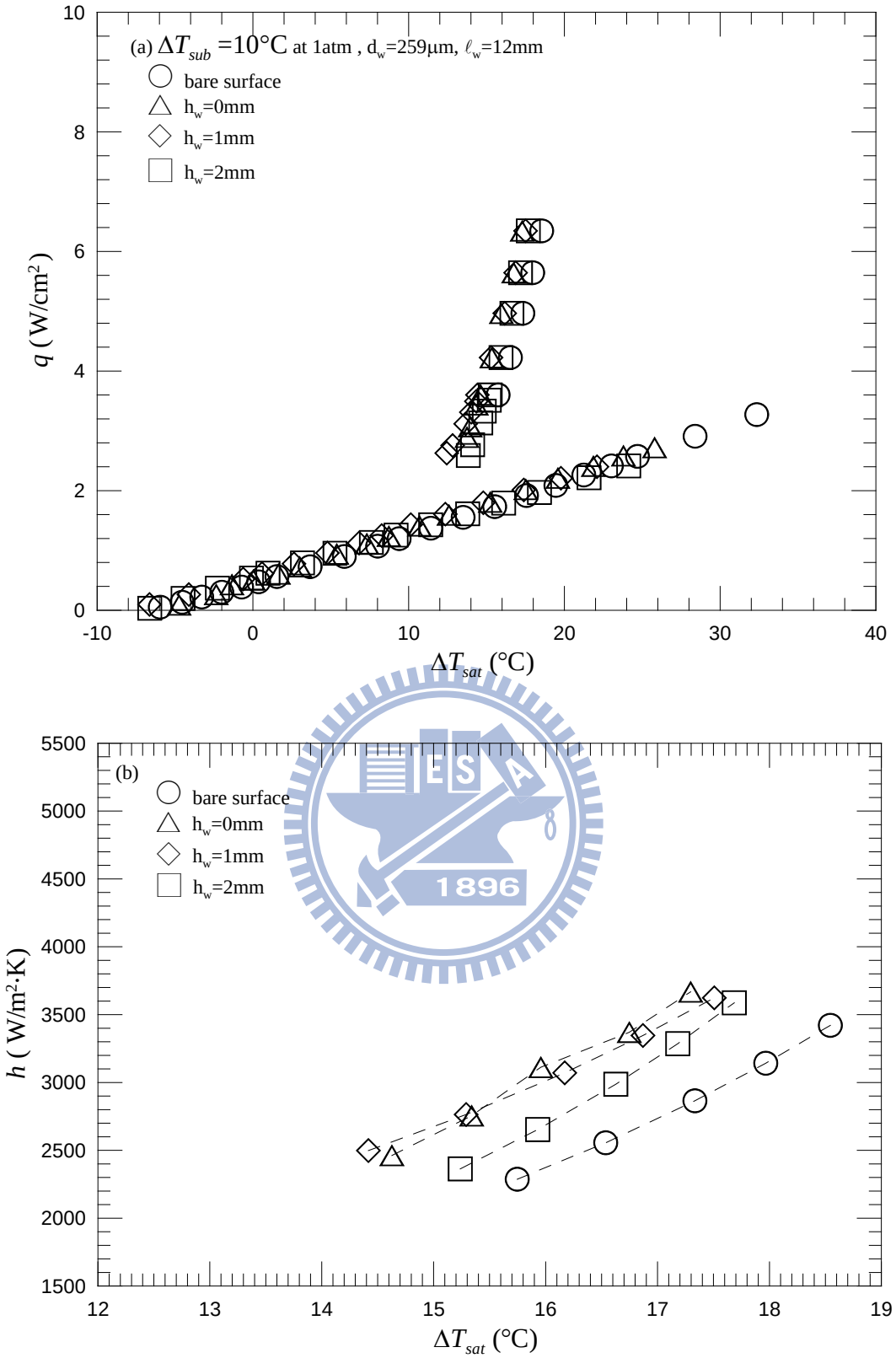

Fig. 5.37 Effects of string height on subcooled pool boiling curves (a) and boiling heat transfer coefficients (b) for ΔT_{sub}= 10°C at d_w=259μm and ℓ_w =12mm.

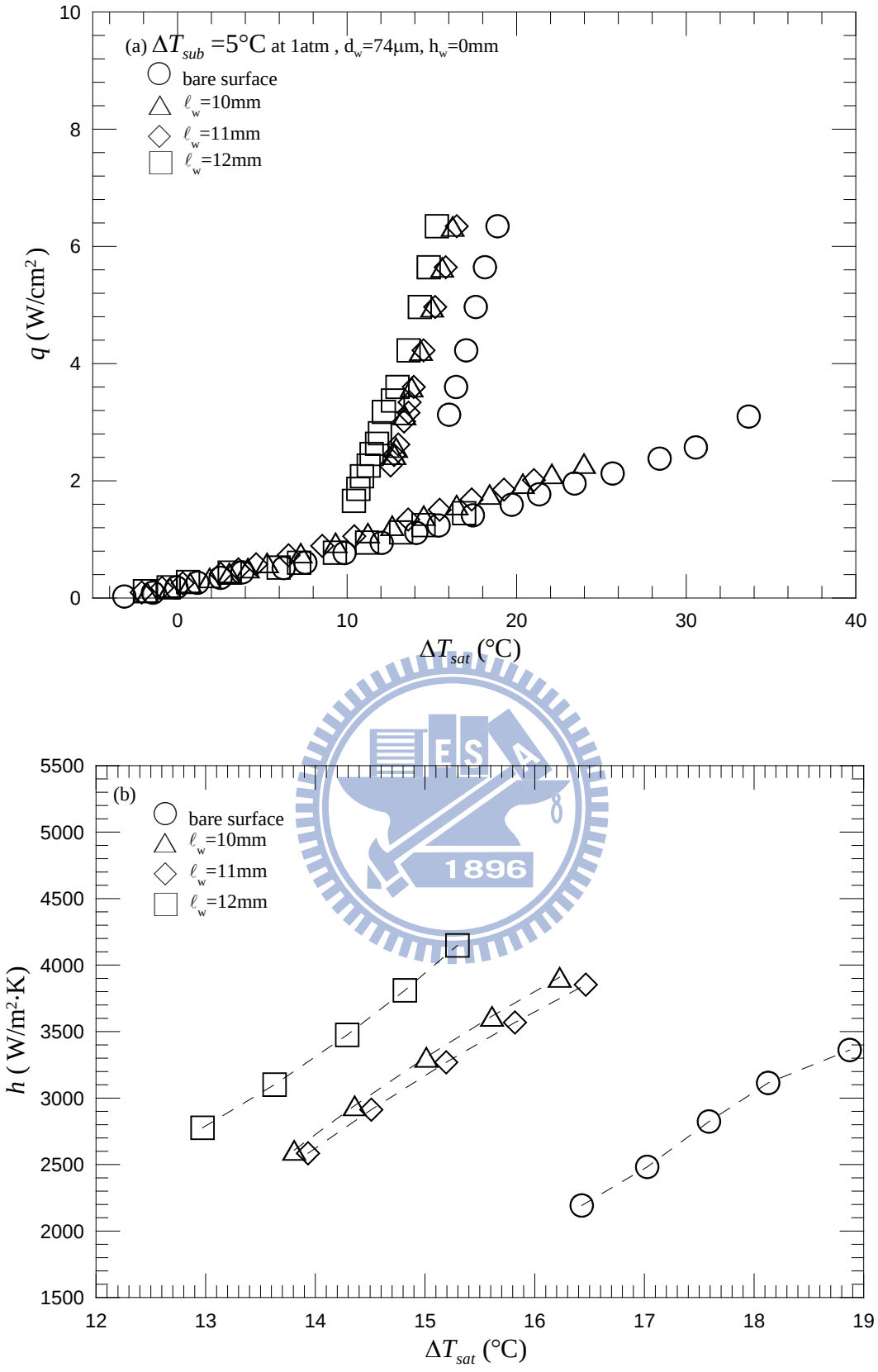

Fig. 5.38 Effects of string length on subcooled pool boiling curves (a) and boiling heat transfer coefficients (b) for ΔT_{sub}= 5°C at d_w=74μm and h_w=0mm.

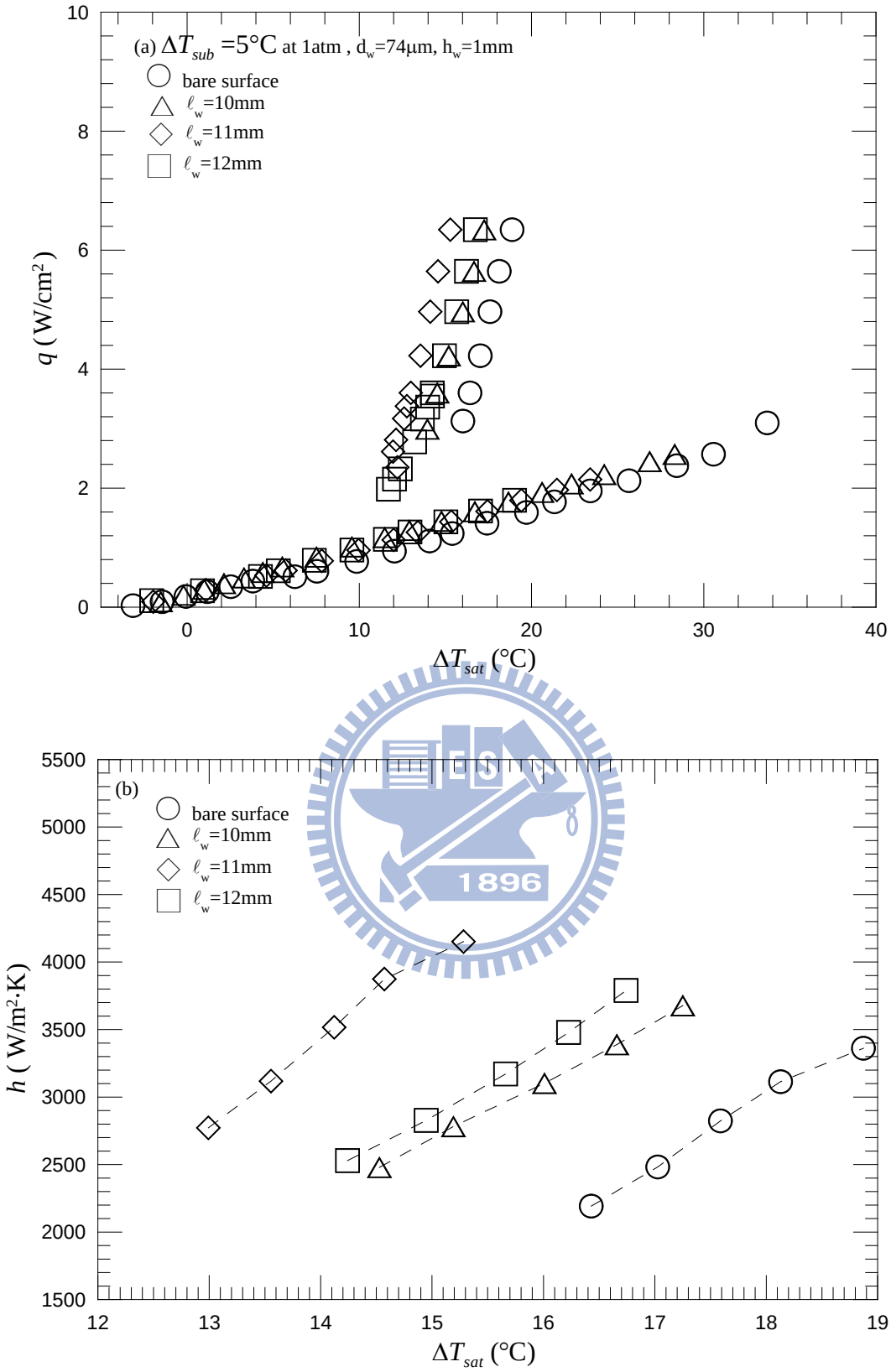

Fig. 5.39 Effects of string length on subcooled pool boiling curves (a) and boiling heat transfer coefficients (b) for ΔT_{sub}= 5°C at d_w=74μm and h_w=1mm.

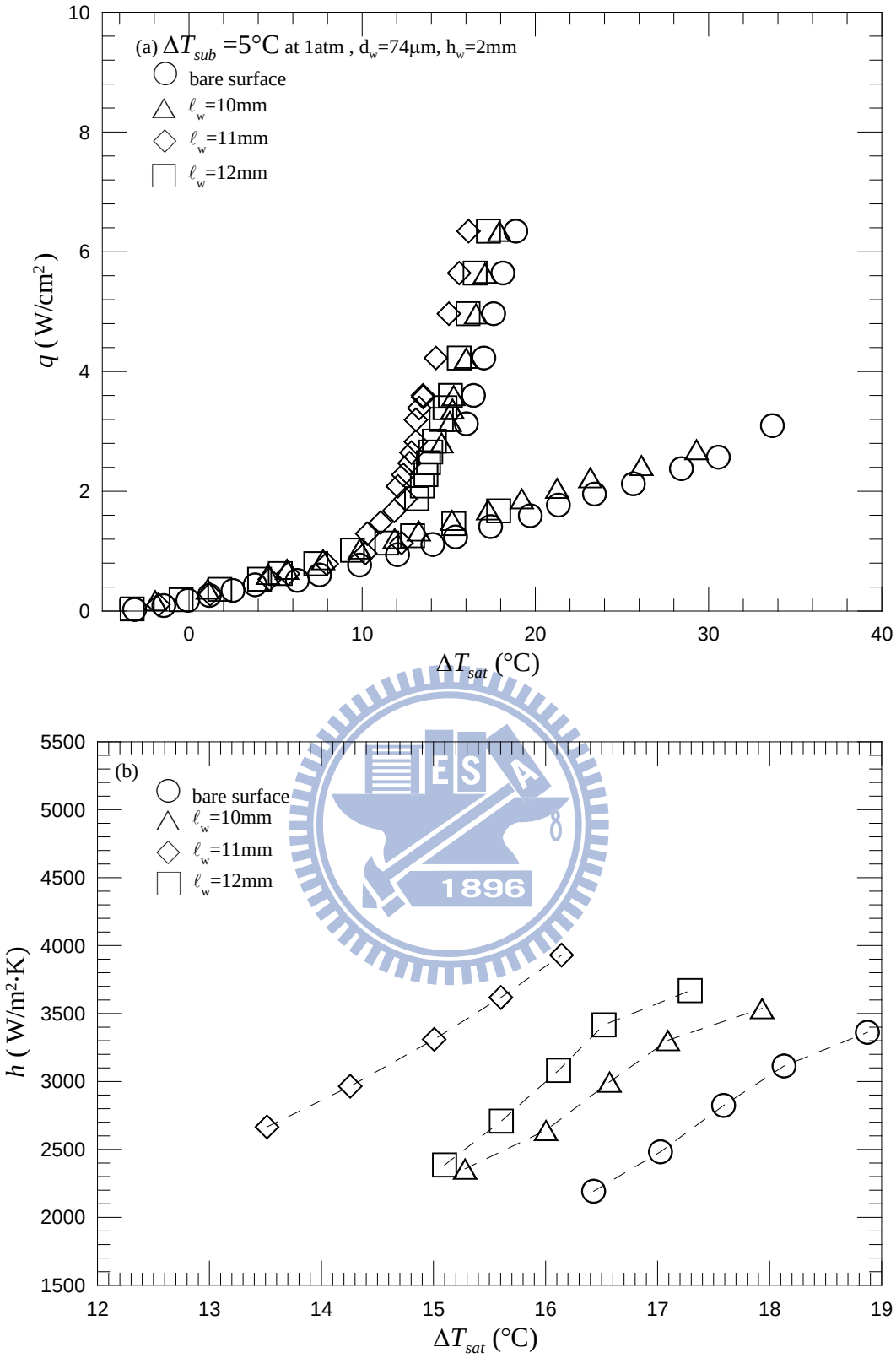

Fig. 5.40 Effects of string length on subcooled pool boiling curves (a) and boiling heat transfer coefficients (b) for ΔT_{sub}= 5°C at d_w=74μm and h_w=2mm.

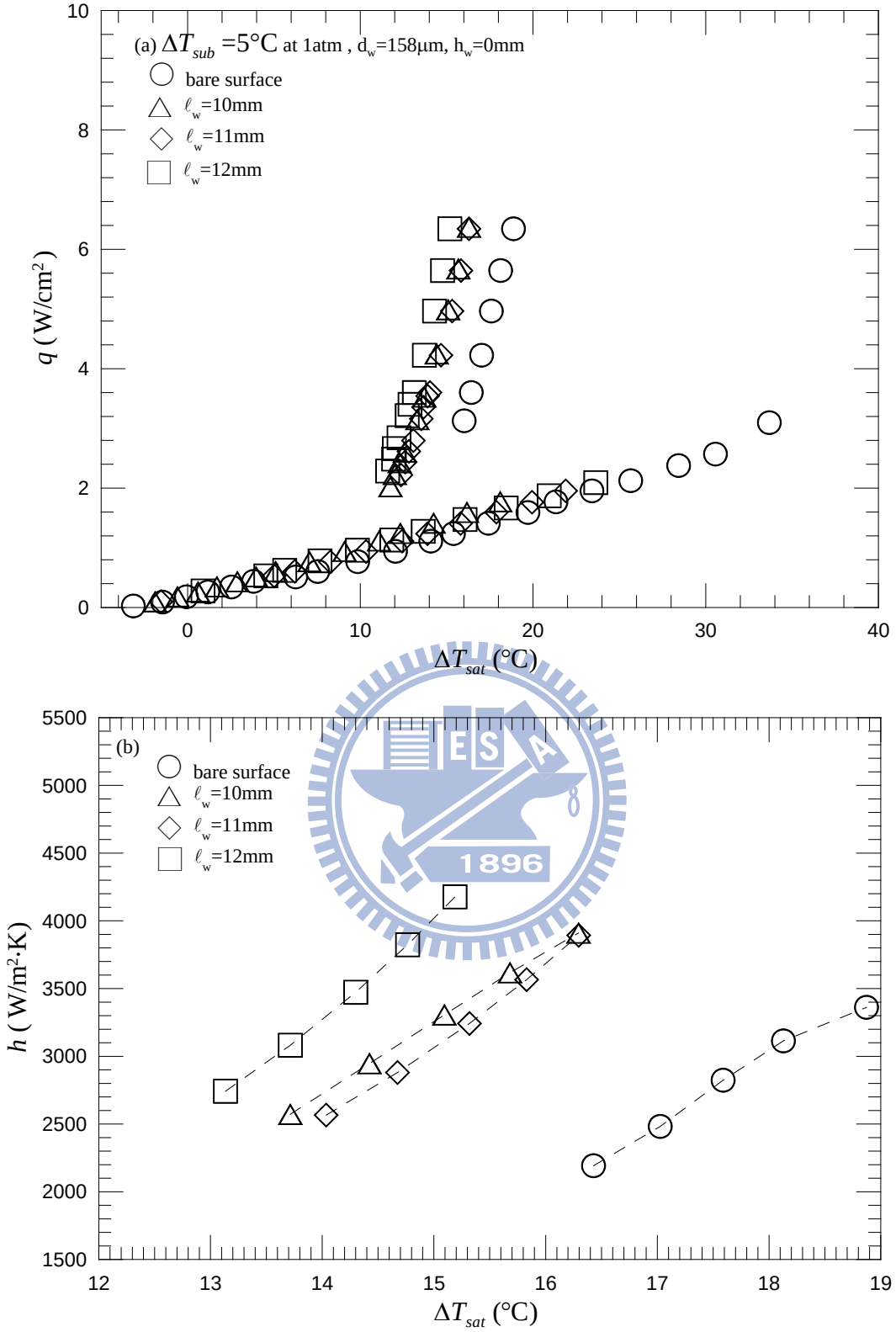

Fig. 5.41 Effects of string length on subcooled pool boiling curves (a) and boiling heat transfer coefficients (b) for ΔT_{sub}= 5°C at d_w=158μm and h_w=0mm.

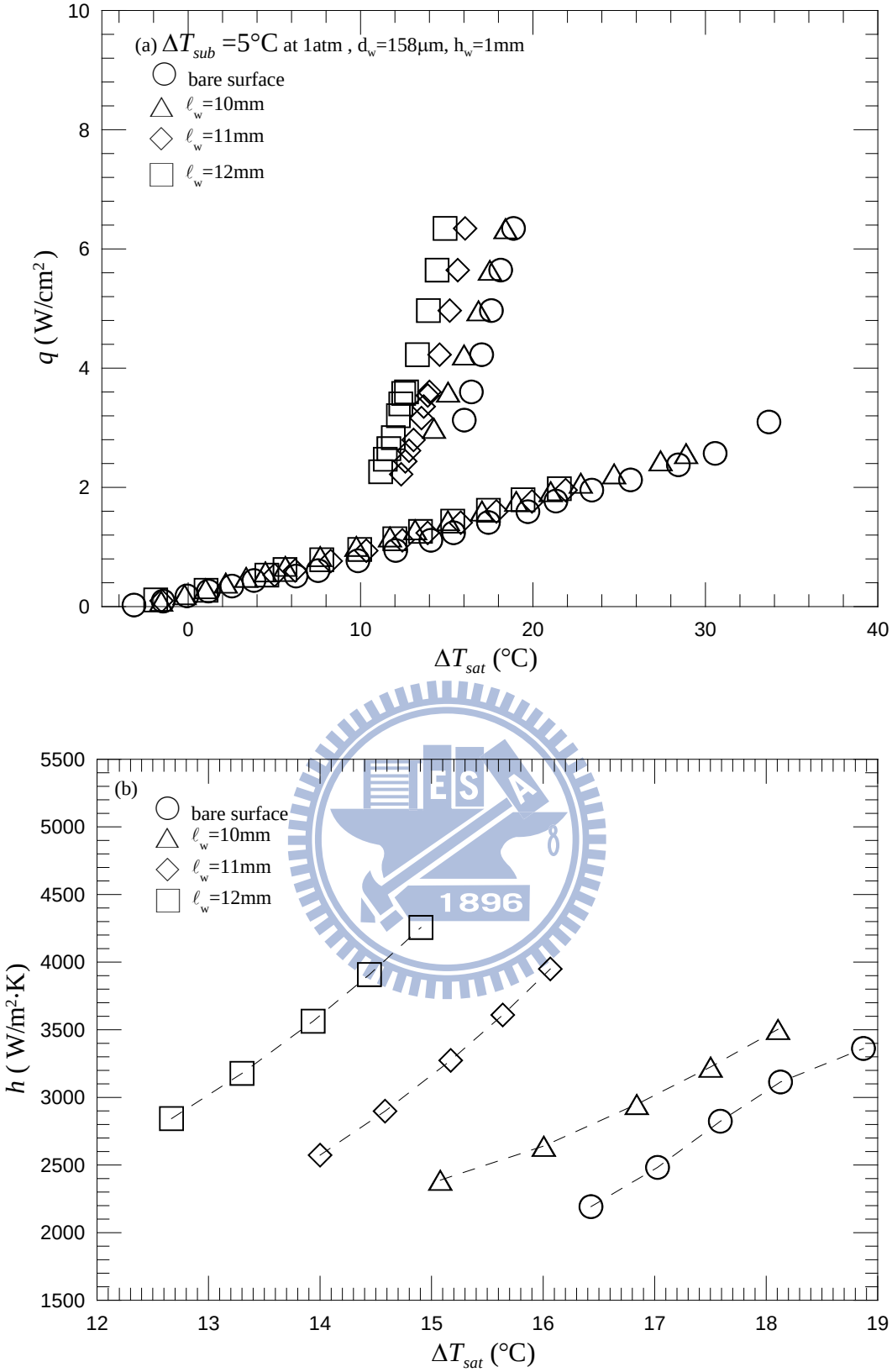

Fig. 5.42 Effects of string length on subcooled pool boiling curves (a) and boiling heat transfer coefficients (b) for ΔT_{sub}= 5°C at d_w=158μm and h_w=1mm.

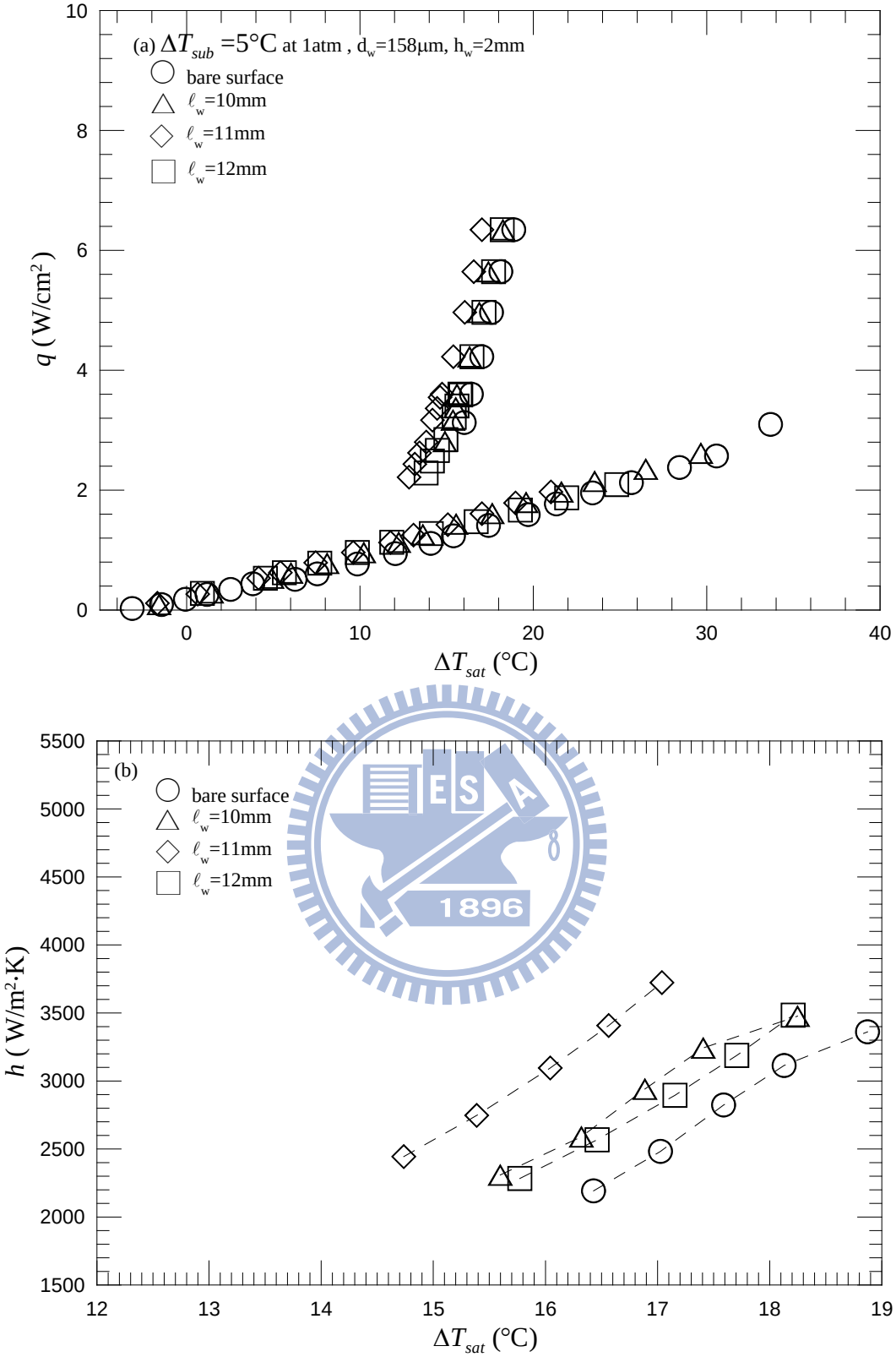

Fig. 5.43 Effects of string length on subcooled pool boiling curves (a) and boiling heat transfer coefficients (b) for ΔT_{sub}= 5°C at d_w=158μm and h_w=2mm.

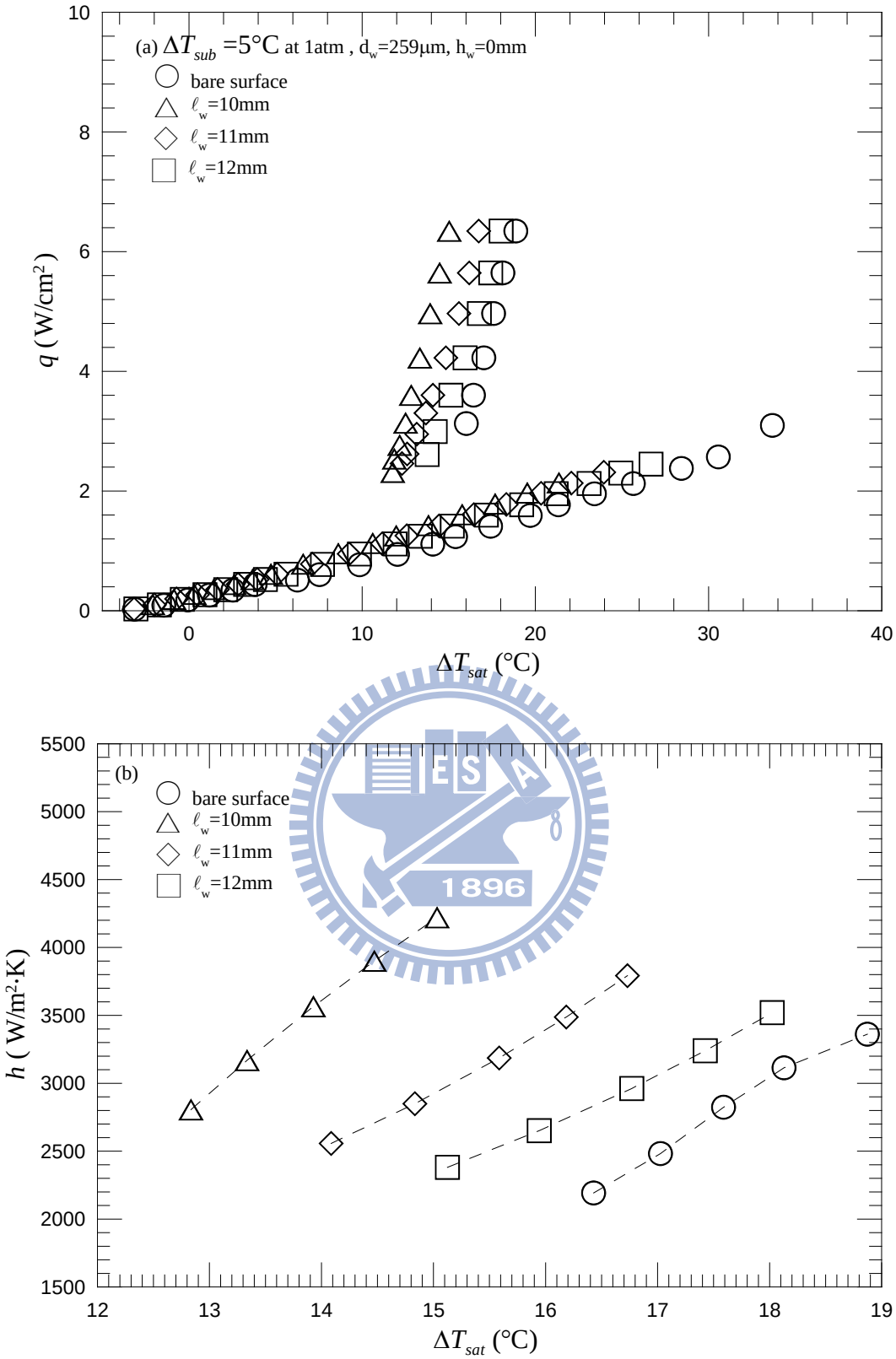

Fig. 5.44 Effects of string length on subcooled pool boiling curves (a) and boiling heat transfer coefficients (b) for ΔT_{sub}= 5°C at d_w=259μm and h_w=0mm.

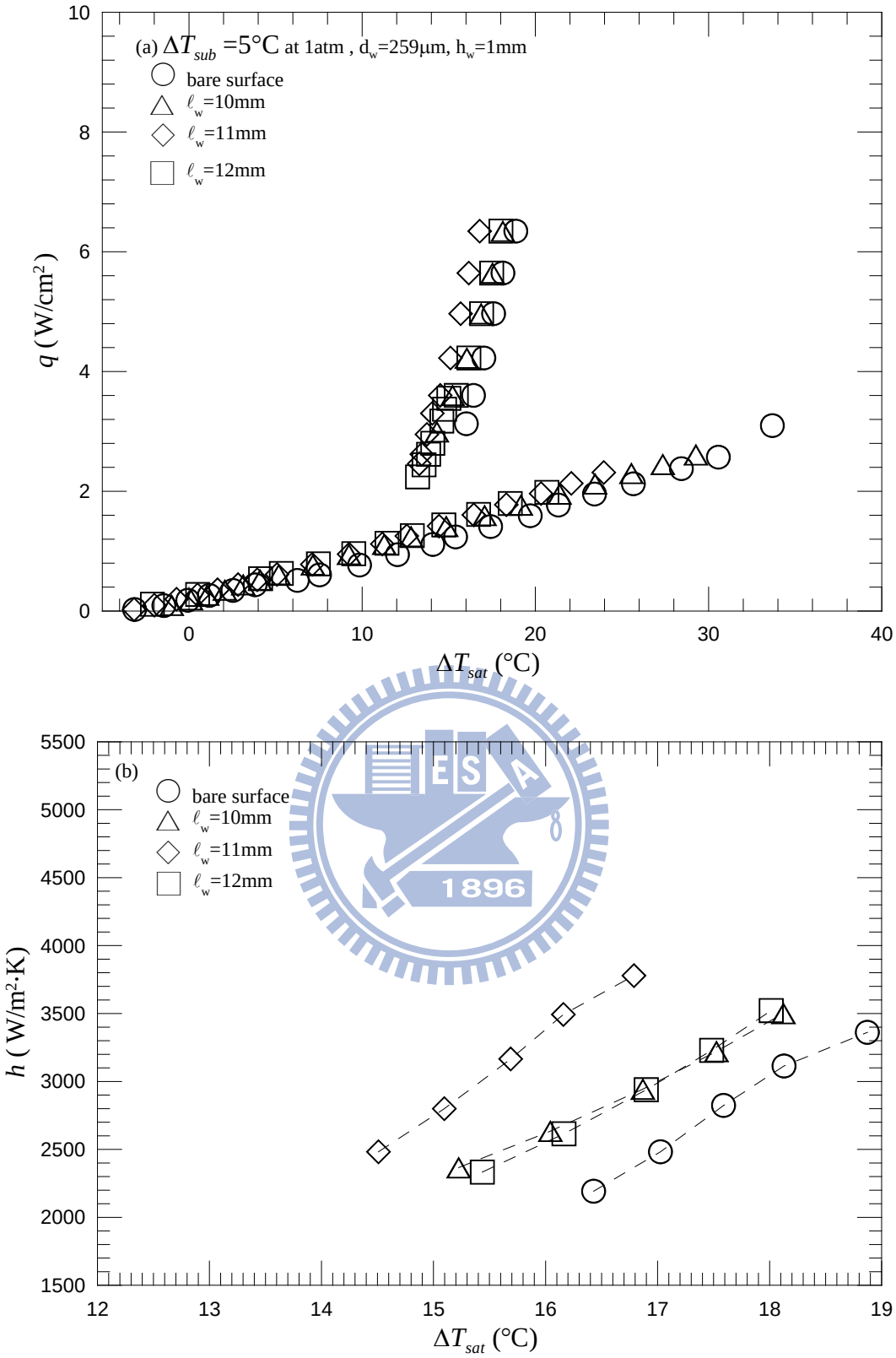

Fig. 5.45 Effects of string length on subcooled pool boiling curves (a) and boiling heat transfer coefficients (b) for ΔT_{sub}= 5°C at d_w=259μm and h_w=1mm.

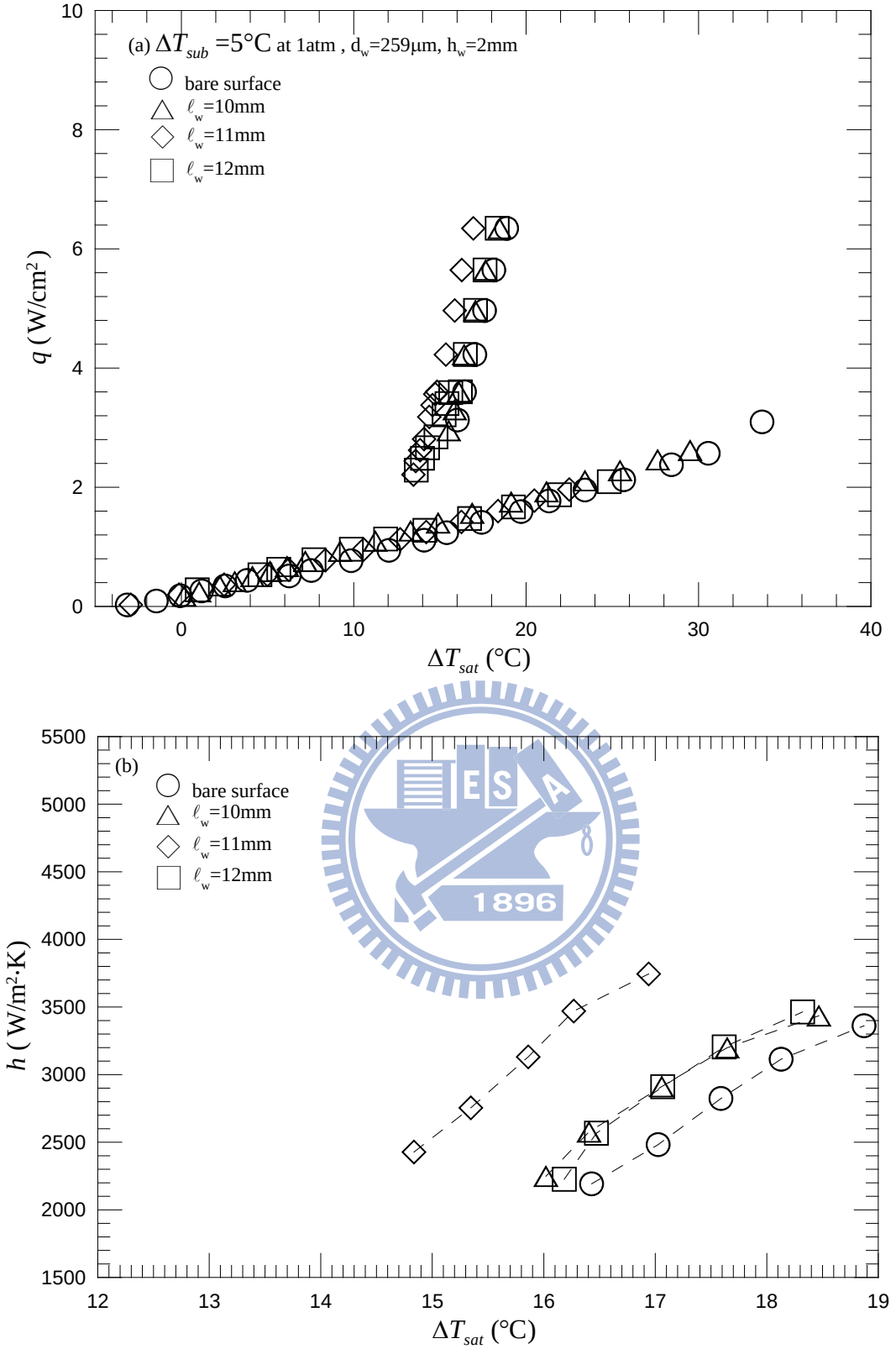

Fig. 5.46 Effects of string length on subcooled pool boiling curves (a) and boiling heat transfer coefficients (b) for ΔT_{sub}= 5°C at d_w=259μm and h_w=2mm.

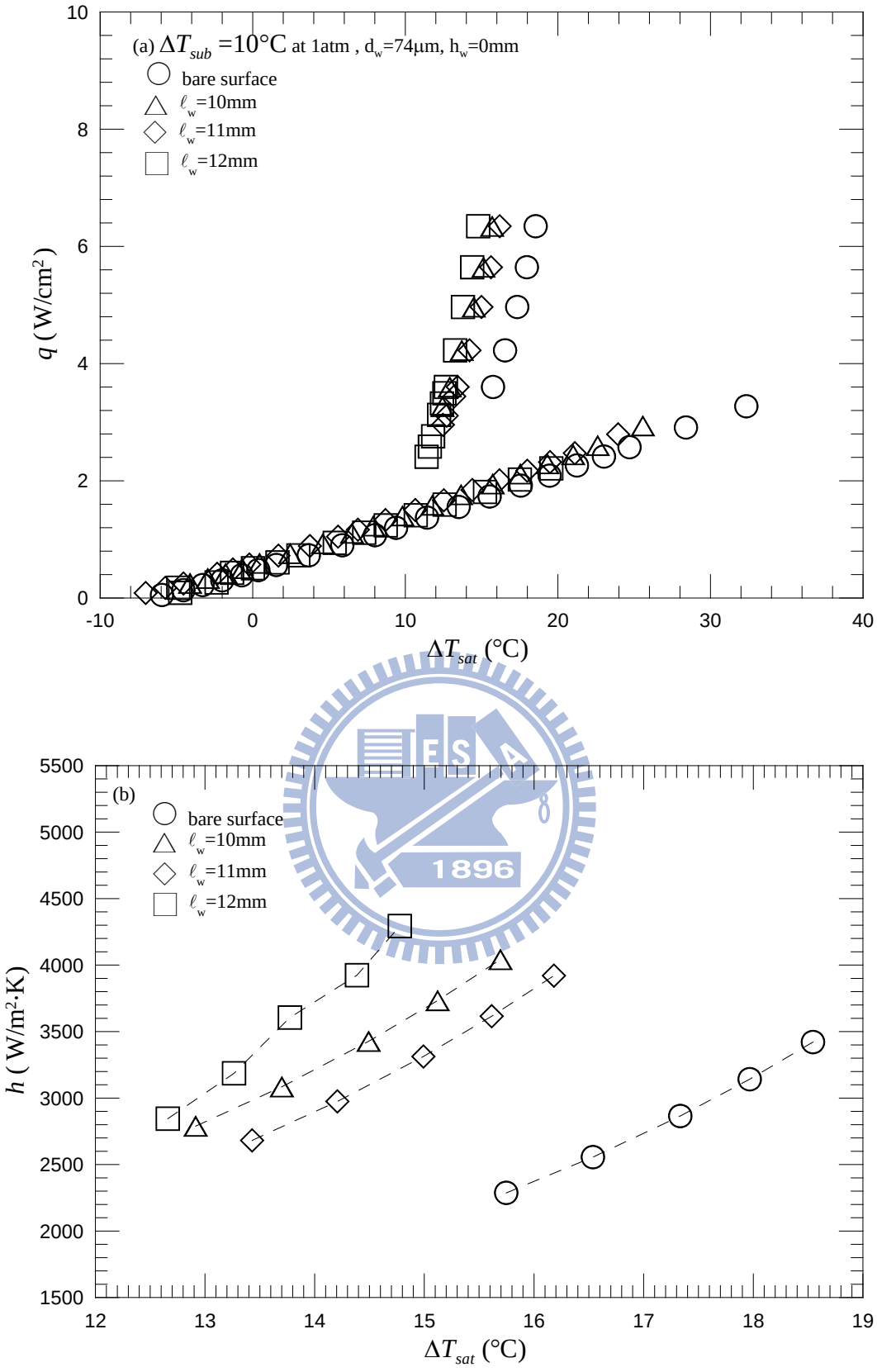

Fig. 5.47 Effects of string length on subcooled pool boiling curves (a) and boiling heat transfer coefficients (b) for ΔT_{sub}= 10°C at d_w=74μm and h_w=0mm.

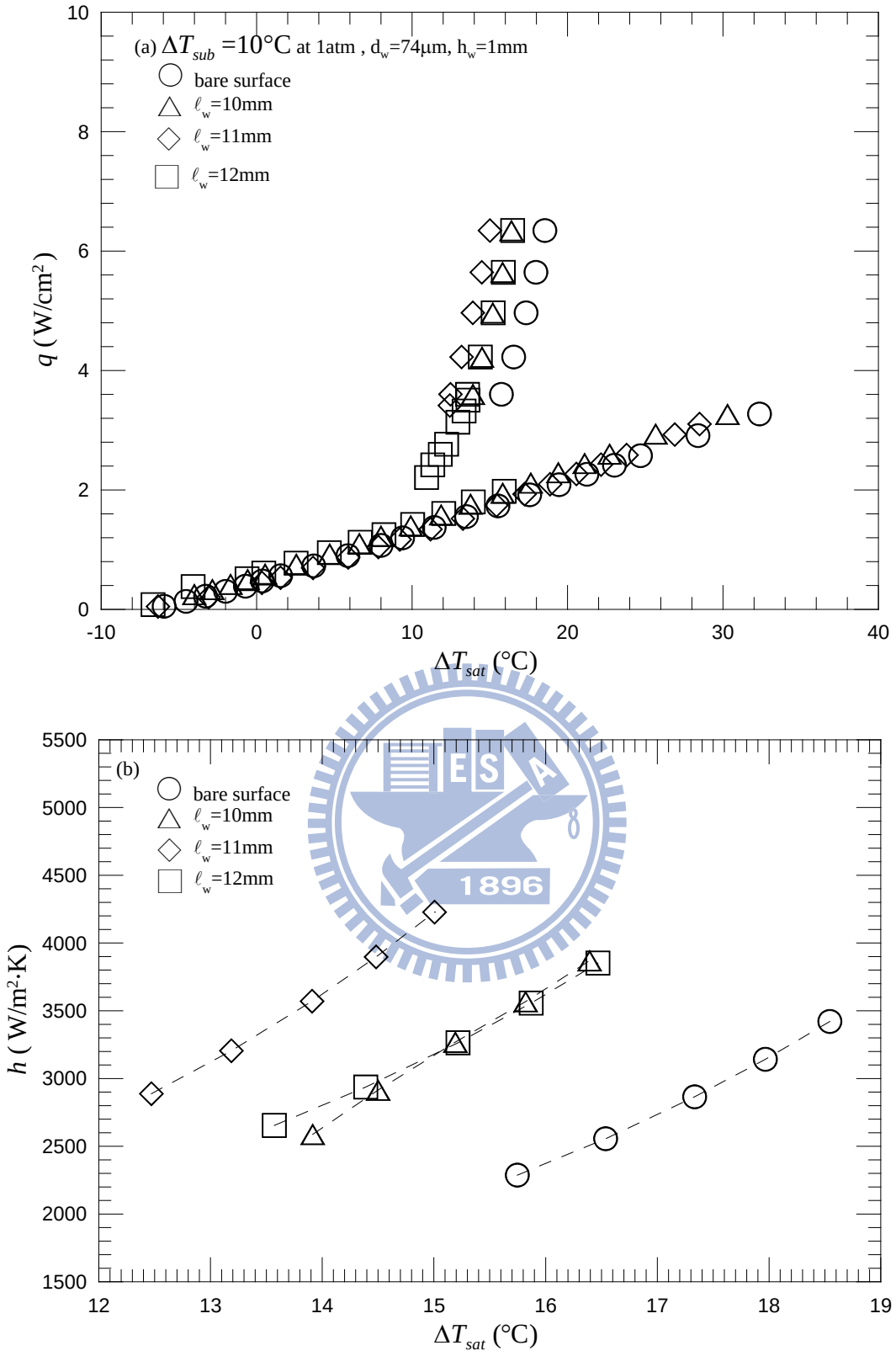

Fig. 5.48 Effects of string length on subcooled pool boiling curves (a) and boiling heat transfer coefficients (b) for ΔT_{sub}= 10°C at d_w=74μm and h_w=1mm.

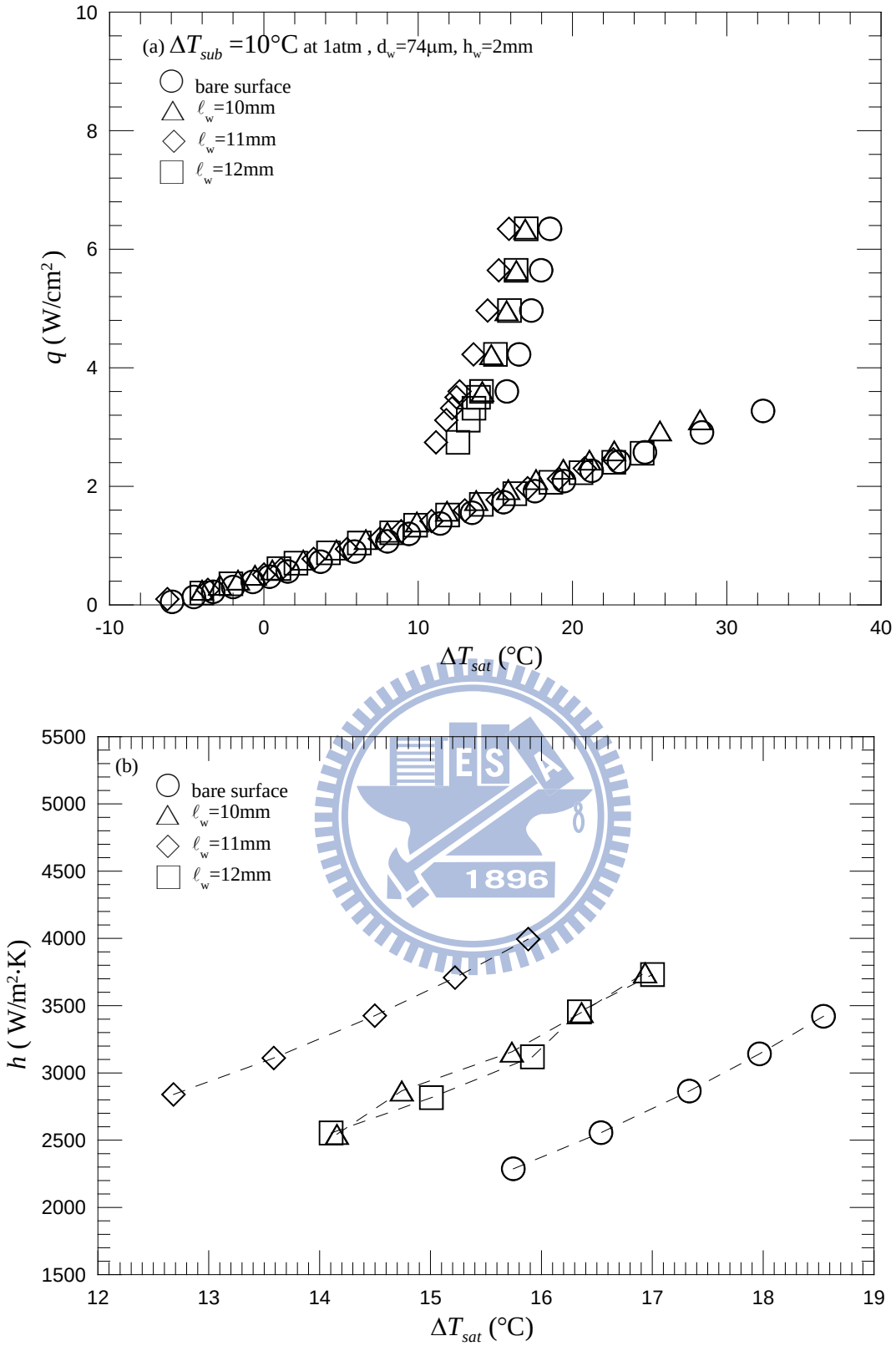

Fig. 5.49 Effects of string length on subcooled pool boiling curves (a) and boiling heat transfer coefficients (b) for ΔT_{sub}= 10°C at d_w=74μm and h_w=2mm.

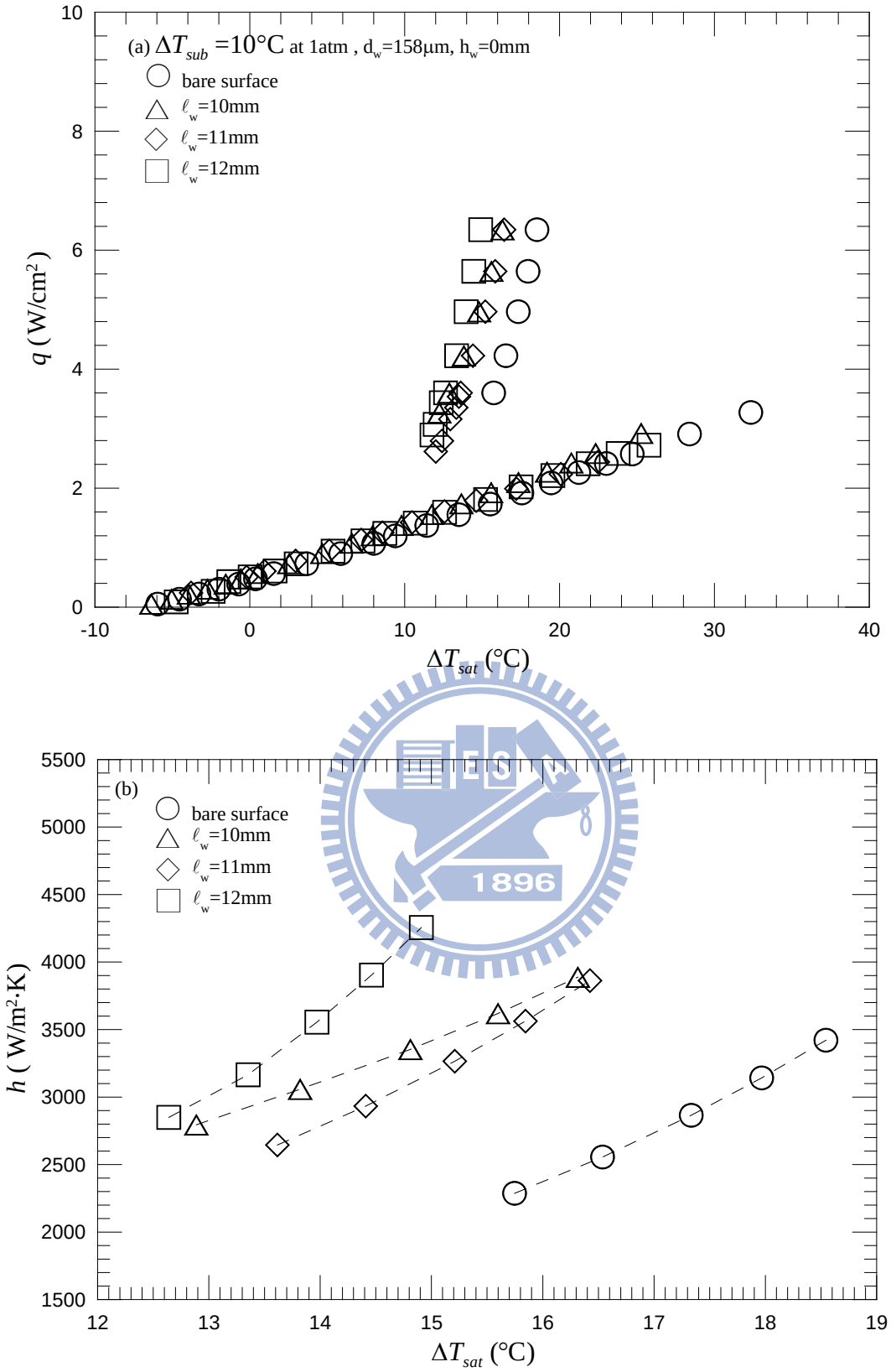

Fig. 5.50 Effects of string length on subcooled pool boiling curves (a) and boiling heat transfer coefficients (b) for ΔT_{sub}= 10°C at d_w=158μm and h_w=0mm.

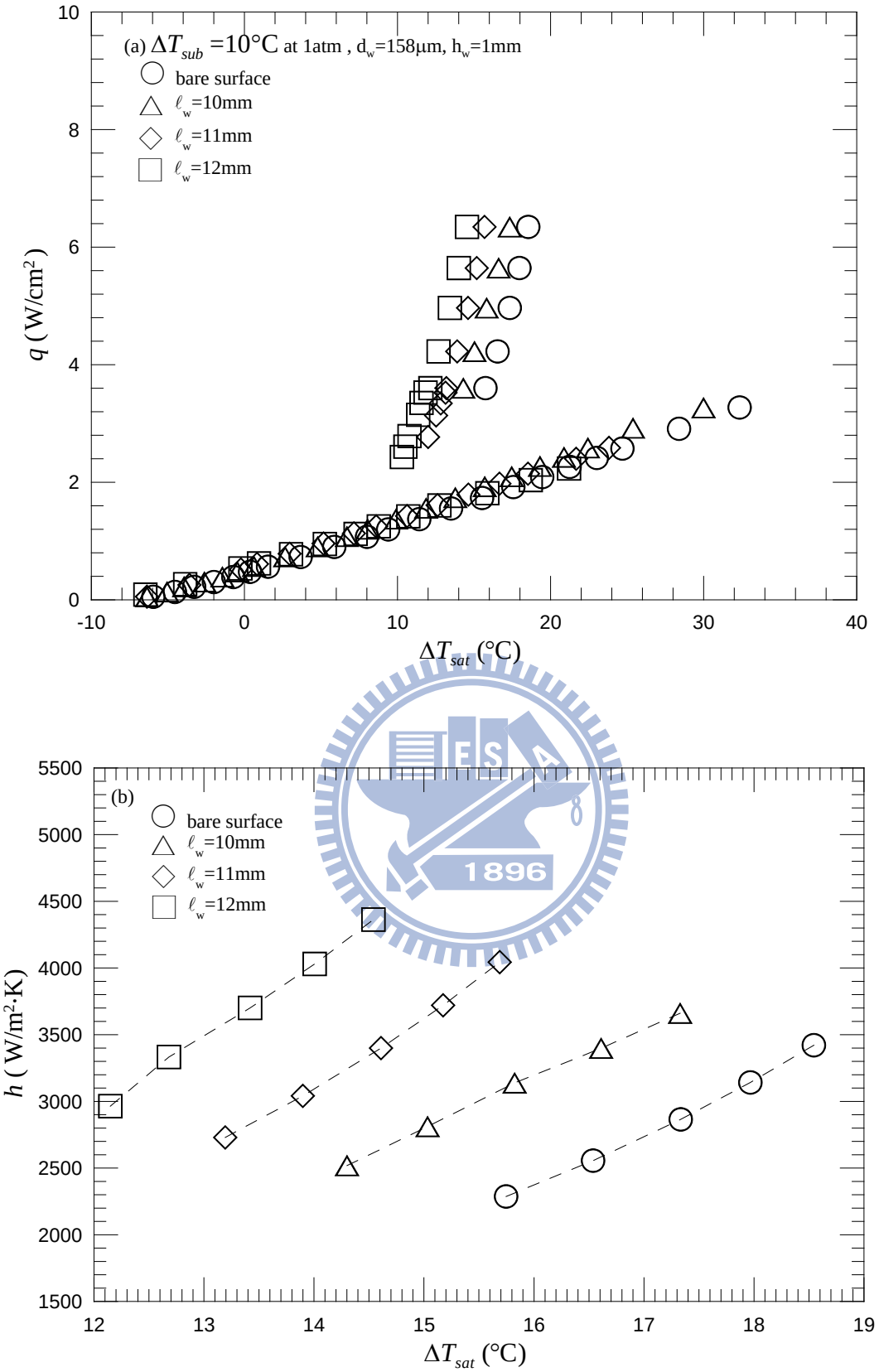

Fig. 5.51 Effects of string length on subcooled pool boiling curves (a) and boiling heat transfer coefficients (b) for ΔT_{sub}= 10°C at d_w=158μm and h_w=1mm.

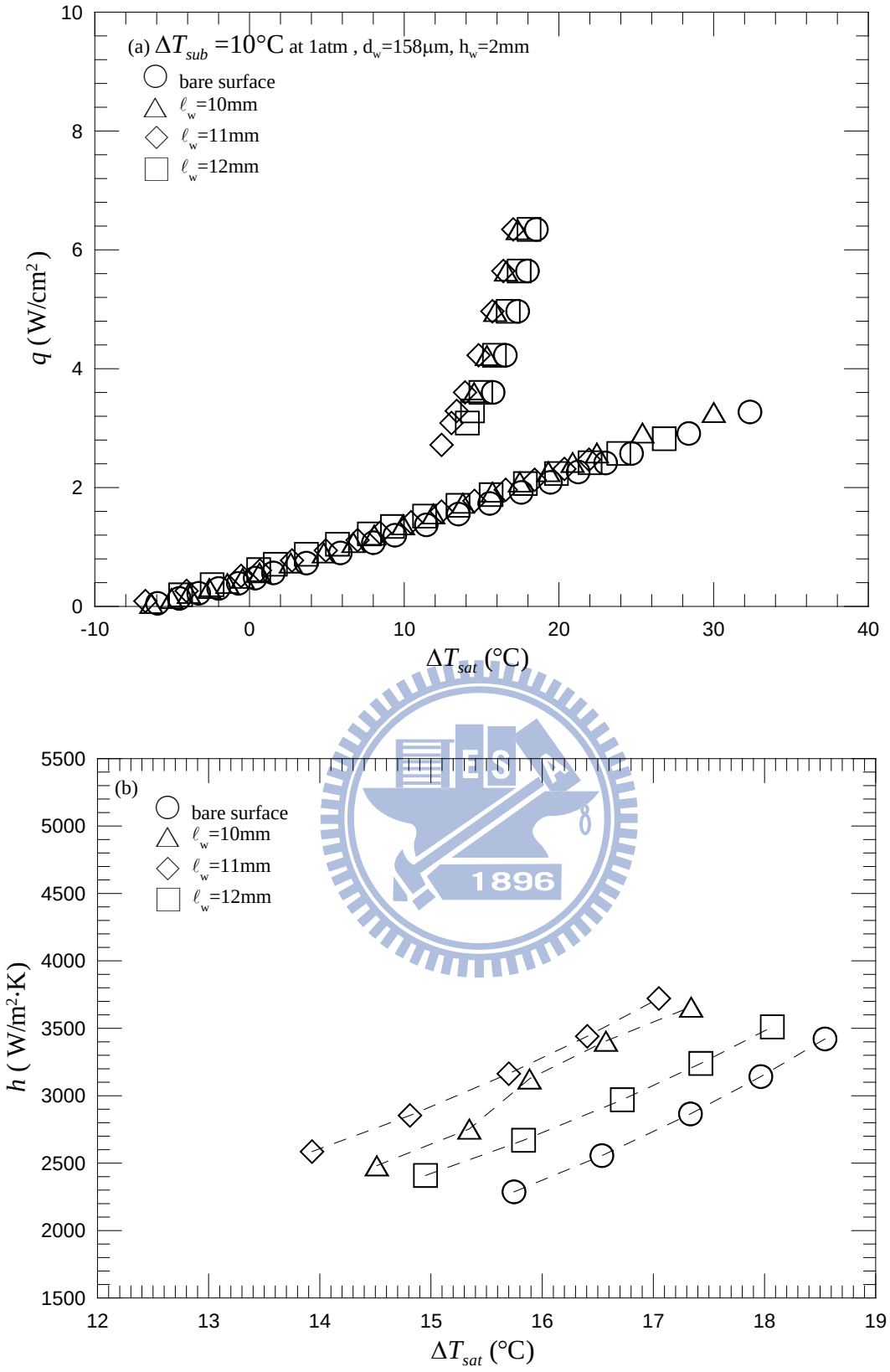

Fig. 5.52 Effects of string length on subcooled pool boiling curves (a) and boiling heat transfer coefficients (b) for ΔT_{sub}= 10°C at d_w=158μm and h_w=2mm.

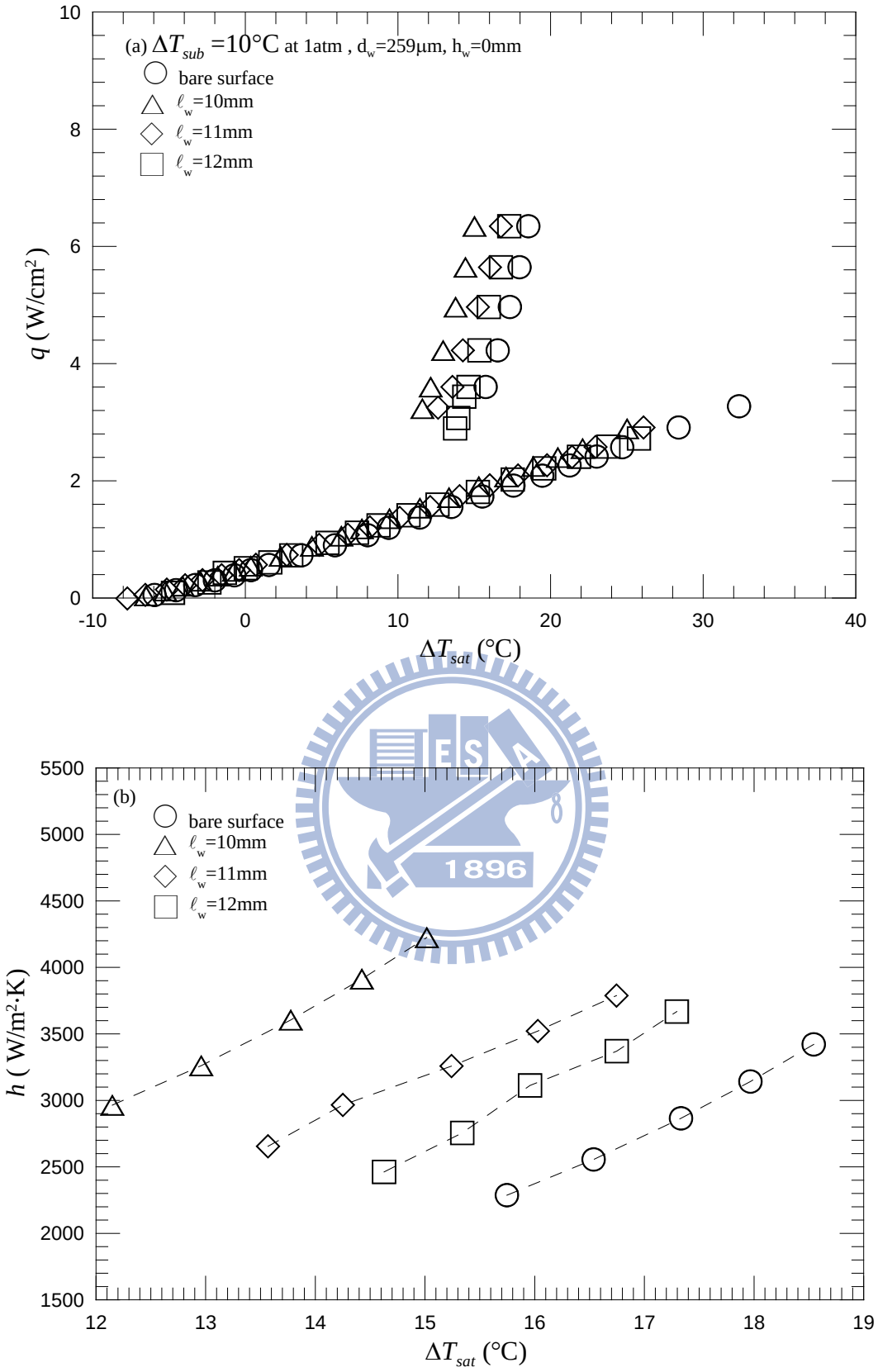

Fig. 5.53 Effects of string length on subcooled pool boiling curves (a) and boiling heat transfer coefficients (b) for ΔT_{sub}= 10°C at d_w=259μm and h_w=0mm.

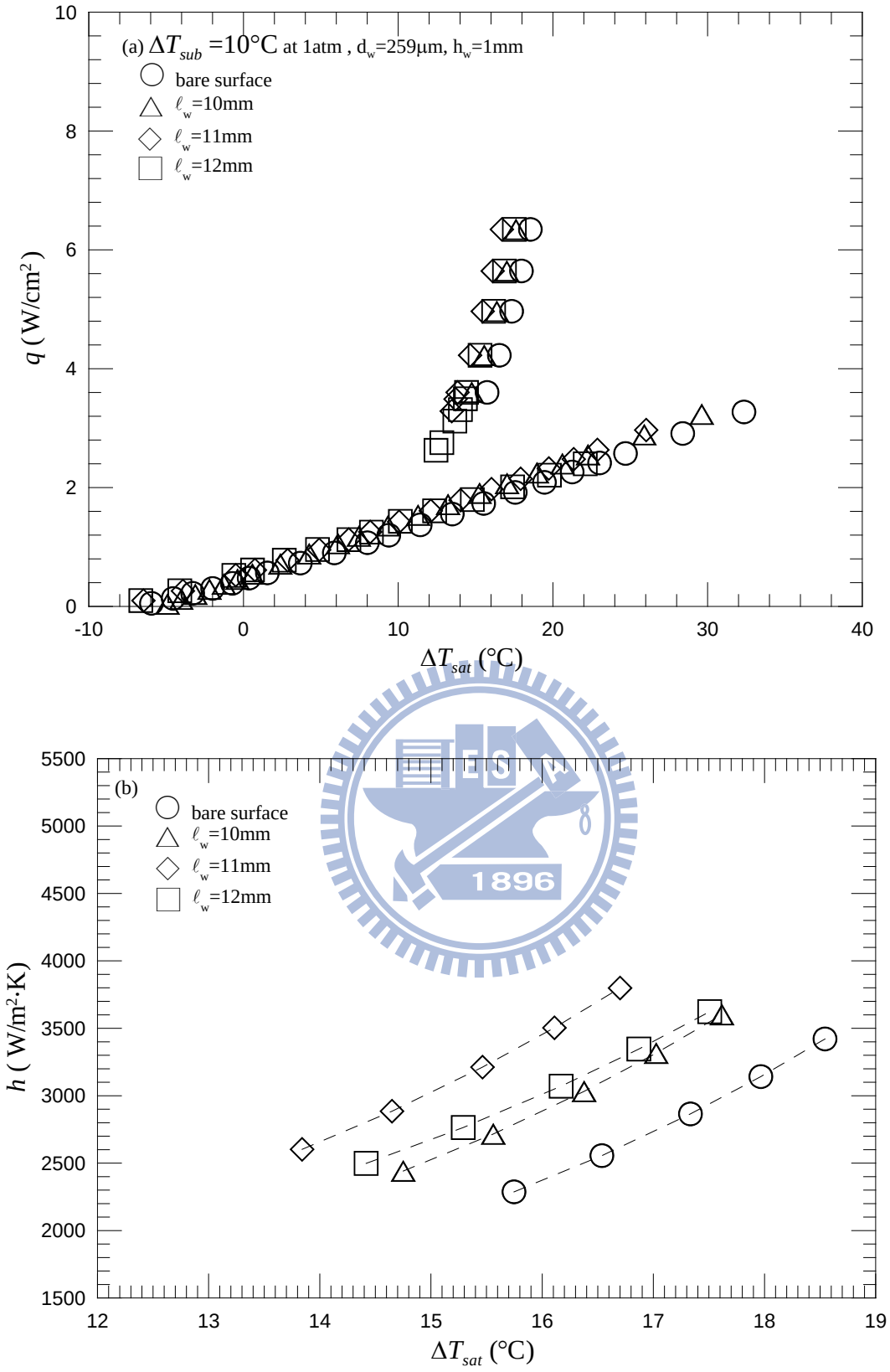

Fig. 5.54 Effects of string length on subcooled pool boiling curves (a) and boiling heat transfer coefficients (b) for ΔT_{sub}= 10°C at d_w=259μm and h_w=1mm.

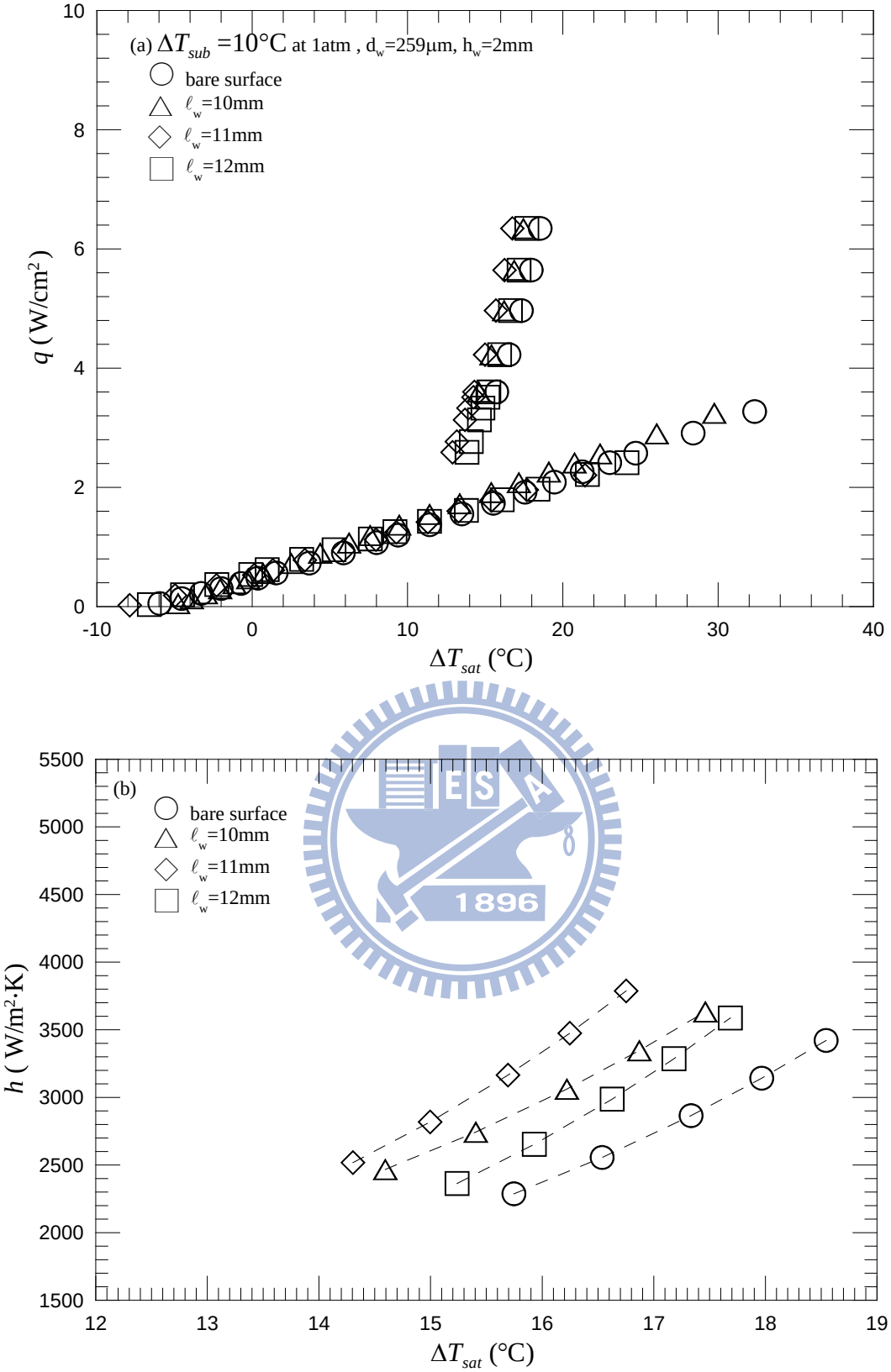

Fig. 5.55 Effects of string length on subcooled pool boiling curves (a) and boiling heat transfer coefficients (b) for ΔT_{sub}= 10°C at d_w=259μm and h_w=2mm.

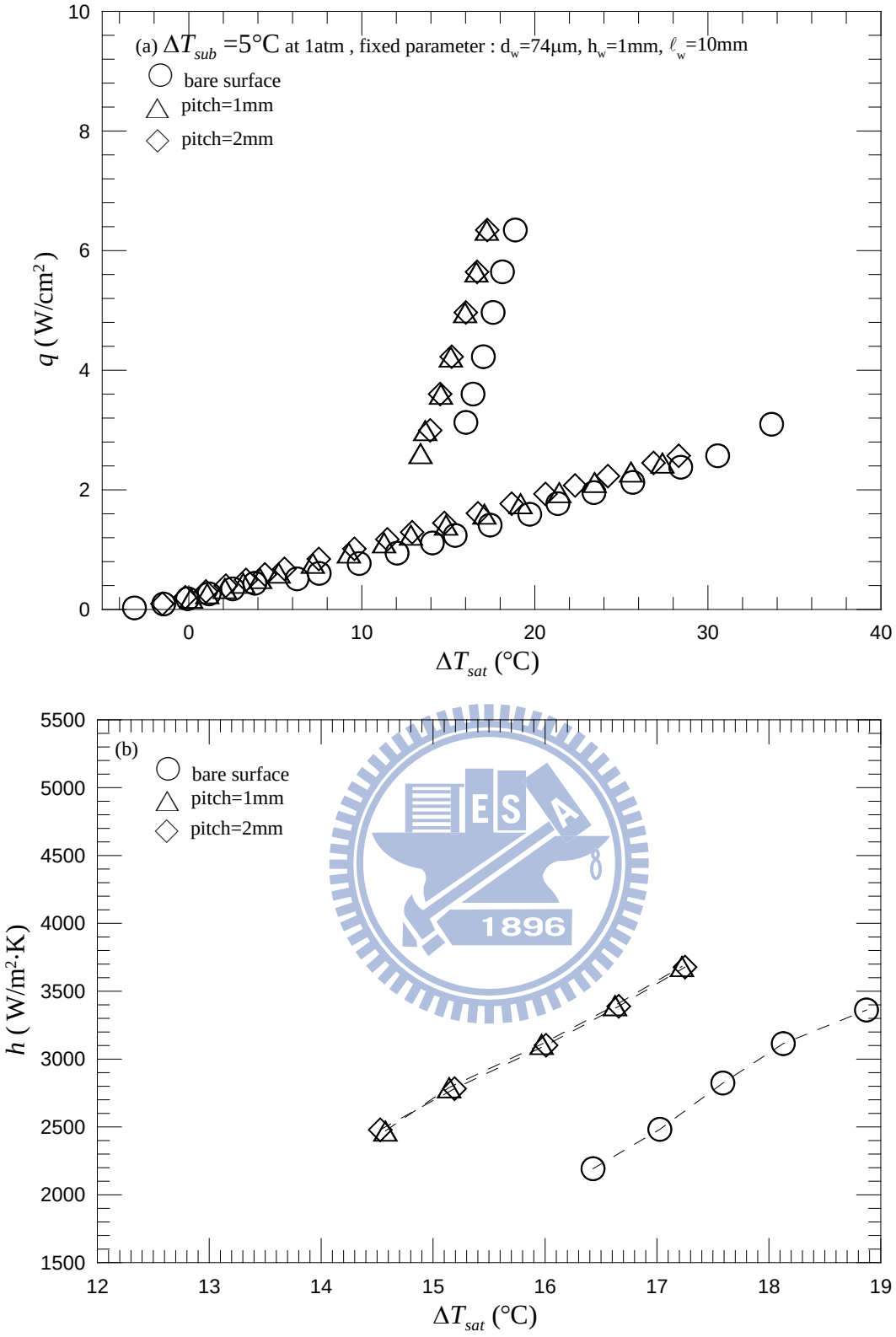

Fig. 5.56 Effects of string string-string pitch on subcooled pool boiling curves (a) and boiling heat transfer coefficients (b) for ΔT_{sub}= 5°C at d_w=74μm, h_w=1mm and ℓ_w =10mm.

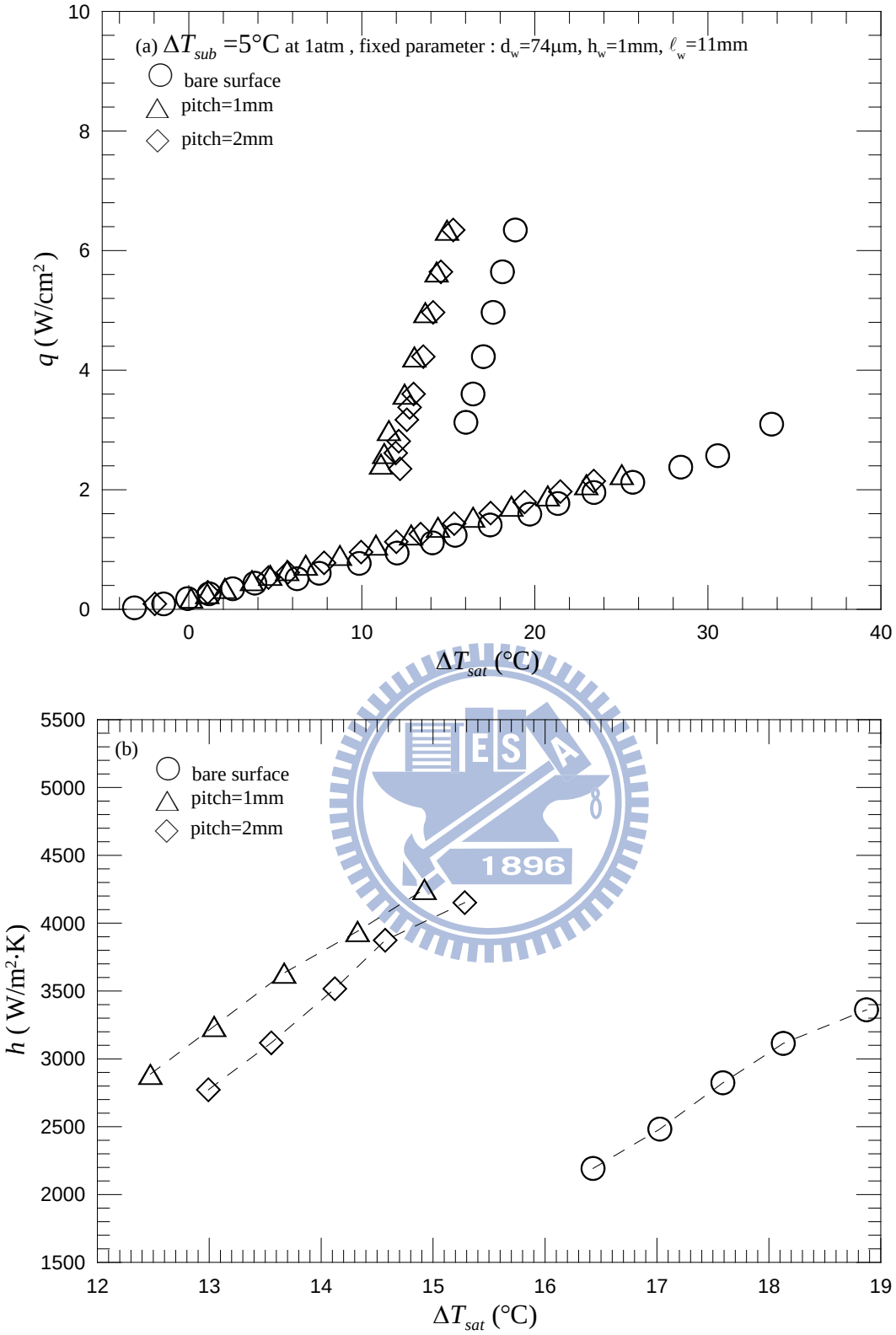

Fig. 5.57 Effects of string string-string pitch on subcooled pool boiling curves (a) and boiling heat transfer coefficients (b) for ΔT_{sub}= 5°C at d_w=74μm, h_w=1mm and ℓ_w =11mm.

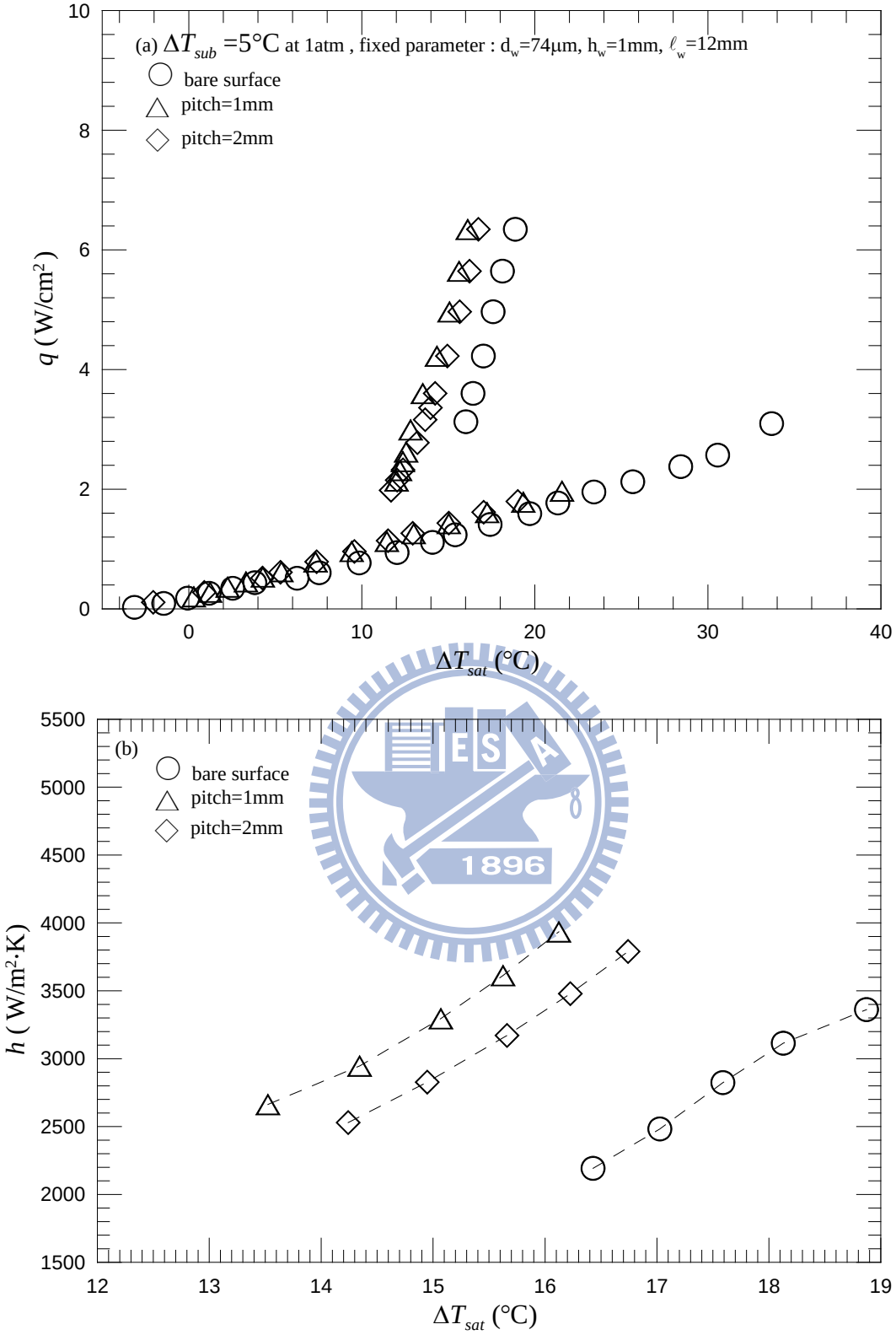

Fig. 5.58 Effects of string string-string pitch on subcooled pool boiling curves (a) and boiling heat transfer coefficients (b) for ΔT_{sub}= 5°C at d_w=74μm, h_w=1mm and ℓ_w =12mm.

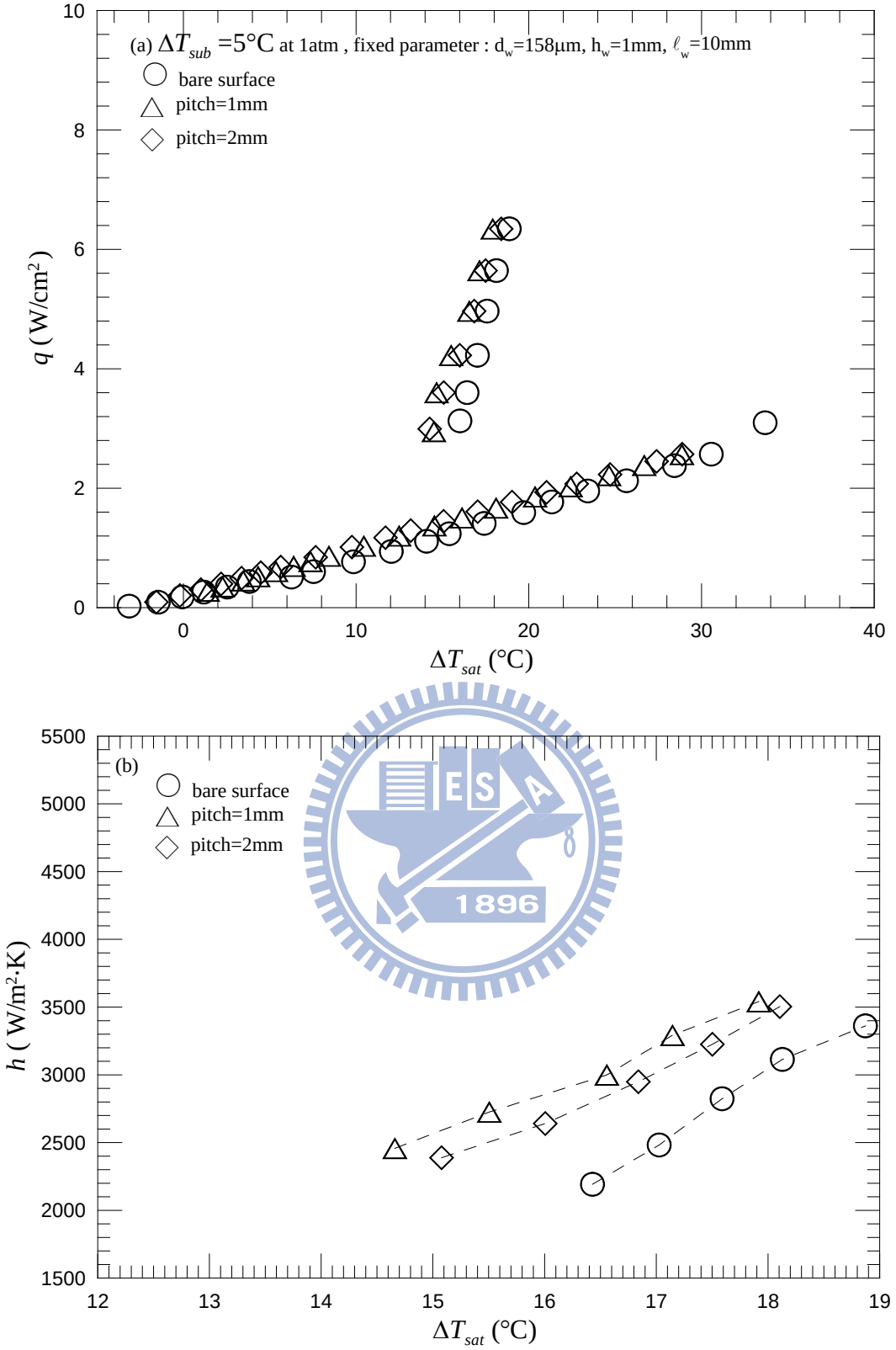

Fig. 5.59 Effects of string string-string pitch on subcooled pool boiling curves (a) and boiling heat transfer coefficients (b) for ΔT_{sub}= 5°C at d_w=158μm, h_w=1mm and ℓ_w =10mm.

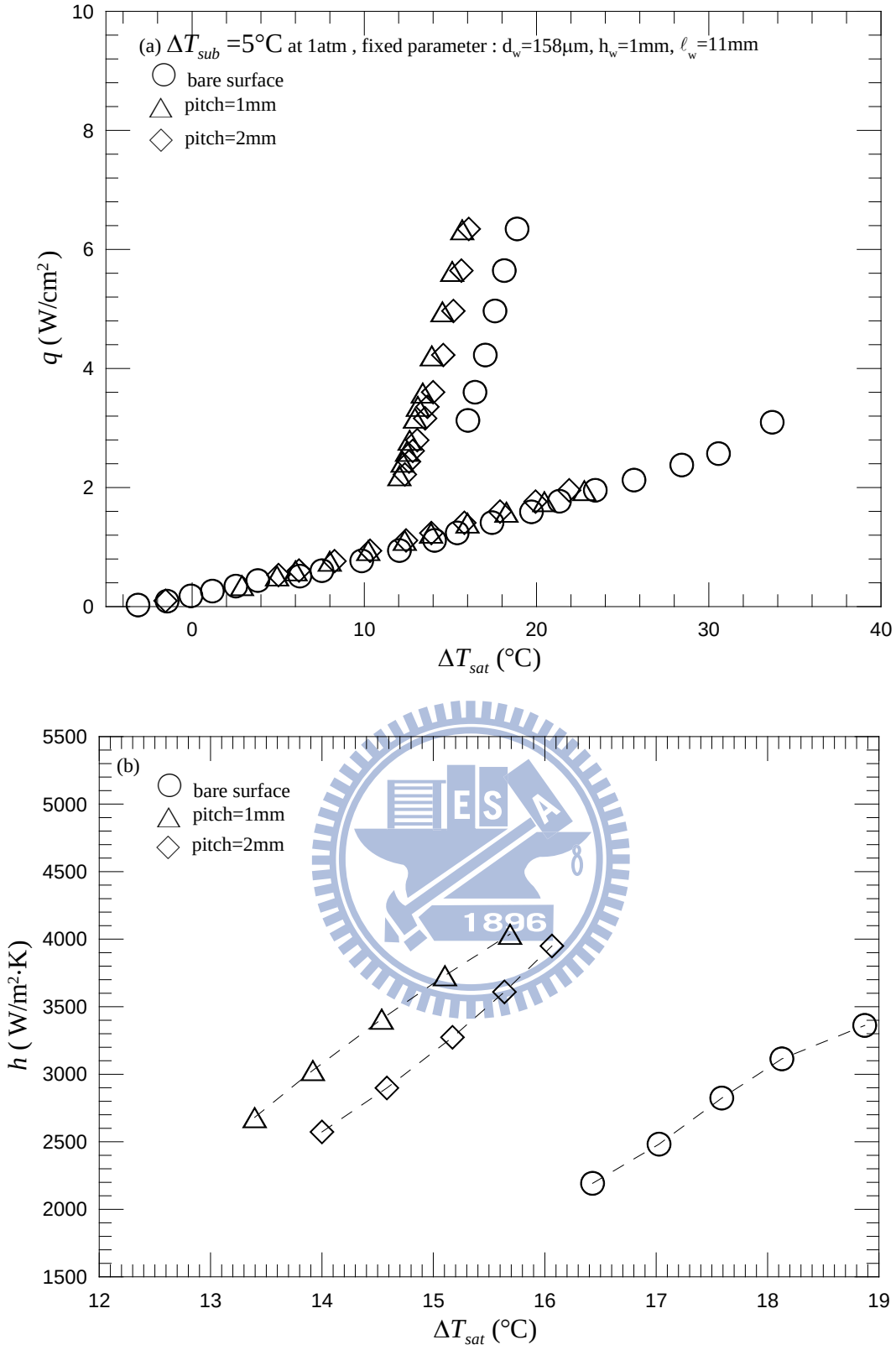

Fig. 5.60 Effects of string string-string pitch on subcooled pool boiling curves (a) and boiling heat transfer coefficients (b) for ΔT_{sub}= 5°C at d_w=158μm, h_w=1mm and ℓ_w =11mm.

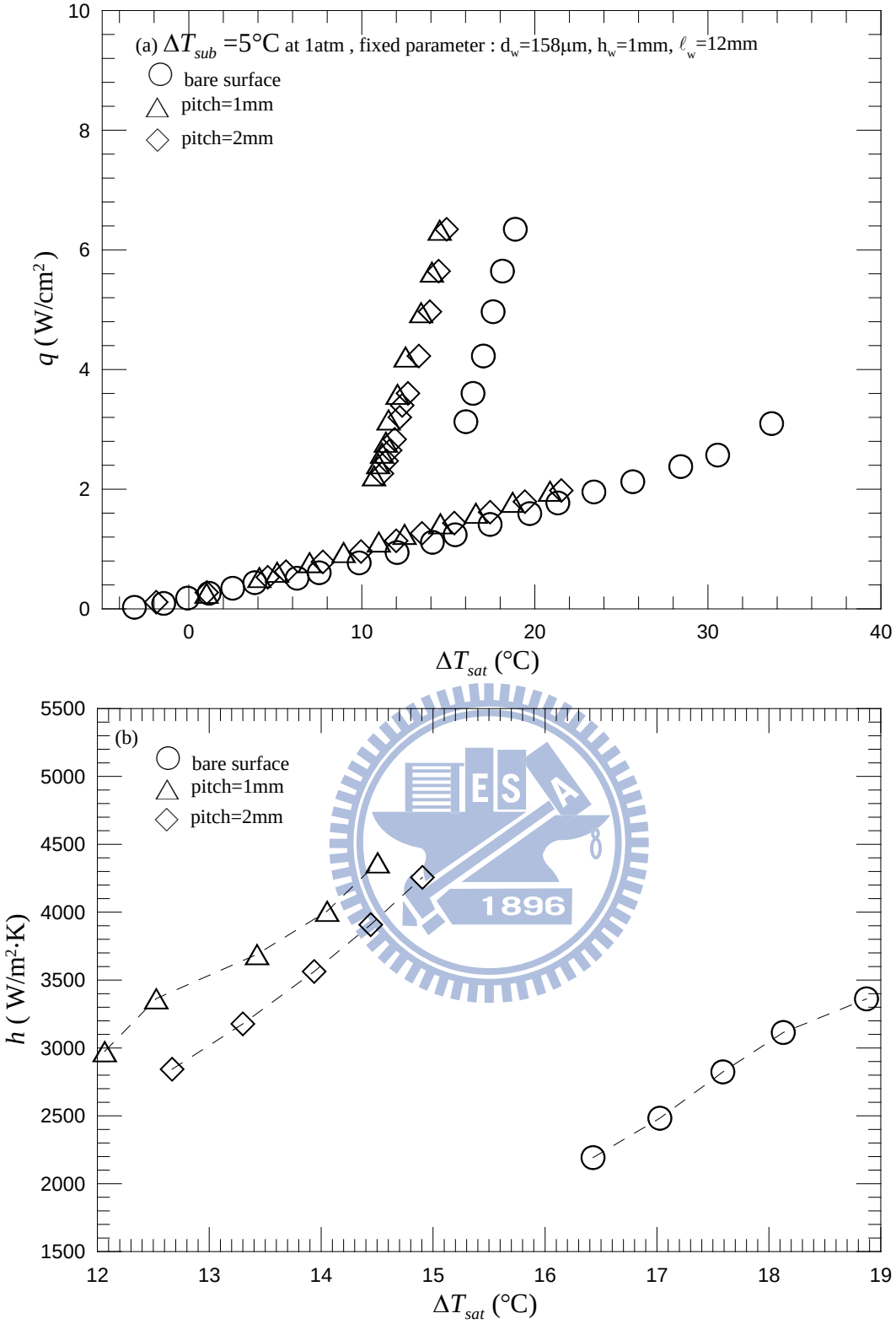

Fig. 5.61 Effects of string string-string pitch on subcooled pool boiling curves (a) and boiling heat transfer coefficients (b) for ΔT_{sub}= 5°C at d_w=158μm, h_w=1mm and ℓ_w =12mm.

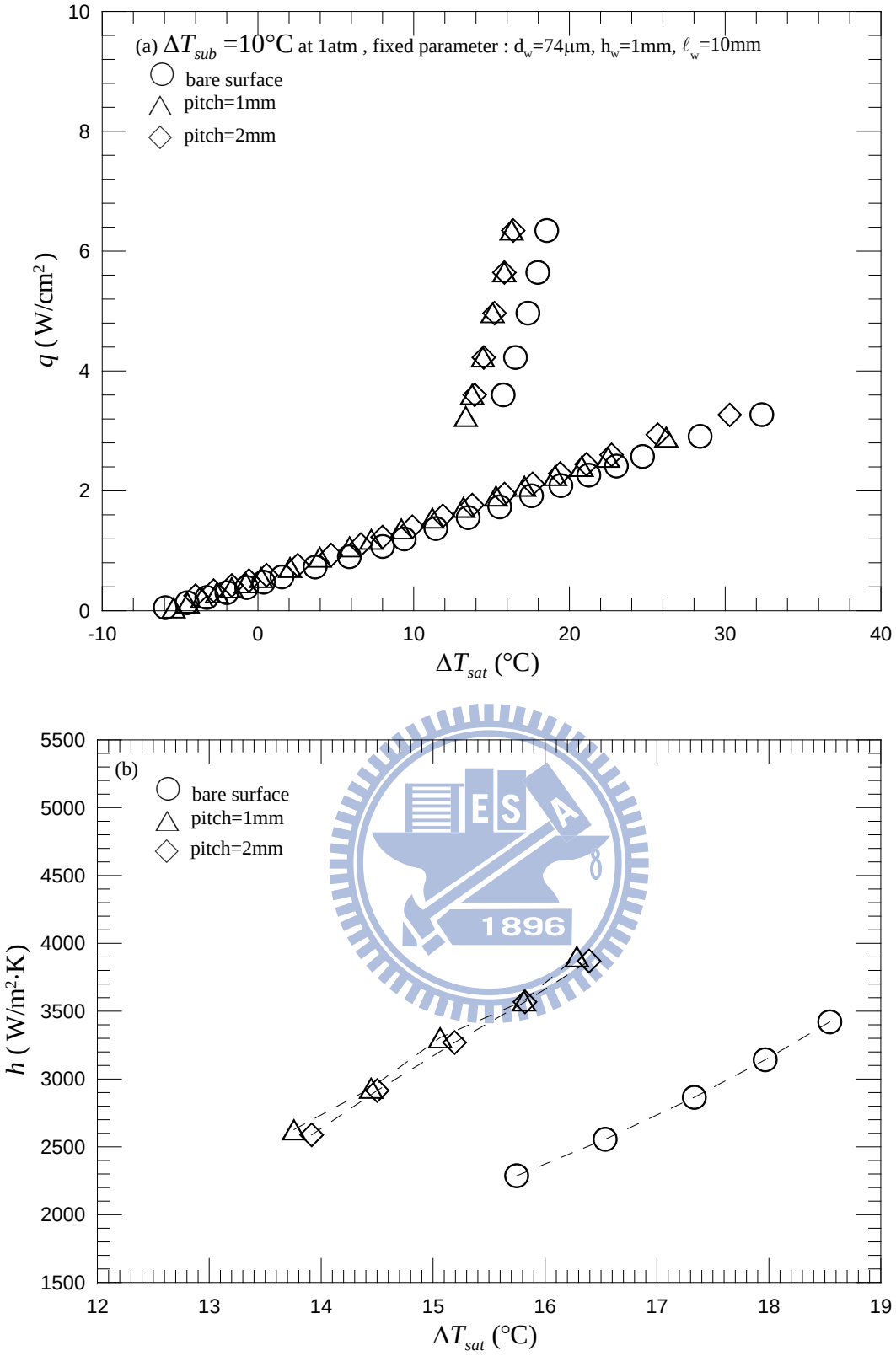

Fig. 5.62 Effects of string string-string pitch on subcooled pool boiling curves (a) and boiling heat transfer coefficients (b) for ΔT_{sub}= 10°C at d_w=74μm, h_w=1mm and ℓ_w =10mm.

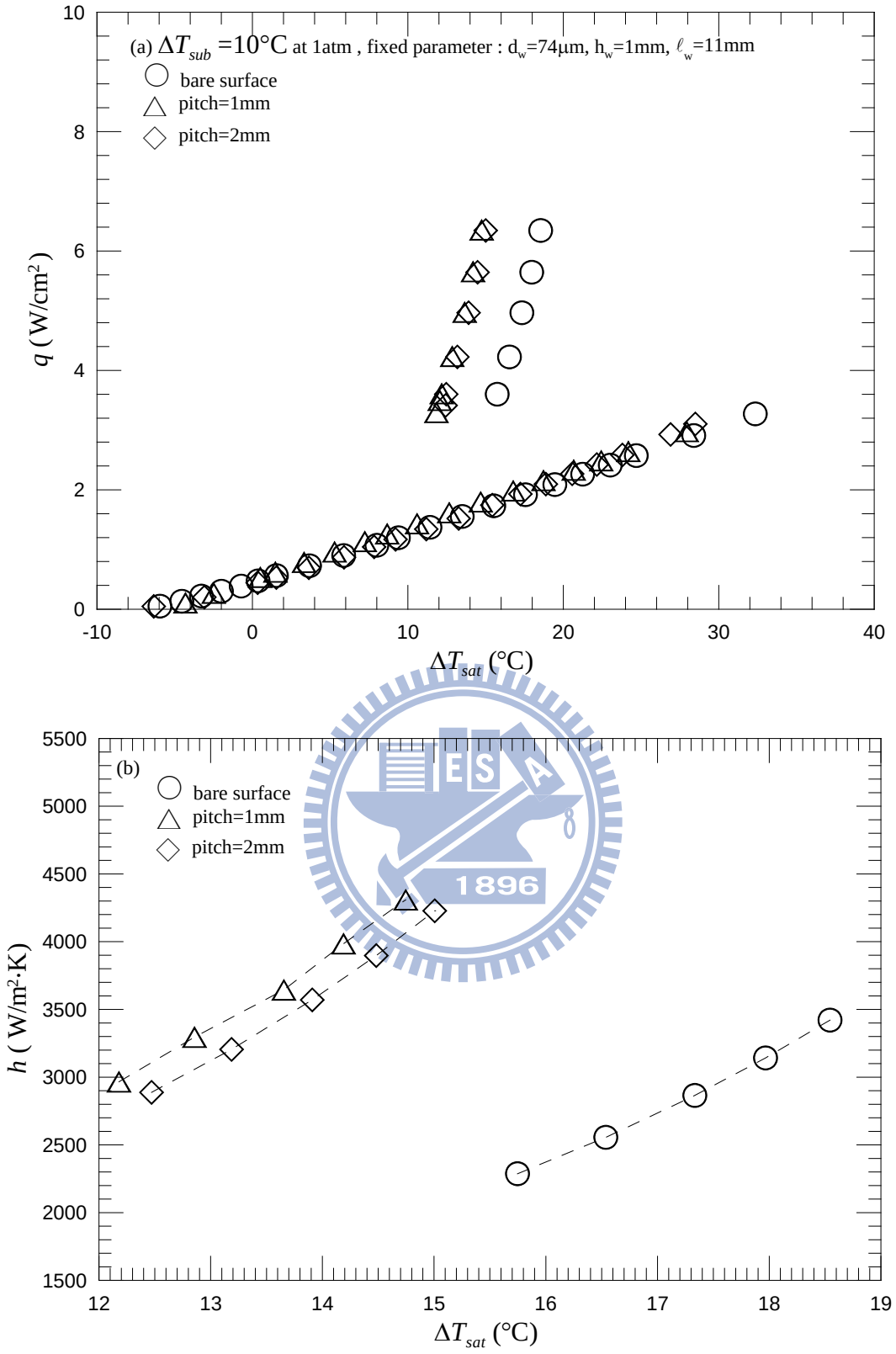

Fig. 5.63 Effects of string string-string pitch on subcooled pool boiling curves (a) and boiling heat transfer coefficients (b) for ΔT_{sub}= 10°C at d_w=74μm, h_w=1mm and ℓ_w =11mm.

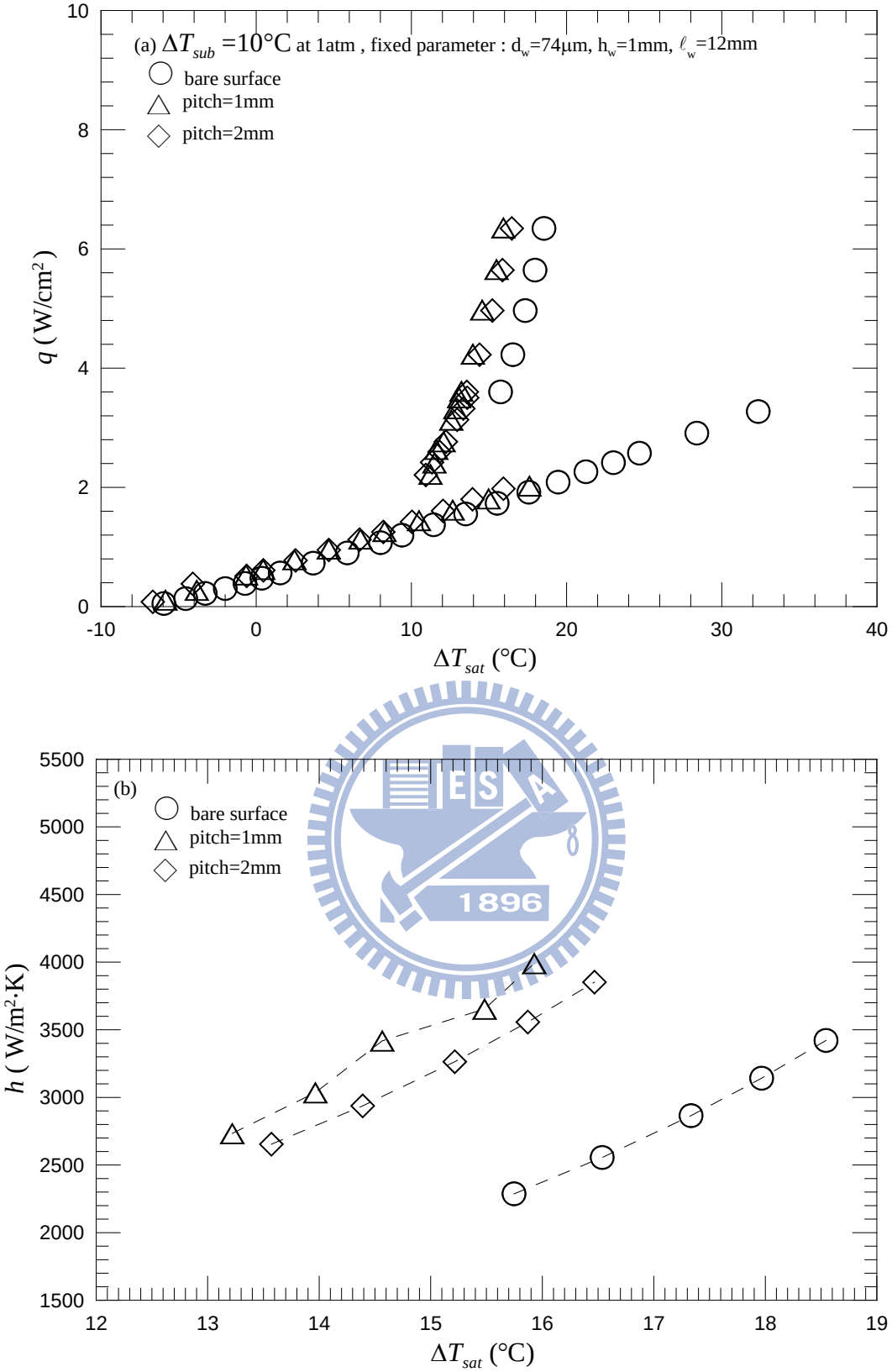

Fig. 5.64 Effects of string string-string pitch on subcooled pool boiling curves (a) and boiling heat transfer coefficients (b) for ΔT_{sub}= 10°C at d_w=74μm, h_w=1mm and ℓ_w =12mm.

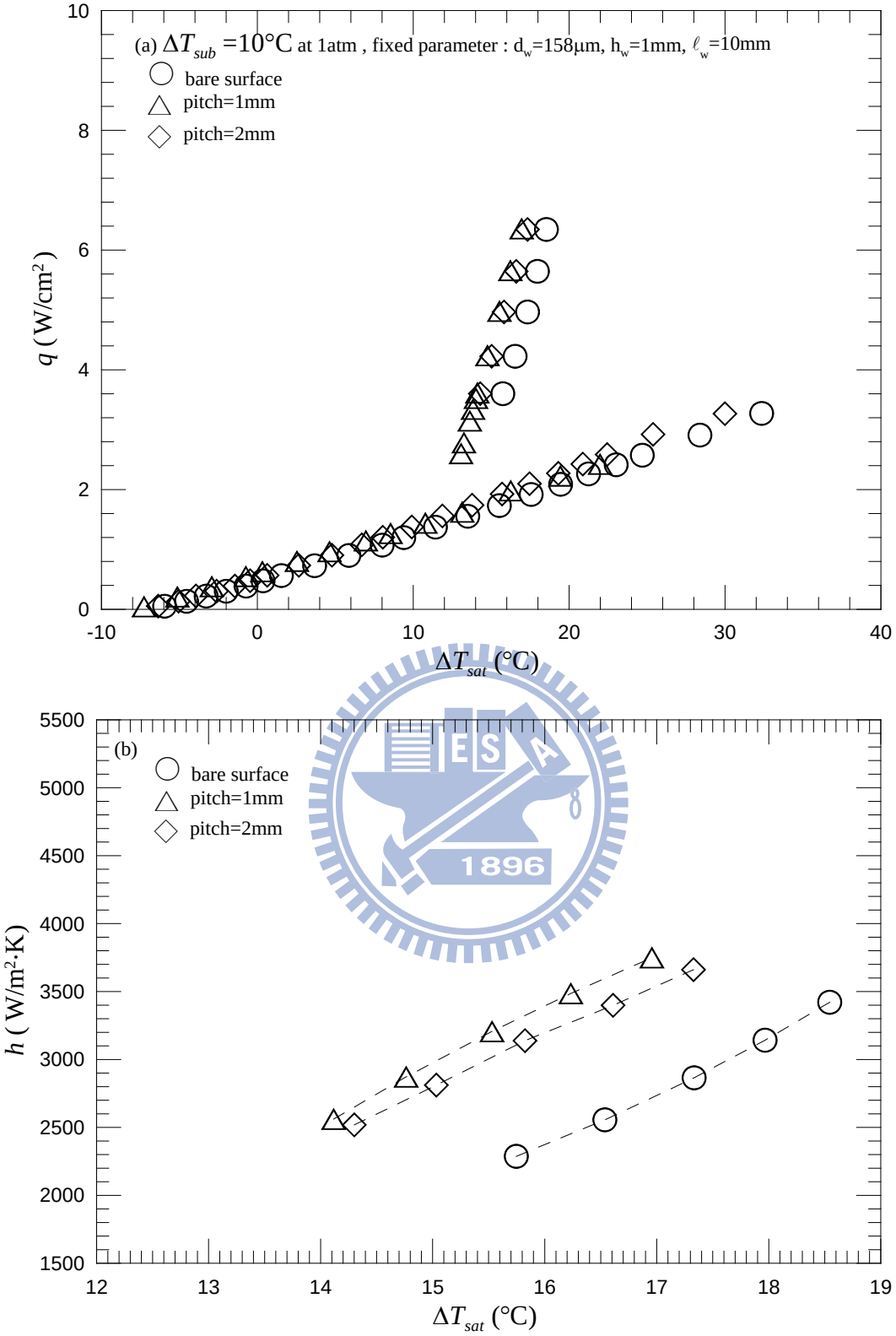

Fig. 5.65 Effects of string string-string pitch on subcooled pool boiling curves (a) and boiling heat transfer coefficients (b) for ΔT_{sub}= 10°C at d_w=158μm, h_w=1mm and ℓ_w =10mm.

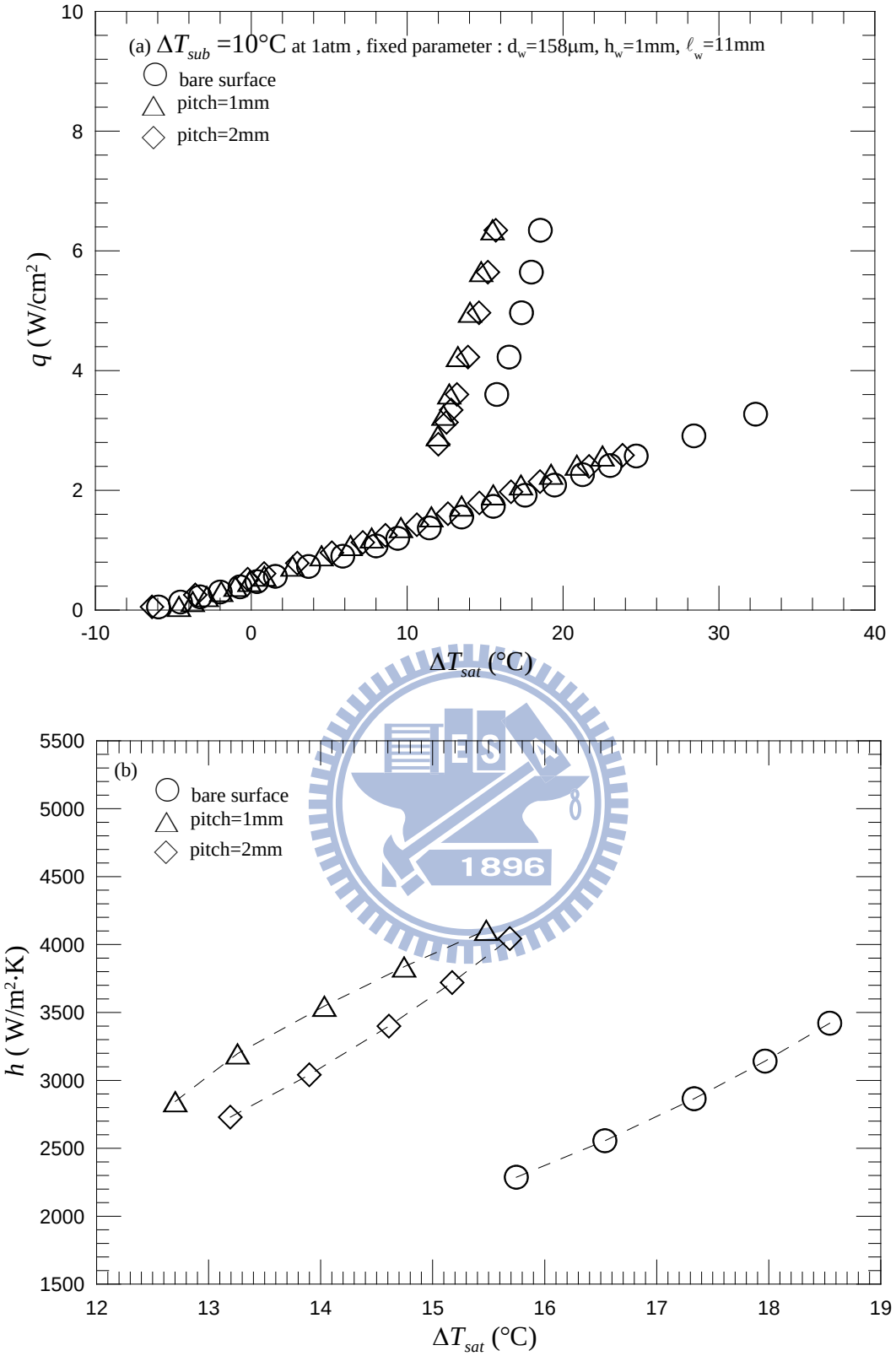

Fig. 5.66 Effects of string string-string pitch on subcooled pool boiling curves (a) and boiling heat transfer coefficients (b) for ΔT_{sub}= 10°C at d_w=158μm, h_w=1mm and ℓ_w =11mm.

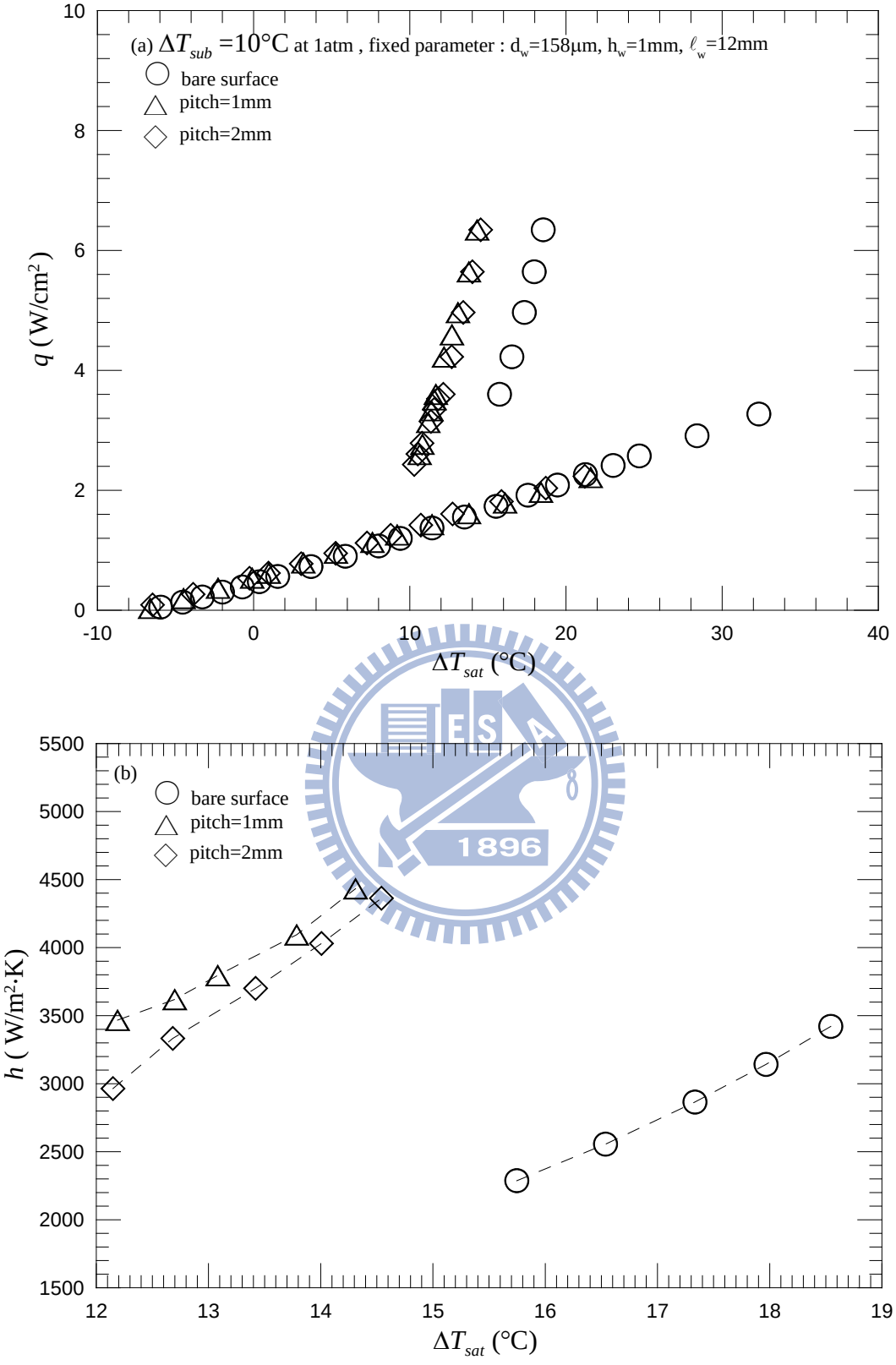

Fig. 5.67 Effects of string string-string pitch on subcooled pool boiling curves (a) and boiling heat transfer coefficients (b) for ΔT_{sub}= 10°C at d_w=158μm, h_w=1mm and ℓ_w =12mm.

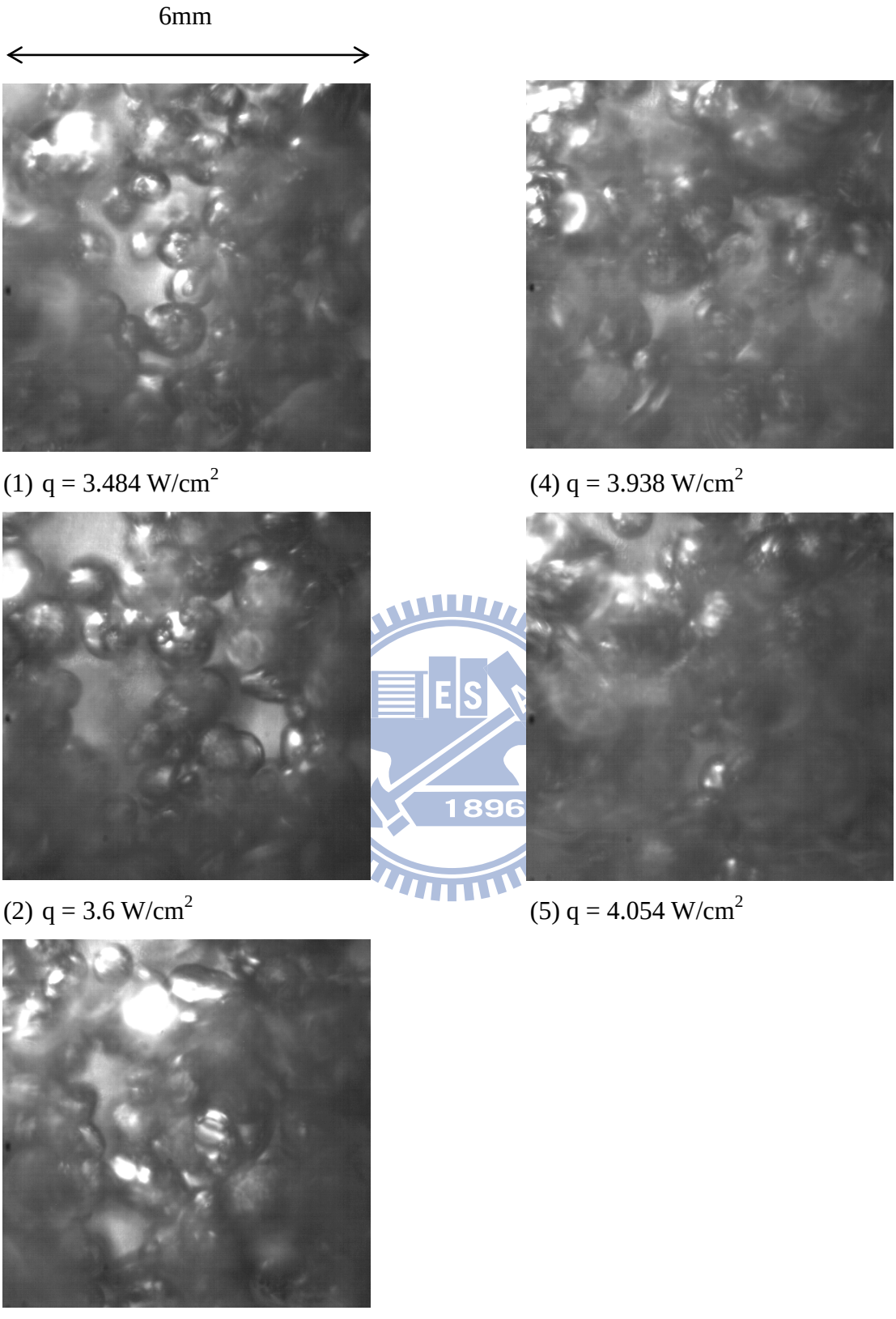

Fig. 5.68 Photos of saturated pool boiling of FC-72 for various imposed heat fluxes for bare surface.

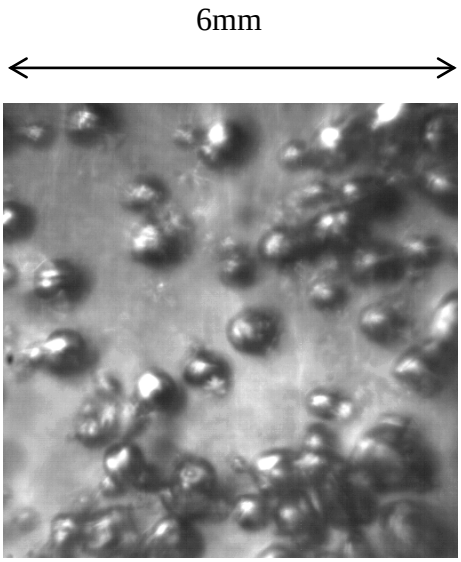

(1) q = 3.484 W/cm^2

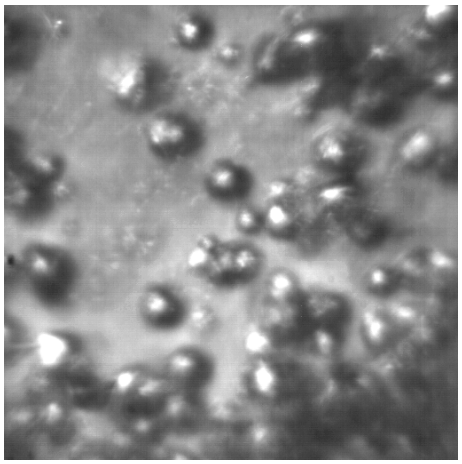

(4) q = 3.938 W/ cm^2

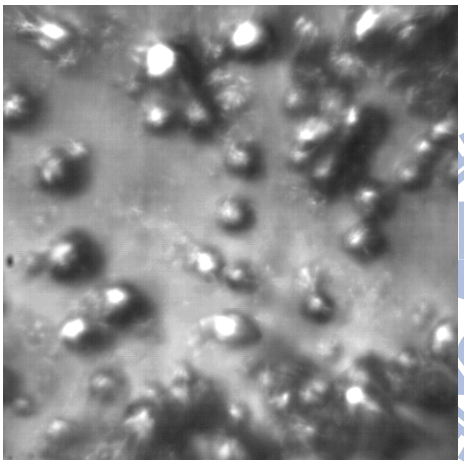

(2) q = 3.6 W/cm^2

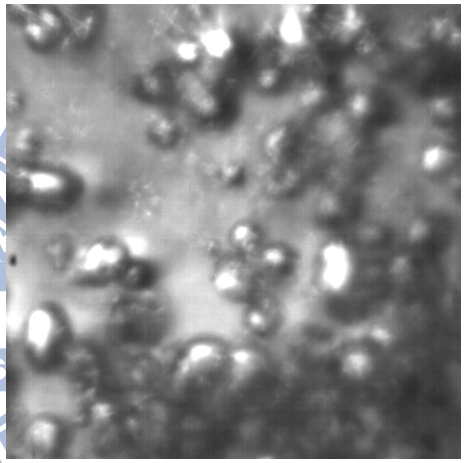

(5) q = 4.054 W/ cm^2

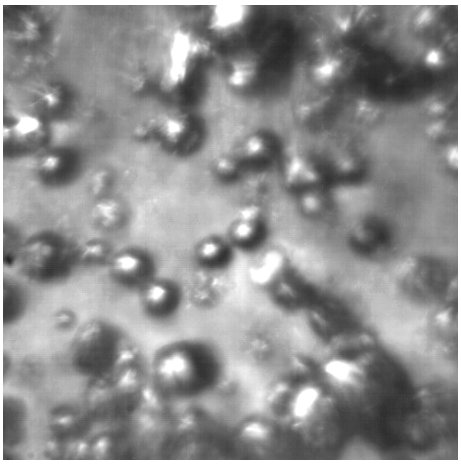

(3) q = 3.715 W/cm^2

Fig. 5.69 Photos of subcooled pool boiling of FC-72 for ΔT_{sub}= 5°C for various imposed heat fluxes for bare surface.

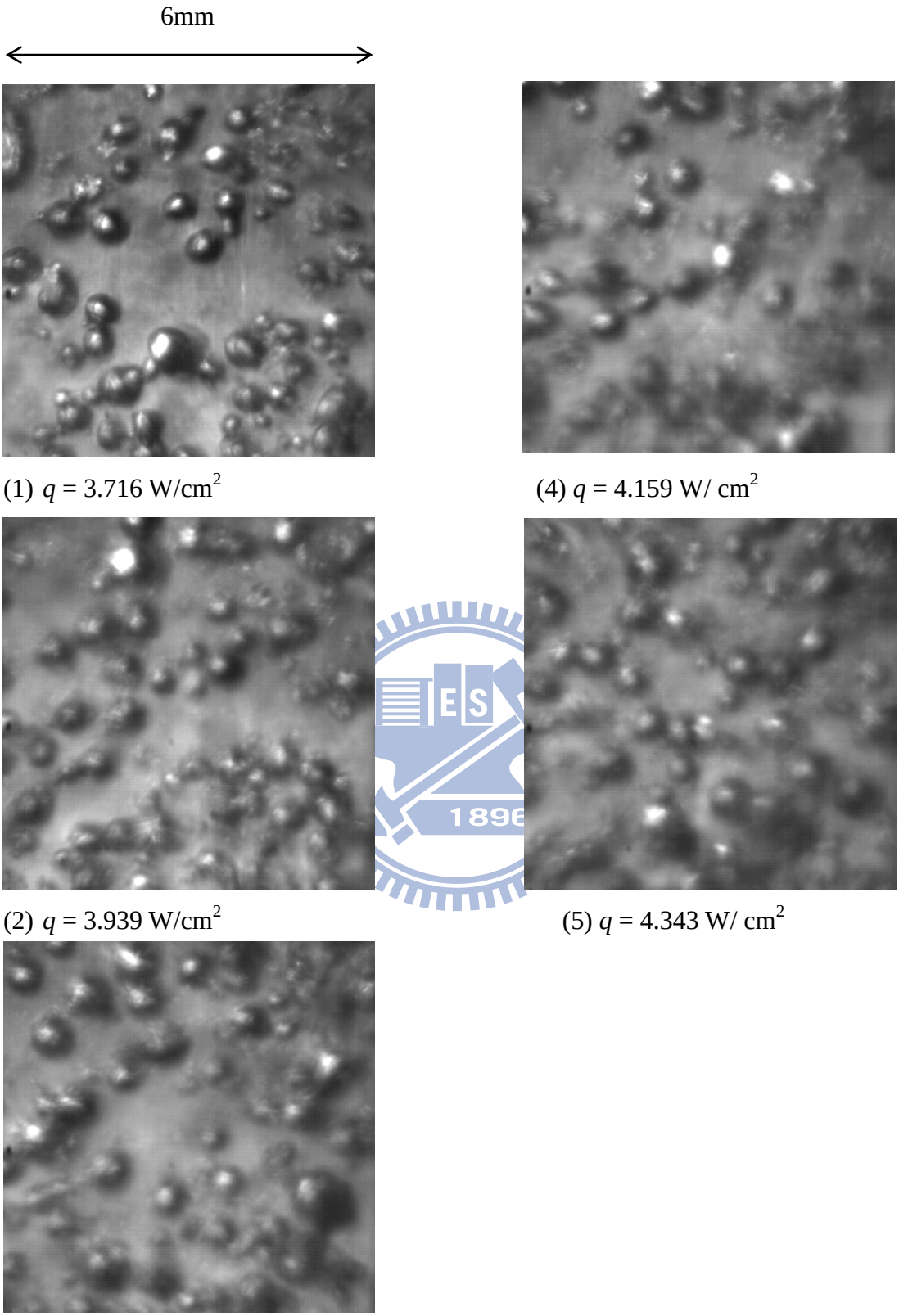

Fig. 5.70 Photos of subcooled pool boiling of FC-72 for ΔT_{sub}= 10°C for various imposed heat fluxes for bare surface.

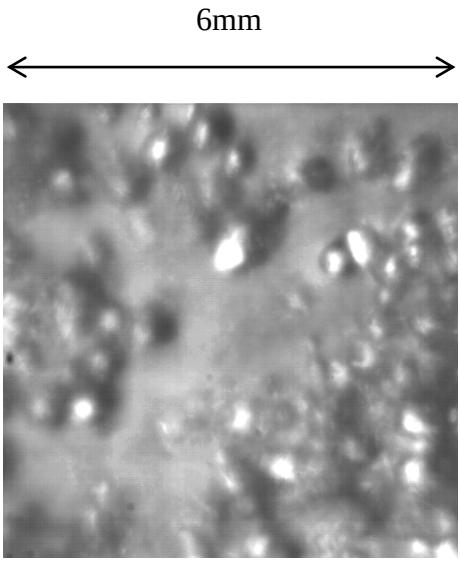

(1) q = 3.75 W/cm^2

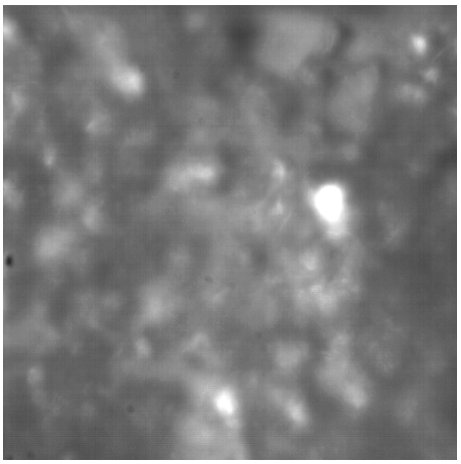

(4) q = 5.78 W/ cm^2

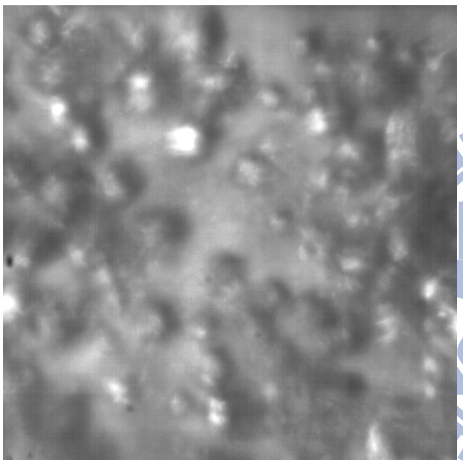

(2) q = 4.33 W/cm^2

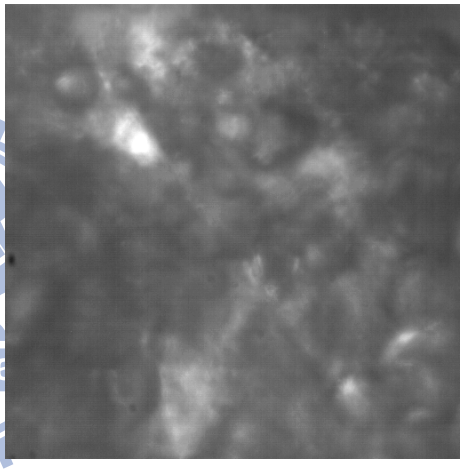

(5) q = 6.48 W/ cm^2

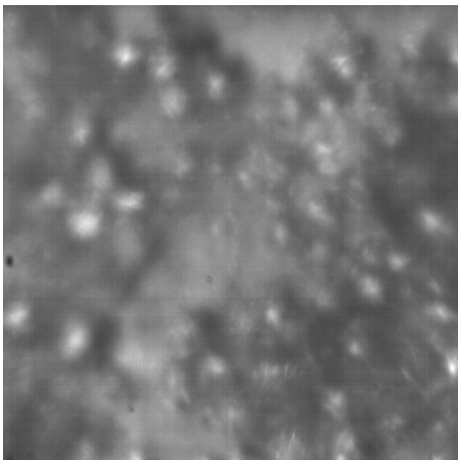

(3) q = 5.71 W/cm^2

Fig. 5.59 Photos of subcooled pool boiling of FC-72 for ΔT_{sub}= 5°C at d_w=74μm, ℓ_w =11mm and h_w=1mm.

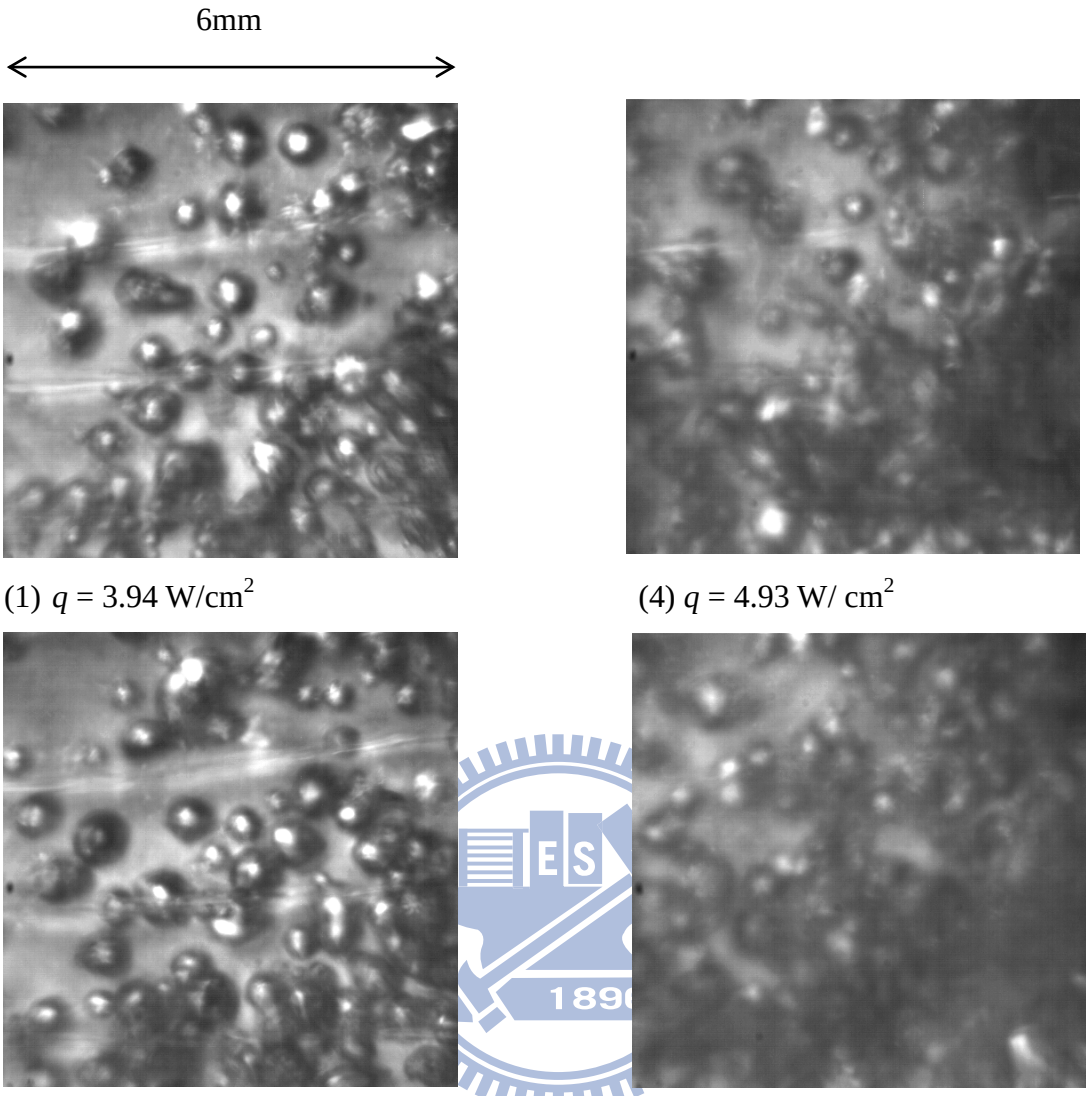

Fig. 5.72 Photos of subcooled pool boiling of FC-72 for ΔT_{sub}= 5°C at d_w=158μm, ℓ_w =11mm and h_w=1mm.

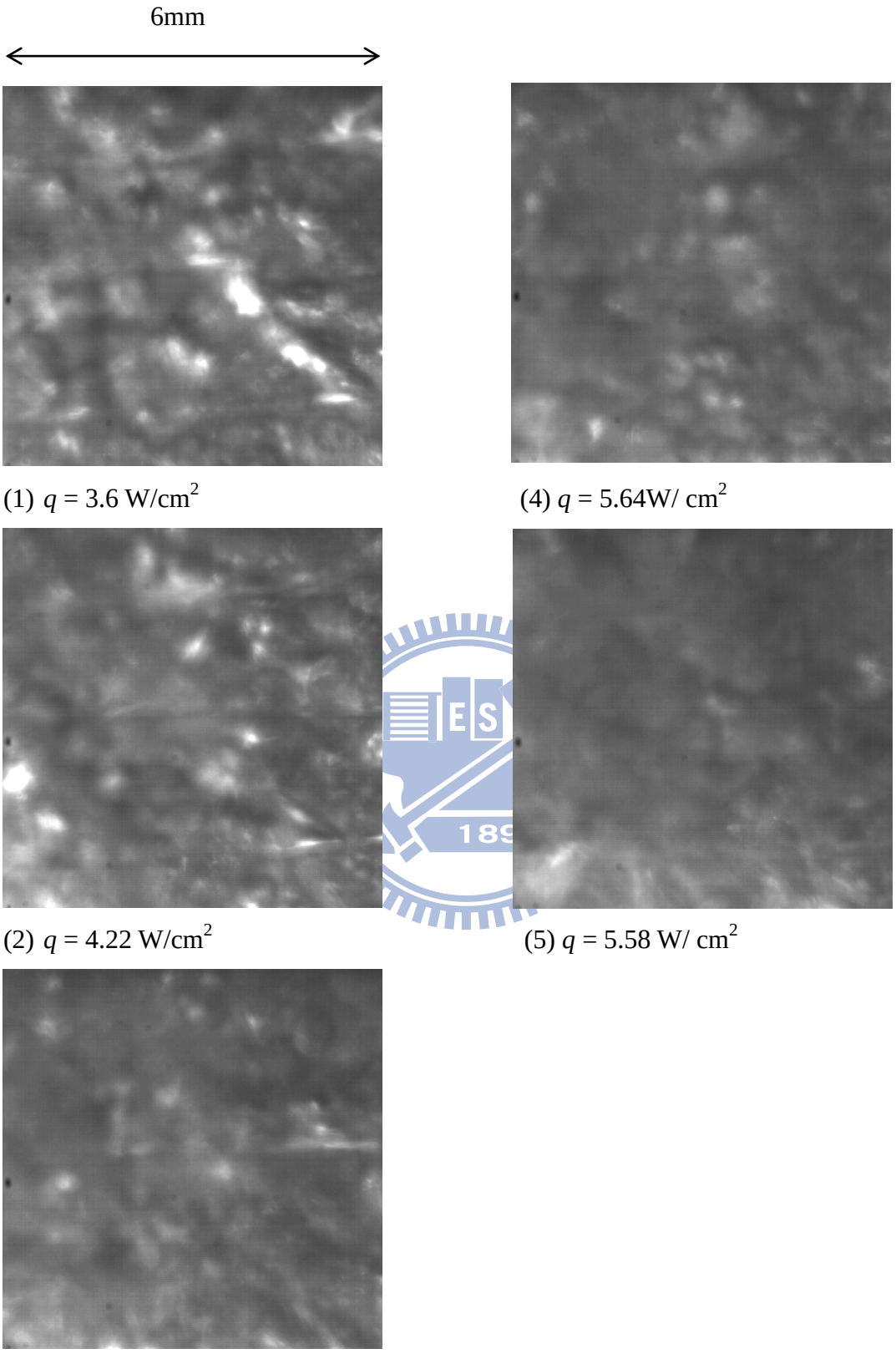

Fig. 5.73 Photos of subcooled pool boiling of FC-72 for ΔT_{sub}= 5°C at d_w=259μm, ℓ_w =11mm and h_w=1mm.

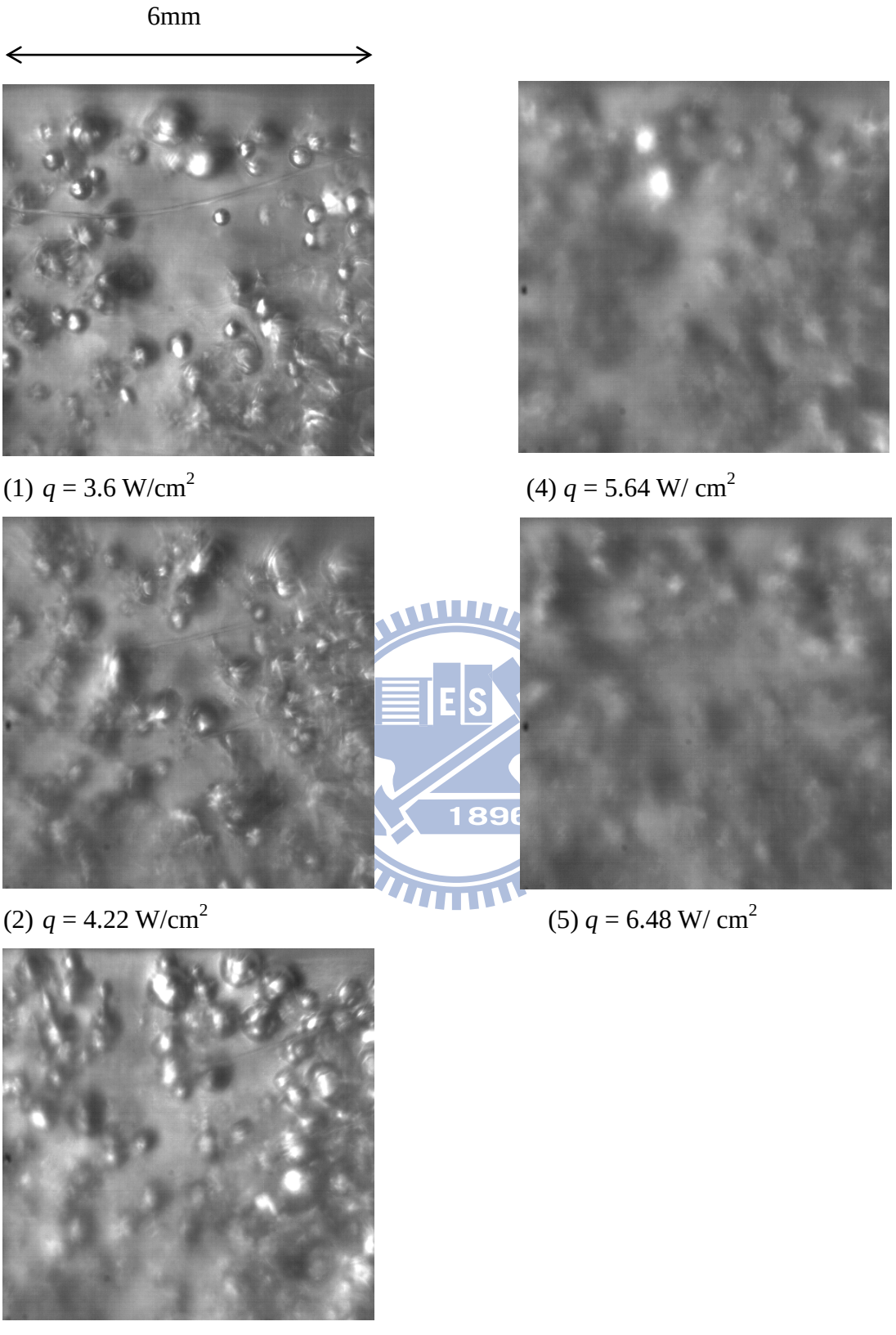

Fig. 5.74 Photos of subcooled pool boiling of FC-72 for ΔT_{sub}= 10°C at d_w=74μm, ℓ_w =11mm and h_w=1mm.

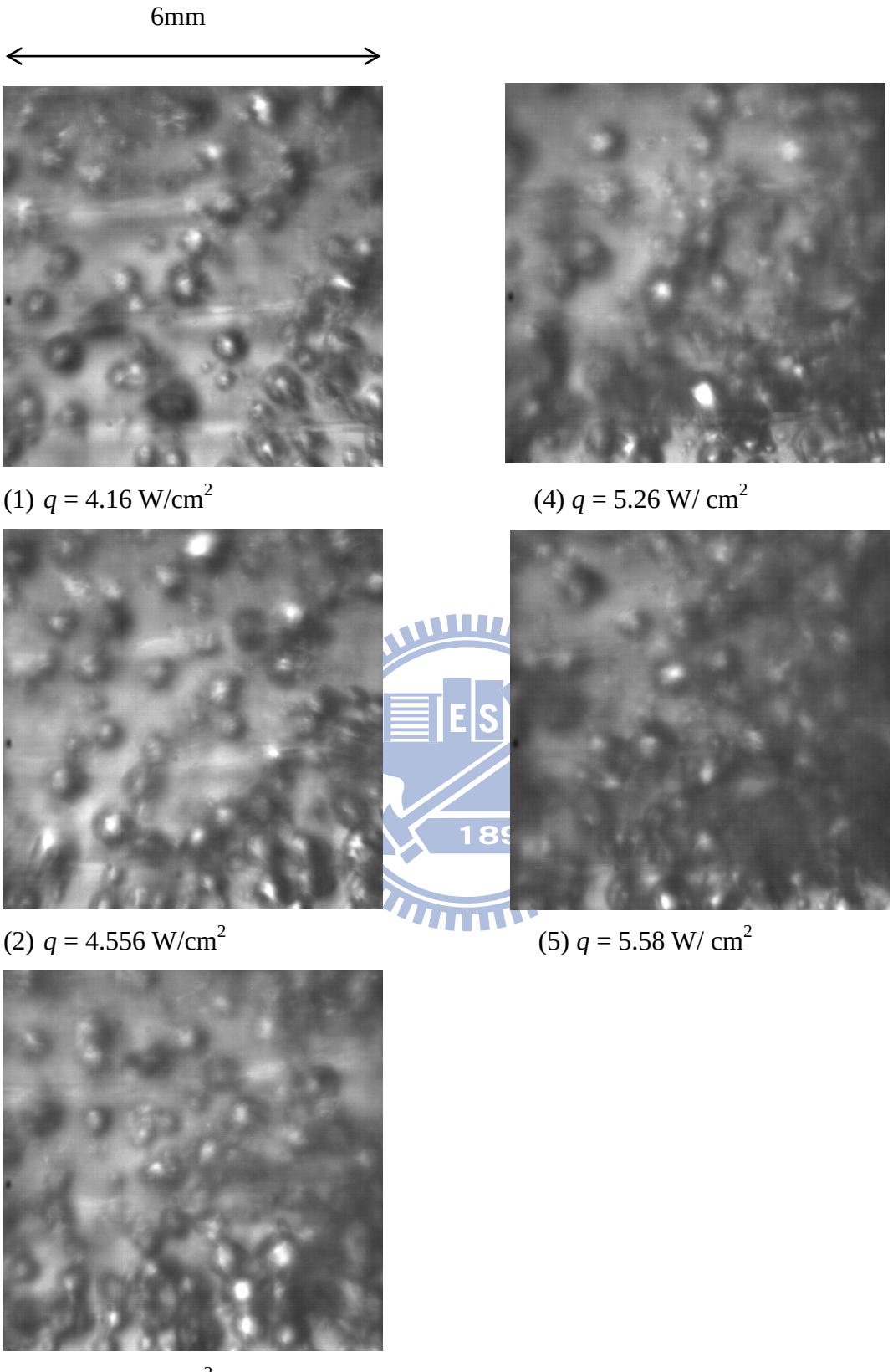

Fig. 5.75 Photos of subcooled pool boiling of FC-72 for ΔT_{sub}= 10°C at d_w=158μm, ℓ_w =11mm and h_w=1mm.

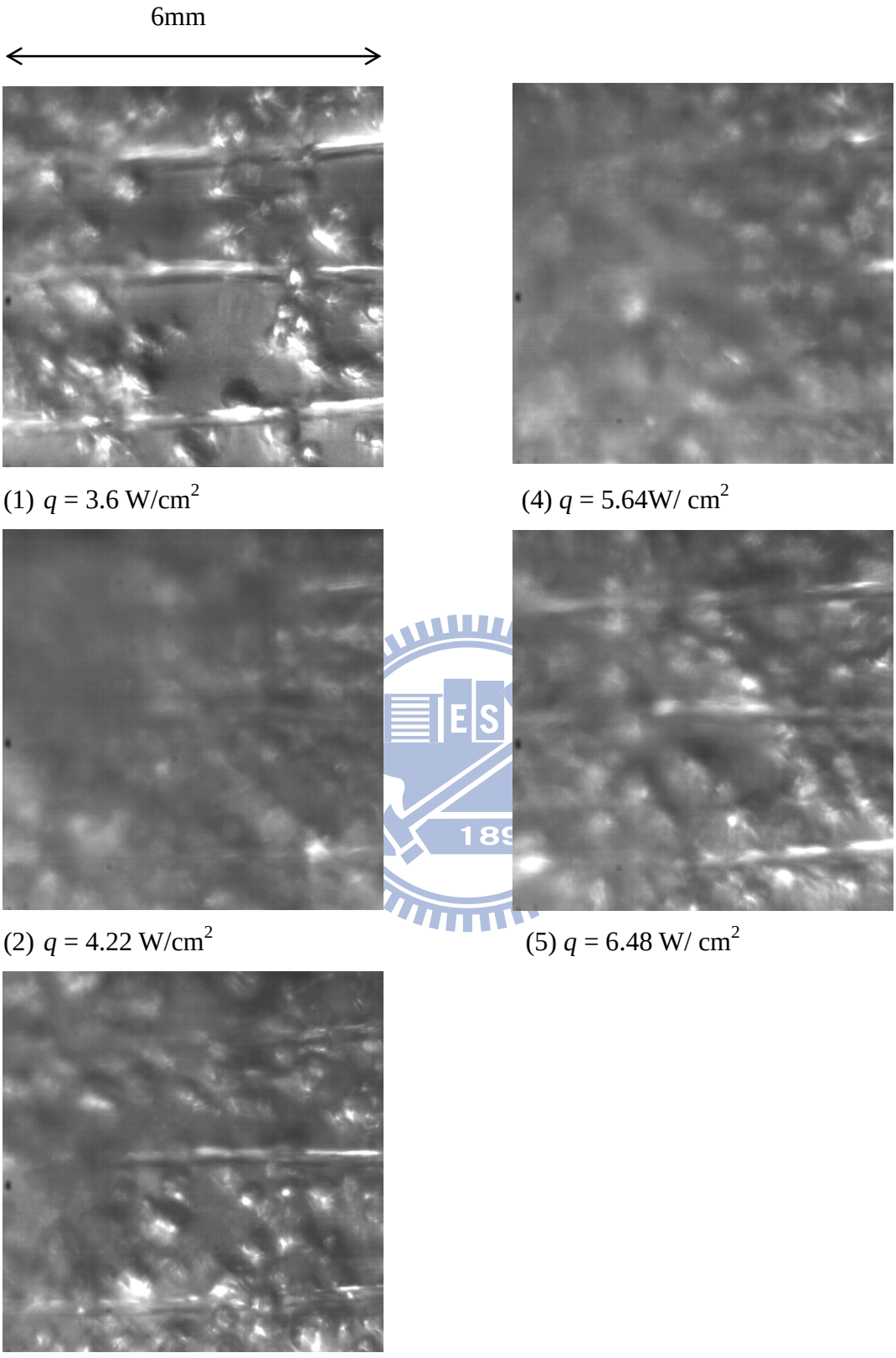

Fig. 5.76 Photos of subcooled pool boiling of FC-72 for ΔT_{sub}= 10°C at d_w=259μm, ℓ_w =11mm and h_w=1mm.

CHAPTER 6

CONCLUDING REMARKS

The enhancement of the saturated and subcooled boiling heat transfer of FC-72 over a small horizontal heated surface by installing nylon strings above the surface is explored in the present study. The effects of the string diameter, height, length and pitch on the boiling heat transfer enhancement are examined. The major results from their study can be summarized as follows.

(1) The extent of the boiling heat transfer enhancement by the flexible strings depends strongly on all experimental parameters, namely, the string diameter, length and height. The dependence is nonmonotonic.

(2) A boiling heat transfer coefficient enhancement to a certain extent can be obtained by a suitable choice of the experimental parameters.

(3) The string pitch reduction can enhance the boiling heat transfer to a noticeable degree only for the small-diameter strings.

(4) The bubble dynamics near the heated surface is conjectured to be affected substantially by the string size, looseness and position. But the details on how these parameters affect the near-wall bubbles requires further investigation.

References

[1] G. Xu, B. Guenin, M. Vogel, “Extension of air cooling for high power processors”, Proceedings 9th Intersociety Conference on Thermal Phenomena 1 (2004) 186-193.

[2] S. Nukiyama, “The maximum and minimum values of the heat *Q* transmitted from metal to boiling water under atmospheric pressure”, Journal Japan Society of Mechanical Engineers 37 (1934) 367-374.
(Translated in Int. J. Heat Mass Transfer 9 (1966) 1419-1433).

[3] A Bar-Cohen, “Thermal management of air-and liquid-cooled multichip modules”, IEEE Transactions on components, hybrids, and manufacturing technology 10 (2) (1987) 159-175.

[4] W. J. Miller, B. Gebhart, N. T. Wright, “Effects of boiling history on a microconfigured surface in a dielectric liquid”, Int. Commun. Heat Mass Transfer 17 (4) (1990) 389-398.

[5] J. Y. Chang, S. M. You, “Enhanced boiling heat transfer from micro-porous surfaces: effects of a coating composition and method”, Int. J. Heat Mass Transfer 40 (18) (1997) 4449-4460.

[6] K. N. Rainey, S. M. You, “Pool boiling heat transfer from plain and microporous, square pin-finned surfaces in saturated FC-72”, Trans. ASME J. Heat Transfer 122 (3) (2000) 509-516.

[7] K. N. Rainey, S. M. You, “Effect of pressure, subcooling, and dissolved gas on pool boiling heat transfer from microporous, square pin-finned surfaces in FC-72”, Int. J. Heat Mass Transfer 46 (1) (2003) 23-35.

[8] H. Honda, H. Takamatsu, J. J. Wei, “Enhanced boiling of FC-72 on silicon chips with micro-pin-fins and submicron-scale roughness”, Trans. ASME J. Heat Transfer 124 (2) (2002) 383-390.

[9] J. J. Wei, L. J. Guo, H. Honda “Experimental study of boiling phenomena and heat transfer performances of FC-72 over micro-pin-finned silicon chips”, Heat and Mass Transfer 41 (8) (2005) 744-755.

[10] T. M. Anderson, I. Mudawar, “Microelectronic cooling by enhanced pool boiling of a dielectric fluorocarbon liquid”, Trans. ASME J. Heat Transfer 111 (3) (1989) 752-759.

[11] J. P. O’Connor, S. M. You, “A painting technique to enhance pool boiling heat transfer in saturated FC-72”, Trans. ASME J. Heat Transfer 117 (2) (1995) 387-393.

[12] J. P. O’Connor, S. M. You, D. C. Price, “A dielectric surface coating technique to enhance boiling heat transfer from high power microelectronics”, IEEE Transactions on components, packaging and manufacturing technology Part A 18 (3) (1995) 656-663.

[13] J. Y. Chang, S. M. You, “Boiling heat transfer phenomena from micro-porous and porous surfaces in saturated FC-72”, Int. J. Heat Mass Transfer 40 (18) (1997) 4437-4447.

[14] J. Y. Jung, H. Y. Kwak, “Effect of surface condition on boiling heat transfer from silicon chip with submicron-scale roughness”, Int. J. Heat Mass Transfer 49 (23-24) (2006) 4543-4551.

[15] H. Honda, J. J. Wei, “Enhanced boiling heat transfer from electronic components by use of surface microstructures”, Experimental Thermal and Fluid Science 28 (2-3) (2004) 159-169.

[16] K. N. Rainey, S. M. You, “Effects of heater size and orientation on pool boiling heat transfer from microporous coated surfaces”, Int. J. Heat Mass Transfer 44 (14) (2001) 2589-2599.

[17] K. N. Rainey, S. M. You, S. Lee, “Effect of pressure, subcooling, and dissolved gas on pool boiling heat transfer from microporous surfaces in FC-72” Trans. ASME J. Heat Transfer 125 (1) (2003) 75-83.

[18] H. M. Chou, R. F. Horng, Y. S. Liu, J. L. Wong, “The effect of grooved pattern on enhanced boiling heat transfer in a cylindrical tank base with a constant surface area”, Int. Comm. Heat Mass Transfer 29 (7) (2002) 951-960.

[19] S. Hasegawa, R. Echigo, S. Irie, “Boiling characteristics and burnout phenomena on heating surface covered with woven screens”, Journal of Nuclear Science and Technology 12 (11) (1975) 722-724.

[20] J. Y. Tsay, Y. Y. Yan, T. F. Lin, “Enhancement of pool boiling heat transfer in a horizontal water layer through surface roughness and screen coverage”, Heat and Mass Transfer 32 (1-2) (1996) 17-26.

[21] J. W. Liu, D. J. Lee, A. Su, “Boiling of methanol and HFE-7100 on heated surface covered with a layer of mesh”, Int. J. Heat Mass Transfer 44 (1) (2001) 241-246.

[22] A. Franco, E. M. Latrofa, V. V. Yagov, “Heat transfer enhancement in pool boiling of a refrigerant fluid with wire nets structures”, Experimental Thermal and Fluid Science 30 (3) (2006) 263-275.

[23] H. M. Kurihara, J. E. Myers, “The effects of superheat and surface roughness on boiling coefficients”, A.I.Ch.E. Journal 6 (1) (1960) 83-91.

[24] F. P. Incropera, D. P. DeWitt, T. L. Bergman, A. S. Lavine, *Introduction to Heat Transfer, 5th ed.*, John Wiley & Sons, Inc., 2007, pp. 535, pp. 541.

[25] S. J. Kline, F. A. McClintock, “Describing uncertainties in single sample experiments”, Mechanical Engineering 75 (1953) 3-8.

[26] R. J. Moffat, “Contributions to the theory of single-sample uncertainty analysis”, Journal of Fluids Engineering 104 (2) (1982) 250-260.

[27] E. Radziemska, W. M. Lewandowski, “The effect of plate size on the natural convective heat transfer intensity of horizontal surfaces”, Heat Transfer Engineering 26 (2) (2005) 50-53.

[28] J. Y. Chang, S. M. You, “Heater orientation effects on pool boiling of micro-porous-enhanced surfaces in saturated FC-72”, Trans. ASME J. Heat Transfer 118 (4) (1996) 937-943.